

# **The role of Atgolgin-84A at the plant ER-Golgi interface**

**Vanessa De Sousa Vieira**

A thesis submitted in partial fulfilment of the requirements of Oxford  
Brookes University for the degree of Doctor of Philosophy

September 2018

# ACKNOWLEDGEMENTS

This work would not have been possible without the support of many people. First of all I would like to thank my supervisor Professor Chris Hawes for giving me the opportunity to be part of his group and to work on this project and for helping me finish this thesis until the end. I want to thank my supervisor Dr. Verena Kriechbaumer for helping me since day one even though she only became my supervisor in a later stage of my studies. Thanks to Dr. Anne Osterrieder for introducing me to Oxford Brookes and to the golgins.

Prof. Stanley Botchway and Dr Andy Ward for their help with the optical tweezers at the Central Laser Facility, Science and Technology Facilities Council, Rutherford Appleton Laboratory, Research Complex at Harwell. Prof. Jurgen Denecke and his students for the help and supervision with  $\alpha$ -amylase assay at the University of Leeds.

Thank you to all the colleagues in the Plant Cell Biology. A special thanks to Frances for sharing her culture and her lovely family with me. For being there as a friend and as a great scientist she is. Always trying to keep me awake with coffee or happy with chocolate. To Alessandra for being a great friend and for hosting me and be there for me when I needed the most. More recently, Charlotte and Bisa, you make the lab and office a better place to work. To the ones far away in Portugal, in particular the Lab 2.61 family that helped in this journey through their support and friendship. To the student from Spain that had the pleasure of working with me and bravely surviving that challenge, Cesar Vesicles Silvestre.

To my family. Especially my mum that has been always there for me, to hear my complaints and enjoy my bad mood during my writing-up stage. My dad for always believing and supporting my choices even the crazy ones. My godfather for being the best godfather in the world. To my grandmother, for all her unconditional love even though she could not understand what I was doing with my life. For the purple flowers she puts on my way every day to make sure I know she is always with me. All the family that makes me feel so welcome and loved every time I return home.

To all the great people I have met in Oxford either through Kineton or through my sports, dances and music. Has definitely been the best time of my life. The most special

thanks to Carina because I could not finish this challenge without her help and friendship. Thank you for everything and I will never be able to thank you enough. Thank you for sharing your lovely baby Ariel. A special thank you to Fátima for being in my life, for the precious friendship and for helping me always in every step I take and for the best conversations and long phone calls that kept me going. To my former housemates from Kineton Road, the best house in Oxford. Thank you for being the best housemates ever. We keep the memories.

And finally, to one of the most important parts of my life, capoeira. A very special thanks to all the Mestres, to the Afro-Brazilian culture that I love, respect and admire. To all the amazing friends I have met here in Oxford through capoeira. To the teachers and Mestres that helped me continue training and being part of this family. Thank you for letting me be part of your lives and always motivate me and believe in me.

# Table of Contents

ABSTRACT .....	1
LIST OF ABBREVIATIONS .....	3
1. Introduction .....	6
1.1 The endomembrane system .....	6
1.1.1 Anterograde transport.....	8
1.1.2 Retrograde transport .....	9
1.2 Endoplasmic reticulum/Golgi interface .....	10
1.3 Function of the Golgi apparatus.....	11
1.3.1 Golgi biogenesis .....	12
1.3.2 Golgi stack maintenance .....	14
1.4 Golgins .....	15
1.4.1 Golgins contribute to specificity in vesicle tethering .....	18
1.4.2 Plant golgins .....	21
Aims .....	25
2. Materials and methods .....	27
2.1 Overview .....	27
2.2 Molecular Biology techniques .....	29
2.2.1 mCh-fusions of Atgolgin-84A and deletion mutant .....	29
2.2.2 Constructs for $\alpha$ -amylase assay.....	31
2.2.3 Bacterial strains and growing conditions.....	34
2.2.4 Bacterial competent cells.....	35
2.2.5 Bacterial transformation.....	35
2.2.6 Plasmid DNA extraction.....	36
2.2.7 Plasmid DNA digestion.....	36
2.2.8 Agarose gels .....	36
2.2.9 DNA extraction and purification.....	37
2.2.10 Zero Blunt PCR cloning .....	37
2.2.11 pB7WGC2-mCherry Gateway cloning .....	37
2.2.12 pJA49 and pFLA39 cloning .....	37
2.3 Plant material- maintenance and transformation- <i>N. tabacum</i> .....	38

2.3.1 <i>Nicotiana</i> species plant system .....	38
2.3.2 <i>N. tabacum</i> growth conditions system .....	38
2.3.3 Agrobacterium-mediated infiltration of <i>N. tabacum</i> leaves .....	39
2.4 Plant material- maintenance and transformation- <i>Arabidopsis thaliana</i> .....	40
2.4.1 Germination and maintenance of <i>A. thaliana</i> .....	40
2.4.2 Transient transformation of <i>A. thaliana</i> .....	41
2.4.3 Stable transformation of <i>A. thaliana</i> by Floral-dip.....	42
2.4.4 Selection of transgenic <i>A. thaliana</i> plants.....	42
2.5 Secretion assay using $\alpha$ -amylase.....	43
2.5.1 Preparation of protoplasts .....	43
2.5.2 Electroporation of protoplasts .....	45
2.5.3 Harvesting of electroporated protoplasts.....	47
2.5.4 $\alpha$ -amylase assay .....	47
2.5.5 Beta-Glucuronidase (GUS) assay.....	48
2.6 Confocal Microscopy.....	49
2.6.1 Image acquisition .....	49
2.6.2 Co-localisation data analysis.....	50
2.7 Drugs treatments .....	51
2.8 Bioinformatics and <i>in silico</i> analysis .....	52
2.9 Optical trapping.....	53
2.9.1 Data collection and analysis of optical trapping.....	53
3. <i>In silico</i> characterisation of Atgolgin-84A .....	55
3.1 Introduction .....	55
3.2 Aims for bioinformatics analysis .....	56
3.3 Results .....	57
3.4 Discussion.....	60
4. Subcellular localisation of Atgolgin-84A using confocal microscopy with Airyscan.....	70
4.1 Introduction to confocal microscopy with Airyscan .....	70
4.2 Results .....	72
4.2.1 Optimisation of high-resolution imaging using the well-described non-functional Golgi marker ST-GFP .....	72
4.2.2 High-resolution imaging of Atgolgin-84A expression in different plant systems .....	72
4.2.3 High-resolution imaging of Atgolgin-84A co-expressed with an ER marker .....	74

4.2.4 High-resolution imaging of Atgolgin-84A co-expressed with different Golgi markers	75
4.2.5 High-resolution imaging of Atgolgin-84A with AtSar1a-GFP, a component of the COPII transporters	77
4.2.6 Co-localisation analysis on Airyscan data	77
4.2.7 High-resolution imaging of Atgolgin-84A expression during BFA treatment	80
4.3 Discussion	83
5. Co-localisation of truncated protein Atgolgin-84A $\Delta$ 1-557	117
5.1 Introduction	117
5.2 Results	118
5.2.1 High-resolution imaging of Atgolgin-84A $\Delta$ 1-557 expression in different plant systems	118
5.2.2 High-resolution imaging of Atgolgin-84A $\Delta$ 1-557 in co-expression with an ER marker	119
5.2.3 High-resolution imaging of Atgolgin-84A $\Delta$ 1-557 co-expression with different Golgi markers	119
5.2.5 High-resolution imaging of Atgolgin-84A $\Delta$ 1-557 with YFP-Sec24A, a component of the COPII transporters	122
5.2.6 Co-localisation analysis on Airyscan imaging data	123
5.2.7 Quantification of sideways ring-shaped structures during expression of Atgolgin-84A $\Delta$ 1-557	124
5.3 Discussion	125
6. Assessing the putative tethering function of the long coiled-coil domains	151
6.1 Introduction	151
6.2 Results	153
6.3 Discussion	156
7: The effect of overexpression of Atgolgin-84A in protein trafficking	168
7.1 Introduction	168
7.2 Results	169
7.2.1 A secretory assay using confocal microscopy	169
7.2.2 A secretory assay using $\alpha$ -amylase	171
7.3 Discussion	174
8. General discussion and future work	190
References	197

# List of tables

Table 1-1: Homologues for the mammalian golgins and their specific tethering ability. ....	19
Table 1-2: Characterized <i>Arabidopsis</i> golgins and their homologues in mammals. ....	22
Table 2-1: List of constructs used during this work including the vector, the optical density (OD <sub>600</sub> ) for <i>N. tabacum</i> infiltration, main features and references. ....	28
Table 2-2: Primers used in the colony PCR amplification and sequencing of Atgolgin-84A and Atgolgin-84Δ1-557 in the mCherry fusions in the pB7WGC2 vector.. ....	30
Table 2-3: PCR conditions for full-length golgins and deletion mutants amplification to add restriction enzyme sites for cloning into pJA49 and pFLA39. ....	32
Table 2-4: Primers used in the amplification of Atgolgin-84A, AtCASP and deletion mutants Atgolgin-84Δ1-557 and AtCASP1-664 for α-amylase assays.....	33
Table 2-5: Antibiotic used to select bacteria and concentrations.. ....	34
Table 2-6: Bacterial strains and growing conditions. ....	34
Table 2-7: Imaging settings with PMT/GaAsP detectors for different fluorophores. ....	49
Table 2-8: Imaging settings with Airyscan detector for different fluorophores.....	50
Table 2-9: Web tools used in chapter 3, web addresses and description of the specific software. ....	52
Table 4-1: Number of pairs of Golgi bodies observed during expression in <i>N. tabacum</i> of ST-GFP and GFP-Atgolgin-84A.....	97
Table 4-2: Co-localisation analysis of Atgolgin-84A and markers for the Golgi, AtCASP and COPII transporters. Pearson's correlation coefficients (PCCs) for the different combinations of markers are given.....	112
Table 5-1: Co-localisation analysis of GFP-Atgolgin-84AΔ1-557 in <i>N. tabacum</i> compared to the previously obtained PCC values for GFP-Atgolgin84A (chapter 4) and Golgi membrane markers. Pearson correlation coefficients (PCCs) are shown for the different combinations of markers.....	148
Table 6-1: Mean of counted trapped Golgi bodies during the overexpression of GFP-Atgolgin-84AΔ1-557 compared to the mean of trapped Golgi bodies expressing ST-GFP.....	164
Table 6-2: Mean of counted trapped Golgi bodies during the co-expression of GFP-Atgolgin-84AΔ1-557 with mRFP-AtCASPΔ1-664 compared to the mean of trapped Golgi bodies expressing ST-GFP.....	166

# List of Figures

Figure 1.1: Schematic representation of transport routes in the secretory pathway in plants. ....	7
Figure 1.2: Diagram showing the spatial relationship between the ER, the Golgi stack and the Golgi matrix.....	14
Figure 1.3: Putative topology and membrane attachment of golgins.....	17
Figure 1.4: Schematic of the putative golgins localization in animal cells according to how golgins appear to tether the different sets of vesicles arriving at the Golgi.....	20
Figure 2.1: Schematic representation of mCherry constructs. (A) mCherry fused to full-length Atgolgin-84A. ....	29
Figure 2.2: Flowchart representation of the procedure for cloning and screening of the constructs for protoplast transformation .....	31
Figure 2.3: Plant leaf enzyme digestion to obtain protoplasts. ....	44
Figure 2.4: Protoplast harvesting after digestion and before electroporation. ....	46
Figure 2.5: Electroporation of <i>N. benthamiana</i> protoplasts.....	46
Figure 3.1: Predicted Hsgolgin-84, Atgolgin-84A and Atgolgin-84B protein structure using Phyre2. ....	63
Figure 3.2: Prediction of TMD insertion in the membrane and alignment of the TMD for different species. ....	64
Figure 3.3: Alignment of the N-terminus of golgin-84 that can capture vesicles in mammalian cells with that from the indicated species. ....	66
Figure 3.4: Mapping of Atgolgin-84A.....	67
Figure 3.5: Phosphorylation sites prediction for Atgolgin-84A C-terminal end using the Arabidopsis Protein Phosphorylation Site Database (PhosPhAt 4.0).....	68
Figure 3.6: Schematic representation of Atgolgin-84A full-length protein and deletion mutant Atgolgin-84A $\Delta$ 1-557.....	69
Figure 4.1: Zeiss LSM 880 with Airyscan detector at Oxford Brookes University with temperature and CO <sub>2</sub> controlled incubator.. ....	91
Figure 4.2: Beam path in the Airyscan unit attached to the Zeiss LSM 880.....	92
Figure 4.3: Airyscan detector design from Huff <i>et al.</i> , (2015).. ....	93



Figure 4.4: <i>Trans</i> -Golgi marker ST-GFP expression in <i>N. tabacum</i> two days post-infiltration (2dpi). Imaging performed using the standard confocal mode of the Zeiss LSM 880.....	94
Figure 4.5: Airyscan high resolution imaging of the <i>trans</i> -Golgi marker ST-GFP stable <i>A. thaliana</i> plants (Appendix I, Movie 1).....	95
Figure 4.6: <i>N. tabacum</i> plants infiltrated with GFP-Atgolgin-84A.....	96
Figure 4.7: Expression of GFP-Atgolgin-84A in <i>N. tabacum</i> (A, B, D and E) and <i>A. thaliana</i> .....	97
Figure 4.8: Co-expression of mCherry-Atgolgin-84A and GFP-HDEL in <i>N. tabacum</i> showing re-shaping of ring-shaped compartment (Appendix I, Movie 2).....	98
Figure 4.9: Enlargement of inset in Figure 4.8B (Appendix I, Movie 2).....	99
Figure 4.10: Co-expression of mCherry-Atgolgin-84A and GFP-HDEL in <i>N. tabacum</i> . (Appendix I, Movie 3 and 4).....	100
Figure 4.11: Enlargement of Figure 4.9. (Appendix I, Movie 3 and 4).....	100
Figure 4.12: Localisation of the different Golgi markers mentioned in this chapter within the Golgi stacks <i>cis</i> -, <i>medial</i> -, <i>trans</i> -Golgi from left to right.....	101
Figure 4.13: Co-expression of GFP-Atgolgin-84A and ST-mRFP in <i>N. tabacum</i> . Atgolgin-84A and ST appear shifted with respect to each other (Appendix I, Movie 5 and 6).....	102
Figure 4.14: Co-expression of MnSI-mRFP and GFP-Atgolgin-84A in <i>N. tabacum</i> .....	103
Figure 4.15: Co-expression of GnTI-mRFP and GFP-Atgolgin-84A in <i>N. tabacum</i> .....	104
Figure 4.16: Co-expression of GFP-Atgolgin-84A and mRFP-AtCASP in <i>N. tabacum</i> leaf epidermal cells.....	105
Figure 4.17: Expression of AtSar1a-GFP in <i>N. tabacum</i> (Appendix I, Movie 7 and 8).....	106
Figure 4.18: Transient expression of mCh-Atgolgin-84A in <i>N. tabacum</i> leaf epidermal cells 3 dpi.....	107
Figure 4.19: Co-expression of AtSar1a-GFP and mCherry-Atgolgin-84A in <i>N. tabacum</i> .....	108
Figure 4.20: Examples of scatterplots for two markers.....	109
Figure 4.21: Schematic representation of different objects selected for analysis.....	110
Figure 4.22: Examples of ROIs used for co-localisation analysis in merged images of green and red channel using Zen (Zeiss) software.....	111
Figure 4.23: BFA treatment on leaves expressing GFP-Atgolgin-84A, AtSar1a-GFP and MnSI-mRFP.....	113

Figure 4.24: Time frames from a movie showing Atgolgin-84A BFA wash-out compartments (Appendix 1, Movie 9).....	114
Figure 4.25: Co-expression of GFP-Atgolgin-84A and mRFP-HDEL after BFA treatment.....	115
Figure 4.26: Co-expression of mCh-Atgolgin-84A and AtSar1a-GFP after BFA treatment.....	116
Figure 5.1: Schematic representation of Atgolgin-84A full-length protein and deletion mutant Atgolgin-84A $\Delta$ 1-557.....	134
Figure 5.2: GFP-Atgolgin-84A $\Delta$ 1-557 transient expression in <i>planta</i> (Appendix 1, Movie 10)....	135
Figure 5.3: Atgolgin-84A $\Delta$ 1-557 stable expression in <i>A. thaliana</i> (Appendix 1, Movie 11).....	136
Figure 5.4: Co-expression of mCh-Atgolgin-84A $\Delta$ 1-557 and GFP-HDEL in <i>N. tabacum</i> (Appendix I, Movie 12).....	137
Figure 5.5: Frames of a time series during co-expression of ST-mRFP and GFP-Atgolgin-84A $\Delta$ 1-557 deletion mutant in <i>N. tabacum</i> (Appendix I, Movie 13).....	138
Figure 5.6: Enlargement of Figure 5.5 showing detail of tubules protruding out of the Golgi bodies and connecting GFP-Atgolgin-84A $\Delta$ 1-557-labelled compartments.....	139
Figure 5.7: Co-expression of GFP-Atgolgin-84A $\Delta$ 1-557 and ST-mRFP with high-magnification of a ring-shaped structure.....	140
Figure 5.8: Co-expression of MnSI-mRFP and GFP-Atgolgin-84A $\Delta$ 1-557 in <i>N. tabacum</i> (Appendix 1, Movie 14 and 15).....	141
Figure 5.9: Frames from a time series of GFP-Atgolgin-84A $\Delta$ 1-557 co-expression with MnSI-mRFP <i>cis</i> -Golgi marker in <i>N. tabacum</i> (Appendix 1, Movie 16).....	142
Figure 5.10: Transient expression of MnSI-mRFP and GFP-Atgolgin-84A $\Delta$ 1-557 in <i>A. thaliana</i> (Appendix I, Movie 17 and 18).....	143
Figure 5.11: Co-expression of plant golgin GFP-Atgolgin-84A $\Delta$ 1-557 and mRFP-AtCASP $\Delta$ 1-164 in <i>N. tabacum</i> (Appendix I, Movie 19 and 20).....	144
Figure 5.12: Co-expression of GFP-Atgolgin-84A $\Delta$ 1-557 and mRFP-AtCASP $\Delta$ 1-164 in <i>N. tabacum</i> (Appendix I, Movie 21).....	145
Figure 5.13: Expression of YFP-Sec24a in <i>N. tabacum</i> leaf epidermal cells (Appendix I, Movie 22).....	146
Figure 5.14: Co-expression of mCh-Atgolgin-84A $\Delta$ 1-557 with YFP-Sec24a in <i>N. tabacum</i> .....	147

Figure 5.15: Examples of ROIs used for co-localisation analysis on Zen (Zeiss) software in merged images of green and red channels.....	148
Figure 5.16: Histogram representing the mean of counted ring-shaped structures that flip sideways during time series during expression of Atgolgin-84A $\Delta$ 1-557 compared to the mean of the number of Golgi bodies expressing only ST-GFP.....	150
Figure 6.1: Trapping event during overexpression of ST-GFP (Appendix I, Movie 23).....	160
Figure 6.2: Trapping event during overexpression of GFP-Atgolgin-84A $\Delta$ 1-557 (Appendix I, Movie 24).....	161
Figure 6.3: Aggregates of Golgi bodies during over expression of GFP-Atgolgin-84A $\Delta$ 1-557 (Appendix I, Movie 25).....	162
Figure 6.4: Golgi bodies labelled by ST-GFP, Atgolgin-84A1-557 and the co-expression of GFP-Atgolgin-84A $\Delta$ 1-557 with mRFP-AtCASP $\Delta$ 1-664 were tested for trapping and their trapping characteristics were scored.....	163
Figure 6.5: Co-expression of GFP-Atgolgin-84A $\Delta$ 1-557 and mRFP-AtCASP $\Delta$ 1-564 imaged with a TIRF microscope with two-colours imaging (Appendix I, Movie 26).....	165
Figure 6.6: Co-expression of GFP-Atgolgin-84A $\Delta$ 1-557 and mRFP-AtCASP $\Delta$ 1-564 imaged with a TIRF microscope (Appendix I, Movie 27).....	166
Figure 7.1: Schematic diagram of secretory pathway blockage by overexpression of Atgolgin-84A or Atgolgin-84A $\Delta$ 1-557.....	180
Figure 7.2: Timeline of infiltration for the secretion assay imaging.....	181
Figure 7.3a: Secretion assay using transient expression in <i>N. tabacum</i> .....	182
Figure 7.3b: Secretion assay using transient expression in <i>N. tabacum</i> .....	183
Figure 7.3c: Secretion assay using transient expression in <i>N. tabacum</i> .....	184
Figure 7.4: Example of each category used for the quantification from the co-expression of SP-mCh with GFP-Atgolgin-84A $\Delta$ 1-557.....	185
Figure 7.5: Quantification of the amount of cells showing different labelling by mCherry.....	186
Figure 7.6: Pilot test for expression of golgins and truncations using GUS assay in transfected <i>N. benthamiana</i> protoplasts.....	187
Figure 7.7: Co-expression of $\alpha$ -amylase and golgins fusions in <i>N. Benthamiana</i> protoplasts.....	188

Figure 7.8: Co-expression of SP-mCherry with GFP-Atgolgin-84A $\Delta$ 1-557 in *N. benthamiana*..... 189

# Appendix I

## List of movies

Movie 1: ST-GFP

Movie 2: mCh-Atgolgin84A+GFP-HDEL

Movie 3: mCh-Atgolgin84A+GFP-HDEL

Movie 4: mCh-Atgolgin84A+GFP-HDEL

Movie 5: GFP-Atgolgin84A+ST-mRFP

Movie 6: GFP-Atgolgin84A+ST-mRFP

Movie 7: AtSar1a-GFP

Movie 8: AtSar1a-GFP

Movie 9: GFP-Atgolgin84A\_BFA\_WO

Movie 10: GFP-Atgolgin84Adel ( $\Delta 1-557$ )

Movie 11: At stable\_GFP-Atgolgin84Adel ( $\Delta 1-557$ )

Movie 12: mCh-Atgolgin84Adel ( $\Delta 1-557$ )+GFP-HDEL

Movie 13: GFP-Atgolgin84Adel ( $\Delta 1-557$ )+ST-mRFP

Movie 14: GFP-Atgolgin84Adel ( $\Delta 1-557$ )+MnSI-mRFP

Movie 15: GFP-Atgolgin84Adel ( $\Delta 1-557$ )+MnSI-mRFP

Movie 16: GFP-Atgolgin84Adel ( $\Delta 1-557$ )+MnSI-mRFP

Movie 17: At\_ transient\_GFP-Atgolgin84Adel ( $\Delta 1-557$ )+MnSI-mRFP

Movie 18: At\_ transient\_GFP-Atgolgin84Adel ( $\Delta 1-557$ )+MnSI-mRFP

Movie 19: At\_ transient\_GFP-Atgolgin84Adel ( $\Delta 1-557$ )+mRFP-AtCASPdel ( $\Delta 1-564$ )

Movie 20: At\_ transient\_GFP-Atgolgin84Adel ( $\Delta 1-557$ )+mRFP-AtCASPdel ( $\Delta 1-564$ )

Movie 21: At\_ transient\_GFP-Atgolgin84Adel ( $\Delta 1-557$ )+mRFP-AtCASPdel ( $\Delta 1-564$ )

Movie 22: mCh-Atgolgin84Adel ( $\Delta 1-557$ )+YFP-AtSec24

Movie 23: Tweezers\_ST-GFP

Movie 24: Tweezers\_ST-GFP

Movie 25: Tweezers\_GFP-Atgolgin84Adel ( $\Delta 1-557$ )

Movie 26: Tweezers\_GFP-Atgolgin84Adel ( $\Delta 1-557$ )+mRFP-AtCASPdel ( $\Delta 1-564$ )

Movie 27: Tweezers\_GFP-Atgolgin84Adel ( $\Delta 1-557$ )+mRFP-AtCASPdel ( $\Delta 1-564$ )

# ABSTRACT

The eukaryotic cell is compartmentalised into an endomembrane system organised into several organelles. Some of these organelles, namely endoplasmic reticulum (ER) and Golgi bodies, are part of a so-called secretory pathway where vital cell components travel to reach the correct final destination or are recycled for further processing. In the plant cell cytoplasm there are numerous stacks of membrane bounded cisternae, each of which constitutes a discrete Golgi body. Golgi bodies are responsible in part for the processing of proteins received from the ER and their distribution to the plasma membrane and other compartments. Exactly how this motile structure is maintained while providing vital functions for the cell is still poorly understood. The ER is physically connected to Golgi bodies, and Golgi matrix components, such as golgins, have been identified and suggested to function as putative tethering factors. Golgins are proteins anchored to the Golgi membrane by the C-terminus either through transmembrane domains (TMDs) or interaction with small regulatory GTPases. The golgin *N*-terminus contains long coiled-coil domains which consist of a number of  $\alpha$ -helices wrapped around each other to form a structure similar to a rope being made from several strands, reaching into the cytoplasm.

Atgolgin84A may act as tethering factor at the ER-Golgi interface and within the Golgi stack. In animal cells golgins are also implicated in specific recognition of cargo at the Golgi. In plants, there is no clear evidence for the localisation of Atgolgin-84A at the Golgi. To investigate Atgolgin-84A subcellular localisation and putative function as a tether, fluorescent fusions to Atgolgin-84A and Atgolgin-84A truncation lacking the coiled-coil domains (Atgolgin-84A $\Delta$ 1-557) were transiently expressed in *Nicotiana tabacum* and imaged by confocal microscopy with Airyscan detector. High-resolution confocal imaging was used to resolve the Golgi cisternae and the ER-Golgi interface. The data presented here shows that Atgolgin-84A seems to be localised at a pre-*cis*-Golgi compartment that is also labelled by one of the COPII proteins.

Optical trapping is a technology in which an infrared laser beam can be used to capture and manipulate Golgi bodies *in planta*. The trapping experiments using optical tweezers revealed differences in Golgi bodies trapping properties when the truncated version Atgolgin-84A $\Delta$ 1-557 was overexpressed in *N. tabacum* leaves.

Under the hypothesis that Atgolgin-84A could also be implicated in ER to Golgi trafficking a secretion assay was optimised using Atgolgin-84A as effector expected to affect the transport of cargo molecules. The trafficking of cargo was imaged when cells were expressing Atgolgin-84A full-length and mutant Atgolgin-84A without coiled-coil domains. The cargo was re-directed to a different compartment. This hypothesis was also tested using an  $\alpha$ -amylase assay and the secretion index decreased when Atgolgin-84A was co-expressed with cargo supporting the effect observed using confocal imaging. The results show strong evidence for a role of Atgolgin-84A in trafficking between ER and Golgi.

## LIST OF ABBREVIATIONS

<b>µg</b>	microgram
<b>µL</b>	microliter
<b>Amy</b>	α-amylase
<b>Arabidopsis</b>	<i>Arabidopsis thaliana</i>
<b>ARF</b>	ADP-ribosylation factor GTPase
<b>BFA</b>	Brefeldin A
<b>BSA</b>	bovine serum albumin
<b>bp</b>	base pairs
<b>CASP</b>	CCAAT-displacement protein alternatively spliced product
<b>COPI</b>	Coatomer protein I coated
<b>COPII</b>	Coatomer protein II coated
<b>C-terminus</b>	carboxy terminus
<b>cv.</b>	cultivar
<b>CW</b>	Cell wall
<b>d</b>	day
<b>DIC</b>	Differential Interference Contrast
<b>DNA</b>	deoxyribonucleic acid
<b><i>E. coli</i></b>	<i>Escherichia coli</i>
<b>EDTA</b>	disodium ethylene diamine tetraacetic acid
<b>En6</b>	6 times enhancer
<b>ER</b>	endoplasmic reticulum
<b>ERD2</b>	ER retention defective 2
<b>ERES</b>	endoplasmic reticulum exit site
<b>ERGIC</b>	ER-Golgi intermediate compartment
<b>FLIM</b>	fluorescence lifetime imaging
<b>FRAP</b>	fluorescence recovery after photobleaching
<b>FRET</b>	Förster/fluorescence resonance energy transfer
<b>GAP</b>	GTPase activating protein



<b>GEF</b>	guanine nucleotide exchange factor
<b>GFP</b>	green fluorescent protein
<b>GRASP</b>	Golgi Reassembly Stacking Proteins
<b>GTP</b>	guanidine triphosphate
<b>h</b>	hour
<b>HEPES</b>	4-(2-hydroxyethyl)-1-piperazineethanesulfonic acid
<b>kD</b>	Kilodalton
<b>LB medium</b>	Luria-Bertani medium
<b>LPVC</b>	Late Protein Storage Vacuole
<b>MES</b>	2-[N-morpholino]ethanesulfonic acid
<b>mins</b>	minutes
<b>mL</b>	milliliter
<b>mM</b>	milimolar
<b>mRFP</b>	monomeric red fluorescent protein
<b>MS</b>	Murashige and Skoog medium
<b>nm</b>	nanometer
<b>N-terminus</b>	amino terminus
<b>OD</b>	optical density
<b>PCR</b>	polymerase chain reaction
<b>PM</b>	Plasma membrane
<b>PSV</b>	Protein Storage Vacuole
<b>s</b>	second
<b>SNARE</b>	soluble NSF [N-ethylmaleimide-sensitive factor] attachment protein receptors
<b>SP</b>	Signal peptide
<b>rpm</b>	revolutions per minute
<b>TAE</b>	Tris-acetate-EDTA buffer
<b>TGN</b>	trans-Golgi network
<b>TMF</b>	TATA element modulatory factor
<b>Trp3 (W)</b>	Tryptophan (amino acid)
<b>Tris</b>	tris(hydroymethyl)aminomethane
<b>UV</b>	Ultraviolet

<b>V</b>	volt
<b>v/v</b>	volume to volume
<b>w/v</b>	weight to volume
<b>YFP</b>	yellow fluorescent protein

# 1. INTRODUCTION

This thesis aims to dissect the interface between two organelles that are part of the plant endomembrane network. The endoplasmic reticulum (ER) and the Golgi apparatus are very dynamic structures in plant cells and the membranes of these two organelles are continuously remodelling. Events between ER and Golgi are still poorly understood. This chapter aims to present a background for this work and an overview about the plant endomembrane system and the secretory pathway focusing on the early events at the secretory pathway.

## 1.1 The endomembrane system

The endomembrane system is a compartmentalised structure of membrane-bounded organelles (Figure 1.1) where the synthesis, modification, trafficking, accumulation and secretion of proteins and other vital cell components occurs (Vitale and Denecke, 1999). In eukaryotic cells the endomembrane system provides correct folding, quality control, processing and packing of proteins, lipids and polysaccharides into transport vectors. In plants the endomembrane system comprises the endoplasmic reticulum (ER), the Golgi apparatus, the vacuolar system and the plasma membrane. These membrane systems are transiently connected by intermediate compartments: the *trans*-Golgi network (TGN), the pre-vacuolar compartments (PVC) or endosomes, and the late pre-vacuolar compartment (LPVC) (De Marcos Lousa *et al.*, 2012; Foresti and Denecke, 2008; Foresti *et al.*, 2010).

The delivery of cargo to different destinations in the cell is in part dependent on vesicular trafficking in the endomembrane system (Andreeva *et al.*, 2000). The transit route from the ER towards the late compartments of the secretory pathway (PM or the vacuole) is the anterograde transport

(Figure 1.1). Endocytosis and trafficking from ER to Golgi are retrograde transport is responsible for constantly recycling proteins and receptors from the PM back to the early compartments of the secretory pathway. Before entering the secretory pathway proteins are synthesised by ribosomes either in the cytosol with ribosomes or on the rough ER membrane.

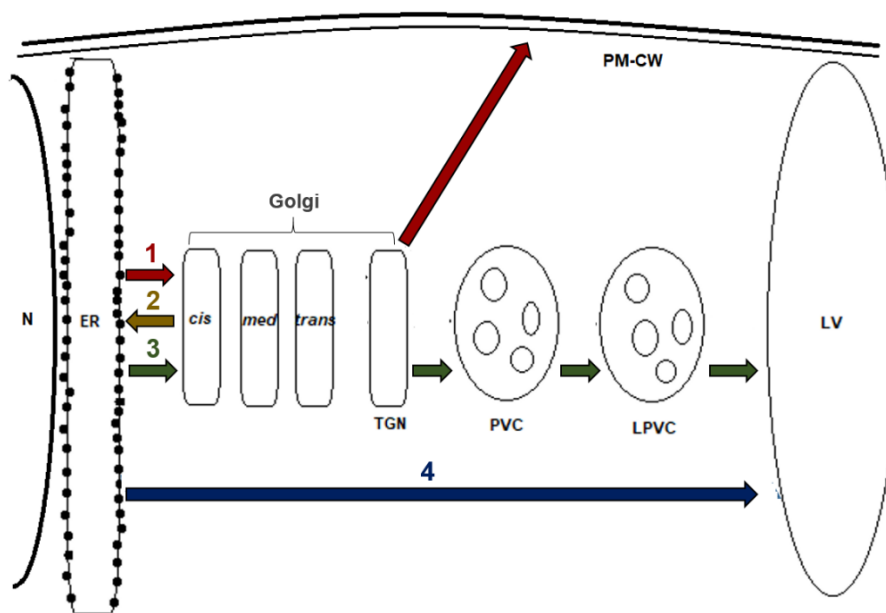


Figure 1.1: Schematic representation of transport routes in the secretory pathway in plants. Proteins encoded in the nucleus (N) enter the secretory pathway via the ER and are transported to the Golgi apparatus via COPII carriers (anterograde transport). (1) Proteins destined to the plasma membrane-cell wall complex or for exocytosis are transported in the free TGN/early endosome. (2) Proteins that need to be recycled back to the ER (retrograde transport) are carried in COPI vesicles. (3) Proteins encoding vacuolar sorting determinants are transported in from the *trans*-Golgi network (TGN) to the pre-vacuolar compartment (PVC) and the late PVC to reach the lytic vacuole (LV). (4) A Golgi-independent transport route has been described to the protein storage vacuoles and to the lytic vacuole when the Golgi-mediated route is impaired (Pereira *et al.*, 2013).

### 1.1.1 Anterograde transport

The transport from the ER to the post-ER compartments is called anterograde transport and is schematically represented in section 1.1, Figure 1.1, excluding route 2 that is representing the retrograde transport). There are several molecular determinants in this process such as receptors to recruit cargo and the Soluble *N*-ethylmaleimide-sensitive factor attachment protein receptors (SNAREs) that are involved in membrane fusion during protein trafficking. Several *Arabidopsis* SNAREs have been localized at the ER, including SYP81, SEC22 and VAMP723 and the plant-specific SYP71, SYP72 and SYP73 (Uemura *et al.*, 2004; Cao *et al.*, 2016). SNARE overexpression has been reported to inhibit ER-to-Golgi trafficking (Chatre *et al.*, 2005). However, the role of plant SNAREs at the ER-Golgi interface is still unclear.

In animal cells ER-to-Golgi trafficking is mediated by the coat protein II (COPII) at specialised ER exit sites (ERES). Assembly of COPII vesicles starts with the activation of a small GTPase Sar1p through a GTP-exchange factor Sec12p. Activated Sar1-GTP recruits the coat subunits Sec23p and Sec24p and these recruit Sec13p and Sec31p in order to form a cage-like structure. Homologues of all animal coat proteins have been identified in plants (d'Enfert *et al.*, 1992; Bar-Peled and Raikhel 1997; Takeuchi *et al.*, 1998; Movafeghi *et al.*, 1999; Yang *et al.*, 2005; Stefano *et al.*, 2006) but there is no clear evidence of COPII vesicles in plants (Kang and Staehelin, 2008). The COPII machinery appears to be conserved in plants, as overexpression of Sec12 and expression of Sar1 mutants impairs ER to Golgi protein transport (Andreeva *et al.*, 2000; Takeuchi *et al.*, 2000; Phillipson *et al.*, 2001).

Proteins that have to exit the Golgi are exocytosed from the cell or are transported to vacuolar compartments. Trafficking to the vacuole can be either through a Golgi-dependent route (Figure 1.1, route (3)) or a Golgi-independent route directly from the ER in precursor accumulating vesicles

(PAC) and fuse directly to the protein storage vacuole (PSV) (Hara-Nishimura *et al.*, 1998; Vitale and Raikhel, 1999; Chrispeels and Herman, 2000). The Golgi-independent route has been described for the plant-specific insert (PSI) in *N. tabacum* cells (Figure 1.1, (4)) when the Golgi-mediated route is impaired by the expression of dominant-negative mutant of GTPases for example the Sar1-GTP locked version (Pereira *et al.*, 2013).

### 1.1.2 Retrograde transport

The coatomer is a set of soluble cytosolic proteins that form the COPI coat and are recruited simultaneously to the Golgi by the small GTPase ADP-ribosylation factor 1 (ARF1). The Golgi membrane forms vesicles with the concentrated cargo and these vesicles bud off the membrane and are uncoated by hydrolysis of GTP by Arf1 and finally they arrive at the ER and fusion occurs. Arf1 is activated and de-activated by ARF-guanine nucleotide exchange factors (ARF-GEFs) and ARF-GTPase-activating proteins (ARF-GAPs) (Spang *et al.*, 2010; Donaldson and Jackson, 2011). The fungal metabolite BFA is used to study ARF-GEFs. The Brefeldin A leads to dissociation of the COPI coat from Golgi membranes (Helms and Rothman, 1992) and generation of ER-Golgi hybrid compartments (BFA bodies) (Satiat-Jeunemaitre *et al.*, 1996). In plants, ARF-GEFs of the Golgi BFA-resistance factor 1 and BFA-inhibited GEF (GBF and BIG) types are known, which exhibit different sensitivity to BFA (Geldner *et al.*, 2003). ARF-GEFs GNOM and GNOM-like1 (GNL1) are sensitive or insensitive to BFA, respectively, and the different expression of these GEFs during development leads to resistance or sensitivity to the drug during growth (Du *et al.*, 2013; Robinson *et al.*, 2008). It has been suggested that Arabidopsis cells have different types of COPI vesicles, COPIa-type and COPIb-type based on electron tomography analyses (Donohoe *et al.*, 2007).

Peptide motifs such as HDEL are typical ER-retention signals and direct the sorting of soluble proteins in the Golgi apparatus to the ER. This motif is recognised by the receptor ER-Retention Defective 2 (ERD2) in the Golgi apparatus which controls the recycling of ER resident proteins (Silva-Alvim *et al.*, 2018).

## 1.2 Endoplasmic reticulum/Golgi interface

The organisation of the ER and Golgi in plant cells is different from other eukaryotes which can be due to the needs of the cell to produce components for the cell wall and the presence of a large vacuole. Mammalian cells have the ER-Golgi intermediate compartment (ERGIC) acting as a bridge between ER and Golgi for docking and budding of protein cargo carriers (Schweizer *et al.*, 1990; Hauri and Schweizer, 1992). The ERGIC is responsible for transport to the Golgi along microtubules (Appenzeller-Herzog and Hauri, 2006). So far, there is no evidence in plants of an intermediate compartment and ER and Golgi appear physically connected (Sparkes *et al.*, 2009a; DaSilva *et al.*, 2004). As in mammalian cells the ER in plants is a network of membranes that assume tubular geometry as well as flattened and enlarged cisternal domains (Stefano *et al.*, 2014) that are constantly remodelling. This is dependent on processes of membrane fusion and tubulation that require proteins such as reticulons (Sparkes *et al.*, 2009b; Kriechbaumer *et al.*, 2015) and RHD3 family of GTPase proteins (Stefano *et al.*, 2012; Chen *et al.*, 2011). The knock-out of certain RHD3 isoforms is lethal (Zhang *et al.*, 2013), implying that the ER re-shaping process is essential. The ER is pushed to the periphery of mature cells by the large central vacuole and is anchored to the PM through ER-PM contact sites (for a review see Wang *et al.*, 2017).

The ER is the entry point into the endomembrane system and the main control station for correct assembly and folding of newly synthesized proteins carrying a signal peptide. Misfolded proteins are recognized by

molecular chaperones and retained in the lumen of the ER in order to refold them to their correct structure. Persistently misfolded proteins are transferred to the cytosol and degraded by the proteasome machinery (Pimpl *et al.*, 2006; Vitale and Boston 2008). Proteins that have erroneously reached the Golgi can also return when ER retrieval signals are present (Pimpl *et al.*, 2006). Important post-translational modifications also occur in the ER such as *N*-glycosylation upon entry into the lumen (Vitale and Denecke, 1999; Strasser, 2016).

### 1.3 Function of the Golgi apparatus

The Golgi apparatus is responsible for the processing of proteins received from the ER and their distribution to multiple destinations within the cell. The plant Golgi apparatus synthesises complex polysaccharides for the cell wall, membrane lipids and glycolipids and is also responsible for further processing of *N*-glycans (for a review see Schoberer and Strasser 2011).

Golgi morphology is different between kingdoms. In animal cells the Golgi apparatus has a perinuclear ribbon-like structure and is mostly stationary. In plants, there are many discrete Golgi stacks and these are dispersed and motile (Boevink *et al.*, 1998). Plant cells have many Golgi bodies that are physically connected to the ER (DaSilva *et al.*, 2004), and each is composed of stacked, flattened membrane cisternae. In each plant Golgi stack, the cisternae are polarized between the *cis*-face, receiving cargo from the ER, and the *trans*-face, sending cargo forward to post-Golgi organelles. This compartmentalisation enables controlled modification of substrates which is well-described based on resident enzyme activities (reviewed by, Schoberer and Strasser, 2011). The Golgi stack is followed by a *trans*-Golgi network (TGN) that also functions as the early endosome (Foresti and Denecke, 2008). Fluorescence recovery after photobleaching (FRAP) analyses showed that the integrity of the Golgi apparatus is maintained through remodelling of the cisternae with their membranes being



reabsorbed in the ER and subsequently retrieved back to the Golgi (Schoberer *et al.*, 2010). It was demonstrated in plant cells that fluorescent protein fusions of integral membrane enzymes distributed to the different cisternae can cycle in and out of the Golgi within 5 minutes (Brandizzi *et al.*, 2002; Schoberer *et al.*, 2010). These results support that the Golgi cisternae are remodelled continuously.

Protein trafficking to and from the Golgi is mediated by coated membranes (as described in sections 1.1.1 and 1.1.2). Expression of COPII dominant negative mutants or for example chemical inhibition of COPI allows the study of these different routes. It is known that disrupting any of these routes leads to reabsorption of Golgi membranes into the ER (Saint-Jore *et al.*, 2002; Satiat-Jeunmaitre *et al.*, 2006; Stefano *et al.*, 2006; Andreeva *et al.*, 2000; Takeuchi *et al.*, 2000) which affects not only Golgi membrane integrity but also ER molecular composition.

### **1.3.1 Golgi biogenesis**

In the plant cell cytoplasm there are numerous membrane bounded cisternae forming stacks, and each of these is a discrete Golgi body characterised by high mobility. In plants Golgi bodies stay intact during cell division. Exactly how these numerous Golgi bodies are generated remains unknown. Different theories have been suggested for animal cells. One claims that a new Golgi stack is generated by a pre-existing template structure (Glick, 2002).

The other hypothesis is the *de novo* formation of a Golgi stack from the ER that would involve the re-organisation of proteins and membrane vesicles (Bevis *et al.*, 2002). The mechanism through which Golgi biogenesis occurs varies from species to species. In fungi and *Toxoplasma gondii* Golgi stacks multiply by cisternal fission (Pelletier *et al.*, 2002). In *Trypanosoma brucei* the

formation of a new Golgi body near to a pre-existing Golgi body and the transport of material between these two Golgi stacks was observed (He *et al.*, 2004). In the yeast *Pichia pastoris*, the new formation of a Golgi stack has been observed at specialised ER sites (Bevis *et al.*, 2002). In mammalian cells it has been suggested that at the start of mitosis, the Golgi apparatus becomes vesiculated and then is reassembled (Misteli and Warren, 1995).

Several methods are used to induce disruption of the Golgi in order to mimic Golgi biogenesis, such as expression of dominant-negative mutants of the small GTPase Sar1 which blocks of COPII-mediated ER-to-Golgi transport and redistribution of Golgi enzymes into the ER (Da Silva *et al.*, 2004; Osterrieder *et al.*, 2009a). Recovery from BFA is also used to mimic Golgi biogenesis (see section 1.1.2).

It has been reported that the number of Golgi stacks in plants increases before cell division (Ueda, 1997). Several studies described the formation of mini-Golgi stacks and lateral cisternal growth after BFA washout followed by the formation of mega-Golgi stacks which then divide into normal-size Golgi stacks (Hummel *et al.*, 2007; Langhans *et al.*, 2007). These experiments suggest a potential for *de novo* Golgi formation and multiplication by fission in order to increase the number of Golgi stacks during cell division (for review, Hawes *et al.*, 2010).

### 1.3.2 Golgi stack maintenance

How the motile structure of Golgi bodies is maintained while providing vital functions for the plant cell is still poorly understood. It has been shown that Golgi distribution and motility is actin-dependent and that stacks move along the ER strands (Boevink *et al.*, 1998; Nebenfuhr *et al.*, 1999; Brandizzi *et al.*, 2002). Contrary to animal cells the plant Golgi appears connected to the ER (Da Silva *et al.*, 2004; Hanton *et al.*, 2005; Runions *et al.*, 2005; Sparkes *et al.*, 2009) but it is unknown what is holding these two compartments together. A matrix (Figure 1.2) that maintains this connection has been suggested (for review, Hawes, 2005; Staehelin and Moore, 1995) and it was observed by electron microscopy as a zone without ribosomes surrounding the Golgi stacks (Staehelin and Moore, 1995). This was hypothesised to be what is maintaining the structural integrity of the stack. Recently in animal cells the importance of upstream ‘tethering’ events prior to fusion when transport vectors are recognised by the Golgi membrane has been shown (Hong and Lev, 2014; Yu and Hughson, 2010). Golgins, proteins with long coiled-coil domains are strongly involved in these tethering events (Wong and Munro, 2014).

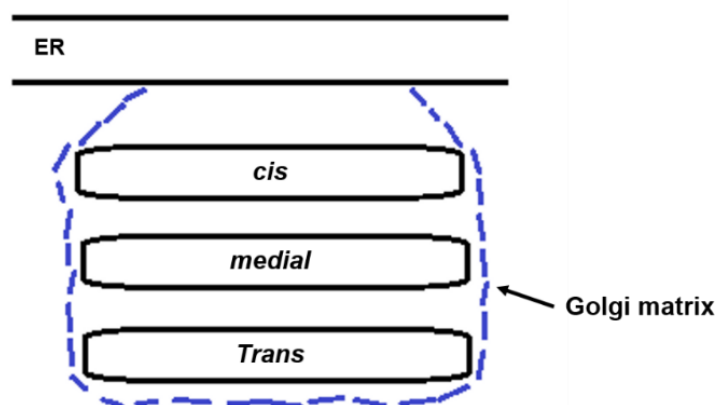


Figure 1.2: Diagram showing the spatial relationship between the ER, the Golgi stack and the Golgi matrix.

## 1.4 Golgins

A putative matrix is suggested to support the Golgi. This matrix should contain proteins and other components to maintain Golgi structure and is most likely involved in transport in and out of the Golgi (Lowe, 2011; Xiang and Wang, 2011). Golgins are suggested to be the main constituents of this matrix. Golgins are proteins with long coiled-coil domains and are attached via their C-terminus to the cytoplasmic face of the Golgi apparatus (Munro, 2011). These features allow the golgins to extend over a significant distance into the cytoplasm, which is an ideal characteristic allowing for capturing or tethering of other membranes such as transport vesicles, Golgi cisternae or cytoskeletal elements. This conformation also enables the golgins to form homo- or heterodimers with other golgins, GTPases or soluble SNARE proteins (Sztul and Lupashin, 2006). Some of the golgins could be involved in tethering between ER and Golgi and tethering at the Golgi cisternae and regulation of the formation of a new Golgi stack (Xiang and Wang, 2011).

In animal cells Golgi matrix proteins respond differently to induced Golgi membrane disassembly as described by Seemann and co-workers (Seemann *et al.*, 2000a) after animal cell exposure to BFA, or a dominant-negative guanosinetriphosphate (GTP)-locked mutant of the COPII small GTP-binding protein (GTPase) Sar1. *Cis*-Golgi matrix proteins would be expected to have a role in stack formation and in regulation of protein transport at the ERES (ER-exit sites). On the other hand golgins localised at the *trans*-face would have other functions such as directing protein cargo exit from the stack to the late compartments of the secretory pathway.

Giantin, golgin-84 and CCAAT-displacement protein alternatively spliced product (CASP) have a C-terminal transmembrane domain (TMD) and were identified in animal cells. Giantin has a cytoplasmic domain around 350 kD being the largest golgin family member and was reported to be resistant to detergent extraction which suggests that this protein could be part of the putative Golgi matrix (Linstedt and Hauri, 1993). Giantin is

reported to interact with the tethering factor p115 that simultaneously binds to another golgin (GM130, Alvarez *et al.*, 2001), Rab1 and Rab6 (Rosing *et al.* 2007). Giantin knock-out cell line show no significant change in Golgi structure but GM130 localisation and the glycosylation enzyme expression patterns were altered in these cells (Stevenson *et al.*, 2017).

Golgin-84 is a mitotic phosphoprotein (Diao *et al.*, 2003), it interacts with the mammalian Rab1 (Diao *et al.*, 2003; Satoh *et al.*, 2003) and features a cytoplasmic coiled-coil domain and a C-terminal transmembrane domain required for Golgi targeting (Bascom *et al.*, 1999). The overexpression of Golgin-84, the expression of a mutant version and the siRNA-mediated depletion of the protein resulted in a disruption of the Golgi ribbon into large cytoplasmic fragments which still retained their stacked organisation but were significantly smaller (Diao *et al.*, 2003). CASP was found in Golgi in mammalian cells and the structure is similar to giantin and golgin-84 (Gillingham *et al.*, 2002). There is some evidence that golgin-84 and CASP bind each other *in vitro* and in a cell-free budding assay followed by production of COPI vesicles (Malsam *et al.*, 2005).

Golgin-97 might play a role in endosome-to-TGN protein transport and is included in another group of golgins containing a GRIP domain (Lu *et al.*, 2003). This domain is a C-terminal sequence consisting of ~42 amino acids with a highly conserved tyrosine residue at position 4 that is essential for Golgi localisation. Golgin-245 is a *trans*-Golgi coiled-coil protein that is known to participate in regulatory transport from the *trans*-Golgi network (TGN) to the cell surface. Another C-terminally localised conserved domain has been identified, the GRAB (GRIP-related ARF binding) domain (Gillingham *et al.*, 2004). An example of this type of golgin is GMAP-210 which on overexpression blocks anterograde and retrograde transport between ER and Golgi and leads to Golgi disassembly (Pernet-Gallay *et al.*, 2002) (Table 1-1).

The majority of golgins are peripheral membrane proteins (Figure 1.3) and interact with other proteins to reach their final destination. Their ability to tether vesicles is best-characterised by GMAP-210 which has an amphipathic lipid packing sensor (APLS) motif at the N-terminus. This motif senses membrane curvature and is able to mediate attachment to lipid vesicles (Drin *et al.*, 2007).

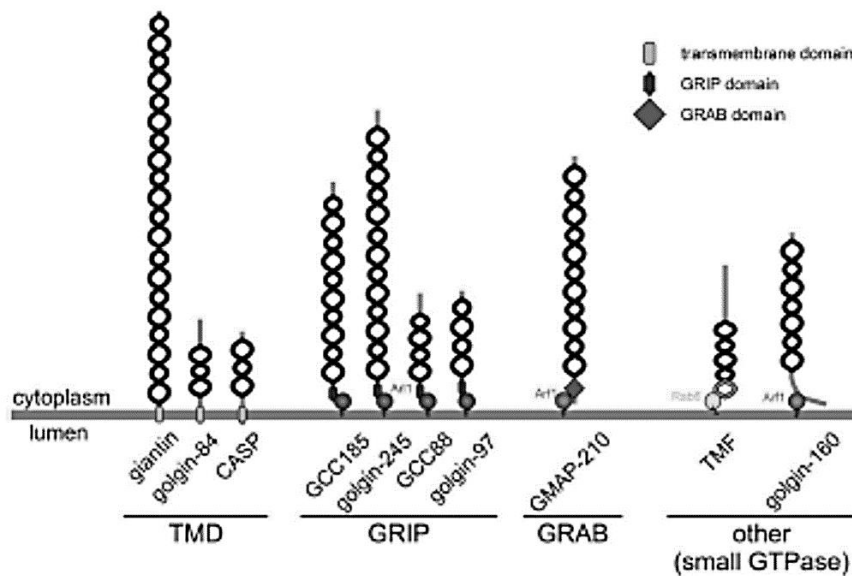


Figure 1.3: Putative topology and membrane attachment of golgins. Coiled-coil regions, membrane targeting domains, and associated proteins are indicated. Golgins are comprised predominantly of coiled-coil regions (depicted by black helices; note that the frequent short breaks found within the coiled-coil regions of golgins are not shown for simplicity) (adapted from Witkos and Lowe, 2016).

The golgin TMF binds to Rab6 in mammalian cells (Fridmann-Sirkis *et al.*, 2004) and RNAi-mediated depletion leads to dispersal of Golgi membranes throughout the cytoplasm suggesting that TMF is involved in organisation of Golgi morphology. Golgin-160 is required for the Golgi membrane sorting of the insulin-responsive glucose transporter GLUT4 in adipocytes (Williams *et al.*, 2006). Furthermore, golgin-160 recruits dynein to

Golgi membranes. This recruitment confers centripetal motility to membranes and is regulated by the GTPase Arf1 (Yadav *et al.*, 2012).

More recently, Barlow *et al.*, (2018) investigated the Golgi as an ancient aspect of eukaryotes and its complexity in the ancestor of eukaryotes. A role in organising the Golgi have been suggested for various proteins, including the golgins. In Barlow *et al.*, (2018) they have analysed genome sequences from organisms which have lost stacked cisternae as a feature of their Golgi and those that have not, using genomics and immunomicroscopy.

The hypothesis is that if a protein has a conserved necessary function in Golgi stacking, such a protein would likely be present in all genomes of organisms showing Golgi stacking, and likely absent from the genomes of those organisms without (i.e., the taxonomic distribution of stacking factors should match that of Golgi stacking). Such a pattern of presence directly correlating with function was not confirmed. The evolutionary analyses performed across 75 taxa with stacked Golgi and 12 without showed that none of the 27 putative stacking factors studied matched this pattern. The data supports the idea that Golgi stacking is an emergent property.

#### **1.4.1 Golgins contribute to specificity in vesicle tethering**

The coiled-coil elongated 'rod-like' structure could allow golgins to extend up to 300 nm away from the surface of the Golgi, thus making them ideal candidates to mediate the first contact with incoming vesicles. There is strong evidence of golgin-84 role in vesicle trafficking. Cells lacking golgin-84 have defects in the maturation of certain plasma membrane proteins and an accumulation of intra-Golgi vesicles containing Golgi residents (Sohda *et al.*, 2010). In 2014, Wong and Munro published an elegant relocation assay, in which golgins were shown to be sufficient for the tethering of transport

vesicles *in vivo*, with different golgins tethering distinct classes of transport vesicles according to their localisation in the Golgi membrane (Table 1-1 and Figure 1.4). Recently a paper was published showing some interesting features of golgin GCC185 including the characterisation of its tethering to vesicles (Cheung *et al.*, 2015). GCC 185 is a GRIP-domain golgin and is C-terminally anchored to the TGN through small GTPases (Burguete *et al.*, 2008). Cheung *et al.* (2015) demonstrated that flexibility in a tethering protein is required for its functionality in cells, both in supporting the arrival of transport vesicles at the Golgi and maintaining Golgi ribbon structure.

Table 1-1: Homologues for the mammalian golgins and their specific tethering ability.

Golgin	Homologs in					Golgi localisation	Confirmed tethering of	
	Fish	Fly	Worm	Plant	Yeast		vesicles	cytoskeleton
GMAP210	✓	✓	✓	✓	✓	Cis-Golgi	✓	
GM130	✓	✓	✓	x	✓		✓	✓
Golgin-160	✓	x	x	x	x			✓
Giantin	✓	✓	x	x	x	Golgi rims		✓
CASP	✓	x	✓	✓	✓			
Golgin-84	✓	✓	✓	✓	x		✓	
TMF	✓	✓	✓	✓	✓		✓	
GCC88	✓	✓	✓	✓	✓	Trans-Golgi	✓	
GCC185	✓	✓	✓				✓	✓
Golgi-97	✓	✓	x				✓	✓
Golgin-245	✓	✓	✓				✓	✓



Transport vesicles can bind to the N-terminus of GCC185, and seem to prefer to bind to the end of this dimeric, coiled-coil tether. Importantly, its structure gives significant flexibility to the protein and would allow it to collapse onto the Golgi surface, bringing vesicles close to the *trans*-Golgi target membrane. GCC185 can bind multiple Rab GTPases along its length (Hayes *et al.*, 2009), as well as syntaxin16, Arl1 and Arl4 GTPases (Burguete *et al.*, 2008; Ganley *et al.*, 2008; Lin *et al.*, 2011). GCC185 also binds to *cytoplasmic linker-associated protein 1* (CLASP1), cytosolic microtubule-associated protein that catalyzes microtubule polymerization from the Golgi surface (Efimov *et al.*, 2007). These additional interactions will pull the tether towards the Golgi surface, bringing N-terminally bound vesicles closer to the Golgi surface for productive vesicle docking (Cheung *et al.*, 2015).

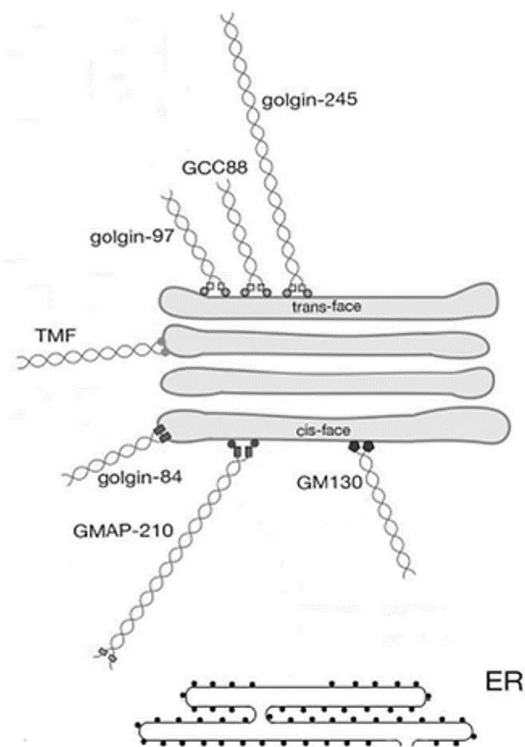


Figure 1.4: Schematic of the putative golgins localization in animal cells according to how golgins appear to tether the different sets of vesicles arriving at the Golgi (adapted from Wong and Munro, 2014).

Golgins are one main factors implicated in Golgi organization and stacking (Ramirez *et al.*, 2009). The golgins are defined in mammalian cells by the presence of coiled-coil domains, attachment to Golgi membranes near their C-termini (either by tail-anchor transmembrane domains or through binding to small GTPases), and functions that include tethering and scaffolding (Munro *et al.*, 2011, Witkos and Lowe, 2016). In addition to apparent roles in stacking, several golgins, including golgin-84, are involved in tethering specific transport vesicles destined for different regions of the Golgi (Wong and Munro, 2014).

### **1.4.2 Plant golgins**

The plant Golgi apparatus is made of many Golgi bodies which are motile in the cell and are connected to the ER that is constantly reorganising its structure. One can hypothesise that the requirements to maintain Golgi structure in plants are different to those in animal cells, but that some components responsible for maintaining the stacking of the cisternae could be conserved between eukaryotic cells. Several putative golgin homologues have been identified in Arabidopsis (Table 1-2): AtCASP, Atgolgin-84 (two isoforms), TATA element modulatory factor (TMF), a GRIP domain protein AtGRIP, two homologues of GMAP-210 with a GRIP-related Arf-binding (GRAB) domain and an homologue for the tethering factor p115 (Latijnhouwers *et al.*, 2005a; Renna *et al.*, 2005; Gilson *et al.*, 2004).

Table 1-2: Characterized *Arabidopsis* golgins and their homologues in mammals.

<i>Arabidopsis</i> Golgins and other tethering factors	Mammalian homologue	Suggested Golgi stack localisation
AtCASP	CASP	<i>cis</i> -Golgi (Latijnhouwers <i>et al.</i> , 2007)
AtGolgin84A	Golgin-84	<i>cis</i> -Golgi (Latijnhouwers <i>et al.</i> , 2007)
AtGolgin84B	Golgin-84	<i>cis</i> -Golgi (Latijnhouwers <i>et al.</i> , 2007)
AtGRIP	Golgin-97	<i>trans</i> -Golgi (Gilson <i>et al.</i> , 2004; Latijnhouwers <i>et al.</i> , 2005b)
AtTMF	TMF	<i>trans</i> -Golgi Latijnhouwers <i>et al.</i> , 2007; Schoberer <i>et al.</i> , 2010)
GDAP1 (GC3), GC4	GMAP-210	<i>cis</i> -Golgi (Latijnhouwers <i>et al.</i> , 2007)
Atp115	p115	<i>cis</i> -Golgi (Latijnhouwers <i>et al.</i> , 2007; Schoberer <i>et al.</i> , 2010)

AtCASP (Latijnhouwers *et al.*, 2005a; Renna *et al.*, 2005) and AtGolgin84 homologues of Golgin84 contain TMDs. AtCASP and AtGolgin84A fluorescent fusions signals were mainly observed at the *cis*-Golgi with a preference for cisternal rims. The fluorescent version GFP-AtCASP was detected in the Golgi body in tobacco leaf epidermal cells and part of the C-terminus was found to be necessary and sufficient for Golgi targeting (Renna *et al.*, 2005). Expression of dominant-negative mutants and optical tweezers experiments pointed to a role of AtCASP in tethering at the ER-Golgi interface (Osterrieder *et al.* 2017). In these trapping events, the ER track coincided almost perfectly with the Golgi track in the control ST-mRFP plants, during trapping of Golgi bodies (Osterrieder *et al.* 2017). In cells expressing AtCASP truncated form without coiled-coil domains, the disruption of the putative tether was clear (Osterrieder *et al.* 2017). Track

patterns were irregular and did not mirror that of the ER compared to control ST-mRFP or full-length mRFP-AtCASP (Osterrieder *et al.* 2017). The gap observed showed the Golgi and ER following the same trajectory, suggesting that AtCASP is not solely responsible for tethering at the ER-Golgi interface but might be part of a more tethering complex/matrix. Other ER-Golgi tethering factors such as Atgolgin-84A might have a role in the tethering to the ER.

AtCASP and AtGolgin-84A (former AtGC1) dynamics were studied during induced Golgi disassembly and reformation and results suggest that AtCASP may be at the ERES and has a role during Golgi biogenesis (Schoberer *et al.*, 2010). Both AtCASP and Atgolgin-84A co-localise with the ERES marker Sar1-GTP-YFP, a mutated form of a GTPase that impairs ER-Golgi trafficking (Osterrieder *et al.*, 2010). During Brefeldin A washout (see section 1.1.2) AtCASP and Atgolgin-84A were labelling the reforming Golgi bodies before resident enzyme markers which suggests a role in early stages of Golgi biogenesis (Schoberer *et al.*, 2010).

AtGRIP has been shown to label the *trans*-Golgi in plants (Gilson *et al.*, 2004; Latijnhouwers *et al.*, 2005b). The *Arabidopsis* homologue of Arl1 binds to the GRIP domain and this interaction is required for Golgi targeting in plants (Latijnhouwers *et al.*, 2005b). AtGRIP shows the highest similarity to the GRIP domains of GCC185 and golgin-97 (Witkos and Lowe, 2016).

The GMAP-210 has two homologues in *Arabidopsis*, termed GC3 (GDAP1) and GC4, and their fluorescent location was slightly shifted from a *medial/trans*-Golgi marker suggesting a localisation at the *cis*-Golgi. GDAP1 interacts with ARF1 (Mathenson *et al.*, 2007) as described for the mammalian homologue and also co-located with additional structures that were labelled by Arf1 in tobacco leaf epidermal cells (Latijnhouwers *et al.*, 2007). The C-terminal sequence of AtTMF (AtcTMF) interacts *in vitro* with Rab6 homologues AtRabH-1b and AtRabH-1c (Johansen *et al.*, 2009) and this interaction was confirmed *in planta* using Fluorescent Lifetime Imaging

of Forster Resonance Energy Transfer of fluorescent protein fusions (FRET-FLIM) (Osterrieder *et al.*, 2009b). So far no homologues of Giantin, GM130 and GRASP have been identified in Arabidopsis.

## Aims

The aim of my thesis was to characterise some of the key-players in plant ER-Golgi interface. A putative Golgi matrix protein suggested to be at the *cis*-Golgi, Atgolgin-84A, was the focus of this study. Another golgin protein, AtCASP, plays a role in ER-Golgi tethering as described in Osterrieder *et al.*, 2017 but there are other tethering factors at this interface. Atgolgin-84A is a good candidate to be a tether considering its predicted protein structure (described in detail in chapter 3 and tested using a truncated version of the protein in chapter 5), its putative subcellular localisation (characterised for the first time with Airyscan high-resolution detection in chapter 4) and ability to tether organelles and cargo vesicles of its homologue in mammalian cells (investigated and discussed in chapter 6 and 7). To accomplish these objectives, *state-of-the-art* microscopy for live cell imaging as well as advanced molecular and cell biology protocols were applied. The main tasks of this study were:

1. Bioinformatics analysis of Atgolgin-84A.

Available software was used to predict the 3-dimensional structure of Atgolgin-84A and to search for functional putative domains. Plant genomic resources were used to search for predicted post-translational modifications that could help understanding results obtained *in vivo* during this work.

2. High-resolution imaging of Atgolgin-84A and deletion mutant for analysis of subcellular localisation:

Confocal laser scanning microscopy with Airyscan detection was used to investigate the localisation of Atgolgin-84A and Atgolgin-84A $\Delta$ 1-557 fluorescent fusions alone and in co-expression with markers for the endomembrane system: sialyl-transferase (ST)-mRFP; mRFP-acetylglucosaminyltransferase I (GnTI); mRFP-Arabidopsis mannosidase I (MnSI); AtSar1a-GFP; Sec24-GFP; mRFP-AtCASP and GFP-HDEL.

**3. To investigate Golgi body tethering properties under overexpression of Atgolgin-84A and Atgolgin-84A $\Delta$ 1-557.**

Optical tweezers combined with Total Internal Reflection Fluorescence (TIRF) microscopy to trap Golgi bodies was used to assess differences in Golgi mobility during expression of the marker ST-GFP when compared against the overexpression of full-length Atgolgin-84 and Atgolgin-84A $\Delta$ 1-557.

**4. To assess the role of Golgins in maintaining trafficking between the ER and Golgi.**

Atgolgin-84A, Atgolgin-84A $\Delta$ 1-557, AtCASP, and AtCASP $\Delta$ 1-564 were co-infiltrated with a fluorescent fusion protein that depends on ER-to-Golgi trafficking to reach its final destination, SP-mCherry. Localisation of the cargo was assessed when expressed alone and when co-expressed with golgins. An  $\alpha$ -amylase secretion assay as a quantitative enzymatic approach was used to confirm these results using.

## 2. MATERIALS AND METHODS

### 2.1 Overview

In order to study Atgolgin-84A localisation and function several GFP-fluorescent fusions of the full-length sequence (AT2G19950) and a deletion mutant were used and were already available in the lab (Latijnhouwers *et al.*, 2007). For co-localisation studies the same Atgolgin-84A and mutant sequences were cloned into a modified version of binary expression vector pB7WGC2 (Karimi *et al.*, 2005) with mCherry fluorescent protein (as described in section 2.2.1). These constructs were used to transform *Nicotiana tabacum* and *Arabidopsis thaliana* using *Agrobacterium tumefaciens* mediated methods, either to achieve a transient expression or to obtain stably transformed plants expressing Atgolgin-84A and mutant (as described in sections 2.3 and 2.4). The expression was evaluated by confocal microscopy (as described in section 2.6) and this set-up also used in optical tweezers coupled to a TIRF (Total Internal Reflection Fluorescence) microscope (as described in section 2.9).

For the enzymatic secretion assay studies the full-length sequences and mutant sequences were cloned into pJA49 (non-fluorescently tagged) and pFLA39 (fluorescently tagged) described in Silva-Alvim *et al.*, (2018) (as described in 2.2.2). These constructs were used to transform protoplast of *N. benthamiana* (as described in 2.5.1).

Table 2-1 displays a list of all constructs used during this work in order of appearance with annotation of which ones were prepared during this PhD work and the ones already available in the lab, as well as main features and optical density for *N. tabacum* infiltration.



Table 2-1: List of constructs used during this work including the vector, the optical density (OD<sub>600</sub>) for *N. tabacum* infiltration, main features and references.

Construct	Vector	OD <sub>600</sub>	Main features	Reference
ST-GFP	pVKH18-EN6 (Batoko <i>et al.</i> , 2000)	0.05	First 52 N-terminal amino acids of the rat $\alpha$ 2,6-sialyltransferase, labels <i>medial/trans</i> -Golgi.	Boevink <i>et al.</i> 1998
GFP-Atgolgin-84A	pMDC43 (Curtis and Grossniklaus, 2003)	0.05	Mammalian golgin-84 homologue.	Latijnhouwers <i>et al.</i> , 2007
mCherry-Atgolgin-84A	pB7WGC2-mCherry (Karimi <i>et al.</i> , 2005; Mckenna and Runions, unpublished)	0.01	Mammalian golgin-84 homologue.	Cloned during this work.
GFP/RFP-HDEL	pVKH18-EN6 (Batoko <i>et al.</i> , 2000)	0.05	ER marker	Batoko <i>et al.</i> , 2000
ST-mRFP	pVKH18-EN6 (Batoko <i>et al.</i> , 2000)	0.05	First 52 N-terminal amino acids of the rat $\alpha$ 2,6-sialyltransferase, labels <i>medial/trans</i> -Golgi.	Renna <i>et al.</i> , 2005
MnSI-mRFP/GFP	pPT2 (Strasser <i>et al.</i> , 2005)	0.05	N-terminal amino acids of the Arabidopsis Golgi $\alpha$ -mannosidase I. Labels <i>cis</i> -Golgi.	Schoberer <i>et al.</i> , unpublished
GnTI-mRFP	pPT2 (Strasser <i>et al.</i> , 2005)	0.05	The first 77 N-terminal amino acids of the tobacco $\beta$ 1,2-N-acetylglucosaminyltransferase I. Labels <i>cis</i> -Golgi.	Schoberer <i>et al.</i> , 2010
mRFP-AtCASP	pB7WGR2 (Karimi <i>et al.</i> , 2005)	0.05	<i>Cis</i> -Golgi transmembrane protein. Homologue for the mammalian CASP.	Latijnhouwers <i>et al.</i> , 2007
AtSar1a-GFP	pVKH18-EN6 (Batoko <i>et al.</i> , 2000)	0.05	Small GTPase Sar1 isoform. Arabidopsis putative ERES (ER-exit site) marker.	Thompson <i>et al.</i> , 1994; Wang <i>et al.</i> , 2014
GFP-Atgolgin-84A $\Delta$ 1-557	pMDC43 (Curtis and Grossniklaus, 2003)	0.05	558-775 last amino acids of the full-length protein (including the transmembrane domain) fused to GFP.	Latijnhouwers <i>et al.</i> , 2007
mCherry-Atgolgin-84A $\Delta$ 1-557	pB7WGC2-mCherry (Karimi <i>et al.</i> , 2005; Mckenna unpublished)	0.05	558-715 last amino acids of the full-length protein (including the transmembrane domain) fused to mCherry.	Cloned during this work.
mRFP-AtCASP $\Delta$ 1-564	pB7WGR2 (Karimi <i>et al.</i> , 2005)	0.05	565-689 last amino acids of the full-length protein (including the transmembrane domain) fused to mCh.	Renna <i>et al.</i> , 2005; Osterrieder <i>et al.</i> , 2017
YFP-Sec24	pVKH18-EN6 (Batoko <i>et al.</i> , 2000)	0.05	Putative ERES marker Arabidopsis SEC24a	Stefano <i>et al.</i> , 2006
SP-mCherry	pVKH18-EN6 (Batoko <i>et al.</i> , 2000)	0.02	Signal peptide of Arabidopsis chitinase fused to mCherry.	Soares da Costa <i>et al.</i> , 2010
PJA-Atgolgin 84-A/ AtCASP/ Atgolgin-84A $\Delta$ 1-557/ AtCASP $\Delta$ 1-564	pJA49 (Silva-Alvim <i>et al.</i> , 2018)	Volume of DNA according to GUS assay activity.	GUS promoter, Protoplast transformation.	Cloned during this work.
PFLA-Atgolgin 84-A/ AtCASP/ Atgolgin-84A $\Delta$ 1-557/ AtCASP $\Delta$ 1-564	pFLA39 (Silva-Alvim <i>et al.</i> , 2018)		GUS promoter, YFP-tag, Protoplast transformation	Cloned during this work.
$\alpha$ -amylase	35S- $\alpha$ -amylase-3' nos (Crofts <i>et al.</i> , 1999)		Amylase expression in protoplasts under 35S promoter.	Crofts <i>et al.</i> , 1999

## 2.2 Molecular Biology techniques

### 2.2.1 mCherry-fusions of Atgolgin-84A and deletion mutant

GFP and mRFP fusions of Atgolgin-84A and the deletion mutant were already available in our lab (Latijnhouwers *et al.*, 2007; Osterrieder *et al.*, 2017). The fusions with mRFP were toxic for the plant cells. Therefore mCherry fusions were obtained in order to understand if the toxicity was due to some instability of the mRFP fluorescent protein. A modified version of pB7WGC2 with mCherry was available in the lab. Full-length Atgolgin-84A (Figure 2.1A) and deletion mutant Atgolgin-84A $\Delta$ 1-557 (Figure 2.1B) chimeras were generated using the previously published pENTR1A clones (Latijnhouwers *et al.*, 2007) for Gateway<sup>®</sup> cloning technology according to the manufacturer's instructions (Invitrogen-ThermoFisher Scientific). The *Escherichia coli* (*E. coli*) positive clones were screened by colony PCR using the primers listed on table 2-2 and confirmed by sequencing (Eurofins-MWG OPERON-Germany).

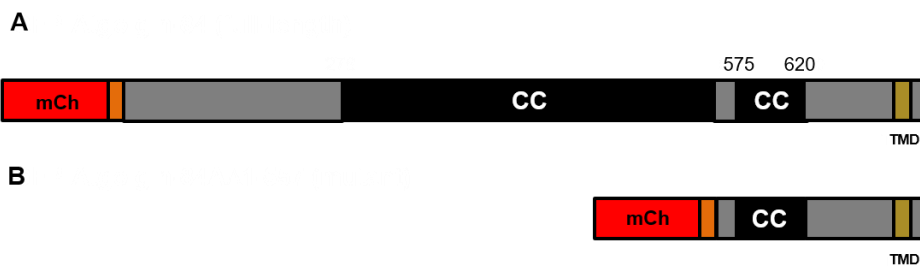


Figure 2.1: Schematic representation of mCherry constructs. (A) mCherry fused to full-length Atgolgin-84A. Short sequence in orange is a linker between mCherry and Atgolgin-84A. (B) mCherry fused to deletion mutant Atgolgin-84A $\Delta$ 1-557.

Table 2-2: Primers used in the colony PCR amplification and sequencing of Atgolgin-84A and Atgolgin-84 $\Delta$ 1-557 in the mCherry fusions in the pB7WGC2 vector.

<b>Primer name</b>	<b>Sequence</b>	<b>Description</b>
Forward 1 (_31_F)	GGCTTAAAGCTGCC GAAGAT	Bind to the 5' of Atgolgin-84A sequence to nucleotides 31, 782 and 1778 respectively.
Forward 2 (_782_F)	CGTAGAGCTGATAC GACTTCCA	
Forward 3 (_1778_F)	TGCAGCAGAGTTTC AGTTGG	
Reverse 2 (_2101_R)	TGCTCCTGGAGTCG GTGTAT	Bind on the 3' of Atgolgin-84A to nucleotides 2101 and 134 respectively.
Reverse 1 (_134_R)	AGAAGCTGGCAACT GCAAAT	
pB7WGC2 Forward (JM129)	GATATCACAAGTTT G TACAAAAAAGC	Binds on the gateway site just after the mCherry before the insert.

## 2.2.2 Constructs for $\alpha$ -amylase assay

The methodology to obtain constructs for protoplast transformation and subsequent screening is shown schematically in figure 2.2 and will be detailed in this section.

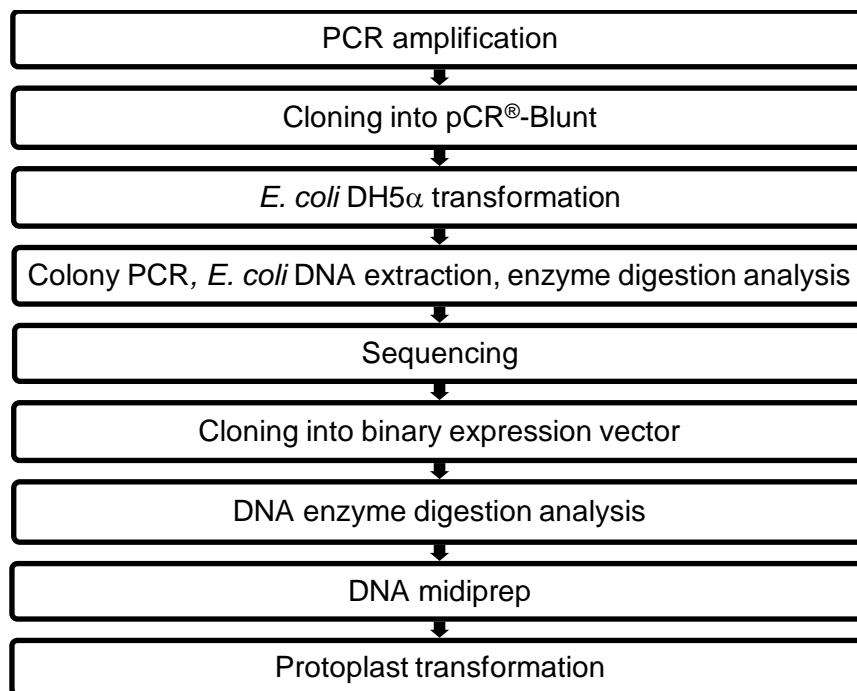


Figure 2.2: Flowchart representation of the procedure for cloning and screening of the constructs for protoplast transformation.

Atgolgin-84A, AtCASP and deletion mutants Atgolgin-84 $\Delta$ 1-557 and AtCASP $\Delta$ 1-664 sequences were amplified from pMDC43-GFP-Atgolgin-84A / Atgolgin-84 $\Delta$ 1-557 and pB7WGR2-mRFP-AtCASP / AtCASP $\Delta$ 1-664 by PCR with primers (Table 2-4) with adapters for restriction enzymes *Xba*I and *Cla*I (New England Biolabs, UK). Primers were ordered from Eurofins MWG Operon (Germany). Q5 high-fidelity DNA polymerase (New England Biolabs, UK) was used for DNA amplification (Table 2-3 and 2-4).

The PCR product was cloned into pCR<sup>®</sup>-Blunt. The product of the ligation was used to transform DH5 $\alpha$  E.coli (New England Biolabs, UK) (as described in section 2.1.5) and colony PCR with One-Taq<sup>®</sup> polymerase (New England Biolabs, UK) was used to screen positive colonies following manufacturer's instructions. The colonies were picked up from the plate with a sterile micropipette tip and dipped into the tube containing the PCR reaction solution. Positive clones were sent for sequencing to Eurofins MWG Operon (Germany). All the PCR reactions were performed in a T100<sup>TM</sup> Thermal Cycler (BioRad, Hemel Hempstead, UK) and the products detected on an agarose gel as described in section 2.1.8.

Table 2-3: PCR conditions for full-length golgins and deletion mutants amplification to add restriction enzyme sites for cloning into pJA49 and pFLA39.

<b>Step</b>		<b>Temperature</b>	<b>Duration</b>
<b>Initial denaturing</b>		98°C	30sec
<b>25 cycles</b>	<b>Denaturing</b>	98°C	10sec
	<b>Annealing</b>	50°C	30sec
	<b>Extension</b>	71°C	2min per Kb
<b>Final extension</b>		72°C	2min

Table 2-4: Primers used in the amplification of Atgolgin-84A, AtCASP and deletion mutants Atgolgin-84 $\Delta$ 1-557 and AtCASP1-664 for  $\alpha$ -amylase assays. All amplified fragments are to be *Cla*I-*Xba*I fragments. They can be ligated in a transient expression vector with or without YFP (pJA49 and PFLA39, respectively). Abbreviation: FL: full length; Del: deletion.

Primer name	Sequence	Description
Atgolgin-84AFL <i>Cla</i> I	TCCGTTCCATCG <u>ATG</u> GCGTCTTGGCTTAAA GCTGCCGAAG	Introduces a methionine before the highlighted region meant to remain after the deletion.
Atgolgin-84Adel <i>Cla</i> I	TCCGTTCCATCGATG TCACGCCAGGAGCAT ACAGAGCTG	Introduces a <i>Cla</i> I recognition site (underlined) at the 5' end of the sequence.
Atgolgin-84A <i>Xba</i> I	TTCGGATCCTCTAGA TTATAGTCTGAAAAC GTTGTTGGTC	Introduces <i>Xba</i> I after the stop codon at the 3' end of the sequence.
CASPFL <i>Cla</i> I	TCCGTTCCATCG <u>ATG</u> GAGGTTTCGCAAGAT GGATCGGA	Introduces a methionine before the highlighted region meant to remain after the deletion.
CASPdel <i>Cla</i> I	TCCGTTCCATCGATG GAGAAGATAGGTTTT CTCACAGAC	Introduces a <i>Cla</i> I recognition site (underlined) at the 5' end of the sequence.
CASP <i>Xba</i> I	TTCGGATCCTCTAGA TTAAAGACCGTGAGG AAGGTTTGTGG	Introduces recognition site <i>Xba</i> I (underlined) is after the stop codon at the 3' end of the sequence.

## 2.2.3 Bacterial strains and growing conditions

The chemical competent (obtained as described in section 2.2.4) *A. tumefaciens* strain GV3101, encoding resistance to Rifampicin and the Gentamycin resistant helper plasmid pMP90, was used for *N. tabacum* and *A. thaliana* plants transformation (Koncz and Schell, 1986) (as described in sections 2.3 and 2.4).

*E. coli* and *A. tumefaciens* strains were grown in liquid LB medium (Lysogeny broth: 10 g/L Bacto-trypton, 5 g/L yeast extract, 10 g/L NaCl in distilled water at pH 7.5 ± 1%). The antibiotic concentrations were used as described in table 2-5 and the incubation conditions are in table 2-6. Glycerol stocks of *E. coli* and *A. tumefaciens* colonies were prepared mixing 800 µl of cell culture with 200 µl of autoclaved 80% glycerol for long term storage at -80°C.

Table 2-5: Antibiotic used to select bacteria and concentrations.

Antibiotic	Concentration (µg/mL)
Gentamycin	10
Rifampicin	25
Kanamycin	100
Spectinomycin	100

Table 2-6: Bacterial strains and growing conditions.

Bacterial strain	Liquid culture	Agar plates
<i>E. coli</i>	16 hrs, 37°C, 200 rpm	16 hrs, 37°C
<i>A. tumefaciens</i>	16 hrs, 28°C, 200 rpm	48hrs, 28°C

## 2.2.4 Bacterial competent cells

Bacterial cloning was done using *E.coli* chemical competent high efficiency strain DH $\alpha$  (NEB).

*Agrobacterium tumefaciens* competent cells were prepared by starting a 5 mL liquid culture with LB and antibiotics and an aliquot of previously prepared competent stocks and incubation for 12h at 28°C. From the pre-culture 2 mL was added to 50 mL LB in 250 mL flask and incubated at 28°C shaking vigorously (250 rpm) until the culture reached OD<sub>600</sub> of 0.5 to 1.0. The culture was spun down in a 50 mL falcon for 20 mins at 4°C and 1540 xg. The supernatant was discarded and the pellet was resuspended in 1 mL of 20 mM ice cold CaCl<sub>2</sub> (for 50 mL of 20 mM CaCl<sub>2</sub> in 15% glycerol: 1 mL of 1 M CaCl<sub>2</sub>, 7.5 mL glycerol, and deionised water to 50mL). Aliquots of 100  $\mu$ L were stored at -80°C in pre-chilled 1.5 mL Eppendorf tubes.

## 2.2.5 Bacterial transformation

*E. coli* transformation was performed according to manufacturer's protocol (New England Biolabs, UK). Isolated colonies were picked and the presence of the cloned construct was confirmed with colony PCR and digestion with restriction enzymes. The positive colonies were grown over night in liquid culture and used to make a glycerol stock (as described in section 2.2.3) and stored at -80°C. Plasmid DNA was isolated from the positive colonies and used to transform *A. tumefaciens*.

For *A. tumefaciens* transformation, 1-5 $\mu$ l of DNA (50-100ng) were added to 25  $\mu$ l of the chemical competent strain GV3101 and kept on ice for 5 mins. After that, the cells were incubated at -80 °C for 5 mins and heat-shocked at 37 °C in a water bath for 5 mins. Cells were then transferred in 1 mL of liquid LB medium and placed in a 28 °C incubator shaking at 200 rpm for 2 h. Aliquots of the cell suspension were plated on LB agar medium



containing selection antibiotics (table 2-5) and allowed to grow for 2 days at 28 °C. Colonies were randomly picked and inoculated in 5 mL of liquid LB with selection antibiotics and infiltrated (see table 2-1 for OD) into *N. tabacum* plants to check for the expression (Sparkes *et al.* 2006). Positive colonies were used to make glycerol stocks for long-term storage (as described in section 2.2.4).

## **2.2.6 Plasmid DNA extraction**

Extraction of *E.coli* plasmid DNA for cloning and screening and Agrobacteria transformation was performed using Monarch® Plasmid Miniprep Kit (New England Biolabs, UK) according to manufacturer's instructions. Extraction of *E.coli* plasmid DNA for protoplast transformation was performed using QIAGEN® Plasmid Midi Kit (Qiagen) and used for protoplast electroporation (as described in section 2.5.2).

## **2.2.7 Plasmid DNA digestion**

Digestion of plasmid DNA digestion either for subcloning into an expression vector or screening after cloning, was carried out according to the manufacturer of the restriction enzymes (New England Biolabs, UK).

## **2.2.8 Agarose gels**

DNA samples were analysed in 0.8-1.0 % (w/v) agarose gel in 1X TAE buffer (TAE: 40 mM Tris, 20 mM acetic acid and 1 mM EDTA). The agarose solution was heated by microwave until the agarose was dissolved in solution and was allowed to cool to 40-50°C before adding 1 µL SYBR Safe DNA Gel Stain (Invitrogen-ThermoFisher Scientific). DNA samples were prepared as follow: 1X gel loading dye (NEB) was added to the DNA sample and was loaded into the gel wells. The electrophoretic separation was carried out at

75V, non-limiting amperage and using 0.25X TAE running buffer. The molecular weight marker used was the Quick load 1 kbp DNA ladder (New England Biolabs, UK). DNA bands were imaged using a transilluminator and images stored as TIFF files.

### **2.2.9 DNA extraction and purification**

The band was cut out of the gel using a razor blade, placed in a 1.5 mL Eppendorf and the PCR products were extracted from agarose gels using the Monarch<sup>®</sup> DNA Gel Extraction Kit (New England Biolabs, UK) following manufacturer's instructions.

### **2.2.10 Zero Blunt<sup>®</sup> PCR cloning**

The ligation of cleaned up DNA fragments obtained by PCR (described in section 2.1.2 and 2.2.9) was performed with a commercial kit for cloning of blunt-ended PCR products - "Zero Blunt<sup>®</sup> PCR Cloning Kit" (Invitrogen) according to the producer instructions in 1.5 mL sterile microtubes for an 1h, at 21°C temperature.

### **2.2.11 pB7WGC2-mCherry Gateway<sup>®</sup> cloning**

A positive pENTR1A clone with Atgolgin-84A and Atgolgin-84A $\Delta$ 1-557 was used in the recombination reaction with pB7WGC2-mCherry (Karimi *et al.*, 2002 modified) using "Gateway<sup>®</sup> LR Clonase<sup>™</sup>II Enzyme Mix", according to manufacturer's instructions (Invitrogen) at 25°C.

### **2.2.12 pJA49 and pFLA39 cloning**

The pJA49 the pFLA39 (Silva-Alvim *et al.*, 2018) vectors were digested with *Xba*I and *Cla*I restriction enzymes (New England Biolabs, UK). The

digestion product was separated in agarose gel electrophoresis (as described in section 2.1.8) and the band corresponding to the linearised vector was recovered and purified (as described in 2.1.9). The plasmid DNA was dephosphorylated with Antarctic Phosphatase following manufacturer's instructions from NEB, to prevent recircularization during ligation. The ligation of fragments excised from pCR®-Blunt positive clones was performed with T4 DNA ligase following instructions from (New England Biolabs, UK).

## **2.3 Plant material - maintenance and transformation - *N. tabacum***

### **2.3.1 *Nicotiana* species plant system**

Transient expression in *N. tabacum* is a fast method to study localisation and co-expression of several constructs for co-localisation studies. This method was used also for the secretion assay by confocal microscopy. For secretion assay by enzymatic assay ( $\alpha$ -amylase assay) *N. Benthamiana* was used as the protoplasting method has more efficiency in this plant species (Silva-Alvim *et al.*, 2018).

### **2.3.2 *N. tabacum* growth conditions**

*Nicotiana tabacum* cv. Petit Havana plants were grown in the greenhouse and used when 5-8 weeks old. Wild type *N. tabacum* plants were used for Agrobacteria-mediated infiltration and transient expression. Plants were potted on compost (Levington F2 Seed and Modular Compost Scotts Miracle-Gro, Ohio, USA), and grown in the greenhouse with 16 hours of light and 8 hours dark. Plants 5-8 weeks old were infiltrated according to Sparkes *et al.* (2006) and observed after 2-3 days from the infiltration event. In the

case of the secretion assay by confocal microscopy experiments the effector (full-length golgins and mutants) was infiltrated 24h prior to cargo infiltration and plants were imaged 3 days after cargo infiltration. For each experimental set, at least two plants were used, and after the infiltration event they were incubated in the growth chamber under controlled conditions (16 hours light and 8 hours dark at 21°C) for 2-4 days.

For  $\alpha$ -amylase enzymatic assay, sterile grown *Nicotiana benthamiana* plants were grown from surface-sterilized seeds in a plant growth room at the University of Leeds. Typically, 20 mg seeds were incubated for 30 mins in 1 mL of 10% bleach supplemented with 0.1% Tween 20 in a microfuge tube, washed 5-times with 1 mL autoclaved distilled water, followed by placing on the surface of Murashige and Skoog medium (MS) (Murashige and Skoog, 1962) supplemented with 2 % sucrose and incubated in a controlled growth room (16 hours of light and 8 hours dark). After 2 weeks incubation, individual seedlings were transferred in glass jars for a further 3-6 week incubation under the same conditions to create sufficient sterile leaves for transient expression analysis. Preparation of *Nicotiana benthamiana* leaf protoplasts and standard transient expression analysis via electroporation, protoplast incubation, harvesting cells and medium were done as described previously for *N. tabacum* (Foresti *et al.*, 2006; Gershlick *et al.*, 2014) and are detailed section 2.5.

### **2.3.3 Agrobacterium-mediated infiltration of *N. tabacum* leaves**

5 mL of Agrobacteria in liquid selection medium were grown overnight (as described in section 2.2.3). From that culture 1 mL was centrifuged for 5 mins at 4000 rpm, the supernatant was discarded and the pellet resuspended in 1 mL of infiltration buffer [50 mM MES hydrate, 2 mM sodium orthophosphate, 5 % D-glucose, 0.1 M acetosyringone (3', 5'-dimethoxy-4'-hidroxiacetofona to 97 % (Sigma-Aldrich) in distilled water]. This step was

repeated once more to wash the pellet and the pellet was re-suspended in 1 mL of infiltration buffer. The optical density (OD) of the cell suspension was measured with the NanoDrop™ ND-1000 UV-Vis Spectrophotometer (Thermoscientific) at a wavelength of 600 nm. The cell culture was then diluted in the infiltration buffer to the optimal infiltration OD<sub>600</sub> as shown in Table 2-1. The agrobacterium suspension was gently injected into the lower epidermis of the leaf using a 1 mL syringe without needle. The expression was checked using confocal microscopy as described in section 2.6.

## **2.4 Plant material - maintenance and transformation - *Arabidopsis thaliana***

In order to confirm the localisation and phenotypes observed during heterologous expression in *N. tabacum* an Agrobacteria-mediated transient expression in the native system was used in *Arabidopsis* seedlings. The protocol was adapted from the Agrobacteria vacuum infiltration method, described by Marion *et al.* (2008) and detailed in section 2.4.2. This method also allows fast expression of more than one construct. The full-length Atgolgin-84A construct was also used to obtain Agrobacteria mediated stable *A. thaliana* plants using the floral-dip method as described in section 2.4.3.

### **2.4.1 Germination and maintenance of *A. thaliana***

*A. thaliana* seeds ecotype Col-0 were sterilized in 70 % (v/v) ethanol for 5 mins under agitation and left to dry onto a filter paper in the flow hood. Seeds were transferred to ½ MS medium (Duchefa Biochemie™) and 1% (w/v) Phytoagar (Duchefa Biochemie™) and stratified for 2 days at 4 °C. Seedlings were germinated in the incubator at 16 hours light and 8 hours dark at 21°C.

For the transient transformation, the germination conditions were the same as described above but the seeds were placed on 35x10mm cell culture dishes (Sigma Aldrich).

To obtain transgenic *A. thaliana* stable lines expressing Atgolgin-84A or Atgolgin-84A $\Delta$ 1-557 after stratification, seeds were incubated in the same growth conditions as above for 12-15 days and then transferred to individual pots on compost (Levington F2 Seed and Modular Compost Scotts Miracle-Gro, Ohio, USA) and maintained in the greenhouse with the same conditions as for *N. tabacum* till flowering stage. The main floral stem was cut relieving apical dominance and encouraging synchronized emergence of multiple secondary bolts (as described in section 2.4.3).

## **2.4.2 Transient transformation of *A. thaliana***

*Agrobacterium tumefaciens* cells transformed with the various constructs were grown overnight in 5 mL pre-culture and used to inoculate a 30 mL culture (LB liquid medium). After overnight growth at 28 °C, *A. tumefaciens* cells were centrifuged at 1537 xg and resuspended at the appropriate OD<sub>600</sub> (2 for one construct, 1 per construct if co-infiltrating two constructs) in 2 mL of MS liquid medium. A 1/20 dilution of the cell suspension was made and the absorbance read at 600 nm. The infiltration solution was diluted in 4 mL of MS liquid medium supplemented with 200  $\mu$ M acetosyringone to the final concentration OD<sub>600</sub>= 2. Infiltration was performed by submerge the seedlings in the *Agrobacterium* solution and by vacuum twice for 1 min. The remaining infiltration medium was subsequently removed and the plates were transferred to a culture room for 3-4 days (as described in section 2.4.1). The expression was checked using confocal microscopy as described in section 2.6.

### **2.4.3 Stable transformation in *A. thaliana* by Floral-dip**

This method was adapted from Clough and Bent, 1998. Arabidopsis plants dipping an Agrobacteria pre-culture was started in 5 mL of LB medium and allowed to grow for 18 h (as described in section 2.2.3). All the cultures were initiated with a 1:100 dilution of a pre-culture in the day before infiltration and grown for 18 hours. The cultures were centrifuged for 15 mins at 1537 xg at room temperature. The supernatant was removed and the cells were resuspended in floral dip inoculation medium [5.0 % (w/v) sucrose, 0.05 % (v/v) Silwet to a final 250 mL volume of water]. The floral dip medium was added to a beaker and the floral parts were inverted into this suspension. A minimum of three flowering plants without siliques were used per transformation. The plants were submerged two times for 2 mins each with agitation. Plants were removed from the beaker and placed in a plastic tray and covered with cling-film to maintain humidity. The cling-film was removed 12-24 hours after dipping. Plants were grown until siliques were brown and dry. The pots from each construct were separated from the neighbouring pots. The seeds were recovered carefully placing the siliques into paper bags that were collected when plants were completely dry. The seeds were separated using a sieve and were stored at room temperature.

### **2.4.4 Selection of transgenic *A. thaliana* plants**

For pMDC43-GFP constructs hygromycin B (Invitrogen) (60µg/mL) was used for selection on MS-agar plates. Seeds of floral-dipped plants were sterilized as described in section 2.4.1. After drying the seeds were sprinkled onto a petri dish with MS agar medium supplemented with selection agent. The petri dish was sealed with micropore tape and placed at 4°C in darkness for 2 days for stratification. Plates were transferred to plant growth cabinet until resistant plants are ready to be transferred to soil. Plants were screened for fluorescence using a confocal microscope.

For pB7WGC2 constructs BASTA® (50µg/mL) was used for selection in silicon dioxide (Sigma Aldrich). 20 mL of silicon dioxide sand were measured using a falcon tube. The sand was poured into a petri dish until the bottom of the petri dish was full. The sand was soaked with MS medium plus herbicide by pouring 10mL of medium into the plates with sand. Seeds from floral-dipped plants were sprinkled onto the sand. Seeds were germinated as described in section 2.4.1. The resistant plants were transferred into soil and screened for fluorescence using a confocal microscope.

## 2.5 Secretion assay using $\alpha$ -amylase

Measurement of  $\alpha$ -amylase activity and calculation of the secretion index (ratio of extracellular to intracellular enzyme activities) were done as described in Foresti *et al.* (2006) and Gershlick *et al.* (2014). For GUS-normalised effector dose-response assays, the GUS enzyme assay was performed as described in Gershlick *et al.* (2014).

### 2.5.1 Preparation of protoplasts

*N. Benthamiana* leaf protoplasts were prepared with a digestion mix which was prepared from TEX buffer (B5 salts, 500 mg/L MES, 750 mg/L CaCl<sub>2</sub> [2 H<sub>2</sub>O] 250 mg/L NH<sub>4</sub>NO<sub>3</sub>, and 0.4 M sucrose [13.7 %], brought to pH 5.7 with KOH) supplemented with 0.2 % Macerozyme R10 and 0.4 % Cellulase R10 (Yakult). Stocks with 10-fold concentrated digestion enzymes were prepared by dissolving the lyophilized powders in TEX buffer for 2 h, followed by centrifugation at 5000 *xg* for 15 mins and filter sterilization (0.2 µm) of the clear supernatant. The filtered supernatant was aliquot in 5 mL and kept at -80°C for routine use. The 1× digestion mix was always prepared freshly by addition of 45 mL of TEX buffer to these stocks. Overnight digestions of floating leaves (Figure 2.3A and C) were prepared by using a



needle bed (Figure 2.3A). These digestions were then filtered through a 100- $\mu\text{m}$  nylon mesh and briefly washed with electroporation buffer (0.4 M sucrose [13.7 %], 2.4 g/L HEPES, 6 g/L KCl, and 600 mg/L  $\text{CaCl}_2$ , brought to pH 7.2 with KOH) to release further protoplasts from the tissue remnants. The protoplast suspensions were then centrifuged in 50 mL Falcon tubes (Figure 2.4A) for 15 mins at 100 xg at room temperature in a swing-out rotor. Centrifugation was stopped without brake to prevent re-suspension of the floating protoplast band. The pellet and the underlying medium were removed and discarded using a peristaltic pump (Figure 2.4B) and a sterile Pasteur pipette until the band of floating living protoplasts reached the bottom. Then the cells were re-suspended in 25 mL of electroporation buffer followed by a centrifugation at 100 xg for 10 mins. The pellet and the underlying medium were removed again (Figure 2.4C) and this procedure was repeated twice.

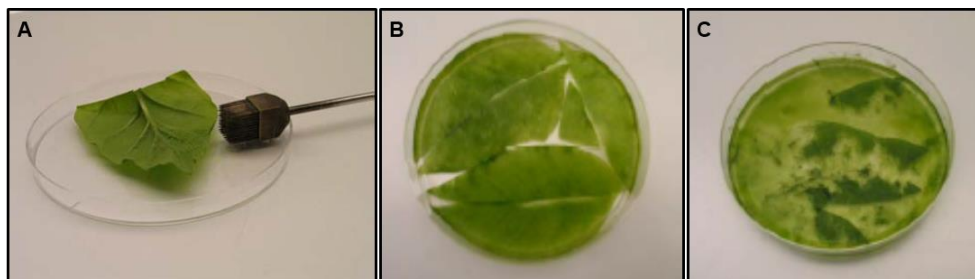


Figure 2.3: Plant leaf enzyme digestion to obtain protoplasts. (A) Leaf and needle bed. (B) Leaf floating in the enzyme solution. (C) Almost all of the leaf is digested and most is protoplasts floating in the enzyme solution.

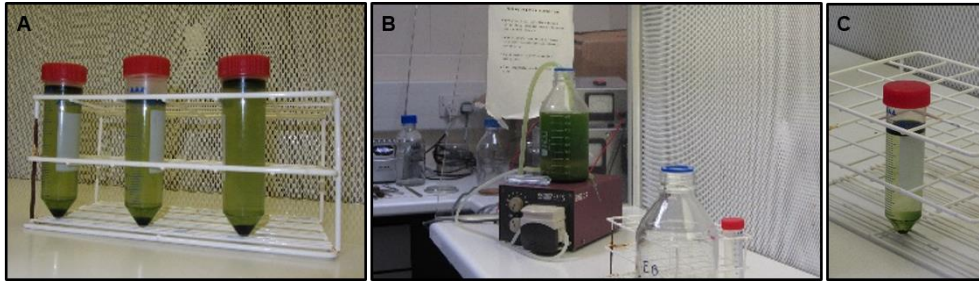


Figure 2.4: Protoplast harvesting after digestion and before electroporation. (A) Protoplast suspensions after first centrifugation in 50 mL Falcon tubes. (B) Peristaltic pump coupled to a sterile Pasteur pipette used to remove the pellet (non-viable cells) and the underlying medium. (C) This procedure was repeated three times.

## 2.5.2 Electroporation of protoplasts

After the final wash, protoplasts were re-suspended in electroporation buffer. 500  $\mu\text{L}$  of the obtained protoplasts mix was then pipetted into a disposable 1-mL plastic cuvette and was mixed with 5  $\mu\text{L}$  of cargo and 7-20  $\mu\text{L}$  effector plasmid DNA depending on relative GUS activity in the pilot assay (Figure 2.5A) (as described in 2.5.5). Negative controls were electroporated with only 5  $\mu\text{L}$  of cargo. The protoplast suspensions were then incubated for 5 mins and electroporated for 5 s with stainless steel electrodes at a distance of 3.5 mm. A complete exponential discharge of a 1000- $\mu\text{F}$  capacitor charged at 160 V was connected to the electrodes (Figure 2.5B). Electroporated protoplasts were rested for 15 mins and were then removed from the cuvettes by washing in 1 mL of TEX buffer twice and transferred to 5 cm Petri dishes (Figure 2.5C). All incubations were performed for 24 h in darkness at room temperature.

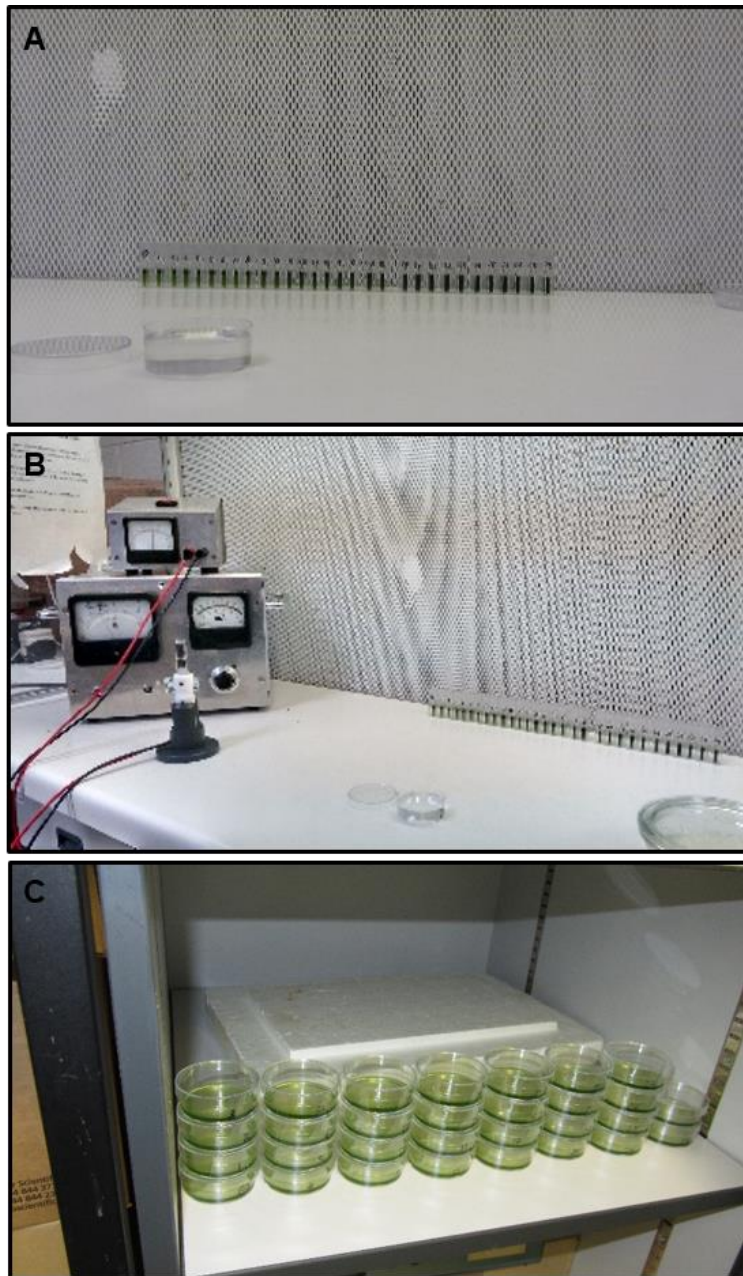


Figure 2.5: Electroporation of *N. benthamiana* protoplasts. (A) 5  $\mu$ L of cargo DNA plasmid was pipetted into a disposable 1-mL plastic cuvette followed by 500  $\mu$ L of the obtained protoplasts and was mixed with 7-20  $\mu$ L effector plasmid DNA and at last the electroporation buffer was added. (B) Electroporation device and set up for electroporation. (C) Protoplasts incubation overnight after electroporation.

### 2.5.3 Harvesting of electroporated protoplasts

After incubation, 2.5 mL of the cell suspension was harvested in a 15 mL Falcon tube and centrifuged at 80 xg for 5 mins. Approximately 1 mL of the underlying medium was manually removed with a refined Pasteur pipette. This obtained medium was further cleared by centrifugation in a refrigerated centrifuge (4°C, 18,000 xg, and 10 mins) and was kept on ice for further analysis (described in section 2.4.4). The cells were diluted 10-fold with 250 mM NaCl in 15 mL Falcon tubes to recover the total cell population of the remaining suspension. The suspension was centrifuged for 3 mins at 200 xg. The supernatant was then removed with a peristaltic pump and the compact cell pellet was kept on ice for subsequent extraction and analysis (described in section 2.4.4).

### 2.5.4 $\alpha$ -amylase assay

$\alpha$ -amylase assay reagents were purchased from Megazyme (<http://secure.megazyme.com>). The supernatant of centrifuged medium suspensions from the harvesting procedure (section 2.5.3) were extracted and diluted with  $\alpha$ -amylase extraction buffer (50 mM malic acid, 50 mM NaCl, 2 mM CaCl<sub>2</sub> and 0.02 % sodium azide, 0.02 % BSA) to obtain suitable dilutions for the assay. In contrast, the cell pellet samples were re-suspended with the same  $\alpha$ -amylase extraction buffer and subsequently sonicated for 5 s (amplitude 10 microns). The sonicated cell pellets were then centrifuged for 10 mins at 18 000 xg at 4°C and the supernatants were recovered. Sample extracts were kept on ice all the time between assays. The assays were carried out at 45°C using 30  $\mu$ L of the extract from the protoplast samples. The reaction was hence initiated by addition of 30  $\mu$ L of the substrate ((R-CAAR4) consisting of blocked *p*-nitrophenyl maltoheptaoside (BPNPG7, 54.5 mg) and thermostable  $\alpha$ -glucosidase (125 units at pH 6.0) which was dissolved according to the manufacturer's instructions in 10 mL of autoclaved distilled water and stored at -80°C as 1 mL aliquots. The reaction

was stopped by the addition of 150  $\mu\text{L}$  of reaction stop buffer (1% (w/v) Tris pH 8.0). Finally the absorbance was measured at 405 nm and readings were recorded.

The  $\alpha$ -amylase activity was calculated in terms of change in optical density ( $\Delta\text{OD}$ ) which was divided per mL of extract used and was then divided by the time period of the assay in mins. The secretion index is the activity of  $\alpha$ -amylase measured in the medium collected 24h after electroporation, divided by the activity of  $\alpha$ -amylase in the cells (measured after sonication of protoplasts). The activity in both medium and cells is the average of two technical repeats.

### **2.5.5 Beta-Glucuronidase (GUS) assay**

From 2.5 mL overnight incubation of the electroporated protoplasts 500  $\mu\text{L}$  were taken and mixed directly with 500  $\mu\text{L}$  of GUS extraction buffer [50 mM Sodium buffer pH7.0, 10 mM  $\text{Na}_2\text{EDTA}$ , 0.1% sodium lauryl sarcosine, 0.1% Triton X-100 and 10 mM  $\beta$ -MeEtOH]. 1 mL diluted protoplasts were then sonicated (60% amplitude for 5s) and vortex before centrifugation at 4°C for 20 mins. 10  $\mu\text{L}$  of supernatant was diluted 10x with GUS extraction buffer and mixed with 100  $\mu\text{L}$  of GUS reaction buffer [50 mM Sodium buffer pH 7.0, 0.1% Triton, 2 mM 4-Nitrophenyl- $\beta$ -D-glucuronic acid (PNPG) and 10mM  $\beta$ -MeEtOH] and incubated at 37°C for 16 h. Reaction is then stopped by adding 80  $\mu\text{L}$  of GUS stop buffer [2.5 M 2-amino-2methyl propanediol] and the optical absorbance was read at  $\lambda 405$ .

## 2.6 Confocal Microscopy

### 2.6.1 Image acquisition

Confocal laser scanning microscope Zeiss LSM 880 AxioObserver with Airyscan (Zeiss) equipped with alpha Plan-Apochromat 100X/ 1.46 Oil DIC M27 Elyra that was used for image and movie acquisition. A segment of approximately 0.5 cm<sup>2</sup> were cut out of *N. tabacum* leaves or a whole cotyledon or first leaf of *A. thaliana* expressing the protein of interest and mounted on a microscope slide with the lower epidermis facing upward. Water was added before mounting the cover slip to keep the sample moisturized. A drop of oil was deposited on the objective to allow the imaging with oil-immersion objectives. Specific settings were used to image different fluorophores (Table 2-7 and 2-8). The acquisition, imaging processing and co-localisation analysis were obtained with ZEN imaging software (Zeiss).

Table 2-7: Imaging settings with PMT/GaAsP detectors for different fluorophores.

<b>Fluorophore</b>	<b>Laser excitation (nm)</b>	<b>Emission spectra (nm)</b>	<b>Beam splitter</b>	<b>Filter</b>
GFP	488:1 %	522	MBS: MBS 488/561	Ch1: 489- 536
mRFP/mCherry	561: 1 %	578	MBS_InVis Plate DBS1: Mirror	ChS1: 588-633

Table 2-8: Imaging settings with Airyscan detector for different fluorophores.

Fluorophore	Laser excitation (nm)	Emission spectra (nm)	Beam splitter	Filter
GFP	ILEXTrack1 488: 1 %	523	MBS: MBS 488/561	BP 495-
mRFP/mCherry	ILEXTrack2 561: 1 %	579	MBS_InVis MBS -405: DBS1: SBS SP 615	550 + LP 570

## 2.6.2 Co-localisation data analysis

Double labelling of *N. tabacum* leaves was imaged using the Zeiss LSM 880 and the Zen (Zeiss) software (<https://www.zeiss.com/microscopy/int/products/microscope-software/zen.htm>). Co-localisation plug-in in Zen software image analysis module was used to analyse the images obtained with Airyscan detector. The Pearson's correlation coefficient (PCC) is a very robust and simple method for quantifying co-localisation (for a review see Zinchuk and Zinchuk, 2008). The equation of PCC is given below for an image of red and green channels.

$$\text{PCC} = \frac{\sum_i (R_i - \bar{R}) \times (G_i - \bar{G})}{\sqrt{\sum_i (R_i - \bar{R})^2 \times \sum_i (G_i - \bar{G})^2}}$$

$R_i$  and  $G_i$  are the intensity values of the red and green channels, respectively, of *pixel*  $i$ , and  $\bar{R}$  and  $\bar{G}$  refer to the mean intensities of the red and green channels, respectively, across the entire image. Because each pixel is subtracted by the average pixel intensity, PCC values can range from -1 to 1. A value of 1 would mean that the patterns are perfectly linearly related, for example every pixel that contains GFP also contains mCherry,

while a value of -1 would mean that the patterns are perfectly but inversely related, every pixel that contains GFP does not contain mCherry and vice versa. PCC measures the pixel-by-pixel covariance in the signal levels of two images. In many image analysis software packages, PCC is measured for entire images by default. Because it subtracts the mean intensity from each pixel's intensity value, PCC is independent of signal levels and signal offset (background). When using the entire image the PCC values will be under-representing the degree of correlation if measured over a field of Golgi bodies and other labelled unidentified structures with heterogeneous expression, since PCC values depend upon a simple linear relationship. Also, unlabelled regions can artificially overestimate PCC values if included in the region of measurement. Therefore, PCC for the Atgolgin-84A co-localisation studies in individual ring-shaped compartments was measured for individual objects, which can be accomplished by hand drawing a "region of interest" (ROI) over the image.

The co-localisation analysis on chapter 4 and 5 aims to set up a methodology for the analysis and give an indication of the quantitative data that can be obtained from imaging with the settings described in section 2.4.1 for objects with the specific characteristics described in chapters 4 and 5.

## **2.7 Drug treatments**

Brefeldin A (BFA) treatment of tobacco leaf samples was carried out as described (Brandizzi *et al*, 2002a). BFA was dissolved in DMSO at 10 mg/mL and stored at -20° C. Tobacco leaf pieces with a size of approximately 3 x 3 mm were cut out and incubated for 30 mins to 2 h in a freshly prepared 100 µg/mL BFA working solution. To wash out BFA, leaf samples were transferred into a petri dish with distilled H<sub>2</sub>O, floating on the water surface for 1-3.5 hours depending on the protein tested.



## 2.8 Bioinformatics and *in silico* analysis

Chapter 3 describes the structural predicted characteristics of Atgolgin-84A in terms of protein structure, evolutionary relationships and post-translational modifications. Table 2-9 summarises the web tools used for the protein predictions described later in chapter 3 and the source for the sequences.

Table 2-9: Web tools used in chapter 3, web addresses and description of the specific software.

Web tool	Web address	Description
The Arabidopsis Information Resource (TAIR)	<a href="https://www.arabidopsis.org/">https://www.arabidopsis.org/</a>	Database for Atgolgin-84A and Atgolgin-84B sequences.
National Centre of Biotechnology Information	<a href="https://www.ncbi.nlm.nih.gov/">https://www.ncbi.nlm.nih.gov/</a>	Database for golgin-84 homologues.
Phyre2	<a href="http://www.sbg.bio.ic.ac.uk/phyre2/">http://www.sbg.bio.ic.ac.uk/phyre2/</a>	Web portal for protein modelling.
Clustal Omega	<a href="https://www.ebi.ac.uk/Tools/msa/clustalo/">https://www.ebi.ac.uk/Tools/msa/clustalo/</a>	Sequences alignment.
Disopred3	<a href="http://bioinf.cs.ucl.ac.uk/psipred_new/">http://bioinf.cs.ucl.ac.uk/psipred_new/</a>	Intrinsic protein disorder and protein binding activity .
The Arabidopsis Protein Phosphorylation Site Database (PhosPhAt 4.0)	<a href="http://phosphat.uni-hohenheim.de/">http://phosphat.uni-hohenheim.de/</a>	Plant specific phosphorylation site predictor and contains information on Arabidopsis phosphorylation sites which were identified in experiments by different research groups.

## 2.9 Optical trapping

The imaging and trapping of Golgi bodies was performed on a TIRF (total internal reflection fluorescence) microscope using a 1090 nm laser and 100X oil-immersion, NA 1.49 TIRF objective lens (Nikon). TIRF uses an excitation laser with a 488-nm for GFP and 561nm for mRFP with a maximum output power of 2 mW, coupled by an optical fiber to a Nikon TIRF adapter system. Emitted fluorescent light was imaged using two electron-multipliers CCD (Andor Ixon EMCCD). This allowed visualization of the excited fluorophores. During each trapping event the trapping laser was maintained in a fixed position while the microscope stage was moved. The positioning of the stage was controlled through a Custom LabVIEW software (National Instruments) which also controlled the EMCCD cameras, microscope stage (Marshauser) and a shutter, which blocked the laser beam used for trapping. The LabVIEW interface was used to set up the stage translation for movies; for scoring Golgi body behaviour on the trap shuttering was manually controlled over approximately 5  $\mu\text{m}$  translation. The trap laser power at the objective was set to the voltage corresponding to 65 mW at the stage which was calibrated before each experiment. A leaf sample was mounted on the microscope slide. Tape was used to seal the sample and avoid coverslip movement and drying of the sample. Each sample was imaged for a maximum of 20 mins.

### 2.9.1 Data collection and analysis of optical trapping data

One-hundred Golgi bodies per *N. tabacum* leaf sample per condition were trapped and classified according to three categories: 'trapped' (if the object is held by the trap and can be displaced from the original position), 'not trapped' (if the object could not be trapped and displaced from the

original position) and 'partially trapped' if the object was trapped but did not stay in the trap during a translation of approximately 5  $\mu\text{m}$ . The trapping data were analysed using the Chi-Squared test in Microsoft Excel. A Chi-Squared test result (indicated as p) smaller than 0.05 indicates that the mean values of the samples are statistically different, and a t-test result higher than 0.05 indicates that the mean values of the samples are not statistically different. The mean values of trapped Golgi bodies were plotted as a histogram where the significance of the differences is represented as (\*)  $p \leq 0.05$ , (\*\*)  $p \leq 0.01$ , (\*\*\*)  $p \leq 0.001$ , (\*\*\*\*)  $p \leq 0.0001$ .

### **3. *In silico* characterisation of Atgolgin-84A**

#### **3.1 Introduction**

In *Arabidopsis* two isoforms of the human golgin-84 were found (Latijnhouwers *et al.*, 2005a). These two isoforms were originally termed golgin candidate (GC) 1 and 2 as they were putative orthologues of human golgin-84. Later these two golgin-84 isoforms were renamed as it is simpler to recognise Atgolgin-84 as being the orthologue of human golgin-84. In this work Atgolgin-84A (AT2G19950) and Atgolgin-84B (AT1G18190) are former GC1 and GC2 respectively. This work will focus on the study of Atgolgin-84A. This chapter describes the predicted structural characteristics of Atgolgin-84A in terms of protein structure, evolutionary relationships and post-translational modifications. Golgins are mainly coiled-coil structured and the first part of the protein is highly disordered (Wong *et al.*, 2017). Therefore, most of the N-terminus of the protein is poorly conserved between species. Golgins in plants could only be identified due to the similarity of conserved domains such as the carboxy-terminal domain (TMD) or the first 30 N-terminal amino acids that for some golgins has more than 60% similarity with mammalian or yeast golgins (Latijnhouwers *et al.*, 2005). Mammalian golgins were used for the plant Atgolgin-84 search (Bascom *et al.*, 1999). In this chapter, some of the Atgolgin-84A protein characteristics are predicted and discussed according to protein analysis software as this revealed some interesting features that can be informative when comparing with the results obtained experimentally during this work. These predictions will generate new theories for the deletion mutant results obtained during this work and described in chapter 5.

### **3.2 Aims for bioinformatics analysis**

The aims of the bioinformatics analysis include the following:

- a) Atgolgin-84A protein structure prediction and comparison with predicted structure for human golgin-84 and Atgolgin-84B;
- b) Compare sequence and domain conservation by BLAST analysis of the protein sequence against other species to compare protein structure, folding and conserved domains;
- c) Search for predictions and/or experimental data on Atgolgin-84A post-translational modifications that in other species are reported to be involved in protein activity and function.

### 3.3 Results

Atgolgin-84A is annotated in TAIR (as annotated in chapter 2, section 2.8) as a predicted member of the golgins subfamily A. *Atgolgin-84A* encodes a protein with a relative molecular mass of 79.534 kDa and an isoelectric point of 4.91. Atgolgin-84A structure and 3D conformation is still unknown. Therefore, as a starting point to study the function and activity of the protein the structure was predicted by submission of Atgolgin-84A and human golgin-84 amino acid sequence to Phyre2: (<http://www.sbg.bio.ic.ac.uk>) (Kelley *et al.*, 2015) web portal for protein modelling. This prediction allowed a comparison of Atgolgin-84A structure with the human golgin-84 and another homologue Atgolgin-84B and Phyre2 compares the submitted sequence to a 10 million known sequences using PSI-BLAST (Altschul *et al.*, 1997). It predicts the secondary structure and disorder with Psipred (Jones, 1999) and Disopred (Ward *et al.*, 2004) and generates a Hidden Markov Model (HMM) which finds the evolutionary fingerprint from the homologues found in PSI-BLAST. This results in a database with HMM known structures for the query sequence by alignment with approximately 65000 known 3D structures in the database. After this, it aligns the query sequence to known structures ranked by confidence and generates a 3D model (Figure 3.1). Atgolgin-84B predicted structure shows  $\beta$ -sheets (Figure 3.1 E, highlighted green arrows in the structure) which was not predicted for human golgin-84 or Atgolgin-84A.

Golgin-84 is represented in several kingdoms including plant species and humans and is anchored in the Golgi membrane by a C-terminal TMD (Burkhard *et al.*, 2001). The sequence identified as Atgolgin-84A has high similarity with other species in terms of specific domains. It was found to have 50% identity with other species in the TM region. The alignment of Atgolgin-84A sequence from different species using CLUSTAL Omega shows the high degree of conservation in this domain (Figure 3.2).

In 2014 Wong and Munro reported that human golgin-84 specifically recognises vesicles moving within the Golgi stack. Later in 2017 (Wong *et al.*, 2017) in order to identify which part of golgin-84 is required for this recognition various truncated forms of the protein were created and tested for the ability of capturing vesicles.

Deletion of Hsgolgin-84A N-terminal 203 residues causes loss of ability to capture vesicles. Although the first 200 amino acids of the protein are poorly conserved, the first 30 residues in the N-terminal are very well conserved (Figure 3.3) and tryptophan 3 is conserved for the species analysed (Figure 3.3). Tryptophan 3 (4 in Atgolgin-84A) is conserved for Arabidopsis as predicted by CLUSTAL Omega BLAST (Figure 3.3). The first part of Hsgolgin-84 is predicted to be unstructured, as it was predicted in this work for Atgolgin-84A (Figure 3.4).

Figure 3.4A shows the region of the structure modelled with high degree of confidence by Phyre2. In order to compare some protein characteristics to human golgin, the coiled-coil regions for Atgolgin-84A were predicted using COILS (Delorenzi and Speed, 2002) (Figure 3.4B), which compares the query sequence to a database of known parallel two-stranded coiled-coils and finds a similarity score. By comparing this score to the distribution of scores in globular and coiled-coil proteins, the program then calculates the probability that the sequence will adopt a coiled-coil conformation. Intrinsic protein disorder and protein binding activity were predicted using Disopred3 (Jones and Cozetto, 2014) (Figure 3.4C). Many eukaryotic proteins contain intrinsically disordered regions (IDRs) (Jones and Cozetto, 2014), which are in unfolded states, or they are transitioning between structured and unstructured conformations.

There is evidence for the regulation of golgin tethering activity by phosphorylation (for review Witkos and Lowe, 2016). The Atgolgin-84A phosphorylation pattern was investigated. The Arabidopsis Protein

Phosphorylation Site Database (PhosPhAt 4.0) contains information on Arabidopsis phosphorylation sites which were identified by mass spectrometry in large scale experiments by different research groups according to PhosPhAt web tool. The PhosPhAt service has a built-in plant specific phosphorylation site predictor recognises on the experimental dataset serine, threonine and tyrosine phosphorylation (pSer, pThr, pTyr). A phosphorylation hotspot is predicted and some sites have been experimentally tested as annotated in Figure 3.5 from the web tool results.



### 3.4 Discussion

Recently, some characteristics of mammalian golgin-84 were described and vesicle tethering activity of this protein was reported (Wong and Munro, 2014). In order to understand similarities and differences between mammalian golgin and the plant golgin Atgolgin-84A, it is important to do a structure analysis for Atgolgin-84A. This is particularly important for the interpretation of the mutant phenotypes observations described later in chapter 5.

The transmembrane domain at the C-terminal end in Arabidopsis and human golgin-84 is predicted with a high degree of confidence (Figure 3.1). Most of the C-terminal region is predicted with high confidence and the confidence decreases towards the N-terminus where structure disorder increases. Therefore the protein could adopt a different conformation *in vivo*, and it could be that human golgin and plant golgin structures are less similar than it is predicted here.

Atgolgin-84A structure was predicted using Phyre2 and 61% of the structure was predicted with more than 90% of confidence (Figure 3.1 A). Necessarily, this has to be considered when making conclusions from this model. Human golgin was predicted with slightly higher degree of confidence as 67% of the structure was predicted with more than 90% of confidence (Figure 3.1 B). These models confirm the TMD region and the long coiled-coil domains. The full-length protein could adopt different conformations as suggested in the recent work with mammalian golgins (for review Wong *et al.*, 2017), where the golgin would be flexible to bring the vesicle into closer proximity with the Golgi membrane.

The structure corresponding to the mutant sequence is predicted with a high degree of confidence (558-707 amino acid residues). When the N-terminus of the protein is deleted in the mutant (which is described in detail

later in chapter 5) this might expose many potential post-translational modification sites. Furthermore, it is described that cleavage of the golgin could also induce fragmentation of the Golgi and unstacking of cisternae and abolish golgin tethering activity (Witkos and Lowe, 2006). The deletion mutant could mimic the cleavage product, as only the C-terminus region of the protein is produced.

As published in previous Atgolgin-84A studies (for review Sztul and Lupashin, 2009), the N-terminus of the protein is predicted to reach out into the cytoplasm, and the transmembrane is predicted to be anchored to the Golgi membrane (Figure 3.2A). The transmembrane domain is one of the most conserved domains between species (Figure 3.2B).

In 2014 one of the most interesting studies on golgin activity was published and showed that golgins are responsible for recognising specific vesicles according to the cargo transported (Wong and Munro, 2014). Later this group investigated the motif for this vesicle tethering activity. This “amphipathic lipid-packing sensor” (APLS) motif was found to be the first 40 amino acids of golgin-84 and it was necessary and sufficient for vesicle capturing activity of the golgin (Wong *et al.*, 2017). Moreover Trp3 is well conserved across species (Figure 3.4) and when this amino acid was mutated the ability to capture vesicles was abolished (Wong *et al.*, 2017). It can be hypothesised that this amino acid is potentially important for tethering activity in Arabidopsis as it very well conserved across kingdoms (Figure 3.3). Most of the Atgolgin-84A structure is predicted to be coiled-coil domains (Figure 3.4 B). The first part of the protein has the highest disorder but the first 30 residues are well conserved across species. It could be hypothesised that the APLS motif could have a function (Figure 3.4C) and it is where the vesicle capturing activity was identified in mammalian golgin-84.

During this work, a mutant of Atgolgin-84A will be described (chapter 5). The mutant was obtained by deletion of 1 to 557 residues (Figure 3.6B).

According to prediction in this mutant, there is one coiled-coil domain remaining, and also according to prediction, in the mutant sequence there is high protein binding activity (Figure 3.4C). This could explain that the mutant has a function, as discussed later in this work. The mutant could be affecting the tethering activity because it does not have the vesicle binding motif, as the N-terminal region was deleted. On the other hand, the region with high protein binding activity could have been exposed, and the phosphorylation sites could also have been exposed to protein kinase activity when the N-terminus of the protein was deleted. Phosphorylation of golgin-84 is suggested to be regulating the tethering activity of other golgins by preventing interaction with binding partners or disassociation of the golgin from the Golgi membrane (Witkos and Lowe *et al.*, 2016). Therefore, the prediction of phosphorylation sites in Atgolgin-84A is important. A phosphorylation hotspot is predicted and several of the sites experimentally confirmed according to PhosPhAt (Figure 3.5). This region is part of the mutant sequence (Figure 3.5 and 3.6). This will be discussed later considering the observations with the mutant overexpression.

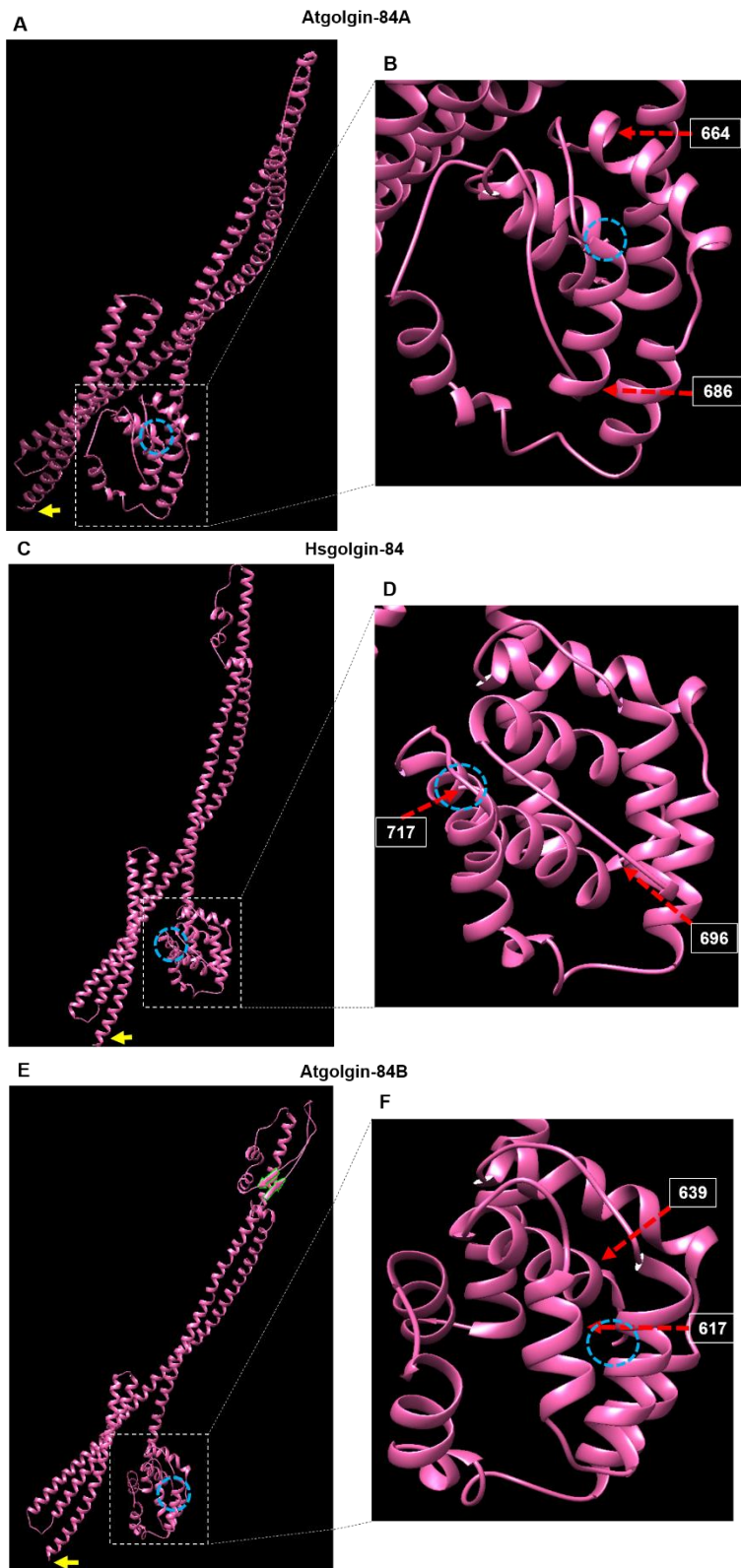


Figure 3.1: Predicted Hsgolgin-84, Atgolgin-84A and Atgolgin-84B protein structure using Phyre2. (A, C and E) General view of the structure predicted on PHYRE2 with indication of N-terminus (yellow arrow) and C-terminus (blue dashed circle). The C-terminal end is more globular than the coiled-coils formed by long  $\alpha$ -helices twisted around each other forming a rope-like structure. (B, D and F) Detail of the C-terminal end of the structure with annotated first and last TMD residues and C-terminus of the modelled structure. 427 residues which is 60% of Atgolgin-84A sequence have been modelled with 97.4% confidence. (B) 67% (489 residues) of Homo sapiens (Hs) golgin-84 sequence has been modelled with 98.2% confidence. (B) (C) Atgolgin-84B predicted secondary structure shows predicted beta-sheets (highlighted in green) which was not predicted for Atgolgin-84A or Hsgolgin-84. 512 residues of Atgolgin-84B (77% of the sequence) have been modelled with 98.4% confidence.

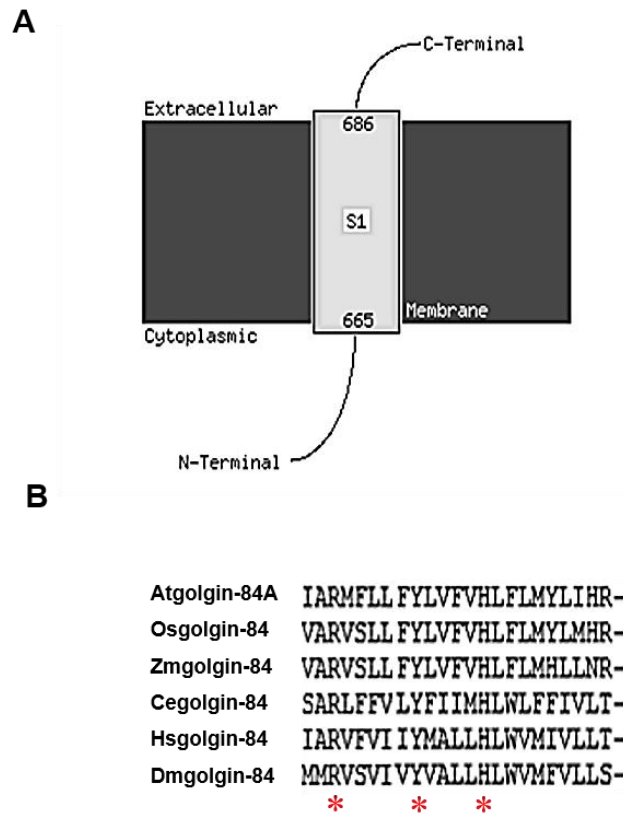


Figure 3.2: Prediction of TMD insertion in the membrane and alignment of the TMD for different species. (A) Schematic representation of Atgolgin-84A insertion into Golgi membrane using Phyre2 prediction. (B) Alignment of predicted golgin-84 TM domains from *Arabidopsis thaliana* (NCBI accession NP\_179585.3), *Oryza sativa* (NCBI accession XP\_015651194.1), *Zea mays* (NCBI accession XP\_008657231.1), *Caenorhabditis elegans* (NCBI accession CAB06546.2), *Homo sapiens* (NCBI accession AAD09753.1) and *Drosophila melanogaster* (NCBI accession NP\_651250.2). \* means conserved across species.

```

Atgolgin-84 MASWL-----KAAEDLFEVVDRAKSVVEDLSEEQNDLQLPASGR--KG
Osgolgin-84 MASWL-----KVAEDLLEVVDRRAKIVATELSDEQSSPQPSGSSS--QE
Zmgolgin-84 MASWL-----KVAEDLLEVVDRRAKIVATELSDEQSTISQPSGPNN--QE
Cegolgin-84 -MSWLSKVSDIAGAAENLLNKLDEKTGDAL---QNARDSAPRTRKSS--T-
Hsgolgin-84 -MSWF---VDLAGKAEDLLNRVDQGAATAL---SRKDNASNIYSKNTIDYTE
Dmgolgin-84 MSSWI---TGLADKAENILNKLDQNAATAL---QTENATGSADPMRRSMTS
          *
```

Figure 3.3: Alignment of the N-terminus of golgin-84 that can capture vesicles in mammalian cells with that from the indicated species. Note that \* Trp3 (red asterisk) is very well conserved in golgin-84 across different species, *Arabidopsis thaliana* (NCBI accession NP\_179585.3), *Oryza sativa* (NCBI accession XP\_015651194.1), *Zea mays* (NCBI accession XP\_008657231.1), *C. elegans* (NCBI accession CAB06546.2), *Homo sapiens* (NCBI accession AAD09753.1) and *Drosophila melanogaster* (NCBI accession NP\_651250.2).

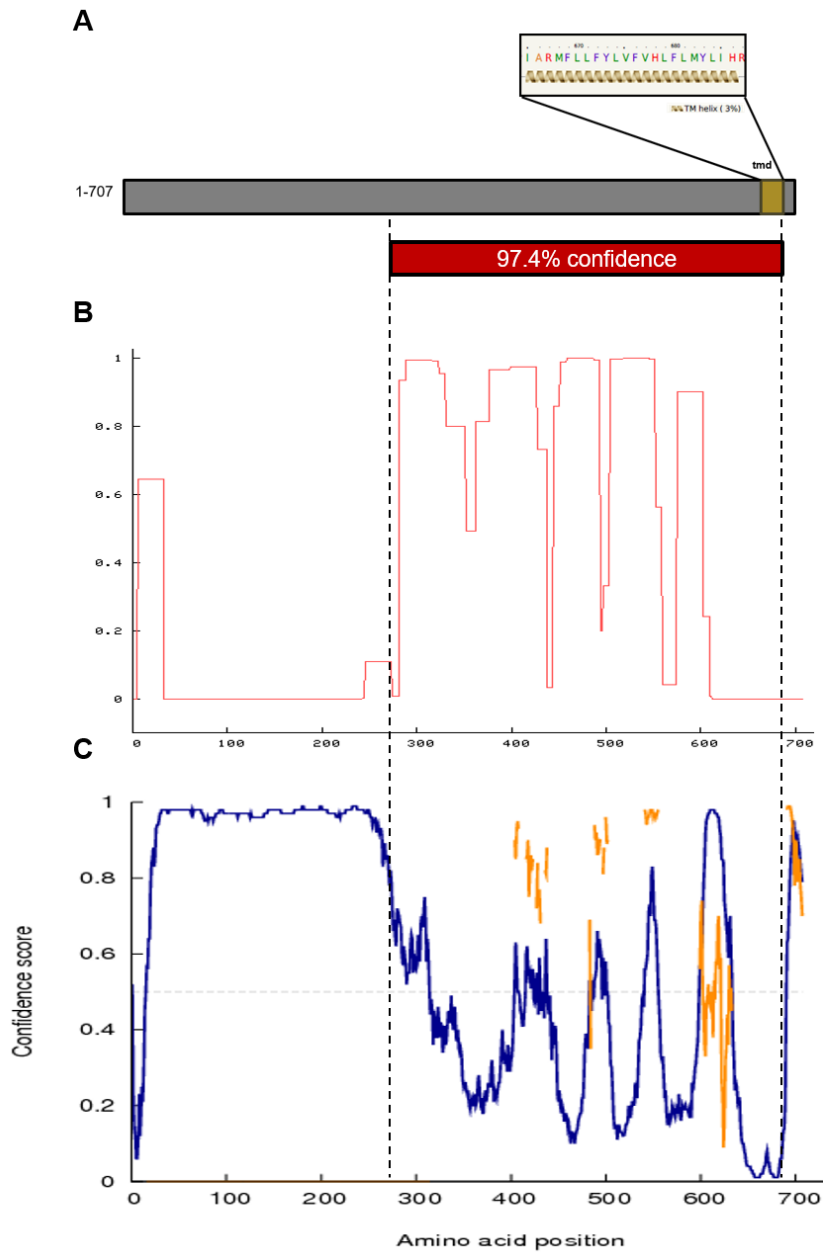


Figure 3.4: Mapping of Atgolgin-84A. (A) Schematic diagram of Atgolgin-84A with detail of TMD sequence and annotation of the residues modelled with 97.4% of confidence in Phyre 2 (red in A). (B) Plot for the predicted degree of coiled-coil. (C) Plot for disorder (blue) and protein-binding activity (C) along Atgolgin-84A length. Amino acids in the input sequence are considered disordered when the confidence score is higher than 0.5. The orange line shows the confidence of disordered protein binding residue predictions.



```

601...650 V E V E K S R V S R R A S A T W E E D S E I K T L E P L P L Y H R H M A T A S T Q L Q N A V K L L D
651...700 S G A V R A I B F L W R Y T P I A R M F L L F Y L V F V H L F L M Y L I H R L Q E Q A E A Q E V A A M
701...750 T N N V F R L

```

Figure 3.5: Phosphorylation sites prediction for Atgolgin-84A C-terminal end using the Arabidopsis Protein Phosphorylation Site Database (PhosPhAt 4.0) (Zulawski *et al.*, 2013; Durek *et al.*, 2010). In residues 603 to 625 the software predicts a hotspot which is a region with several residues predicted to be phosphorylated. **RASATWEEDSEIK** were found in experiments according to PhosPhAt and more details on these experiments can be found in the website. The residues in bold has higher score in the prediction. HMATASTQLQNAVKLLDSGAVRATR were not predicted but were found in experiments and more details on the experiments can be found in the website (<http://phosphat.uni-hohenheim.de/>).

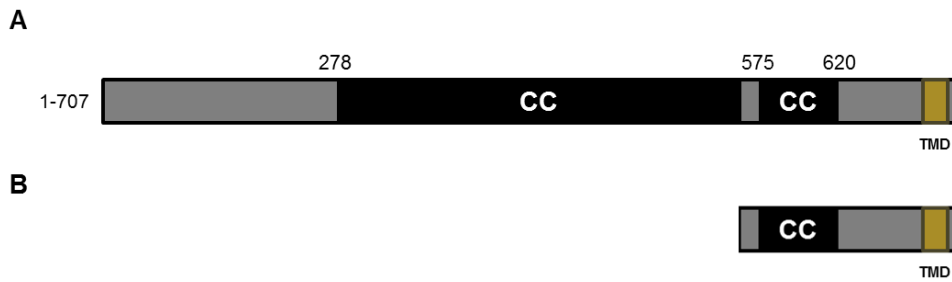


Figure 3.6: Schematic representation of Atgolgin-84A full-length protein and deletion mutant Atgolgin-84A $\Delta$ 1-557. (A) Most of Atgolgin-84A structure is predicted to be coiled-coil domains (CC). The N-terminal is disordered except for the first 30 amino acids that are well conserved across species. The TMD at the C-terminus anchors the golgin to the Golgi membrane. (B) Using a similar approach as for the human golgin-84 in the Atgolgin-84A deletion mutant is the TMD and approximately 100 amino acids preceding the TMD and this region (amino acids 558–707) is necessary and sufficient for Golgi localisation (Latijnhouwers *et al.*, 2007).

## 4. Subcellular localisation of Atgolgin-84A using confocal microscopy with Airyscan

### 4.1 Introduction to confocal microscopy with Airyscan

GFP-Atgolgin-84A was overexpressed as fluorescent fusions *in planta* in order to study the specific localisation of the full-length protein. For this a ZEISS LSM 880 confocal microscope with an Airyscan detector was used (Figure 4.1). This new microscope is the best combination of high-resolution coupled with sensitive confocal image acquisition (Figure 4.2). The resolution of a conventional widefield microscope is restricted by the diffraction. Conventional confocal laser scanning microscopes combine a physical aperture, the pinhole, and a unitary detector to create an optically sectioned image by blocking any light that does not originate from the focal plane. The standard confocal microscope has maximum resolution when the pinhole diameter is 0.2 Airy Unit (AU) and this means 1.4x increase in resolution. In reality, if the pinhole is less than 1 AU there is a decrease in signal reaching the detector and therefore the image quality decreases. The Airyscan detector combines the resolution benefits of imaging with a small pinhole with the collection efficiency of a large pinhole. The Airyscan detector is a 32-channel Gallium arsenide phosphide (GaAsP) photomultiplier tube (PMT) area detector. Each detector element acts as a pinhole and will produce its own image. The image of the central detector element will be centred, whereas the images of the other detector elements will be displaced by approximately half their distance they have to the centre (Figure 4.3). Therefore, a detector array of 32 elements will produce 32 images with different displacements. By shifting back all the images to the central position, because the amounts of their displacements are known, an image called the "Sheppard sum" is generated. For a comparison of standard confocal detection to confocal with Airyscan detection see Figures 4.4 and 4.5. The 1.25 AU allows pinhole to collect up to 50% more light than a

conventional 1 AU pinhole that is in theory the optimal for a traditional confocal system. Each Airyscan detector element behaves as a small 0.2 AU pinhole but is collected by a 1.25 AU pinhole. To extend the resolution from the 0.2 AU pinhole Airyscan uses linear deconvolution which in theory results in a 1.7x increase in resolution which in three spatial dimensions means 140 nm in x and y and 400 nm in z.

This chapter aims to assess the resolution improvement using a confocal microscope with Airyscan detector and optimise this system for the imaging of Golgi bodies in order to characterise Atgolgin-84A subcellular localisation.

## **4.2 Results**

### **4.2.1 Optimisation of high-resolution imaging using the well-described non-functional Golgi marker ST-GFP**

Plant Golgi cisternae morphology has never been described using high-resolution confocal microscopy. During this work one of the aims was to assess the resolution improvement using a confocal microscope with Airyscan detector compared to a standard confocal microscope (Figure 4.4.). The Airyscan is a new technology and therefore the first approach was to image the best known Golgi marker, ST-GFP (Boevink *et al.*, 1998), to better understand the improvement in resolution.

In order to do so ST-GFP expression was imaged in *A. thaliana* with a Zeiss LSM 880 confocal microscope with an Airyscan detector. Several secondary structures and more fine details on the *trans*-Golgi structure were detected with Airyscan imaging compared to standard confocal resolution. Golgi bodies showed short tentacle-like structures (Figure 4.5, arrows, Appendix I, Movie 1) that move in and out of the Golgi bodies that are less than 1  $\mu\text{m}$  long. Some Golgi bodies appear to have sub-structures in a ring-shape that often look like as there was a boundary in the middle of the ring-shape (Figure 4.5, red circle).

### **4.2.2 High-resolution imaging of Atgolgin-84A expression in different plant systems**

In order to characterise the localisation of Atgolgin-84A predicted to be at the ER-Golgi interface, the subcellular expression of fluorescently tagged Atgolgin-84A was investigated. Therefore, GFP-Atgolgin-84A was infiltrated

in *N. tabacum* leaves as described in chapter 2. Overexpression of full-length GFP-Atgolgin-84A is toxic for the leaf cells. Expression of Atgolgin-84A fluorescent fusions can cause necrosis in leaf cells as observed in Figure 4.6. To control this effect reduced expression using only 0.02 Agrobacteria optical density ( $OD_{600}$ ) was used to infiltrate the full-length protein (Figure 4.7). Cytoplasmic localisation of Atgolgin-84A 2dpi showing distinct puncta can be observed 2 dpi (Figure 4.7A). GFP-Atgolgin-84A labels ring-shaped structures at 3dpi. Accumulation of Atgolgin-84A between ring-shaped structures can also be detected (Figure 4.7B). The plants were imaged with a confocal microscope with Airyscan detector two or three days post-infiltration (2 or 3 dpi). In order to confirm the phenotype observed in tobacco *A. thaliana* Columbia-0 (Col-0) plants were stably transformed with GFP-Atgolgin-84A by floral dip as described in chapter 2. Plants expressing Atgolgin-84A full-length are shorter with less leaves and flowers than wild-type plants and only few survived to the flowering stage. The fluorescence was not detected in the T2 generation, therefore T1 plants were imaged (Figure 4.7C).

Due to the high resolution it was possible to resolve substructures in the compartments labelled by Atgolgin-84A. In *N. tabacum* 2 dpi. Atgolgin-84A labels the cytoplasm and pleomorphic aggregates. The plants were imaged 24 hours later (3 dpi) and ring-shape structures were labelled and some were connected in pairs (Figure 4.7B and C). As a preliminary indication several Golgi bodies were counted from at least 8 movies from Atgolgin-84A and ST-GFP expression in *N. tabacum* (Table 4-1). This preliminary result from a single experiment shows detection of pairs of ring-shaped structures in the Atgolgin-84A expression when compared to ST-GFP where no Golgi pairs were observed in 273 Golgi bodies counted. Further experiments are needed to interpret this phenotype. There was a higher intensity of fluorescence where the two Golgi bodies connect as confirmed by the line profile across the aggregate of ring-shapes (Figure 4.7D and E). Transient expression in *N. tabacum* (Figure 4.7B) and stable

expression in *A. thaliana* (Figure 4.7C) show a very similar phenotype as in both expression systems GFP-Atgolgin-84A labeled ring-shaped structures and several Golgi pairs are observed but not all ring-shapes were connected.

### **4.2.3 High-resolution imaging of Atgolgin-84A co-expressed with an ER marker**

The hypothesis was that Atgolgin-84A is a tethering factor between ER and Golgi and therefore it was of interest to look at the dynamics between the ER and the compartment labelled by the golgin. The use of Airyscan imaging allowed for fine structures to be resolved and change in shape of the structures to be monitored. Atgolgin-84A fused to mCherry fluorescent protein was co-infiltrated with the ER marker GFP-HDEL.

The compartment labelled by the golgin appeared to change in shape constantly and in some time-frames the shape was not completely round (Figure 4.8A, Appendix I, Movie 2 and Figure 4.9A). The red compartment labelled by the golgin seemed to be re-shaping according to the ER or possibly the other way around being the ER re-shaping around the ring-shaped structure (Figure 4.8A and 4.9A, white arrow). The ring-shaped structure seems to fit to the ER lacunae as the ER moves. It is possible to observe the ER structure in the cisterna part of the ER and how some of them do not look like a homogeneous sheet as was previously observed with conventional confocal imaging. Some of the cisternae appear to be made of a set of tubules connected together (Figure 4.8A-C, Appendix I, Movie 2). Short tubular connections appear to emanate from the ring-shaped structure to the ER (Figure 4.8B and Figure 4.9B, E and H, white arrow). An ER tubules can be seen crossing the lacunae above a ring-shaped structure labelled by the golgin (Figure 4.8C, Figure 4.10C and 4.11B, Appendix I, Movie 3 and 4) or possibly going inside the Golgi (Figure 4.8C and 4.9C, F and I). The high definition of these structures shows the improvement in resolution with the

Airyscan detection. In Figure 4.10C some ER cisternae seem to be very homogeneous compared to the ER structures in Figure 4.8 which shows the high plasticity and fast structural changes in the ER. The aggregates of ring-shaped structures observed when Atgolgin-84A is overexpressed seem to be disconnected from the ER (Figure 4.10F and 4.11B) and some aggregates appear not to move as much as single Golgi bodies. Further experiments are needed to understand the significance of this phenotype.

#### **4.2.4 High-resolution imaging of Atgolgin-84A co-expressed with different Golgi markers**

Atgolgin-84A is a putative *cis*-Golgi protein and if it is a tethering factor it can be hypothesised that Atgolgin-84A would also localise at the ER-exit sites (ERES) where it could have a function. In order to characterize its localisation in the Golgi stack, GFP-Atgolgin-84A was co-infiltrated in *N. tabacum* with various Golgi markers (Figure 4.12) starting with the well-described Golgi marker ST (Figure 4.13, Appendix I, Movie 5 and 6). ST-mRFP labels the *medial/trans*-Golgi (Munro, 1995; Boevink *et al.*, 1998; Renna *et al.*, 2005). The co-expression in tobacco leaves was imaged 3 dpi with a Zeiss LSM 880 with Airyscan.

The ring-shaped structures labelled by Atgolgin-84A and ST-mRFP move together but the golgin and ST appear to label different sub-compartments (Figure 4.13C, F and I). Short (0.5-1  $\mu\text{m}$ ) tubular structures are observed protruding out of the ring-shape structure labelled by Atgolgin-84A (Figure 4.13F and I, insets). Several ring-shaped structures labelled by Atgolgin-84A are connected by a tubular structure (Figure 4.13F, inset).

Due to the lack of co-localisation with the *trans/medial*-Golgi marker ST and in order to understand the specific localisation of Atgolgin-84A, two previously described Golgi glycosylation enzymes were infiltrated into leaves



alongside Atgolgin-84A. One is resident on the *cis*-Golgi, the Golgi- $\alpha$ -mannosidase I (MnSI) (Figure 4.14) and another resident on the *cis*/medial-Golgi N-acetylglucosaminyltransferase I (GnTI) (Figure 4.15) (Schoberer *et al.*, 2009; Schoberer and Strasser, 2011). Atgolgin-84A is detected in a ring-like structure (Figure 4.14B, red arrow), whereas MnSI and GnTI labelling looks more homogeneous in the Golgi cisternae (Figure 4.14A, yellow arrow and Figure 4.15A). Atgolgin-84A shows a shift from the MnSI labelling (Figure 4.14C). Some Golgi shaped compartments labeled by MnSI were not labeled by Atgolgin-84A (Figure 4.14, white arrow). With GnTI expression Atgolgin-84A fluorescence also accumulated between several Golgi bodies (Figure 4.15C-E). It appears that Atgolgin-84A is connecting several Golgi bodies and is likely to be the reason why these move in aggregates (Figure 4.15).

Atgolgin-84A expression (Figure 4.16A) is more constricted to the rims of the round-shape than AtCASP (Figure 4.16B). Most of Atgolgin-84A and AtCASP co-localise, but when the ring-shaped structure is slightly tilted it seems that the shift between green and red is more distinguishable (Figure 4.16C, white arrow).

The degree of co-localisation for the co-expression of Atgolgin-84A with the markers described in this section will be analysed in detail in section 4.2.6.

## 4.2.5 High-resolution imaging of Atgolgin-84A with AtSar1a-GFP, a component of the COPII transporters

Atgolgin-84A did not completely co-localise with Golgi markers and it appears that the golgin labels a pre-*cis*-Golgi subcompartment. This could co-localise with ER-exit sites (ERES) described in the literature (Zeng *et al.*, 2015). The marker AtSar1a-GFP (Figure 4.17, Appendix I, Movie 7 and 8) was chosen as an ERES marker and was co-infiltrated with mCherry-Atgolgin-84A (Figure 4.18). Sar1 being a GTPase associated with COPII coat formation.

Single expression of AtSar1a-GFP labels the cytoplasm but also ring-shaped and punctate structures (Figure 4.17). On co-expression of mCherry-Atgolgin-84A with AtSar1A-GFP most of the ring-shaped structures are no longer observed. mCherry-Atgolgin-84A labels structures that are surrounded by AtSar1a-GFP (Figure 4.19C and F).

## 4.2.6 Co-localisation analysis

To further investigate the specific localisation of the golgins compared to the markers described above, the data obtained from co-expression was analysed in Zen (Zeiss) image analysis software for co-localisation in section 4.2.6. The method is described in detail in chapter 2.

The subcellular distributions of two fluorescently labelled proteins can be used to understand the function of a protein when for example the protein is found to co-localise with a marker of a specific compartment or subcompartment, or to understand intracellular trafficking or transport when the protein is found to co-localise with markers known to follow a particular

pathway. Often co-localisation is a subjective feature, such as the appearance of the colour that reflects the combined contribution of both channels when the images of each channel are merged. This judgement can be ambiguous and relies on the detection of a combination of colours. Recently with the resolution obtained from the Airyscan that allows resolving subcompartments this is not enough to characterise the localisation of two probes in very close proximity. Also, the combined colour from merged images is obtained only if the intensities of both fluorescent proteins are similar. Nevertheless, the third colour observed by merging two channels is very useful for identifying regions of the cell or compartments where molecules co-localise in order to identify specific regions of interest to quantify co-localisation. Additionally these observations can be represented graphically in scatterplots where the intensity of one colour is plotted against the intensity of the other colour for each pixel (Figure 4.20). In the case of proportional co-distribution the points in the scatterplot cluster around a straight line (Figure 4.20A). On the other hand, the lack of co-localisation of two markers is represented by the distribution of points into two separate groups. Values near zero reflect distributions of probes that are uncorrelated (Figure 4.20B).

Using the Airyscan high resolution detector it is possible to distinguish in different time-frames Golgi bodies that look like a ring and this ring is facing the coverslip and other rings are sideways on (as represented in Figure 4.21). The PCC was analysed separately for side view and for face view to the coverslip as shown in Figure 4.22. The co-expression of MnSI-GFP and GnTI-mRFP was used as a positive control for co-localisation. Both proteins are described as being localised in the *cis/medial*-Golgi and therefore the distribution of these two markers should mostly overlap and also have very similar proportion to one another within the *cis/medial*-Golgi cisternae (Figure 4.22A). For a comparison with the proteins tested in this work, the co-expression of MnSI-GFP and GnTI-mRFP will be representing a high degree of correlation between two probes as the side view PCC of 0.76 and the face

view 0.78 obtained indicates reasonably strong correlation. The structures observed in Figure 4.22 were used to measure co-localisation between Atgolgin-84A and AtSar1a-GFP as observed in Figure 4.22B. A PCC of 0.63 was obtained which is lower than the positive control but higher than 0.4 which indicates a positive correlation for the two proteins (Table 4-2). The number of objects analysed for this condition is low which is due to the toxicity of mCherry-Atgolgin-84A and also to the phenotype observed during co-expression of both proteins. When co-expressed the ring-shaped structures are not present as observed for single expression and only few structures as shown in Figure 4.22B are found. Due to the toxicity of Atgolgin-84A it was only possible to obtain one object for co-localisation analysis with mRFP-MnSI and therefore this result is shown in Table 4-2 but it is not sufficient to be compared to the other conditions. The PCC value of 0.63 for the co-expression with AtSar1a-GFP is a preliminary indication that the golgin is not in the *cis*-Golgi and it is possibly towards the ER just before the *cis*-Golgi. The PCC of 0.40 indicating no correlation of the proteins for the co-expression with ST-mRFP (*medial/trans*-Golgi marker) also confirms the localisation of the golgin in the initial compartments of the Golgi towards the ER (Table 4-2).

The strong degree of correlation between mCherry-Atgolgin-84A and AtSar1a-GFP suggests both proteins are at least partially in the same subcompartment, since the proteins are also distributed in other regions of the cell that like the cytoplasm for example. BFA was used to look further into the localisation of these two proteins as described next.

#### 4.2.7 High-resolution imaging of Atgolgin-84A expression during BFA treatment

*N. tabacum* infiltrated leaves were treated with Brefeldin A (BFA) that impairs COPI transport vesicle formation and as consequence Golgi bodies and ER form a hybrid compartment fusing together. As Atgolgin-84A seems to be in a different sub-compartment than the *cis*-Golgi marker MnSI, the BFA treatment could reveal differences in the response from Atgolgin-84A compared to markers for ERES or the *cis*-Golgi as these are well described in the literature when treated with BFA (Schoberer *et al.*, 2010; Osterrieder *et al.*, 2009b). The leaves expressing GFP-Atgolgin-84A were incubated in BFA for 1.5h (Figure 4.23). A component of the COPII transporters (AtSar1a-GFP) and a *cis*-Golgi marker, MnSI-mRFP were used as controls for the BFA activity and as comparison to Atgolgin-84A. As BFA is dissolved in DMSO control samples were incubated in DMSO and imaged with the BFA treated samples.

Atgolgin-84A and AtSar1a-GFP label the cytoplasm and puncta after BFA treatment (Figure 4.23D and E). The patterns of AtSar1a-GFP and Atgolgin-84A are similar after BFA treatment. Atgolgin-84A does not re-localise to the ER as the *cis*-Golgi marker does but instead after BFA treatment localises to cytoplasm and small puncta (Figure 4.23D). MnSI-mRFP re-localises to an ER network pattern (Figure 4.23F). After wash-out of BFA Atgolgin-84A starts to label ring-shaped structures with long tubules (Figure 4.23G). Some of the ring-shaped structures are connected in pairs (Figure 4.23G, inset).

Some rings show protruding tubular structures (Figure 4.24) that are retractable (Figure 4.24A-C). A round structure is connected to the tubules and disconnects from the tubules and moves away (Figure 4.24E-G). AtSar1a-GFP labels ring-shaped structures but these do not show tubules

as Atgolgin-84A (Figure 4.24H, arrow). MnSI re-localises to Golgi bodies and also to the ER (Figure 4.24I, arrow).

To find out if the GFP-Atgolgin-84A puncta observed after BFA treatment were ER-localised GFP-Atgolgin-84A was co-infiltrated with mRFP-HDEL and treated with BFA 3dpi (Figure 4.25). The puncta seem to not co-localise with mRFP-HDEL (Figure 4.25).

GFP-Atgolgin-84A showed a similar pattern to AtSar1a-GFP upon BFA treatment. The Atgolgin-84A puncta resulting from BFA treatment are not ER localised (Figure 4.25). Therefore the localisation of these puncta remains unclear. AtSar1a-GFP showed a similar pattern as Atgolgin-84A in distribution after BFA treatment (Figure 4.23D and E) and therefore the puncta in both patterns as well as the cytoplasmic distribution could co-localise. Therefore, the construct mCherry-Atgolgin-84A (Figure 4.24) was used for co-expression with the AtSar1a-GFP. When infiltrated alone, mCherry-Atgolgin-84A labels aggregates of ring-shaped structures (Figure 4.18, arrow and inset) similar to what was observed for GFP-Atgolgin-84A. Therefore mCherry-Atgolgin-84A was co-infiltrated with AtSar1a-GFP in *N. tabacum* leaves to understand if both constructs would co-localise after BFA treatment. Infiltrated leaves 3 dpi were treated with BFA (Figure 4.26). mCherry-Atgolgin-84A and AtSar1a-GFP partially co-localise in cytoplasmic labelling but most of the puncta for both constructs seem to be at the same localisation as shown in yellow (Figure 4.26, white arrow).

When infiltrated alone, mCherry-Atgolgin-84A labels aggregates of ring-shaped structures (Figure 4.18, arrow and inset) similar to what was observed for GFP-Atgolgin-84A. Therefore mCherry-Atgolgin-84A was co-infiltrated with AtSar1a-GFP in *N. tabacum* leaves to understand if both constructs would co-localise after BFA treatment. Infiltrated leaves 3 dpi were treated with BFA (Figure 4.26). mCherry-Atgolgin-84A and AtSar1a-GFP partially co-localise in cytoplasmic labelling but most of the puncta for both

constructs seem to be at the same localisation as shown in yellow (Figure 4.26, white arrow). Would be interesting to do co-localisation in Zen software but the data obtained was not Airyscan data therefore repetitions using the Airyscan detector would be needed to obtain the PCC for this co-expression upon BFA treatment.

## 4.3 Discussion

### **Golgi cisterna re-shape constantly and show several tubular protrusions**

The imaging on the LSM 880 with an Airyscan detector revealed for the first time details and increased resolution of substructures in the Golgi cisternae labelled by ST-GFP, a non-functional *medial/trans*-Golgi marker (Figure 4.5). The structure seems to be very flexible and plastic and as the Golgi body moves its structure re-shapes and changes constantly. Therefore the Golgi body is not a well-defined round structure (in some time-frames as it moves it can look less round). Protrusions emanating from the Golgi body that are likely to be membrane extensions or structures more similar to tubules. These protrusions extend into the cytosol constantly reaching out and retracting back to the Golgi body (Figure 4.5A to B white arrow). Some time-frames show Golgi bodies with what looks like a boundary in the cisternae (Figure 4.5D). This is visually different from what is described in Figure 4.7B. In ST-GFP two non-fluorescent spaces are observed in the middle of the Golgi body (Figure 4.5D, red circle) like a boundary. These substructures have not been resolved before with conventional confocal microscopy (Figure 4.4). In tobacco leaf epidermal cells, 2 dpi GFP-Atgolgin-84A was detected in aggregates and puncta (Figure 4.7A) and at 3 dpi GFP-Atgolgin-84A labels ring-shaped structures that are in pairs, and fluorescence is more intense in between the 2 rings suggesting that is the region where the GFP-Atgolgin-84A is accumulating and could be causing the connection between the ring-shaped structures (Figure 4.7B). This supports the hypothesis of Atgolgin-84A being a tether and perhaps the higher levels of expression result in aggregates of ring-shaped structures. The distribution of fluorescence in the ring-pairs could be seen from a line profile (Figure 4.7E) from the red arrow of Figure 4.7D. This result is confirmed in the native system by the stable expression in *A. thaliana* where



the ring-shapes pairs were also observed with GFP fluorescence accumulating in middle of the pair (Figure 4.7C) which suggests that the Golgi phenotype observed is not due to expression in an heterologous system and therefore this validates *N. tabacum* as a good system to study Atgolgin-84A.

### **Tubular protrusions from Atgolgin-84A-labelled structures reach out to ER that re-shapes around these structures**

Protrusions emanating from the ring-shaped structures labelled by the golgin reach out to the ER when the ER is labelled with a fluorescent marker (Figure 4.8). This could be the contact site between ER and Golgi or a tether that could help the docking of the ring-shape structure to the ER and could be facilitating or preventing Golgi movement. The ring-shaped structure labelled by the golgin appears to re-shape constantly and according to the ER lacunae shape (Figure 4.8) suggesting that this specific subcompartment of the Golgi labelled by Atgolgin-84A is in close proximity and interaction with the ER. During this work the ring-shaped structures were never observed moving on top of the ER cisternae but always moving between tubules and lacunae. Aggregates of more than two ring-shaped structures were often observed (Figure 4.10D) and these appear not to move much compared single ring-shaped structures labelled by GFP-Atgolgin-84A or Golgi bodies labelled by ST-GFP. Furthermore, no tubular structures were observed to or from the red aggregate. The aggregates appear to be floating in the lacunae (Figure 4.10F) as if it had lost connection to what drives movement or possibly the machinery responsible for movement is unable to move the aggregate that is 4 times the usual ring-shaped structure. Another explanation would be that the overexpression of the motif for tethering not only tethers several ring shapes but also tethers the ring-shapes to other

structures and this is preventing movement, like a glue causing the aggregate to be blocked in its track.

### **Atgolgin-84A seems to co-localise more with COPII carriers than with Golgi markers and its localisation is distinguishable from AtCASP**

The use of Airyscan detection requires a re-definition of co-localisation and a more accurate and objective method to describe the localisation of markers that are in very close proximity or even only partially in the same compartment. The structures labelled by Atgolgin-84A and the markers described in this chapter were analysed using Zen (Zeiss) software. These data suggests that Atgolgin-84A is at least in part in a subcompartment between the ER and the *cis*-Golgi. When was co-expressed with AtSar1a-GFP, a COPII component and co-localisation was assessed. Both proteins alone labeled ring-shaped structures but together only small structures (variable but less than 1  $\mu\text{m}$ ) (Figure 4.19). Further independent experiments are needed to confirm these results but the preliminary data here shows that Atgolgin-84A and AtSar1a might have the same interactors or be recruited to the same subdomains and therefore competing with each other during overexpression which might cause them to fall off the Golgi. This suggests that Atgolgin-84A might have a role in the tethering COPII components to the Golgi during assembly of the transporters. The ability of golgins, including golgin-84, to tether vesicles in mammalian cells was shown *in vitro* using purified golgins and isolated vesicle fractions by Malsam *et al.*, (2005) and later this was confirmed in intact cells by Wong and Munro, (2014).

GFP-Atgolgin-84A and MnSI-mRFP are shifted with respect to each other and only partially co-localise and some ring-shaped compartments are only labelled by MnSI-mRFP which could indicate unstacking of the Golgi cisternae when GFP-Atgolgin-84A is overexpressed. GFP-Atgolgin-84A was

not detected in the centre of the round-shape structures whereas MnSI-mRFP often labeled the centres of cisterna (Figure 4.14) which supports the hypothesis that Atgolgin-84A is tethered at the rims of the cisternae. The different distribution is explained by the first studies using fluorescent proteins when GFP-tagged Golgi proteins such as resident glycosylation enzymes, like mannosidase were found to diffuse freely without constraints within the Golgi membranes in photobleaching experiments (for review see Schoberer and Strasser, 2011). Due to the shift observed between another *cis*-Golgi marker N-acetylglucosaminyltransferase I (GnTI-mRFP) was used for *cis*-Golgi labelling. GFP-Atgolgin-84A was detected in aggregates with high intensity of fluorescence connecting the ring-shaped structures. GnTI-mRFP does not accumulate in-between the ring-shapes where the intensity of Atgolgin-84A is higher at the rims of the cisternae. GnTI-mRFP, as observed for MnSI, has higher intensity in the centre of the cisternae, decreases intensity in the centre of the aggregate which is the region where GFP-Atgolgin-84A increases drastically in intensity.

AtCASP (AT3G18480) is a golgin homologue of human CASP identified in *A. thaliana*. AtCASP has been implicated in tethering between the ER and Golgi (Osterrieder *et al.*, 2017). When the mutant AtCASP $\Delta$ 1-564 without coiled-coil domains was expressed in Arabidopsis the tethering between ER and Golgi was affected. In Osterrieder *et al.* (2017) AtCASP full-length and mutant Golgi body speed and displacement were analysed using standard confocal microscopy. Golgi body speed and displacement were significantly reduced in the mutant overexpression. Optical tweezers were used to assess any ER-Golgi connection. The trapping power required to trap and move Golgi bodies was reduced from that required to manipulate Golgi bodies during expression of ST-mRFP (Osterrieder *et al.*, 2017). Therefore, Atgolgin-84A and AtCASP were co-infiltrated in tobacco in order to check for possible co-localisation of both golgins (Figure 4.16). Given the shift between *cis*-Golgi markers and GFP-Atgolgin-84A, another *cis*-golgin mRFP-AtCASP (Renna *et al.*, 2005; Latijnhouwers *et al.*, 2007;

Osterrieder *et al.*, 2017) was co-infiltrated with GFP-Atgolgin-84A. If both golgins are localised at the *cis*-Golgi cisternae there should be a co-localisation of both golgins, but the co-expression of both golgins showed only a partial co-localisation. This preliminary data was analysed with Zen software and the PCC value is higher than any other combination of markers tested (Table 4-2) but due to the low *n* numbers more repeats are needed to further investigate the subcompartment specific localisation.

GFP-Atgolgin-84A is localised towards the ER, partially at the *cis*-face of the Golgi but not entirely as it does not completely co-localise with any of the *cis*-Golgi markers used. This data points to a possible localisation of GFP-Atgolgin-84A at a sub-region of the *cis*-face of the Golgi. The overexpression of the protein that is fused to a fluorescent protein it has to be taken into account as this could have an effect on the golgin localisation and could be disrupting the tethering ability of the golgin which could increase the distance to the *cis*-cisternae or the high amount of golgin could be inducing oligomerisation of the golgin which could lead to the aggregates of ring-shapes observed. Mammalian golgin-84 has been suggested to be a tether of vesicles to Golgi membranes and to be involved in maintaining Golgi stacking (Seemann *et al.*, 2000b; Short *et al.*, 2005).

One possibility is that a new Golgi stack is generated by producing two Golgi stacks from a pre-existing stack or ERES (Hawes *et al.*, 2010). It could be that when the golgin is overexpressed and not fully functional then one effect could be the non-separation of the stacks and reflected in the presence of the clusters.

## **BFA treatment shows that Atgolgin-84A does not redistribute to the ER as is documented for other Golgi markers**

If Atgolgin-84A is located at the *cis*-Golgi we could predict to see a redistribution of the protein into the ER with BFA as it happens for the *cis*-Golgi markers (Schoberer *et al.*, 2010). On BFA treatment the *medial/trans*-Golgi marker ST redistributes to the ER before the golgin AtCASP which indicates differences in distributional persistence of a golgin and a membrane-bound Golgi enzyme (Osterrieder *et al.*, 2009b). Here the distribution of GFP-Atgolgin-84A was compared to the distribution of an ERES marker AtSar1a-GFP and a *cis/medial*-Golgi marker, MnSI-mRFP. After BFA incubation MnSI-mRFP redistributed to the ER (Figure 4.23F) as described for the *cis*-Golgi enzyme GnTI-mRFP (Schoberer *et al.*, 2010). AtSar1a-GFP labelled the cytoplasm and small puncta (Figure 4.23E) but not the ER. AtSar1a-GFP should be in the cytoplasm before BFA treatment as it should be only recruited to the ERES during assembly of the transport carrier. Therefore the protein stays in the cytoplasm when ER and Golgi hybridise in one compartment on BFA treatment. This might mean there is a disassembly of the ERES or this is not fully functional during treatment or the other components for the COPII carrier formation are not able to recruit AtSar1a during BFA treatment. GFP-Atgolgin-84A distribution was similar to AtSar1a-GFP (Figure 4.23D and E) in the cytoplasm and small puncta. After washout MnSI-mRFP labelled the Golgi and also the ER (Figure 4.23I) in a similar to the pattern of GnTI-mRFP described in Schoberer *et al.*, (2010). The ER labelling may be due to newly synthesised protein that should be transported to the Golgi if the washout was monitored for longer. AtSar1a-GFP was found in the cytoplasm and in ring-shaped structures (Figure 4.23H), presumably Golgi bodies. GFP-Atgolgin-84A labeled ring-shaped structures with long tubules protruding out of the rings (Figure 4.23G). Pairs of ring-shaped structures were observed with fluorescence accumulating in

between them. GFP-Atgolgin-84A redistribution is similar to the ERES marker AtSar1a-GFP and does not redistribute to the ER during BFA treatment. After washout Atgolgin-84A was often found in puncta, which support the theory that during biogenesis, the golgin has a role in maintaining the Golgi stack like a scaffolding linked to other elements of a putative Golgi matrix, and this is affected when GFP-Atgolgin-84A is overexpressed. More interestingly, these puncta look very similar to the pattern observed for the expression of Atgolgin-84A 2 dpi (Figure 4.7A). With the high-resolution afforded by the Airyscan detector it is possible to resolve substructures during reassembly of the Golgi. These structures labelled by Atgolgin-84A were not completely round and had several long protruding structures that could be tubules or remnants of membrane. These long structures elongate and retract back to the ring-shaped structure several times during imaging (Figure 4.24, Appendix I, Movie 9).

In order to understand where the GFP-Atgolgin-84A small puncta observed were located, the same BFA treatment was performed after co-expression of GFP-Atgolgin-84A with mRFP-HDEL for ER labelling. The puncta did not colocalise with the mRFP-HDEL labelling and thus the ER, and seem to be in a different focal plane than the mRFP-HDEL network (Figure 4.25). Considering GFP-Atgolgin-84A and AtSar1a-GFP have similar patterns during BFA treatment, both proteins were co-infiltrated and incubated in BFA under the same conditions (Figure 4.26). mCherry-Atgolgin-84A showed the same phenotype as the GFP version showing clusters of ring-shaped structures and the labelling was restricted to the rims of the cisternae with accumulation of fluorescence in the connection of several ring-shaped structures (Figure 4.18). After BFA incubation both proteins labelled the cytoplasm and small puncta (Figure 4.26) and seem to co-localise. Further experiments would be necessary for PCC analysis. These data indicate that the golgin falls off Golgi membranes easily and possibly stays forming a scaffold for the formation of the Golgi stack. This supports the hypothesis that a putative Golgi matrix of, which the golgins are

suggested to be part of, would be holding the stack together. The Golgi matrix was suggested in mammalian cells when after detergent-treatment of Golgi membranes a proteinaceous exoskeleton remained, retaining Golgi structure. Electron microscopy showed the existence of intercisternal elements and a ribosome-excluding zone around the stack, in plant cells which was suggested to be the equivalent of the Golgi matrix (Kristen, 1978; Staehelin and Moore 1995). These results indicate similar sub-localisation of the ERES marker and Atgolgin-84A and similar order of redistribution during deconstruction of the Golgi.

**The data presented in this chapter not only highlights the difficulties associated with PCC analysis but for the first time suggests the presence of a new pre-*cis*-Golgi compartment post-ER which may contain COPII ERES components. The localisation of Atgolgin-84A 2dpi is very similar to what is observed after BFA treatment which suggests a localisation of the golgin in a suggested matrix that could be holding the Golgi stack together and could be the scaffolding for the reassembly of a new stack.**



Figure 4.1: Zeiss LSM 880 with Airyscan detector at Oxford Brookes University with temperature and CO<sub>2</sub> controlled incubator.



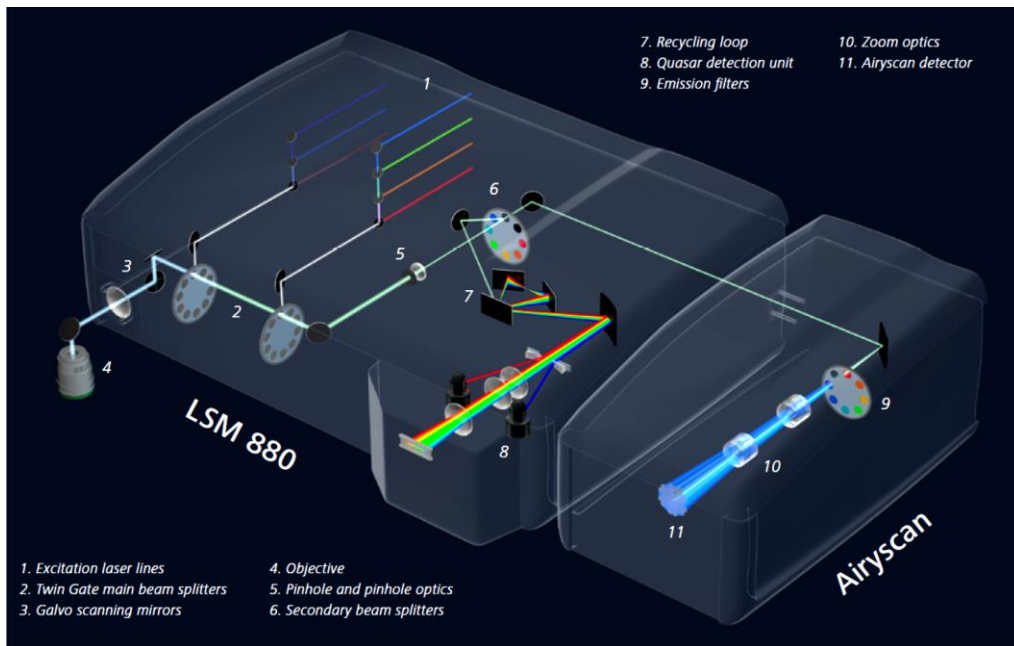


Figure 4.2: Beam path in the Airyscan unit attached to the Zeiss LSM 880 (from Huff *et al.*, 2015).

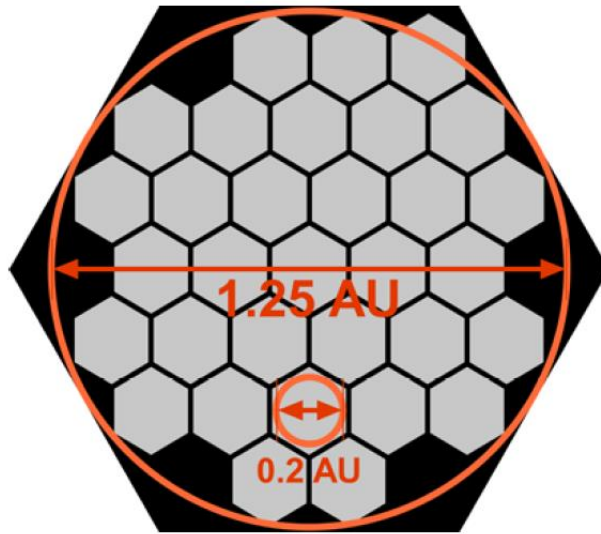


Figure 4.3: Airyscan detector design from Huff *et al.*, (2015). One element lies on the optical axis and acts like a classical point detector. The other elements are grouped around the central one, in a hexagonal pattern. In the example each detector element acts as a pinhole of size 0.2 Airy units (AU) but the whole detector area captures light of 1.25 AU. The 0.2 AU determines the sectioning and resolution in x, y and z, whereas the 1.25 AU determines the sensitivity.

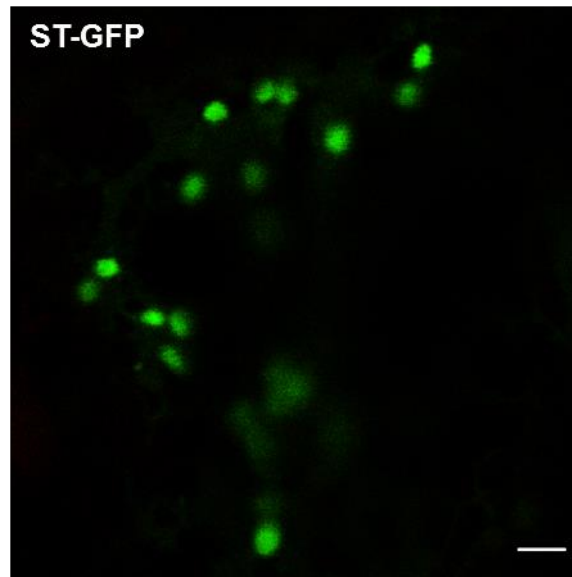


Figure 4.4: *Trans*-Golgi marker ST-GFP expression in *N. tabacum* two days post-infiltration (2dpi). Imaging performed using the standard confocal mode of the Zeiss LSM 880. Scale bar, 2  $\mu$ m.

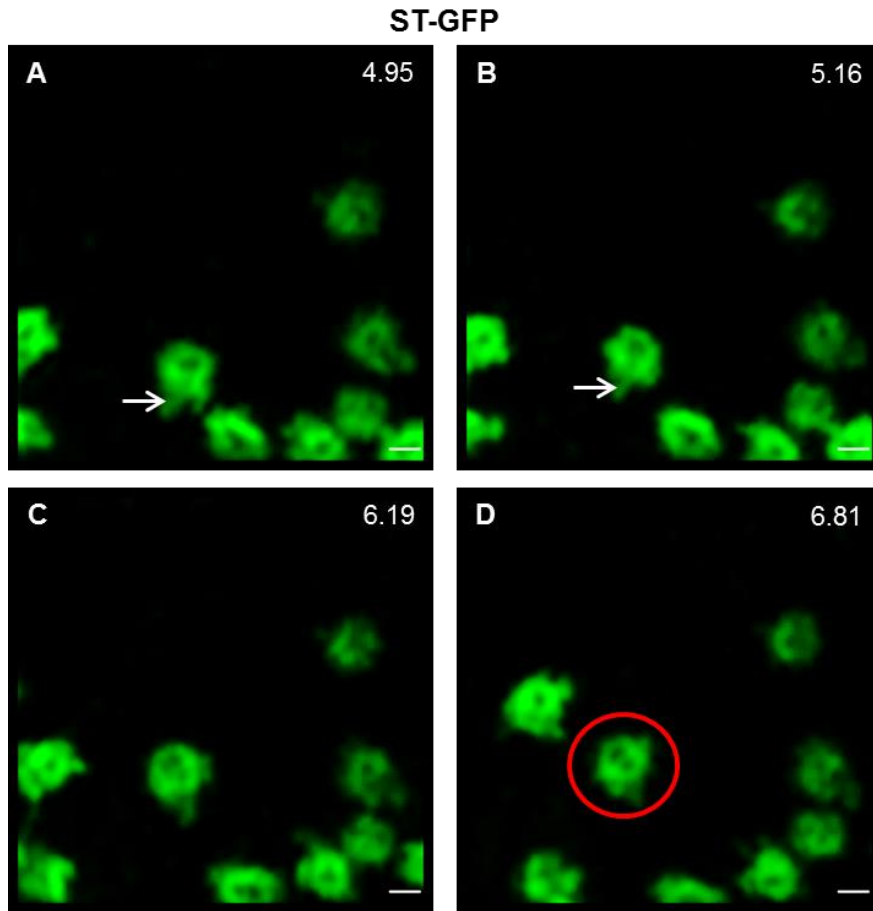


Figure 4.5: Airyscan high resolution imaging of the *trans*-Golgi marker ST-GFP stable *A. thaliana* plants (Appendix I, Movie 1). (A) Golgi bodies detected are ring-shaped structures with protruding retractable structures emanating from the Golgi bodies (white arrows). (B) These tubules look retractable as observed from (A) to (B) white arrow. (C) Most of the Golgi bodies have short protrusions. (D) High resolution shows several Golgi bodies with substructure at the centre of the ring (red circle). Time-frames in seconds. Scale bars, 1  $\mu\text{m}$ .

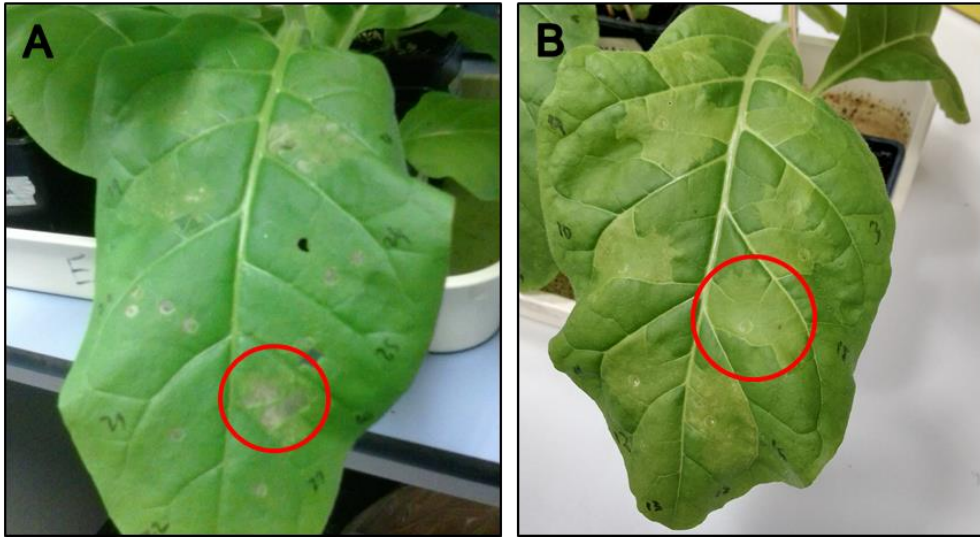


Figure 4.6: *N. tabacum* plants infiltrated with GFP-Atgolgin-84A. (A) 3 dpi leaf region using *Agrobacteria*  $OD_{600}=0.1$  (red circle). (B) 3 dpi infiltrated leaf region using *Agrobacteria*  $OD_{600}=0.02$  (red circle).

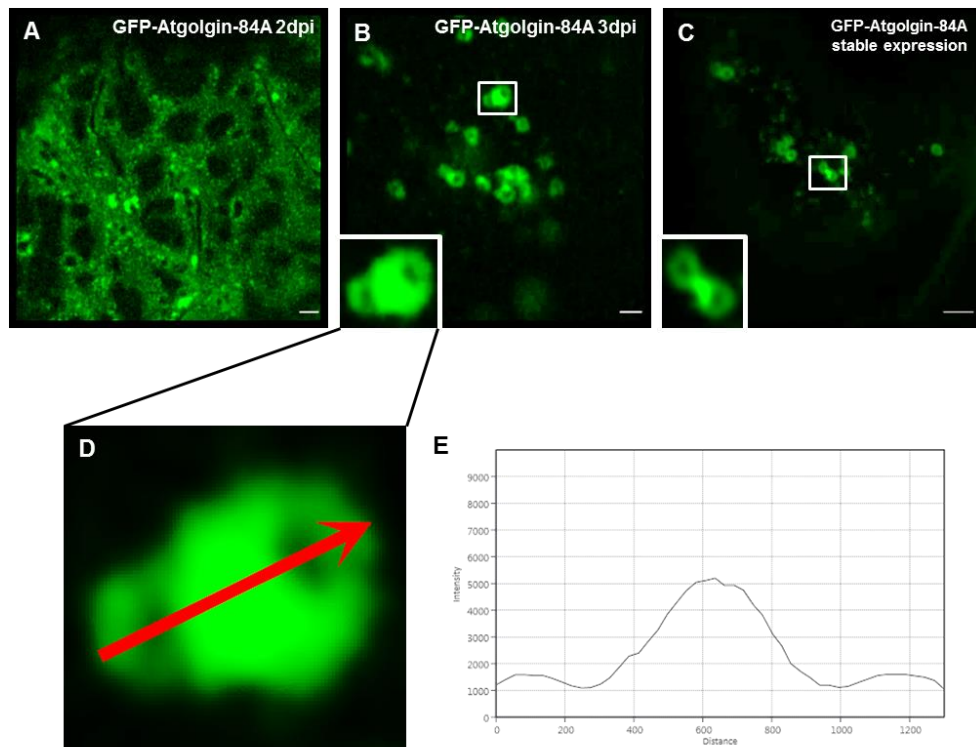


Figure 4.7: Expression of GFP-Atgolgin-84A in *N. tabacum* (A, B, D and E) and *A. thaliana*. (A) Cytoplasmic localisation of Atgolgin-84A 2dpi showing distinct puncta. (B) GFP-Atgolgin-84A labels ring-shaped structures at 3dpi. Accumulation of Atgolgin-84A between ring-shaped structures can also be seen (inset). (C) GFP- Atgolgin-84A stable expression in *A. thaliana* showing pairs of ring-shaped structures. (D) Magnification of a pair of ring-shaped structures labelled by Atgolgin-84A. (E) Line profile showing the intensity of fluorescence across the arrow in D. Scale bars, 1  $\mu\text{m}$ .

Table 4-1: Number of pairs of Golgi bodies observed during expression in *N. tabacum* of ST-GFP and GFP-Atgolgin-84A.

Construct	Total <i>n</i> of movies	Total <i>n</i> of Golgi bodies observed	Total <i>n</i> of pairs observed
ST-GFP	11	273	0
GFP-Atgolgin-84A	8	163	16

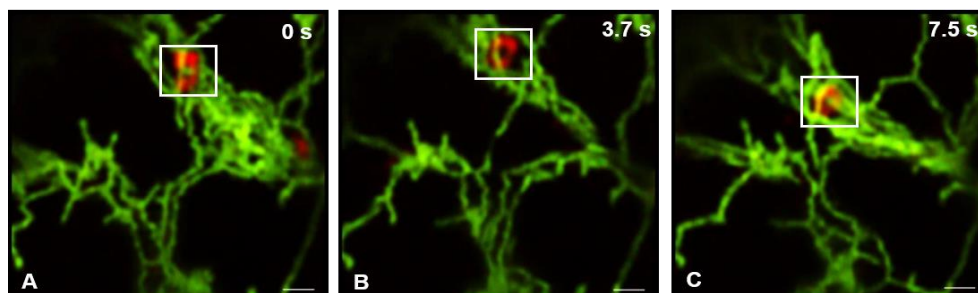


Figure 4.8: Co-expression of mCherry-Atgolgin-84A and GFP-HDEL in *N. tabacum* showing re-shaping of ring-shaped compartment (Appendix I, Movie 2). (A) Ring-shape is not round and shows a distorted shape adjusted to the ER lacunae (white arrows). (B) Golgi body changes shape and a tubular structure is detected extruding from the ring-shape labelled by Atgolgin-84A. (C) ER strands seem to be directed to the middle of the Golgi body. Scale bars, 1  $\mu\text{m}$ .

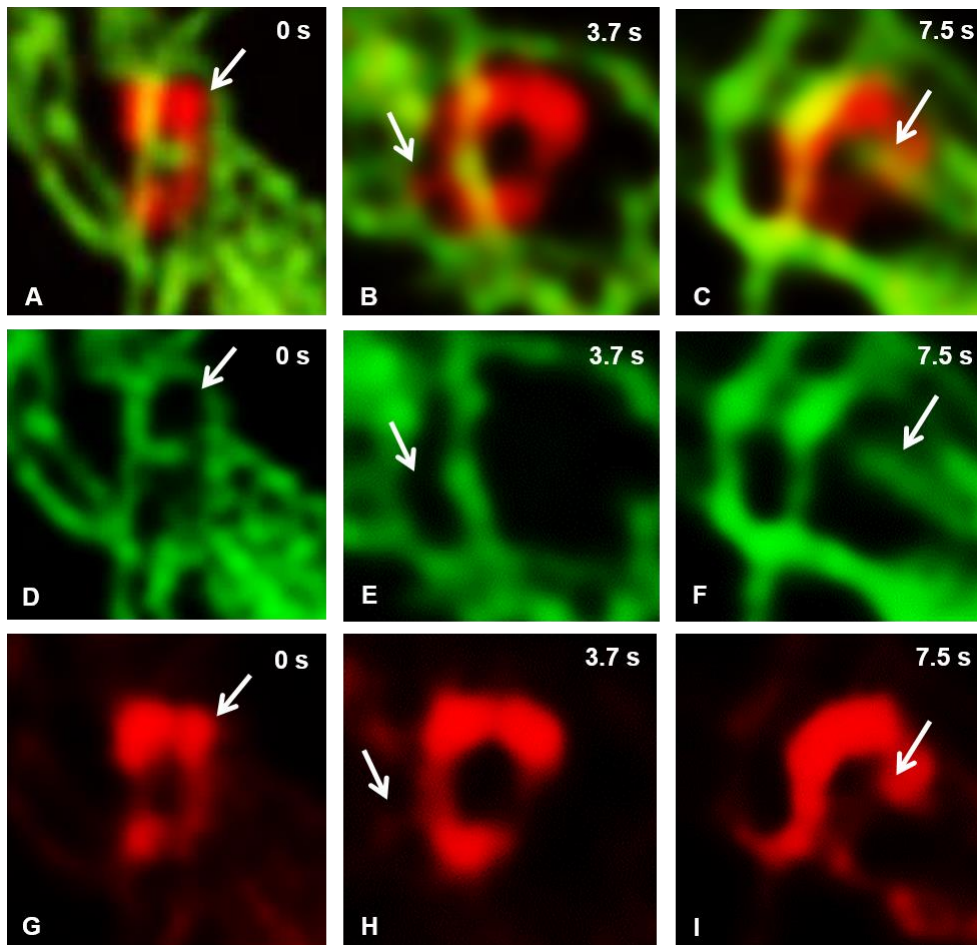


Figure 4.9: Enlargement of inset in Figure 4.8B. (A-C) Overlay of green and red channels. (D-F) Green channel. (G-I) Red channel. (A) Atgolgin-84A-labelled structure seems to adjust to ER lacunae shape adopting an almost square-shape. (B) Tubular protrusion from the ring-shaped structure to the ER. (C) ER tubule seems to disappear into the black space in the middle of the ring-shaped structure and ER tubules seem to surround the Atgolgin-84A structure.



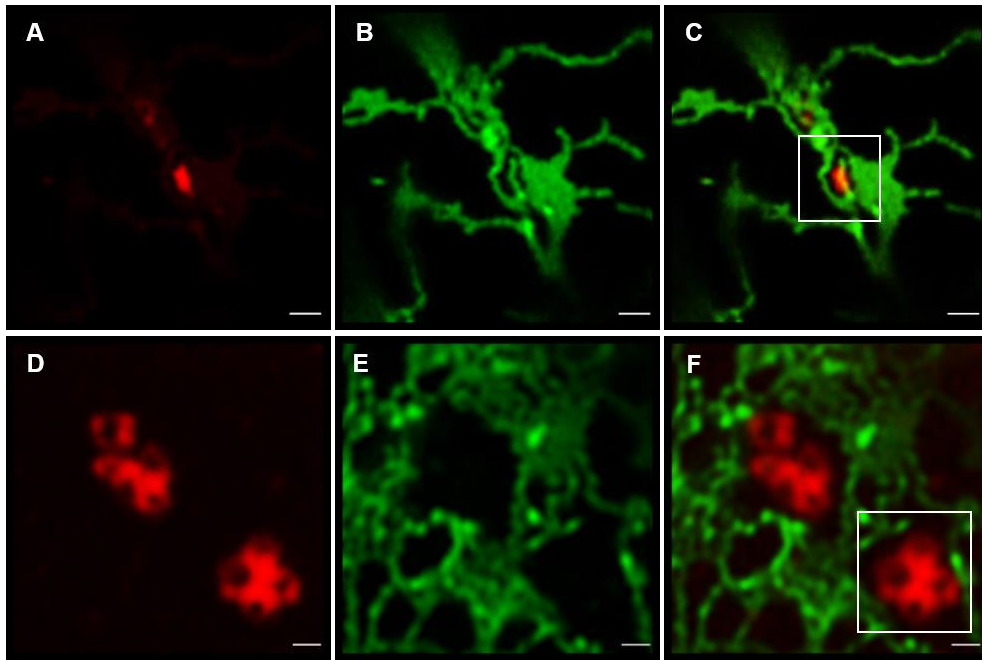


Figure 4.10: Co-expression of mCherry-Atgolgin-84A and GFP-HDEL in *N. tabacum*. (A-C) Detail of ER tubule above golgin-labelled compartment (Appendix 1, Movie 3). (D-F) Aggregates of ring-shaped structures in the ER lacunae (Appendix 1, Movie 4). Scale bar, 1  $\mu$ m.

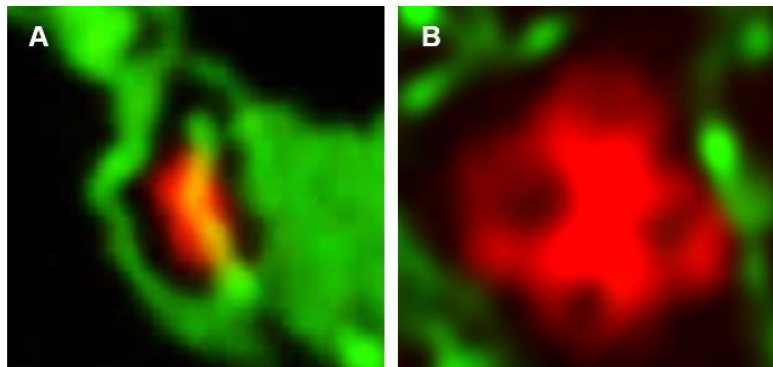


Figure 4.11: Enlargement of Figure 4.9. (A) A tubule from the ER is in the middle of lacunae, appearing to be above the Atgolgin-84A-labelled compartment, in another focal plane. (B) An aggregate of four ring-shaped compartments in the ER lacunae.

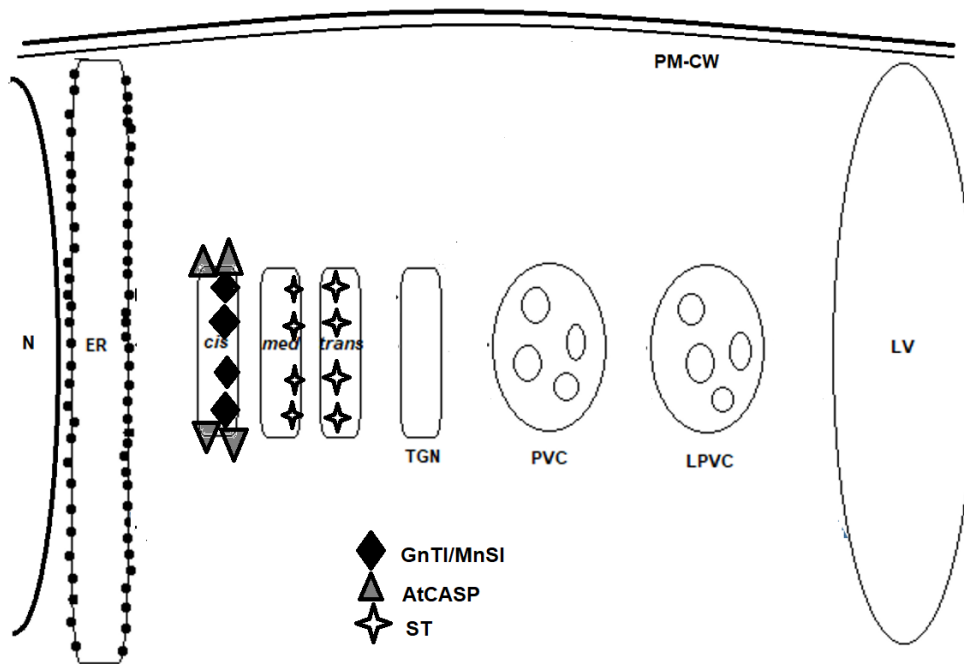


Figure 4.12: Localisation of the different Golgi markers mentioned in this chapter within the Golgi stacks *cis*-, *medial*-, *trans*-Golgi from left to right.

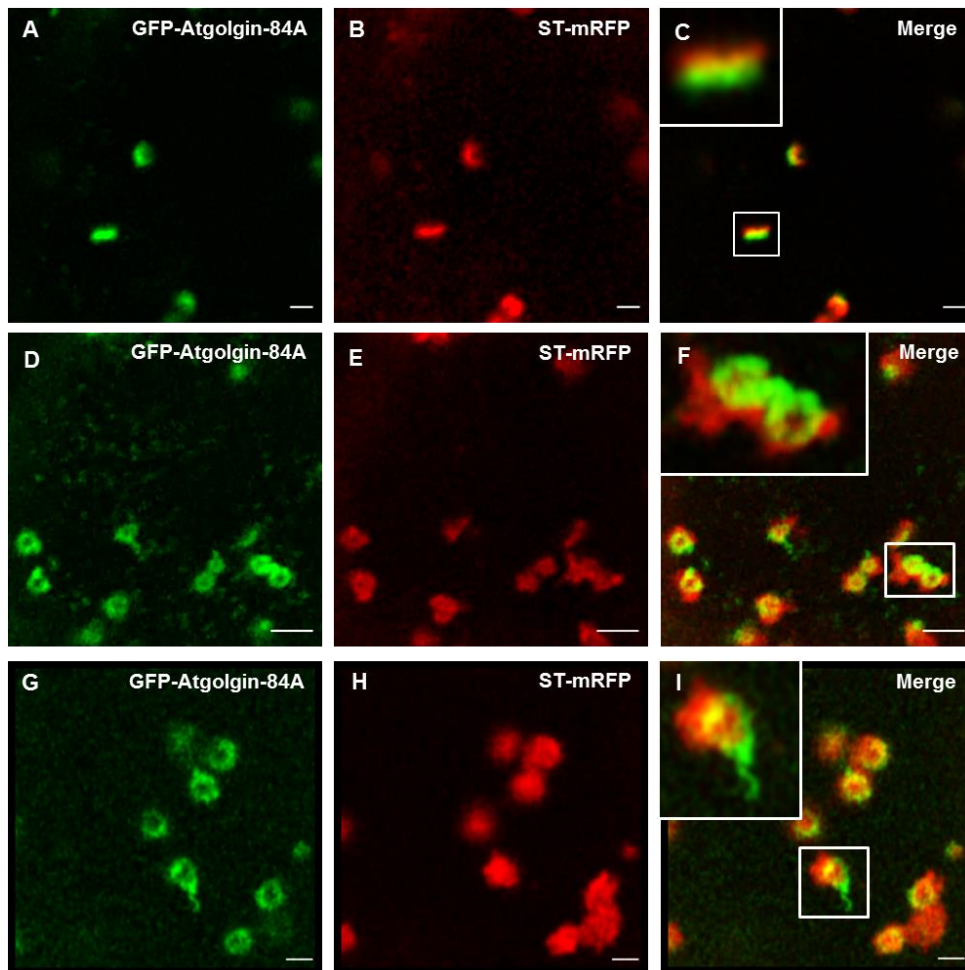


Figure 4.13: Co-expression of GFP-Atgolgin-84A and ST-mRFP in *N. tabacum*. Atgolgin-84A and ST appear shifted with respect to each other. (A-C) The shift between both colours is clearly visualized using high-resolution confocal microscopy. (C) Atgolgin-84A partially co-localises with ST-mRFP but in side view appears to be in different cisternae (inset). Often Atgolgin-84A shows protruding tubular structures (D-F) (Appendix 1, Movie 5). Several pairs of ring-shaped structures are linked by a tubular structure (G-I) (Appendix 1, Movie 6). The protruding tubules are only labelled by GFP-Atgolgin-84A (I, inset). Imaging was performed using a Zeiss LSM 880 with Airyscan. Scale bars, 1  $\mu\text{m}$ .

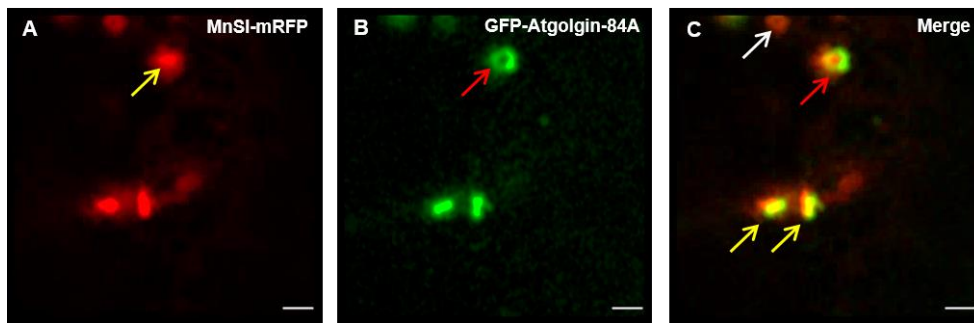


Figure 4.14: Co-expression of MnSI-mRFP and GFP-Atgolgin-84A in *N. tabacum*. (A-B) Atgolgin-84A is more restricted to the rims of the cisternae than MnSI that is more evenly distributed across the cisternae (yellow arrow). (C) Atgolgin-84A labels ring-shaped structures and only partially co-localises with MnSI and appears shifted with respect to each other (red arrow). Some Golgi bodies labelled by MnSI do not seem to be labelled by Atgolgin-84A in the same cell (C, white arrow). In side view (C, yellow arrows) there is labelling of two different subcompartments of the Golgi body and only the region between cisternae shows some co-localisation. Scale bars, 1  $\mu\text{m}$ .

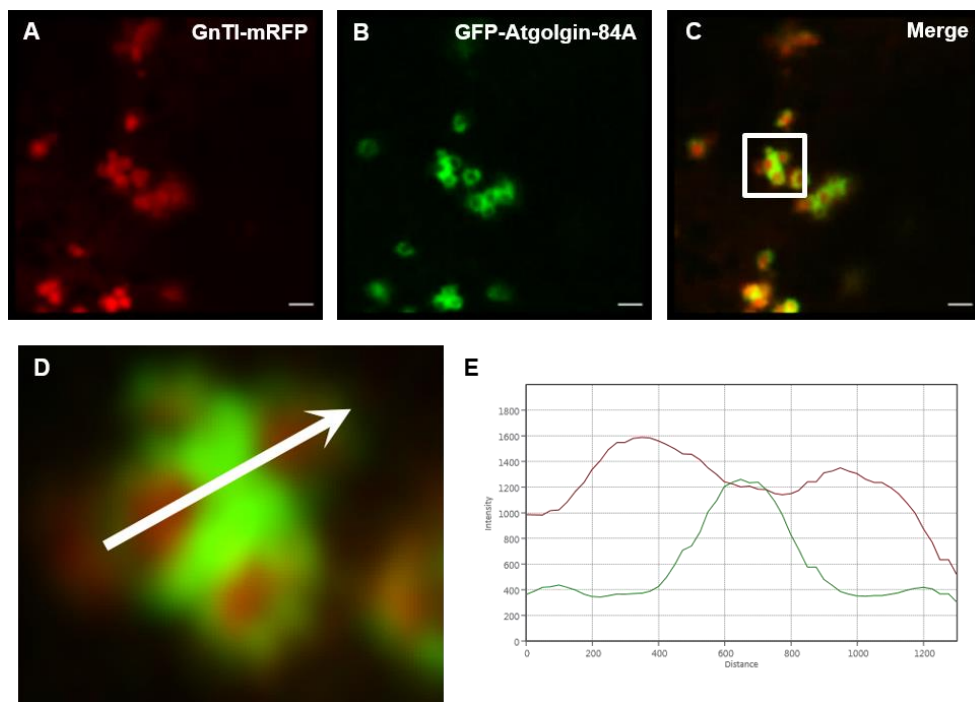


Figure 4.15: Co-expression of GnTI-mRFP and GFP-Atgolgin-84A in *N. tabacum*. (A) GnTI labels *cis*-cisternae in Golgi bodies. (B) Ring shaped structures labelled by GFP-Atgolgin-84A appear connected. (C) Co-expression with GnTI shows that Atgolgin-84A labels a ring-shaped structure, does not label the centre of the *cis*-cisternae compared to GnTI and clusters several Golgi bodies together (inset). (D) Magnification of aggregate in figure 4.15C. (E) Line profile showing distribution of Atgolgin-84A (green line) compared to the *cis*-Golgi marker GnTI (red line) in the Golgi cluster. For GnTI the intensity is higher in the Golgi bodies and lower in the middle of the aggregate. Atgolgin-84A has higher intensity in the middle of the aggregate and is almost absent from the centre of the Golgi bodies. Scale bars, 1  $\mu\text{m}$ .

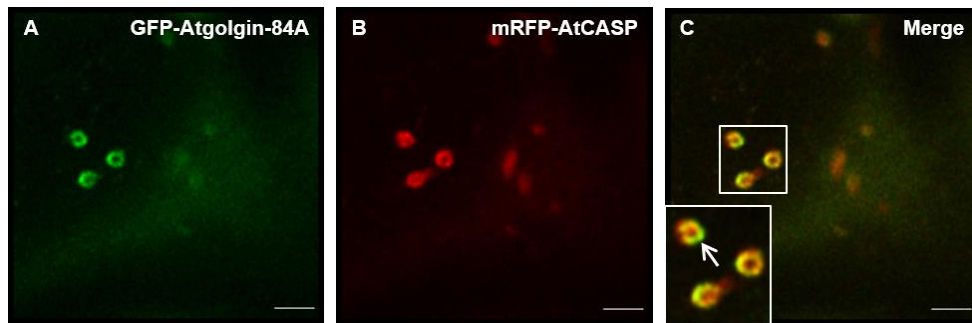


Figure 4.16: Co-expression of GFP-Atgolgin-84A and mRFP-AtCASP in *N. tabacum* leaf epidermal cells. (A and B) GFP-Atgolgin-84A and mRFP-AtCASP label ring-shape compartments. (C) Green and red channel do not overlay completely suggesting that Atgolgin-84A and AtCASP might have at least partially different sub-domain localization. Scale bars, 2  $\mu$ m.

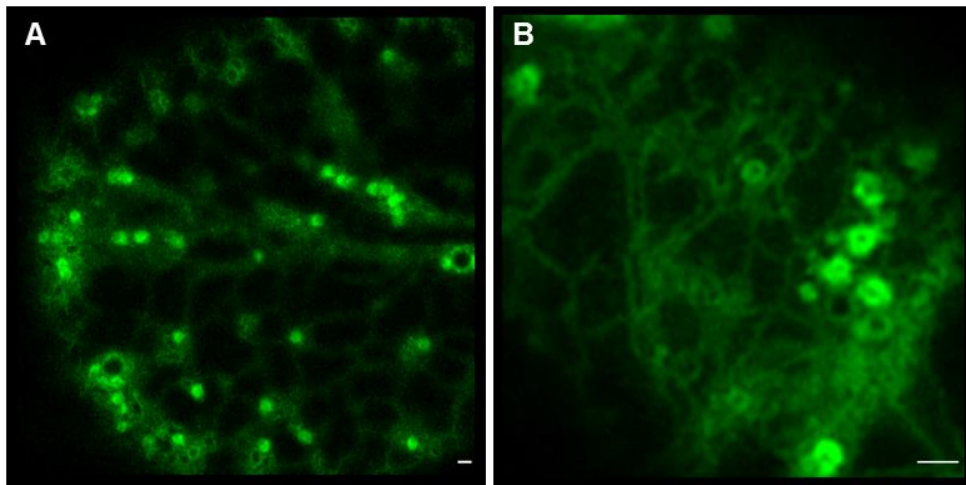


Figure 4.17: Expression of AtSar1a-GFP in *N. tabacum*. (A) AtSar1a-GFP labels round-shaped structures and the cytoplasm (Appendix 1, Movie 7). (B) The round-shaped structures are ring-shaped with some protruding structures (Appendix 1, Movie 8). Scale bars, 1  $\mu\text{m}$ .

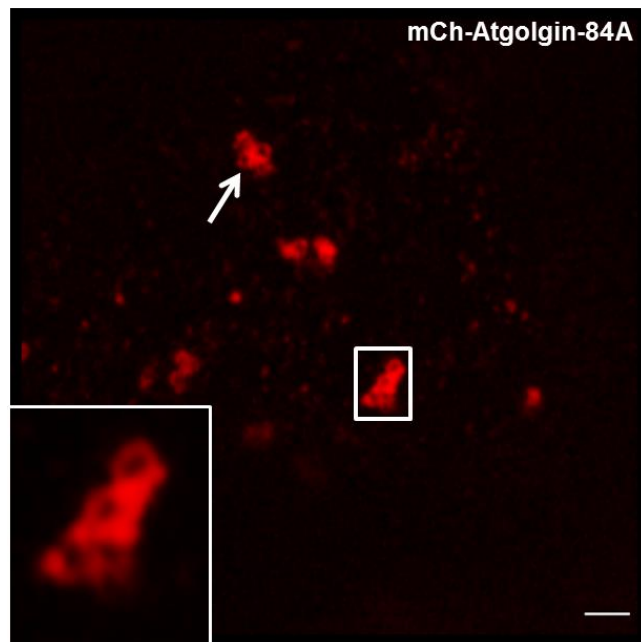


Figure 4.18: Transient expression of mCh-Atgolgin-84A in *N. tabacum* leaf epidermal cells 3 dpi. mCherry-Atgolgin-84A ring-shaped structures are in aggregates and fluorescence of mCherry is more intense in some regions mainly where the ring-shaped structures connect to each other similar to what was observed for GFP-Atgolgin-84A. Scale bar, 2  $\mu\text{m}$ .



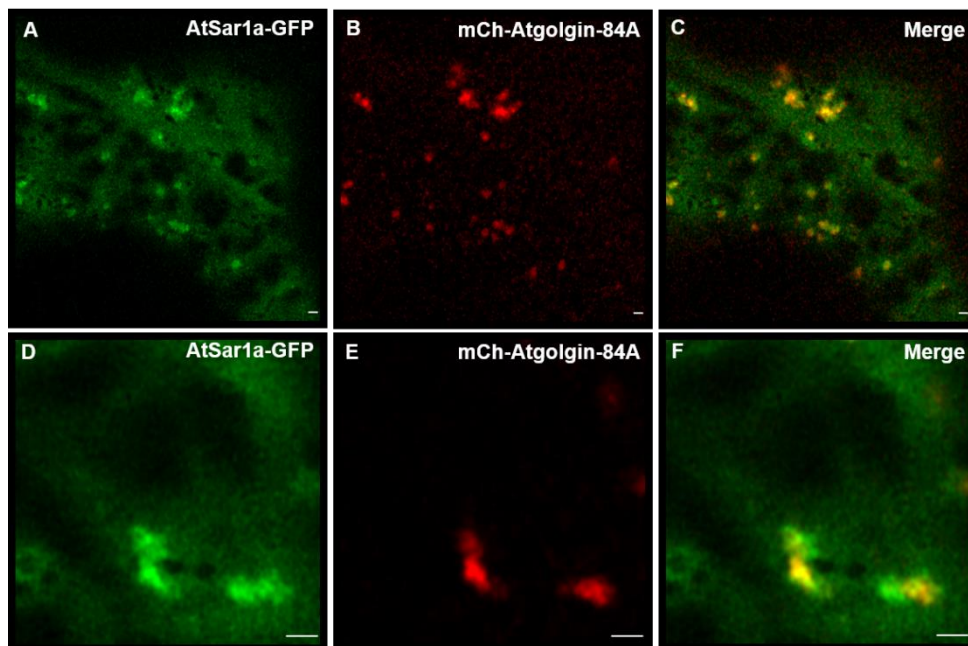


Figure 4.19: Co-expression of AtSar1a-GFP and mCherry-Atgolgin-84A in *N. tabacum*. (A) AtSar1a-GFP expression. (B) mCherry-Atgolgin-84A expression. (C) Overlay of both channels showing co-localisation of Atgolgin-84A and AtSar1a. (D-F) Enlargement of some structures labelled by both markers. (D) Green channel for AtSar1a-GFP. (E) Red channel for mCherry-Atgolgin-84A. (F) Overlay of structures labelled by both markers showing AtSar1a-GFP surrounding mCherry-Atgolgin-84A labelled structures. Scale bars, 1  $\mu\text{m}$ .

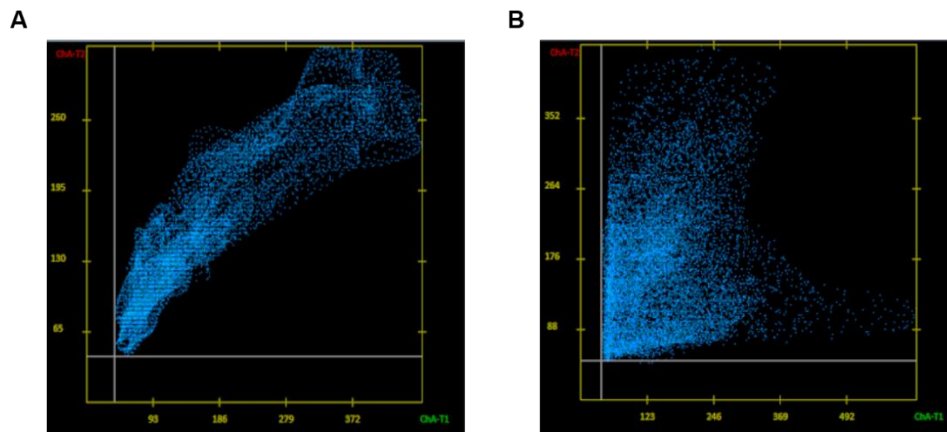


Figure 4.20: Examples of scatterplots for two markers. (A) PCC values close to 1 for GnTI-mRFP and MnSI-GFP. (B) PCC close to 0 for two markers uncorrelated, GFP-Atgolgin-84A and ST-mRFP.

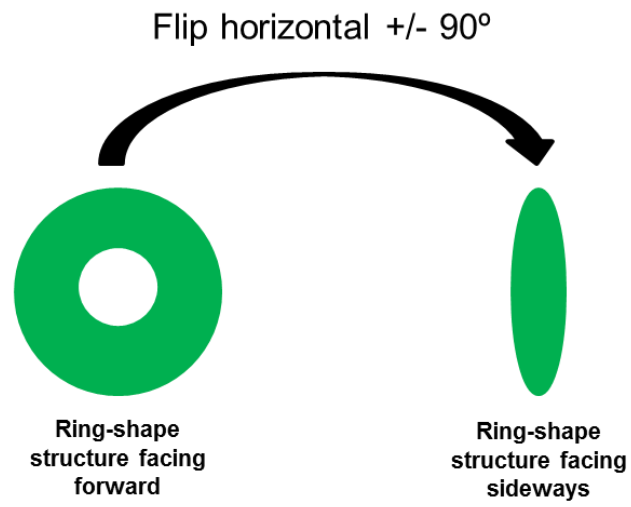


Figure 4.21: Schematic representation of different objects selected for analysis. In each frame some Golgi bodies are facing the coverslip showing the ring shape and others are facing sideways towards the coverslip.

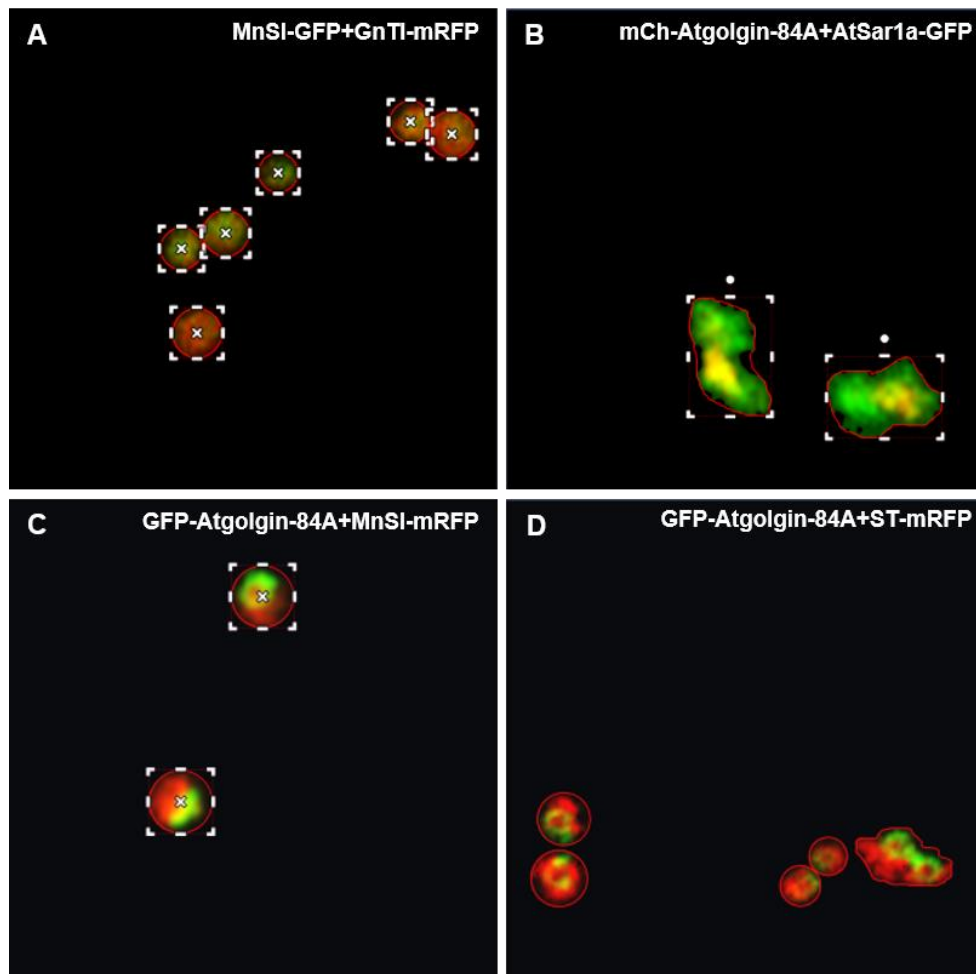




Figure 4.22: Examples of ROIs used for co-localisation analysis in merged images of green and red channel using Zen (Zeiss) software. (A) MnSI-GFP and GnTI-mRFP. (B) mCherry-Atgolgin-84A and AtSar1a-GFP. (C) GFP-Atgolgin-84A+MnSI-mRFP. (D) GFP-golgin-84A and ST-mRFP.

Table 4-2: Co-localisation analysis of Atgolgin-84A and markers for the Golgi, AtCASP and COPII transporters. Pearson's correlation coefficients (PCCs) for the different combinations of markers are given.

<b>Pearson's correlation coefficient (PCC)</b>				
<b>Object's position</b>			<b>n</b>	
	<b>Side view</b>	<b>Face view</b>	<b>Side view</b>	<b>Face view</b>
<b>MnSI-GFP + GnTI-mRFP</b>	0.76	0.78	23	28
<b>GFP-Atgolgin-84A + AtSar1a-GFP</b>		0.63		19
<b>GFP-Atgolgin-84A+AtCASP</b>		0.81		9
<b>GFP-Atgolgin-84A + MnSI-mRFP</b>	0.44	0.43	1	1
<b>GFP-Atgolgin-84A + ST-mRFP</b>	0.49	0.40	8	25

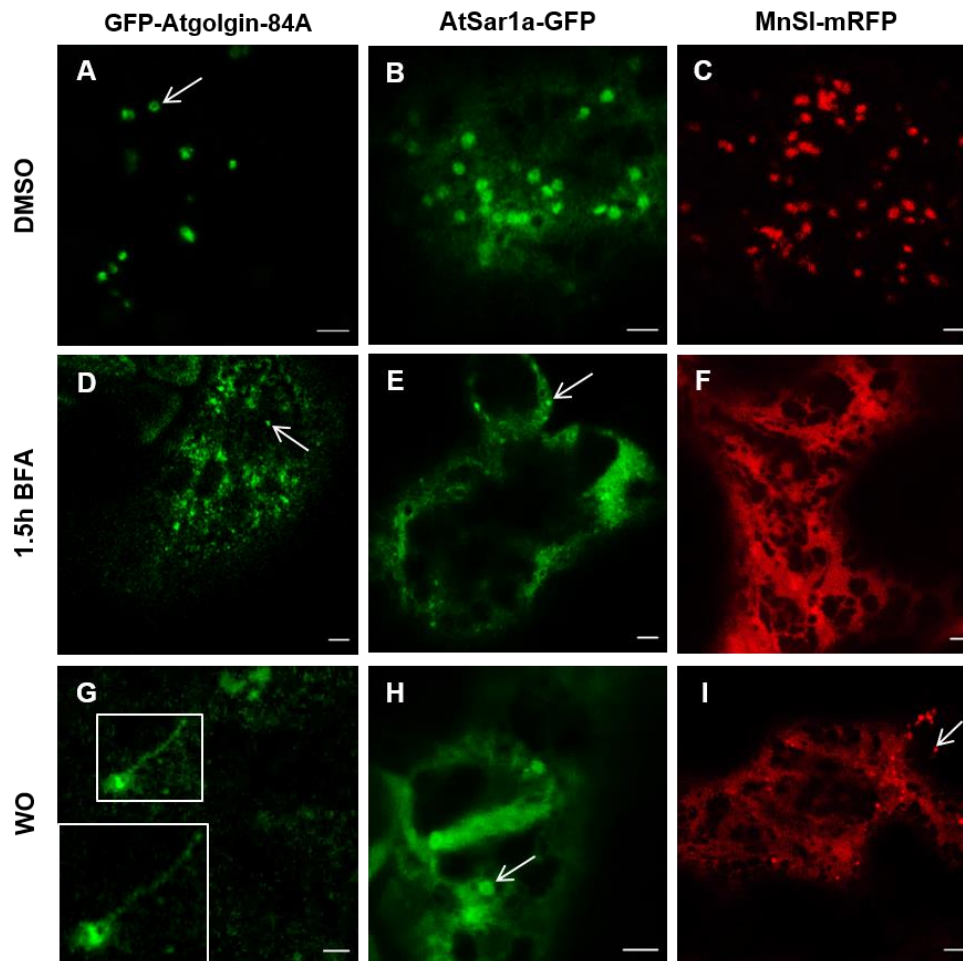


Figure 4.23: BFA treatment on leaves expressing GFP-Atgolgin-84A, AtSar1a-GFP and MnSI-mRFP. Leaves expressing Atgolgin-84A (A), AtSar1a (B) and MnSI (C) were incubated in DMSO and motile round-shaped structures (A, arrow) similar to non-treated leaves incubated in water. After incubation in BFA for 1.5h Atgolgin-84A (D) and AtSar1a (E) re-localises to the cytoplasm and pleomorphic puncta (D and E, arrows). MnSI-mRFP (F) re-localise to the ER that shows mainly cisternal regions and few tubular structures. After BFA wash-out (WO) for 3.5h Atgolgin-84A starts to localise to ring-shaped structures and 6.5  $\mu\text{m}$  long tubular structures extruding (G, inset) from ring-shapes are observed (G). AtSar1a re-localises to ring-shaped structures (H, arrow) and MnSI re-localises to round-shaped *cis*-Golgi structures (I, arrow). Scale bars, 1  $\mu\text{m}$ .

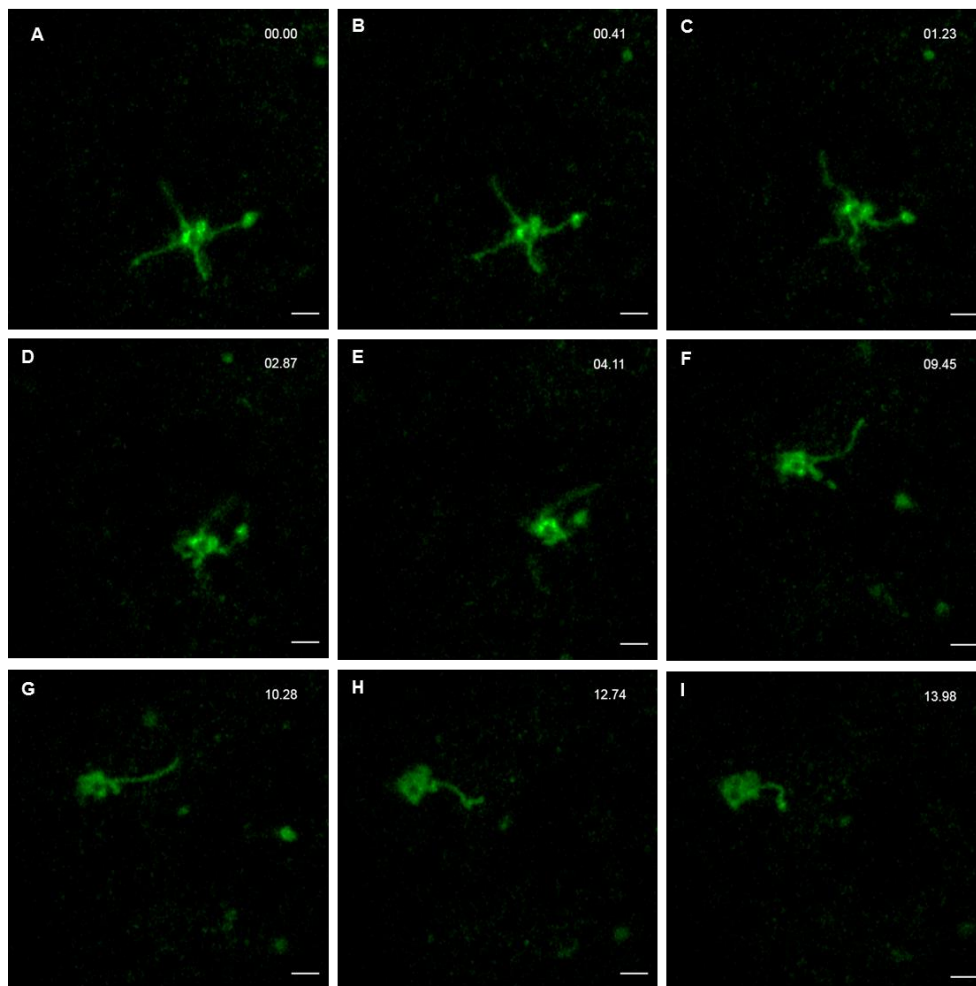


Figure 4.24: Time frames from a movie showing Atgolgin-84A BFA wash-out compartments (Appendix 1, Movie 9). (A) Round-shape structure shows four tubules protruding out of the ring structure. The tubular structures appear to extend and contract. (B-E). The smaller round structure connected to one of the tubules disconnects from the tubule (F). The small structure moves alone (G). The ring only shows one tubule (H). In (I) the ring shape structure appears to be in fact two ring-shapes. Time frames in seconds. Scale bars, 1  $\mu\text{m}$ .

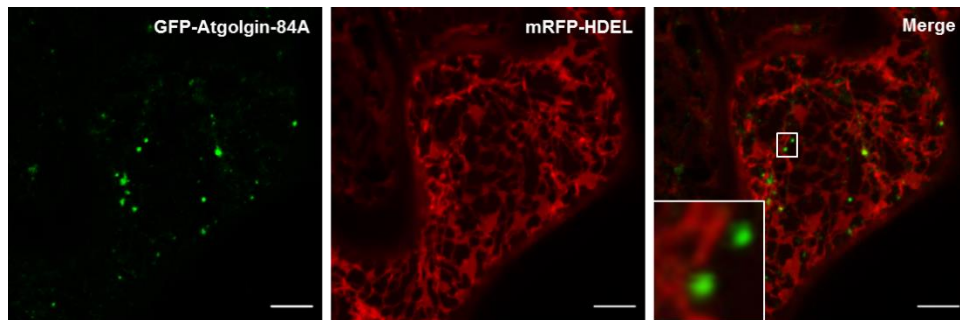


Figure 4.25: Co-expression of GFP-Atgolgin-84A and mRFP-HDEL after BFA treatment. GFP-Atgolgin-84A punctae do not co-localise with mRFP-HDEL (inset). Scale bars, 5  $\mu$ m.



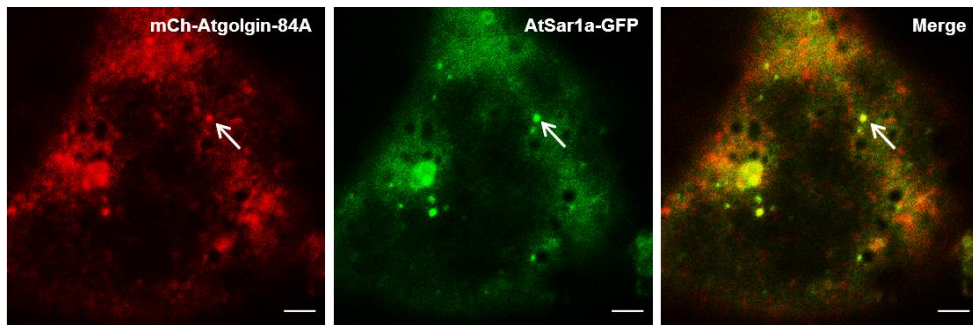


Figure 4.26: Co-expression of mCh-Atgolgin-84A and AtSar1a-GFP after BFA treatment. mCherry-Atgolgin-84A and AtSar1a-GFP co-localise and show cytoplasmic localisation and the puncta from both proteins co-localise (inset). Scale bars, 2  $\mu$ m.

## 5. Co-localisation of truncated protein Atgolgin-84A $\Delta$ 1-557

### 5.1 Introduction

Atgolgin-84A is predicted to have long coiled-coil domains and these are suggested to be the tethering motif in the golgin structure (Figure 5.1). In order to investigate the function of the coiled-coil domains, an Atgolgin-84A $\Delta$ 1-557 construct was obtained by deleting the N-terminal region predicted to be coiled-coil (Latijnhouwers *et al.*, 2007) (Figure 5.1). Using a similar approach as for the human golgin-84, the Atgolgin-84A deletion mutant comprises the TMD, and approximately 100 amino acids preceding the TMD and this region (amino acids 558–707) is necessary and sufficient for Golgi localisation (Latijnhouwers *et al.*, 2007).

This mutant lacks amino acids 1-557. Atgolgin-84A $\Delta$ 1-557 fused to the C-terminus of GFP (Latijnhouwers *et al.*, 2007) was infiltrated in *Nicotiana tabacum* as described in chapter 2 to observe if there would be changes in localization compared to the full-length expression or a different phenotype. In order to confirm localisation of Atgolgin-84A $\Delta$ 1-557 in the native system, *A. thaliana* cotyledons were transiently transformed with GFP-Atgolgin-84A $\Delta$ 1-557 as described in chapter 2. Additionally, stable expression of GFP-Atgolgin-84A $\Delta$ 1-557 in *A. thaliana* was obtained by floral-dip transformation described in chapter 2, in order to confirm the localisation when the mutant is stably and constitutively expressed in the native system. The mutant was co-infiltrated in *N. tabacum* with several markers in order to understand if the coiled-coil domains deletion affects the localisation of the protein. To do this, markers for the *medial-trans*-Golgi, *cis*-Golgi, and ERES were infiltrated. A red version of Atgolgin-84A $\Delta$ 1-557 using the mCherry fluorescent protein (mCh-Atgolgin-84A $\Delta$ 1-557) was also obtained for co-localisation studies with GFP markers well described in the literature for the COPII components.

## 5.2 Results

### 5.2.1 High-resolution imaging of Atgolgin-84A $\Delta$ 1-557 expression in different plant systems

Figure 5.1 is a schematic representation of the region deleted from the full-length Atgolgin-84A to obtain the mutant Atgolgin-84A $\Delta$ 1-557.

GFP-Atgolgin-84A $\Delta$ 1-557 transient expression in *N. tabacum* shows ring-shaped structures with protruding tubular structures (Figure 5.2A and B, Appendix I, Movie 10). In *A. thaliana* transient expression, the ring shapes are similar to those found in tobacco (Figure 5.2C and D). Several ring shapes smaller than 1  $\mu$ m in diameter labelled with GFP-Atgolgin-84A $\Delta$ 1-557 are also detected (Figure 5.2D, arrows).

To confirm the localisation and phenotype observed in *N. tabacum* transient expression, *A. thaliana* plants were floral-dipped with GFP-Atgolgin-84A $\Delta$ 1-557 and mCh-Atgolgin-84A $\Delta$ 1-557. Both fluorescent fusions were detected in ring-shaped structures that often show tubules protruding out of the ring (Figure 5.3A, arrow, Appendix I, Movie 11). The ring-shaped structures detected re-shaped constantly during movement. The structures showed short tubular extensions in what looks like movement in and out of the ring-shaped structure (Figure 5.3A, white arrow). Additionally long tail-like structures (tubules) were detected (Figure 5.3 A, inset). Smaller ring (<1  $\mu$ m, often 0.5  $\mu$ m) shapes are detected similar to what was observed in transient expression (Figure 5.3B, white arrow and also C, yellow arrow). Clusters are also observed (Figure 5.3D).

## 5.2.2 High-resolution imaging of Atgolgin-84A $\Delta$ 1-557 in co-expression with an ER marker

mCh-Atgolgin-84A $\Delta$ 1-557 labelled compartments appear more rounded ring-shaped structures and the ER surrounds the ring shaped structure shaping as if accommodating the ring-shaped structure (Figure 5.4 in enlargement E-G). In Figure 5.4A anchor points of ER can be observed (white arrows) that stay in the same position during the time series (Figure 5.4 B-D, Appendix I, Movie 12) (Staehelein and Chapman, 1987; Staehelein, 1997; Perico and Sparkes, 2018). Fine tubular protrusions can be observed emanating from the ring-shaped compartment labelled by mCherry-Atgolgin-84A $\Delta$ 1-557 (Figure 5.4E). ER tubular extensions were detected and it is not clear if they are connecting to the ring-shaped structure (note the yellow colour in Figure 5.4 F, white arrow) or if the ER tubules are in another focal plane above the ring-shaped compartment as it was observed in the expression of Atgolgin-84A (Chapter 4, Figure 4.8, 4.9 and 4.10).

## 5.2.3 High-resolution imaging of Atgolgin-84A $\Delta$ 1-557 co-expression with different Golgi markers

Several Golgi markers (described in chapter 4, section 4.2.4) were co-expressed with GFP-Atgolgin-84A $\Delta$ 1-557. In this chapter first the phenotypes and localisations observed are described. First the best known Golgi marker ST-mRFP for *medial/trans*-Golgi labelling was co-infiltrated with GFP-Atgolgin-84A $\Delta$ 1-557.

Both GFP-Atgolgin-84A $\Delta$ 1-557 and ST-mRFP label ring-shaped structures but they are shifted with respect to one another, not completely overlapping (Figure 5.5, Appendix I, Movie 13). This indicates that GFP-

Atgolgin-84A $\Delta$ 1-557 is not at the *medial/trans*-Golgi. Some of the ring-shaped structures have protruding tubules (Figures 5.5 and 5.6, yellow arrows). A ring-shaped structure labelled by both markers shows a protruding structure only labelled by GFP-Atgolgin-84A $\Delta$ 1-557, which in Figure 5.5 and 5.6A is very close to another ring-shape structure, but does not look connected. In frame Figure 5.5 and 5.6B, this protruding structure seems to connect with another tubule from another ring-shaped structure (white arrow). The first tubule slides on the second one (Figure 5.5 and 5.6C) before disconnecting and moving away from the second structure. In Figure 5.5 and 5.6D what looks like a free tubular structure (blue arrow) moves between Golgi bodies.

In Figure 5.7 GFP-Atgolgin-84A $\Delta$ 1-557 appears to be in a different subcompartment that seems to sit on the ST-mRFP labelled cisternae and shows some protruding structures not labelled by ST-mRFP.

GFP-Atgolgin-84A $\Delta$ 1-557 was co-infiltrated with the *cis*-Golgi marker  $\alpha$ -mannosidase MnSI-mRFP. GFP-Atgolgin-84A $\Delta$ 1-557 co-localises more with MnSI-mRFP than the full-length (PCC 0.80 and 0.64). Some of the ring-shaped structures look like they are only labelled by MnSI-mRFP with only very weak GFP-Atgolgin-84A $\Delta$ 1-557 expression (Figure 5.8C, white arrows, Appendix I, Movie 14 and 15). This was also observed in the expression of full-length GFP-Atgolgin-84A (chapter 4, Figure 4.14). GFP-Atgolgin-84A $\Delta$ 1-557 is more restricted to the rims, while MnSI is detected in the whole cisterna (Figure 5.8F, white arrow).

During overexpression of GFP-Atgolgin-84A $\Delta$ 1-557 several protruding structures similar to tubules were observed (Figure 5.9, yellow and white arrows, Appendix I, Movie 16). Some of these structures are connecting ring-shaped structures (Figure 5.9, yellow arrow) and others are moving as if they are reaching into the cytoplasm in a random movement (Figure 5.9, white

arrows). In Figure 5.9F (white arrow) the protruding structure branches off into two tubular structures while reaching into the cytoplasm.

Considering the partial co-localisation of GFP-Atgolgin-84A $\Delta$ 1-557 with MnSI-mRFP a *cis*-Golgi marker, the same co-infiltration was performed in the native system *A. thaliana* using transient expression in order to confirm the phenotypes observed in tobacco transient expression. Here the shift between the two proteins seems to be more obvious than in tobacco as smaller ring-shaped structures are observed and the structures labelled by MnSI are 1  $\mu$ m size in diameter but few GFP-Atgolgin-84A $\Delta$ 1-557 are approximately 0.5 $\mu$ m (Figure 5.10C, yellow arrow, Appendix I, Movie 17 and 18). Two small rings labelled by GFP-Atgolgin-84A $\Delta$ 1-557 are connected to larger *cis*-Golgi shapes (Figure 5.10, yellow arrow). The rings labelled by GFP-Atgolgin-84A $\Delta$ 1-557 are closer, more connected in the aggregate in Figure 5.9C (white arrow). This is different from the expression of GFP-Atgolgin-84A where the Golgi aggregates showed an accumulation of GFP-Atgolgin-84A in between ring-shaped compartments (chapter 4, Figure 4.15). Both proteins appear in different subcompartments (Figure 5.10F, inset). In the ring, GFP-Atgolgin-84A $\Delta$ 1-557 is labelling regions as if it is constricted to certain regions (Figure 5.10A).

GFP-Atgolgin-84A $\Delta$ 1-557 seems to be in a different sub-compartment from the *cis*-Golgi marker in Figure 5.10F. Therefore GFP-Atgolgin-84A $\Delta$ 1-557 was co-infiltrated with a *cis*-golgin mutant mRFP-AtCASP $\Delta$ 1-164 in order to understand if the localisation of coiled-coil deletions is the same as full-length.

GFP-Atgolgin-84A $\Delta$ 1-557 appears more restricted to specific regions of the rims of cisternae than mRFP-AtCASP $\Delta$ 1-164 (Figure 5.11C, Appendix I, Movie 19 and 20) Ring-shaped structures appear flipped very often when both mutants are co-expressed (Figure 5.11F). They seem to co-localise in

the side view, i.e. flipped sideways (Figure 5.11C) but not in completely in face view (Figure 5.11F).

When both mutants are co-expressed the long tubular protusions are more visible, even though this still an extremely dynamic and fast event, but it was possible to measure the length of one tubule linking two ring-shaped structures (Figure 5.12C and F, white arrows, Appendix I, Movie 21). This was the longest tubule (approximately 7  $\mu\text{m}$ ) that was visible for a measurement and it is only an example which means the tubules that can possibly be longer or smaller.

### **5.2.5 High-resolution imaging of Atgolgin-84A $\Delta$ 1-557 with YFP-Sec24A, a component of the COPII transporters**

Similar to the full-length golgin, it was difficult to co-express the golgin with AtSar1a-GFP, as it does not label distinct ring-shaped structures anymore and instead just a few pleomorphic structures with very weak expression not sufficient for imaging (data not shown). Figure 5.14 is a rare example of what was observed in co-expression with a fluorescent fusion of the *A. thaliana* Sec24a, YFP-Sec24a construct another COPII component marker. YFP-Sec24a alone labels round-shape compartments (Figure 5.12). In co-expression with the mCherry-Atgolgin-84A $\Delta$ 1-557 smaller round shapes (different sizes less than 1  $\mu\text{m}$ ) are also observed labelled by YFP-Sec24a (Figure 5.14, yellow arrow, Appendix I, Movie 22). As it was a rare event to obtain expression of both markers, it was not possible to do statistically meaningful co-localisation analysis using Zen software. Although the indication was that both markers were in the same compartment.

## 5.2.6 Co-localisation analysis on Airyscan imaging data

To better understand if the deletion of the long-coiled domain region affects the localisation of the golgin, co-localisation analysis was performed in the software Zen (Zeiss) using the same method as described in chapter 4 for the full-length protein. Co-localisation was analysed for the co-expression of the mutant with MnSI-mRFP and ST-mRFP. Figure 5.14 shows examples of the ROIs selected for the analyses. Side view ring-shaped compartments (Figure 5.15A and C) were counted separately from the face view ring-shaped labelled compartments (Figure 5.15B and D). PCC was obtained for each object, and the graph and table in Table 5-1 shows the PCC mean for each co-expression. The co-expression of GnTI-mRFP with MnSI-GFP was used as a positive control for co-localisation as for the analysis for the full-length golgin (chapter 4, section 4.2.4).

The deletion mutant seems to co-localise more with MnSI with a PCC of 0.80 than the full-length golgin with a PCC of 0.44. In the case of the mutant there is a strong correlation with the *cis*-Golgi marker, which was not the case for the protein with coiled-coil domains. For the face view objects the PCC decreases, but still is a positively strong correlation. The PCC is low for the side view objects of co-expression with ST-mRFP (0.23) (Figure 5.5, 5.6, 5.7 and table 5-1), lower than the co-expression for the full-length (0.49) (table 5-1). For the face view the PCC increases to 0.56, which indicates a positive correlation between the two fluorescent fusions which is due to the imaging face view versus side view (table 5-1).



## 5.2.7 Quantification of sideways ring-shaped structures during expression of Atgolgin-84A $\Delta$ 1-557

During imaging of Atgolgin-84A $\Delta$ 1-557 it was observed that the ring-shaped structures often flip, i.e. they turn 90° with respect to the cell surface (for example, Figure 5.8D) which is not the case for expression of a standard Golgi marker such as ST-GFP alone (chapter 4, Figure 4.5). This means that during a time series, ST-GFP labelled structures would look like a ring, and in case of Atgolgin-84A $\Delta$ 1-557 flipped structures, the side of the shaped is observed instead of the ring, as represented in chapter 4, Figure 4.21. This ability to flip sideways by 90° was quantified for ST-GFP and GFP-Atgolgin-84A $\Delta$ 1-557 by counting how many ring-shaped structures flip during a time series (Figure 5.16).

The ring-shaped structures were assessed for flipping or not flipping during a time series. Obtained data indicates that only 9% of the total of Golgi structures observed during ST-GFP expression were flipping sideways which is 13 of the 140 Golgi bodies that were counted and 90% were facing forwards (Figure 5.16) i.e., not flipping during the time series. When Atgolgin-84A $\Delta$ 1-557 is expressing 43% of the ring-shaped structures flip sideways which is 59 of the 136 total objects counted and only 58% are observed facing forward (Figure 5.16) throughout the duration of the time series. The hypothesis that the differences between ST-GFP and deletion mutant are due to randomness is rejected. The Golgi bodies flipping to side view more often than in ST-GFP is a real pattern in the population of all the Golgi bodies given the p-value of  $1.123 \times 10^{-10}$  in the Chi-squared test.

## 5.3 Discussion

The Atgolgin-84A deletion mutant was obtained by amplification of the 125 amino acids C-terminal region. This region was found to be sufficient for transport of the protein to the Golgi (Renna *et al.*, 2005). Therefore, in the final deletion mutant sequence, used throughout this work, remains part of a predicted coiled-coil domain and a transmembrane domain (Figure 5.1).

In chapter 3 the structure of the Atgolgin-84A full-length protein was bioinformatically analysed and the region corresponding to the mutant sequence is predicted with a high degree of confidence (558-707 amino acid residues) as described in chapter 3 (Figure 3.4). This sequence contains mainly a small coiled-coil region and a transmembrane domain (Figure 5.1B). A phosphorylation hotspot is predicted, which means a region with several amino acids predicted to be phosphorylated, and several of the sites are experimentally confirmed (PhosPhAt 4.0). This region is part of the mutant sequence (Figure 3.5).

When the N-terminus of the protein was deleted this could expose any potential post-translational modification sites such as phosphorylation sites. Both cleavage of golgins and phosphorylation have been suggested to induce Golgi disassembly (for review see Witkos and Lowe, 2016). Furthermore it is described that cleavage of the golgin could also induce fragmentation of the Golgi and unstacking of cisternae as a consequence of impaired golgin tethering activity as has been described for mammalian golgins (Witkos and Lowe, 2006) This could be compared to expression of the deletion mutant, as it could be considered as a fragment of the protein. This could explain the observations in Figure 5.2D and 5.3 of smaller size ring-shaped structures which could be the fragmentation of the Golgi bodies in plant cells and these structures could resemble Figure 5.6 subcompartments/cisternae are strongly labelled by one protein and weakly by the other marker which could be due to the unstacking of cisternae. The

deletion mutant could mimic the cleavage product as only the C-terminal region of the protein is produced. According to prediction in this mutant there is one coiled-coil domain remaining and also according to prediction in the mutant sequence there is high protein binding activity (Figure 3.4C). This could mean that there is still some tethering function or interaction with other proteins present. Although by deleting the N-terminus, the remaining domains in the mutant protein structure may be more exposed to interaction or to post-translational modifications.

If the function affects tethering and maintenance of Golgi the stack as previously suggested (for review see Osterrieder *et al.*, 2012) this would explain the observed phenotype in Figures 5.2B, 5.5 and 5.9.

### **Expression of GFP-Atgolgin-84A $\Delta$ 1-557 *in planta* shows that mutant expression induces a different phenotype in Golgi bodies**

The phenotypes observed during transient expression in both plant systems are very similar but in *A. thaliana* expression seems to be more constricted to the rims and subdomains of the ring-shaped structure (Figure 5.2D) which is something that was not observed for the expression of the full-length GFP-Atgolgin-84A and mRFP-AtCASP (chapter 4, Figure 4.16). In the native system the smaller size ring-shaped structures seem to be more abundant (Figure 5.2D). Indicating that in Arabidopsis the mutant might be titrating out a native Atgolgin-84A more efficiently than in *N. tabacum*. Also Atgolgin-84A in the native system may increase the quantity of golgin but in *N. tabacum* will compete with the native golgin.

The phenotype was confirmed in stable expression (Figure 5.3) and long tubules were observed (Figure 5.3A) that could be compensating as a form of a membrane connection for the lack of the long coiled-coil domains and therefore the fully functional tethers.

## **Co-expression with an ER marker shows the re-shaping is associated to ER movement and connections between both compartments**

In chapter 4, the full-length golgin tagged with mCherry was co-infiltrated with the ER marker GFP-HDEL. It was observed that the ring-shaped structures labelled by Atgolgin-84A were re-shaping constantly in and appeared to be to filling the ER lacunae and adjusting to the edges of the ER cisternae. Another possibility is that the ER re-shapes to follow the Golgi changes. The coiled-coil domains contain the putative tethering motif and the hypothesis is that these domains have a role in tethering ER to Golgi. Therefore, as in chapter 4 the deletion mutant Atgolgin-84A $\Delta$ 1-557 was also co-infiltrated with the ER marker GFP-HDEL.

The enhanced resolution of the Airyscan detector permits imaging of the structure and re-shaping of the ER including what may be anchor points to the plasma membrane that stay very stable during the duration of the movie (Figure 5.4A, white arrows). Similar to what was observed for the full-length construct the ring-shaped structures labeled by the deletion mutant fits the ER lacunae like in a key-lock arrangement (Figure 5.4E-G). As the ring-shaped structure and the ER move there seems to be a protruding structure emanating from one of the organelles (Figure 5.4F and G, white arrows) that seems to connect both organelles.

The co-expression with the ER-marker GFP-HDEL shows that the mutant it is not so constricted to the rims of the cisternae (Figure 5.4) as the full-length protein (see also chapter 4, Figure 4.8 and 4.9). The ring-shaped structure also changes shaped during movement and the ER and ring shaped structure still act as a key-lock arrangements re-shaping according to each other and appears to be even more adjusted to the ER lacunae (Figure 5.4E-G) than the ring-shaped structures labelled by the full-length construct (see chapter 4, Figure 4.8 and 4.9). There seems to be short, fine tubular emanations from the ER to the ring-shaped structure (Figure 5.4B-G)

which are additional evidence for the close relationship between the two compartments.

### **Co-expression with Golgi markers confirms the differences in phenotype between full-length and mutant**

Long tubules labelled by the mutant protein seem to connect Golgi bodies (Figure 5.5) and some seem to slide on each other (Figure 5.5 and 5.6A-C). Some tubules are labelled by the *trans*-Golgi marker and not by the mutant golgin, which could indicate that even though the mutant is not in the same cisternae as ST-mRFP, it is affecting the whole structure of the stack as the tubules are also present in the *trans*-Golgi (Figure 5.5B). Although both cisternae with different fluorophores move together, both proteins do not seem to co-localise confirmed by the low (<0.5) PCC in Table 5-1.

When GFP-Atgolgin-84A $\Delta$ 1-557 was also co-expressed with a *cis*-Golgi marker the Golgi  $\alpha$ -mannosidase I, the mutant seems to co-localise more with the *cis*-Golgi marker than the full-length GFP-Atgolgin-84A. This is observed in Figure 5.7 and was confirmed by the PCC value in Table 5-1. Surprisingly, in Arabidopsis, when the cisternae are flipped sideways as in Figure 5.8D-F these two markers do not seem to co-localise. This difference might be due to the fact that in Arabidopsis the deletion mutant titrates out the native protein faster than happens in *N. tabacum* as it may be more similar to the native protein. On the other hand, the remaining coiled coil domain may be functional in the native system and not in the heterologous system.

The long tubules emanating from Golgi bodies were not observed in each experiment and this may be due to levels of protein expression. These tubules were often detected with the TIRF microscope (discussed later in

chapter 6). Here only one tubule (Figure 5.12) was imaged long enough to enable measurement. This may be due to the fact that the tubule extension and movement is a transient and very dynamic event. Such tubules are mainly labelled by the mutant construct (Figure 5.9 and 5.11), and the tubules branch into two tubules that show a random movement as if they are attempting to connect or reach to something (Figure 5.9F white arrow). The Atgolgin-84A long coiled-coil domains may be maintaining Golgi stack structure. Such tubules were not observed during the expression the full-length Atgolgin-84A in chapter 4. Dynamic extensions have been observed in other organelles: stromules from plastids, peroxules from peroxisomes and matrixules from mitochondria (reviewed in Mathur *et al.*, 2012). The stromules extend along microtubules, are dependent on microtubule organisation and have anchor points to actin (reviewed in Hanson and Sattarzadeh, 2013). They have been suggested to direct movement of chloroplasts during the immune response. Similar to other dynamic extensions, the protruding tubules from the golgin mutant labelled compartment could be a response to the effect of expression of a golgin without long coiled-coil domains in order to maintain the homeostasis of the cell. On the other hand the tubules could increase the contact area between ER and Golgi in the absence of a tether to stabilise the connection between compartments.

In *A. thaliana* transient expression several subpopulations of Golgi bodies were observed. Some *cis*-cisternae labelled by MnSI-mRFP are connected to smaller ring-shaped structures in aggregates (Figure 5.9A-C), which might indicate that the golgin mutant is in another subcompartment or a pre-*cis*-Golgi compartment. Also the *A. thaliana* system the different subcompartment localisation of the mutant and MnSI is more distinguishable on the sideways facing view (Figure 5.10D-F). Considering that MnSI is localised at the *cis*-cisternae of the Golgi, which has been confirmed (Table 5-1) by the strong positive correlation with the *cis*-Golgi marker GnTI well-described in the literature (Schoberer and Strasser, 2011), the Atgolgin-84A

deletion mutant has to be at least partially in another compartment or subcompartment of the Golgi body.

Another *cis*-golgin AtCASP has been described in more detail recently (Osterrieder *et al.*, 2017) as well as its mutant form mRFP-AtCASP $\Delta$ 1-564 without the coiled-coil domains. In order to understand the localisation of Atgolgin-84A $\Delta$ 1-557, since it does not co-localise with the *cis*-Golgi marker, both mutants were co-infiltrated. The aim was to look at localisation of proteins with similar size and domains. Therefore both mutants were used, AtCASP $\Delta$ 1-564 only has the TMD and only has the necessary sequence for Golgi targeting. The mutants only partially co-localise in X, and Y (Figure 5.11C). and GFP-Atgolgin-84A $\Delta$ 1-557 appeared to be constricted to regions of the rims (Figure 5.11C). whereas the mutant AtCASP seems to be more evenly distributed across the ring-shaped structure (Figure 5.11B). The overexpression of GFP-Atgolgin-84A $\Delta$ 1-557 induces long tubular extensions emanating from the ring-shaped structures, and this is more evident during expression of both golgins deletion mutants (Figure 5.12). The tubule measured here serves as an example of the distance that these tubules can reach, which is only indicative, meaning that possibly the tubules can extend longer and shorter ones were also observed as shown in Figure 5.9C and F, yellow arrow). These tubules appear to be labelled only by mCherry-Atgolgin-84A $\Delta$ 1-557 and do not co-localise with GFP-HDEL (data not shown) and some of these tubules connect two ring-shaped structures or more. These tubular extensions can break and disconnect from the ring shaped structures and move free. A tubular extension can be as long as 7  $\mu$ m (Figure 5.12) or possibly longer. If the long coiled-coil domains from Atgolgin-84A are maintaining the cisterna morphological identity by holding them as a disk, then the tubules can be a result of the deletion of the coiled-coil domains creating a membrane surplus. If the golgins act as tethers it could be that they are also involved in movement and without the long coiled-coil domains the tether is not functional and the tubules would be the way to slow down the Golgi bodies and therefore having a more mechanical function

in order to facilitate transport from ER-to-Golgi. If golgins are tethering transport carriers, without the long coiled-coils, the tubules could help increase the contact sites between ER and Golgi or other organelles facilitating the transport. Investigating the function of these tubules requires further experiments such as using tracking software to compare velocity of Golgi bodies with tubules and without tubules.

### **Co-expression with COPII components indicate the golgin and these markers might be involved in the same transport events**

The full-length golgin was co-infiltrated with COPII components such as AtSar1a, but it was very difficult to obtain co-expression. The ring-shaped compartments were rarely detected, and instead pleomorphic structures were visualised. Therefore, the deletion mutant was co-infiltrated with AtSec24 (Figure 5.13) (Faso *et al.*, 2009), labelling was very similar to the full-length protein. The deletion mutant was not labelling specific structures in most of the experiments, and rarely some ring-shaped structures or round-shaped objects could be detected labelled by the mutant. It was possible to obtain co-expression with Sec24a, and the deletion mutant. YFP-Sec24a was diffused around the ring-shaped structures labelled by the mutant and also concentrated at subdomains in the ring (Figure 5.14). This might indicate that both mutant and COPII components are involved in the same events and are competing for the same interactors or interact with each other and consequently mCherry-Atgolgin-84A $\Delta$ 1-557 cannot be incorporated in the Golgi membrane when YFP-Sec24a is overexpressed because both are being recruited at cytoplasm or at the putative Golgi matrix.

The co-expression with ST-mRFP and MnSI-mRFP was analysed using Zen software. The mutant seems to co-localise more with the ST-mRFP marker than the full-length in the face view (Table 5-1). This might



indicate that if the coiled-coils are responsible for keeping the golgin possible interacting or tethering to other cytoplasmic or Golgi matrix components at the rims of Golgi body. Therefore the protein without coiled-coil domains is looser in the membrane and able to move towards the lumen of the Golgi cisternae. This also confirms that the mutant is less constricted to the rims of the cisternae than the full-length. Other imaging methods could be used to confirm localisation differences within the Golgi stack such as immunoelectron microscopy. If the coiled-coil domains are keeping the stacking of the Golgi body it is not surprising that without coiled-coil domains the stack is not so connected between cisternae and the mutant expression has a much lower PCC (0.23) with the *trans*-Golgi marker than the full-length protein (Table 5-1). For the co-expression with *cis*-Golgi markers the mutant co-localises more with these than the full-length protein. Nevertheless, the PCC values for the mutant co-localisation with *cis* markers are lower than the control (co-localisation of the two *cis*-Golgi markers) which indicates the mutant as is only partially in the *cis*-Golgi as observed in Figure 5.9. This is only an indication, since the number of objects analysed was very low, as it was the case also for some of the other combinations tested. Therefore, more repeats are needed to analyse these data and test the significance. But this is now possible due to the fact that methods for co-localisation developed here. During this work only the pleomorphic structures in Figure 5.14 were observed during the co-expression of COPII components and Atgolgin-84A $\Delta$ 1-557, most of them, such as AtSar1 had such a low fluorescent marker signal which did not allow imaging with the Airyscan detector (data not shown). It would be interesting to obtain co-expression with a range of COPII and ERES markers to confirm the data presented here.

## **Structures labelled by Atgolgin-84A $\Delta$ 1-557 flip side on more often than Golgi bodies labelled by the Golgi marker ST indicating less tethering to other organelles or structures**

Several ring-shaped structures appear flipped sideways by 90° (Figure 5.11D) (as schematically represented in chapter 4, Figure 4.21) which could be due to overexpression of the Atgolgin-84A $\Delta$ 1-557. Compared to the overexpression of Atgolgin-84A no aggregates were observed indicating that the coiled-coil domains were inducing the pairs of Golgi bodies. Ring-shaped structures facing sideways were counted for expression of the mutant Atgolgin-84A $\Delta$ 1-557 compared to the expression of the non-functional *trans*-Golgi marker ST-GFP. During ST-GFP expression only 10% of the ring-shaped structures observed were flipped and 90% were facing forward. Interestingly for the mutant labelled structures 42% flipped during the time-series and only 58% of the structures observed were facing forward for the duration of the time-series. This data indicates that the Atgolgin-84A region that was deleted from the sequence, which includes the predicted long coiled-coil domains is responsible for maintaining the Golgi body facing forward as preferred orientation considering that this is the orientation observed in the most common Golgi markers. This suggests that during expression of GFP-Atgolgin-84A $\Delta$ 1-557 the tethering to the ER is impaired. This supports the hypothesis that Atgolgin-84A may be involved in tethering the Golgi to the ER.

**Altogether the data indicates that a fully functional Atgolgin-84A with its long coiled-coil domains can act as an ER tether and could be responsible in part for maintaining the Golgi body shape, size and orientation. The deletion mutant golgin may still retain some function as the remaining sequence has a coiled-coil domain where phosphorylation and protein interaction sites have been predicted.**

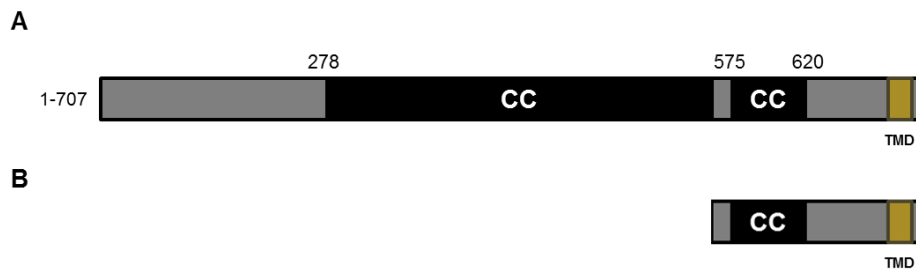


Figure 5.1: Schematic representation of Atgolgin-84A full-length protein and deletion mutant Atgolgin-84A $\Delta$ 1-557. (A) Full-length Atgolgin-84A, where most of the structure is predicted to be coiled-coil domains (CC). (B) Using a similar approach as for the human golgin-84, the Atgolgin-84A deletion mutant comprises the TMD and approximately 100 amino acids preceding the TMD and this region (amino acids 558–707) is necessary and sufficient for Golgi localisation (Latijnhouwers *et al.*, 2007).

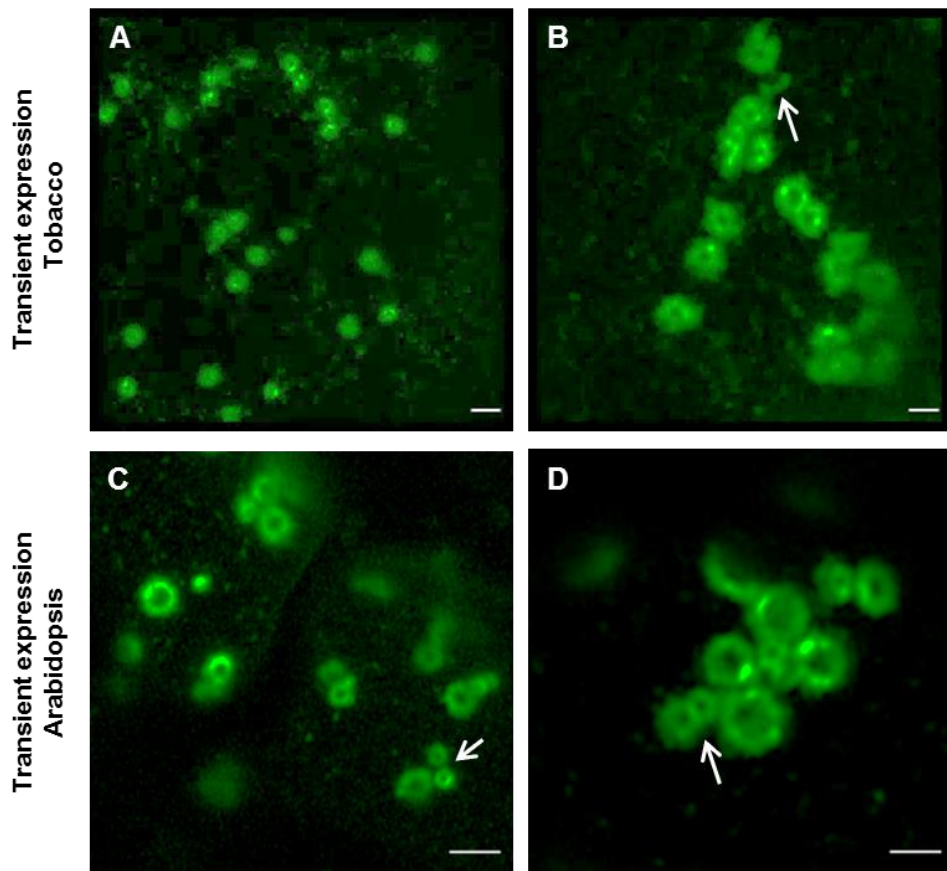


Figure 5.2: GFP-Atgolgin-84A $\Delta$ 1-557 transient expression in *planta*. (A and B) *N. tabacum* leaf epidermal cells transiently expressing GFP-Atgolgin-84A $\Delta$ 1-557. GFP-Atgolgin-84A $\Delta$ 1-557 labels ring shaped structures (A), which show tubular structures protruding out of the ring and longer ones reaching into the cytoplasm which retract and extend constantly (B, arrow) (Appendix I, Movie 10). (C and D) Transient expression in *A. thaliana* showing ring shaped structures and smaller ring shapes (C and D, arrows). Scale bars, (A) 0.5  $\mu$ m, (B-D) 1  $\mu$ m.

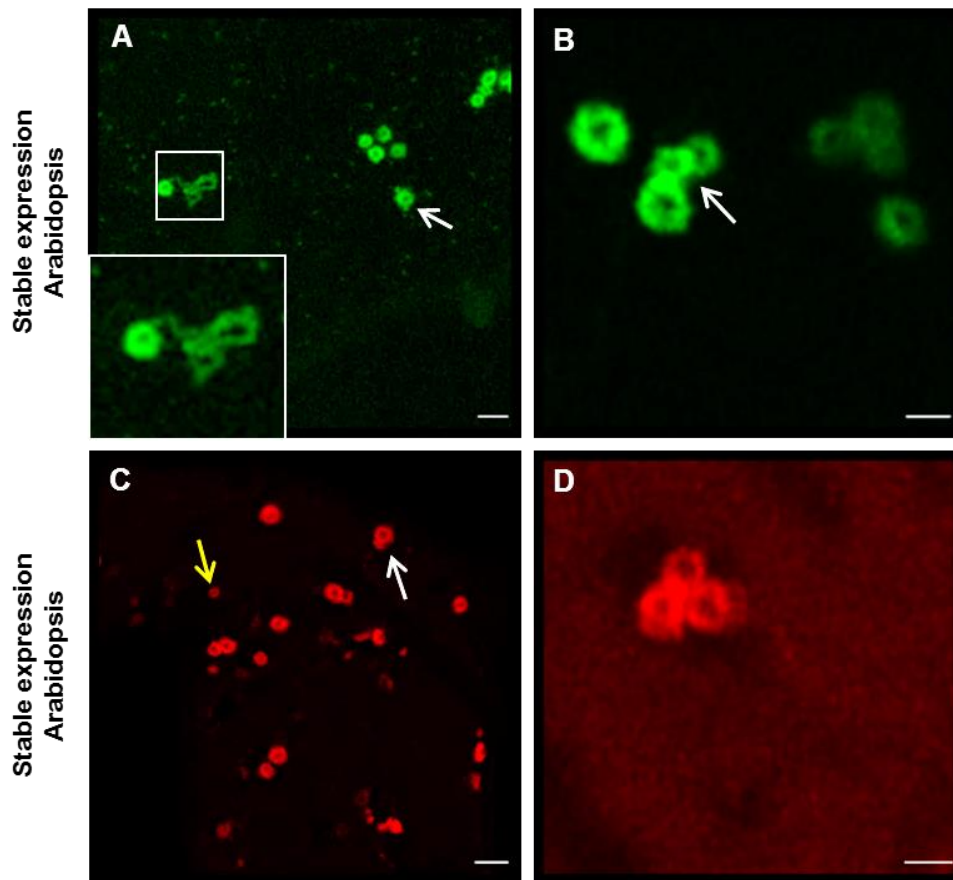


Figure 5.3: Atgolgin-84A $\Delta$ 1-557 stable expression in *A. thaliana*. (A and B) stable expression of GFP-Atgolgin-84A $\Delta$ 1-557 in *A. thaliana*, which shows ring shape structures and long tubules that often connect ring shapes or are reaching into the cytoplasm and occasionally forming a loop (inset in A) (Appendix I, Movie 11). (C and D) stable expression of mCh-Atgolgin-84A $\Delta$ 1-557 shows different ring sizes, some in pairs very similar to the GFP version. Scale bars, (A and C), 2  $\mu$ m; (B and D), 1  $\mu$ m.

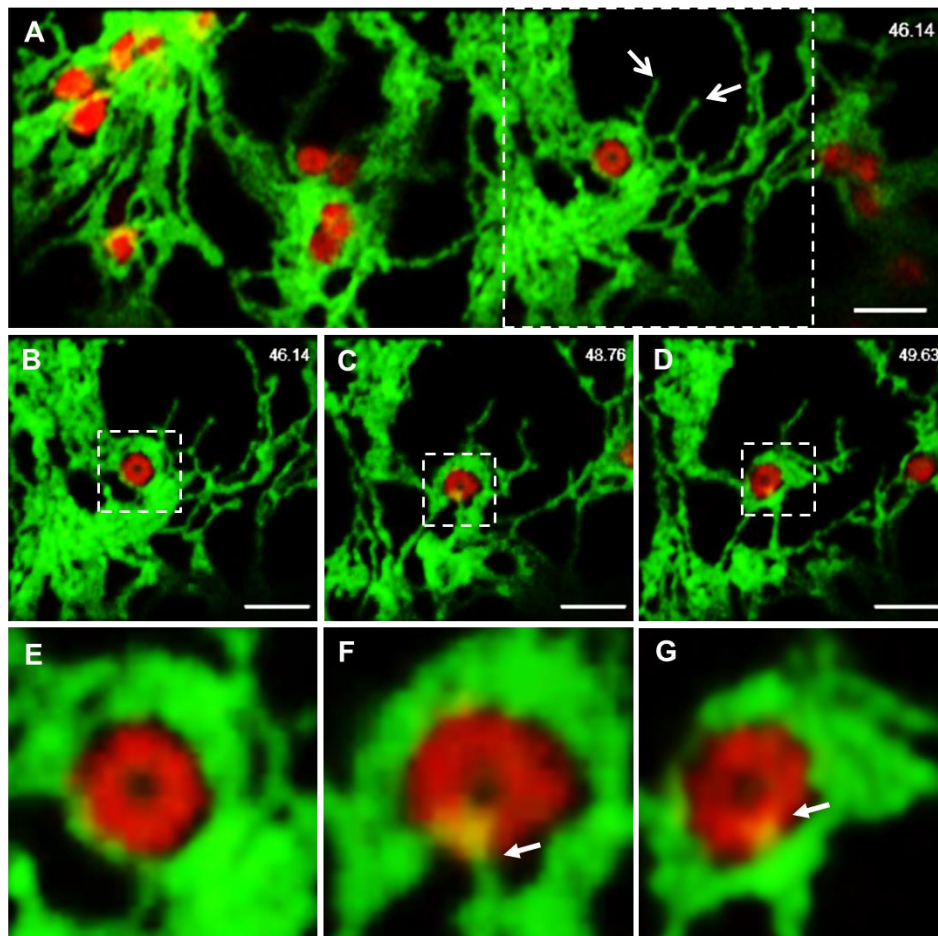


Figure 5.4: Co-expression of mCh-Atgolgin-84A $\Delta$ 1-557 and GFP-HDEL in *N. tabacum* (Appendix I, Movie 12). (A) The compartment labelled by the deletion mutant sits in the ER lacunae and there is an ER tubule above the ring-shaped compartment. Some structures are very stable, do not move and look like if they are anchored (white arrows). (B-D) The ring-shaped structure is flipping to side view. (E-G) Enlargement of (B-D) showing detail close proximity to ER (E) , ER tubules above ring-shaped compartment (F) and an ER protrusion that seems to connect with the mCherry-Atgolgin-84A $\Delta$ 1-557 labelled compartment (G, white arrow). Scale bar, 2  $\mu$ m. Time in seconds.

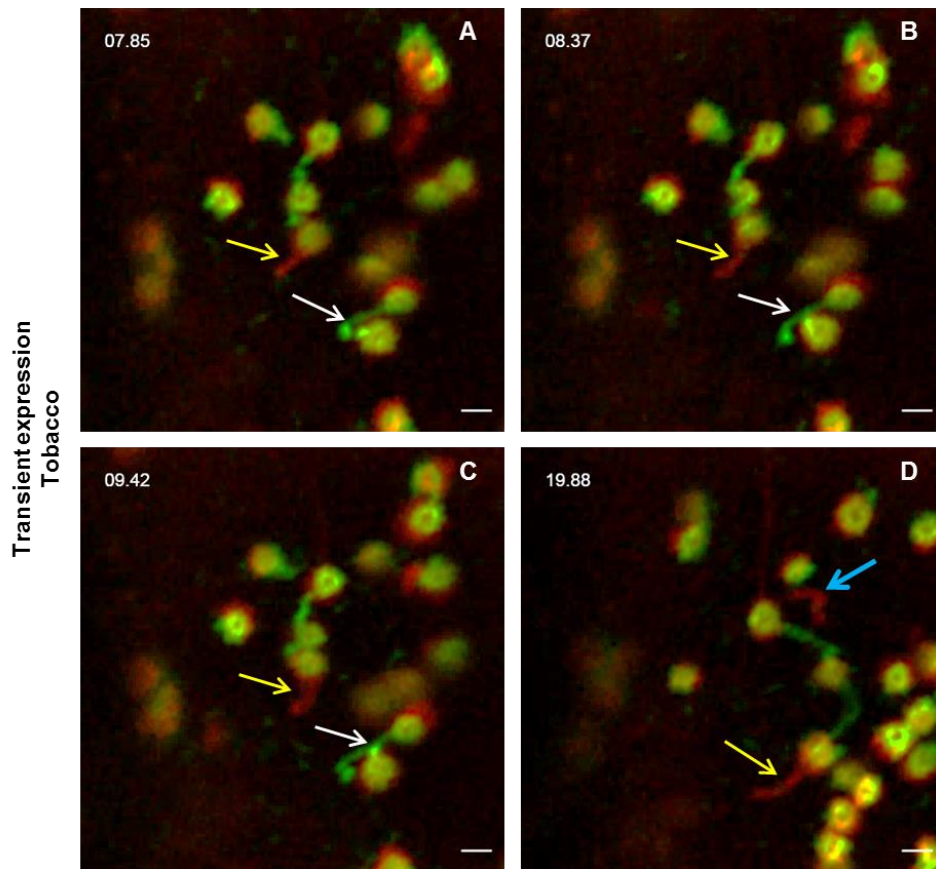


Figure 5.5: Frames of a time series during co-expression of ST-mRFP and GFP-Atgolgin-84A $\Delta$ 1-557 deletion mutant in *N. tabacum* (Appendix I, Movie 13). (A) GFP-Atgolgin-84A $\Delta$ 1-557 and ST-mRFP partially co-localise and both show tubular structures that do not co-localise (yellow arrow). (B) A tubule gets very close to other tubule and they seem to connect (white arrow). (C) Some tubules slide on other tubules (white arrow). (D) A tubule moving alone, not connected to other labelled structures is observed (blue arrow) Scale bars, 1  $\mu$ m. Time series in seconds.



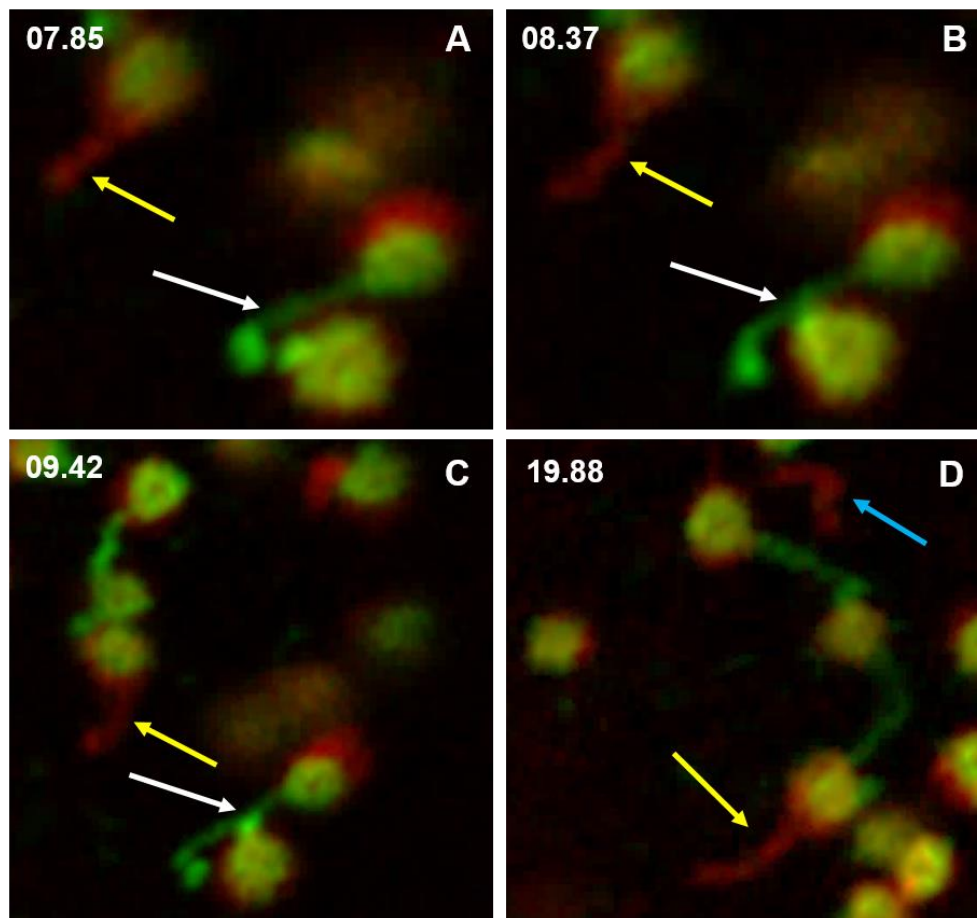


Figure 5.6: Enlargement of Figure 5.5 showing detail of tubules protruding out of the Golgi bodies and connecting GFP-Atgolgin-84A $\Delta$ 1-557-labelled compartments. (A) GFP-Atgolgin-84A $\Delta$ 1-557 and ST-mRFP partially co-localise and both show tubular structures that do not co-localise (yellow arrow). The green tubule ends in a more globular structure. (B) A tubule gets very close to other tubule and they seem to connect (white arrow). It is possible to see the labelling of the markers in different cisternae. (C) Some tubules slide on other tubules (white arrow). (D) A tubule moving alone, appears not connected to other labelled structures is observed (blue arrow). This tubule moves disconnected from any other labelled structures. Time series in seconds.



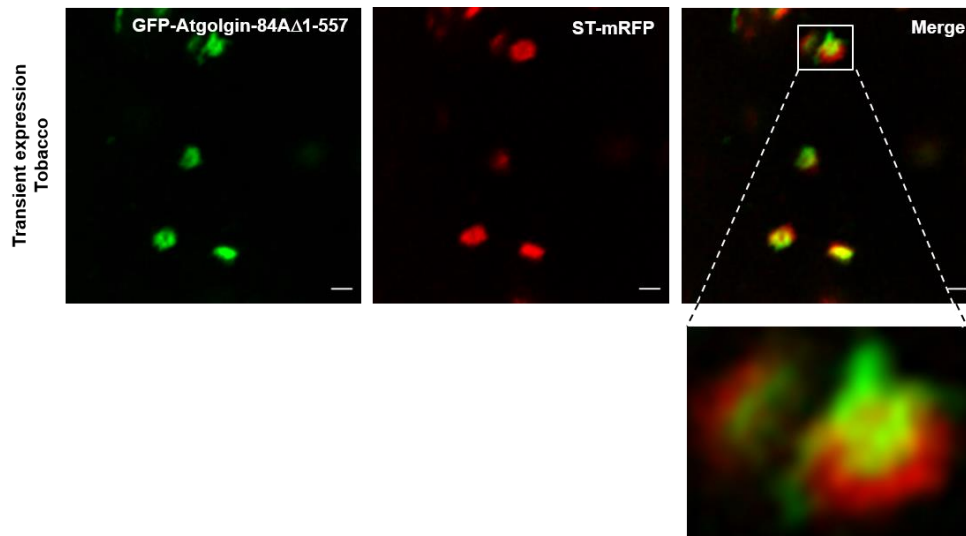


Figure 5.7: Co-expression of GFP-Atgolgin-84A $\Delta$ 1-557 and ST-mRFP with high-magnification of a ring-shaped structure. GFP-Atgolgin-84A $\Delta$ 1-557 shows protruding structures and seems to be in a different subcompartment than ST-mRFP (inset). Scale bars, 1  $\mu$ m.

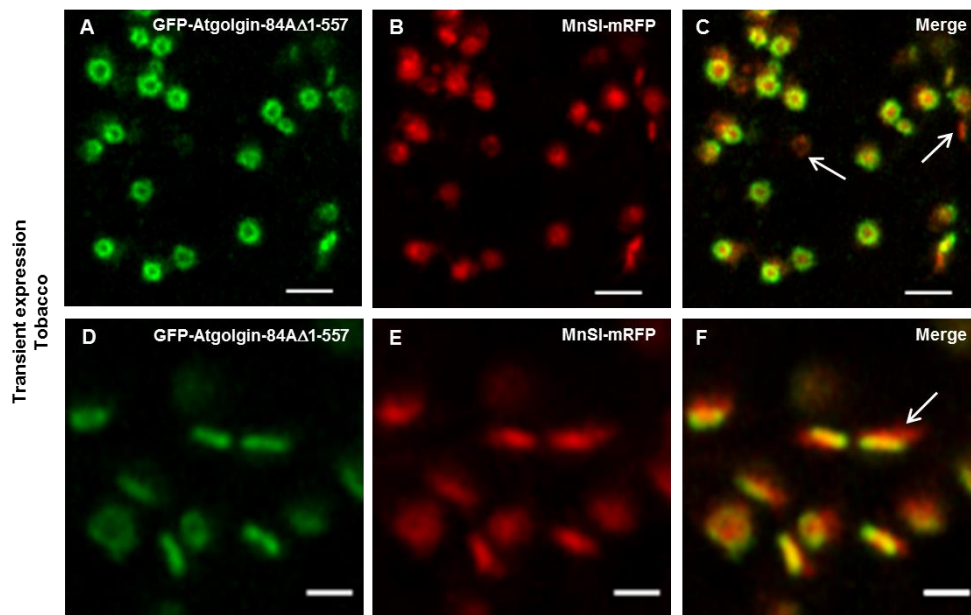


Figure 5.8: Co-expression of MnSI-mRFP and GFP-Atgolgin-84A $\Delta$ 1-557 in *N. tabacum*. (A-B) MnSI-mRFP and GFP-Atgolgin-84A $\Delta$ 1-557 only partially co-localise and in some Golgi only MnSI-mRFP is detected (C, white arrows) (Appendix I, Movie 14). (D-F) Golgi are flipped 90°; side view and not face view, as it is usually observed for Golgi bodies. The *cis*-Golgi marker MnSI appears shifted with respect to GFP-Atgolgin-84A $\Delta$ 1-557 (F, white arrow) (Appendix I, Movie 15). Scale bars, (A-C) 2  $\mu$ m; (D-F) 1  $\mu$ m.

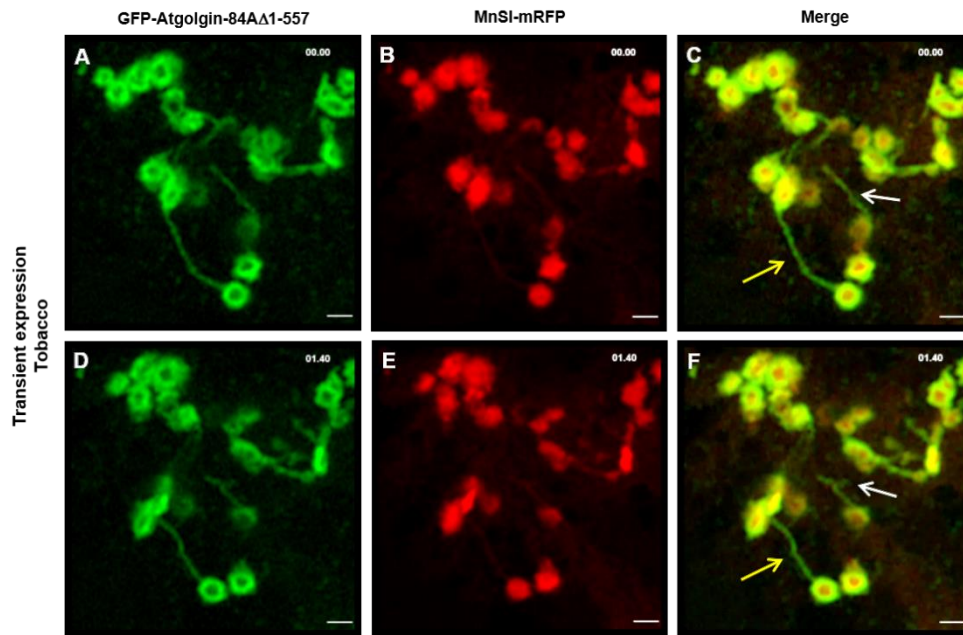


Figure 5.9: Frames from a time series of GFP-Atgolgin-84A $\Delta$ 1-557 co-expression with MnSI-mRFP *cis*-Golgi marker in *N. tabacum*. GFP-Atgolgin-84A $\Delta$ 1-557 labels ring-shaped structures with long tubules. Some tubular structures connect several ring-shaped structures (yellow arrows). The tubular structures elongate and retract. Some tubular structures are reaching out and some of them branch into two tubular structures (white arrows). MnSI-mRFP labels round disc shaped structures. GFP-Atgolgin-84A $\Delta$ 1-557 and MnSI-mRFP only partially co-localise as it is possible to distinguish between green and red without yellow in parts of the round shaped structures (Appendix I, Movie 16). Scale bars, 1  $\mu$ m. Time in seconds.

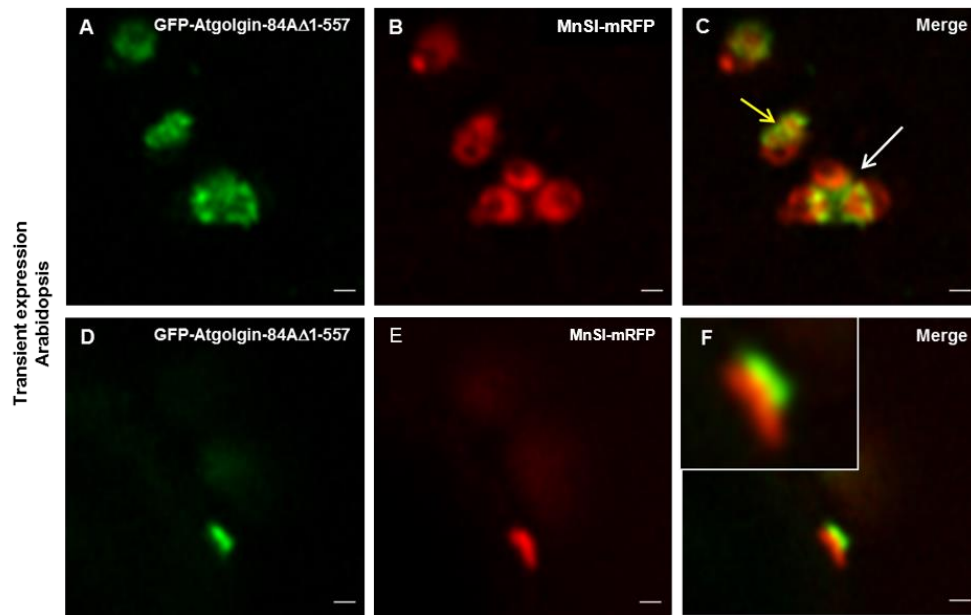


Figure 5.10: Transient expression of MnSI-mRFP and GFP-Atgolgin-84AΔ1-557 in *A. thaliana*. (A-C) Aggregates of Golgi bodies are observed (Appendix I, Movie 17). (D-E) Golgi body flipped sideways shows different localisation of the two markers (Appendix I, Movie 18). (F) Detail of Golgi body flipped sideways. Scale bars, 1  $\mu\text{m}$ .

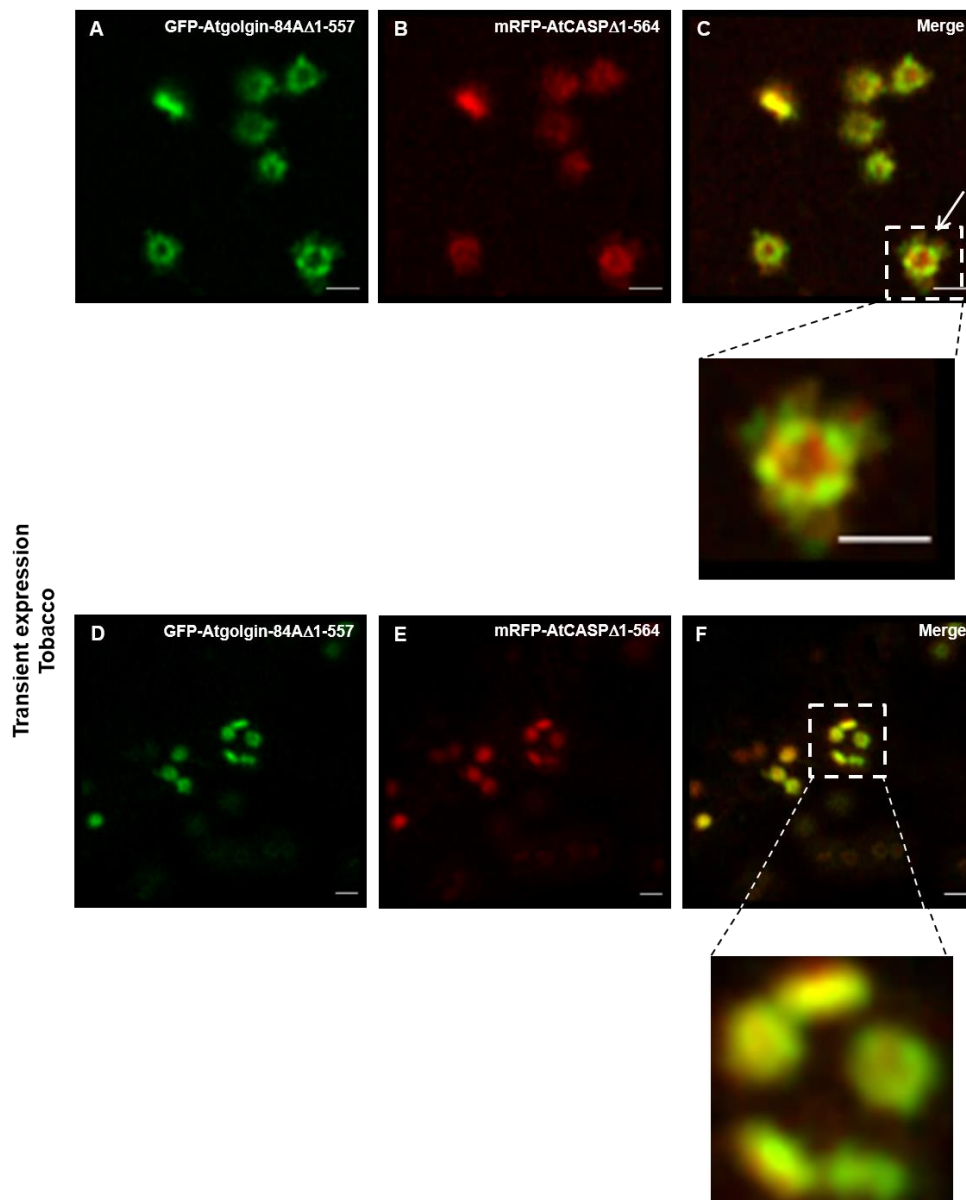


Figure 5.11: Co-expression of plant golgin GFP-Atgolgin-84A $\Delta$ 1-557 and mRFP-AtCASP $\Delta$ 1-164 in *N. tabacum*. (A-C) AtCASP deletion mutant seems to label more the centre of the cisterna and the rim, whereas GFP-Atgolgin-84A $\Delta$ 1-557 labelling appears restricted to parts of the rims of the cisternae (white arrow) (Appendix I, Movie 19). (D-F) Round-shape compartments labelled by both deletion mutants appear sideways (inset) (Appendix I, Movie 20). Scale bars, (A-C) 1  $\mu$ m, (D-F) 2  $\mu$ m.

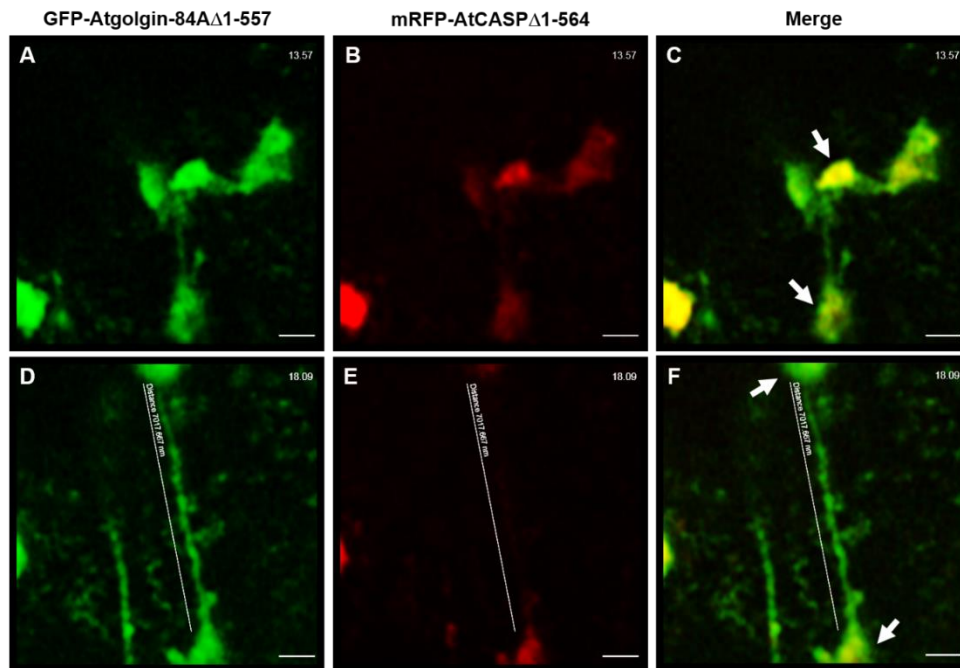


Figure 5.12: Co-expression of GFP-Atgolgin-84A $\Delta$ 1-557 and mRFP-AtCASP $\Delta$ 1-164 in *N. tabacum*. (A-C) Two compartments labelled by both deletion mutants are linked by a tubule. (D-F) The round shapes move apart (white arrows) but the tubule is still visible and the maximum length observed is 7  $\mu$ m (Appendix I, Movie 21). Scale bars, 1  $\mu$ m.

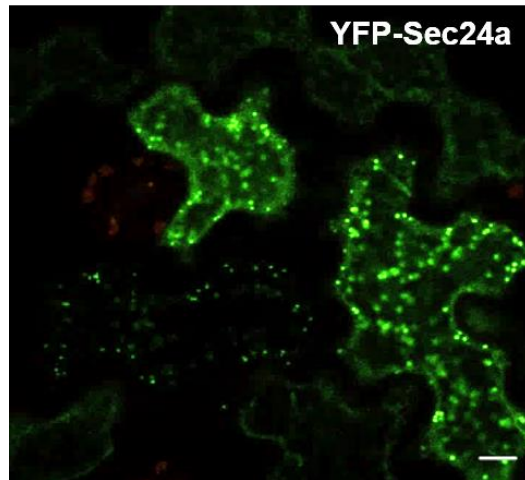


Figure 5.13: Expression of YFP-Sec24a in *N. tabacum* leaf epidermal cells. The cytoplasm is labelled at a low level as well as round-shaped compartments. Scale bars, 10  $\mu\text{m}$ .

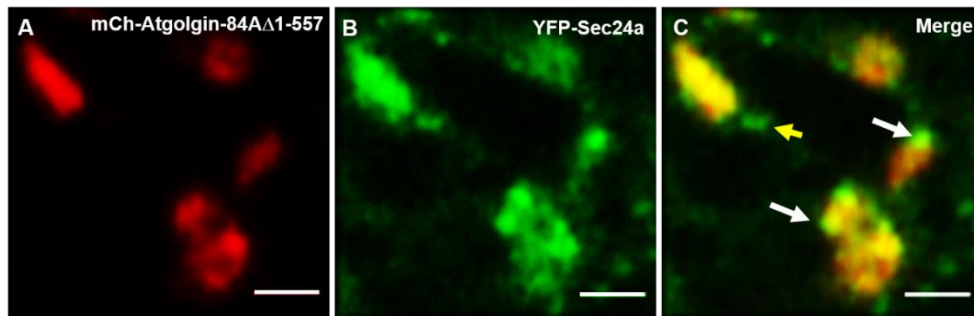


Figure 5.14: Co-expression of mCh-Atgolgin-84A $\Delta$ 1-557 with YFP-Sec24a in *N. tabacum* (Appendix I, Movie 22). (A) The deletion mutant labels ring-shaped compartments and the intensity seems to be higher in subdomains of the ring. (B) The COPII components localises in a diffuse pattern around the subcompartment labelled by the golgin mutant and more specifically in subdomains where the mutant fluorescence is also more intense (C, white arrows). (C) YFP-Sec24a localises around the golgin mutant ring-shaped compartment. Some smaller round compartments are detected labelled only by YFP-Sec24 (yellow arrows). Scale bars, 1  $\mu$ m.



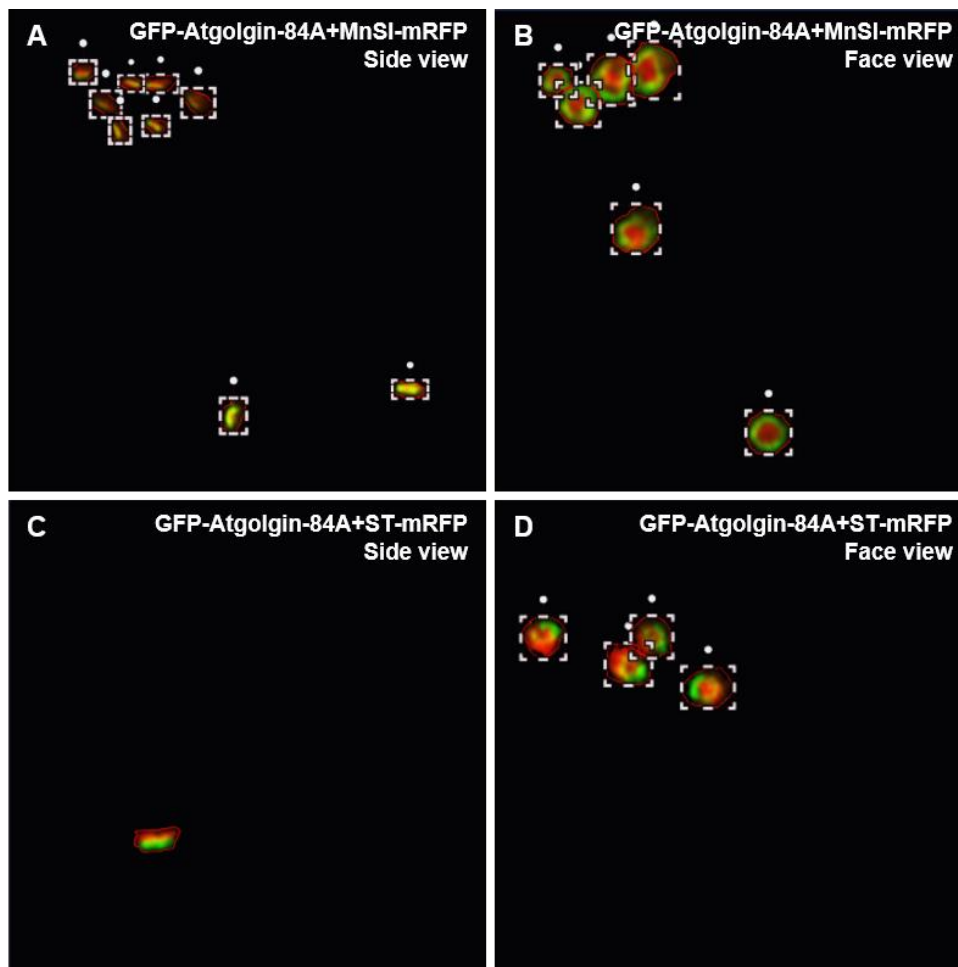




Figure 5.15: Examples of ROIs used for co-localisation analysis on Zen (Zeiss) software in merged images of green and red channels. (A) GFP-Atgolgin-84A $\Delta$ 1-557 and MnSI-mRFP side view of Golgi bodies. (B) GFP-Atgolgin-84A $\Delta$ 1-557 and MnSI-mRFP face view of Golgi bodies. (C) GFP-Atgolgin-84A $\Delta$ 1-557 and ST-mRFP side view of Golgi bodies. (D) GFP-Atgolgin-84A $\Delta$ 1-557 and ST-mRFP face view objects.

Table 5-1: Co-localisation analysis of GFP-Atgolgin-84A $\Delta$ 1-557 in *N. tabacum* compared to the previously obtained PCC values for GFP-Atgolgin84A (chapter 4) and Golgi membrane markers. Pearson correlation coefficients (PCCs) are shown for the different combinations of markers.

<b>Pearson's correlation coefficient (PCC)</b>				
<b>Object's position</b>			<b>n</b>	
	<b>Side view</b>	<b>Face view</b>	<b>Side view</b>	<b>Face view</b>
<b>MnSI-GFP + GnTI-mRFP</b>	0.76	0.78	23	28
<b>GFP-Atgolgin-84A + MnSI-mRFP</b>	0.44	0.43	1	1
<b>GFP-Atgolgin-84A<math>\Delta</math>1-557 + MnSI-mRFP</b>	0.80	0.64	9	47
<b>GFP-Atgolgin-84A + ST-mRFP</b>	0.49	0.40	8	25
<b>GFP-Atgolgin-84A<math>\Delta</math>1-557 + ST-mRFP</b>	0.23	0.56	16	8

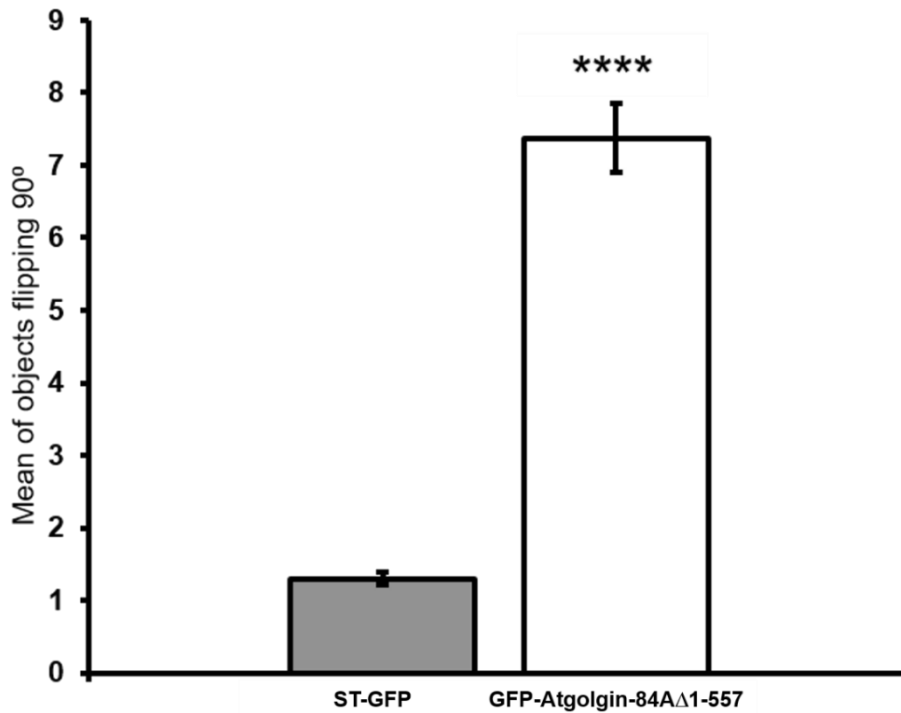


Figure 5.16: Histogram representing the mean of counted ring-shaped structures that flip sideways during time series during expression of Atgolgin-84AΔ1-557 compared to the mean of the number of Golgi bodies expressing only ST-GFP. Ring-shaped structures as shown in Figure 5.1 A were quantified in 2 independent experiments;  $n \geq 60$  ring-shaped structures were assessed per independent experiment. Data represent mean  $\pm$  SEM\*\*\*\* $p < 0.0001$  (Chi-Square test).

## **6. Assessing the putative tethering function of the long coiled-coil domains with optical tweezers**

### **6.1 Introduction**

Golgi bodies are highly motile in plant cells and therefore characterisation of tether components is challenging particularly in highly vacuolated leaf epidermal cells because all organelles are constricted to a limited space and close to each other and interactions might happen because of the limited space. In order to test the importance of the coiled-coil domains for the putative tethering function of Atgolgin-84A the behaviour of Golgi bodies in the optical trap during the expression of GFP-Atgolgin-84A $\Delta$ 1-557 was analysed. In this chapter optical tweezers coupled to a Total Internal reflection fluorescence-TIRF microscope were used to assess the effect of overexpression of the GFP-Atgolgin-84A $\Delta$ 1-557 alone or in combination with mRFP-AtCASP $\Delta$ 1-664. The optical trap is a highly focused infrared beam that captures the objects that have a significantly different refractive index from the surrounding medium (Fazal and Block, 2011; Sparkes *et al.*, 2018). For example, unlike the ER, Golgi bodies due to their size and density are amenable to trapping (Sparkes *et al.*, 2009b). By comparing how objects respond to the optical trap in the wild-type against the overexpression of Atgolgin-84A $\Delta$ 1-557 it is possible to infer the putative tethering function of the long coiled-coil domains. In this chapter the objects tested in the trap will be named 'Golgi bodies' since all cisternae in the Golgi stack seem to move together, even though as described in chapter 4 and 5 the Atgolgin-84A-labelled structures seem to be a subcompartment of the Golgi. This means that the Golgi stack moves together including the subcompartment that is labelled by GFP-Atgolgin-84A $\Delta$ 1-557, therefore it will be assumed that the

Golgi body responds the same way in the trap as the golgin-labelled subcompartment.

## 6.2 Results

*N. tabacum* cells expressing Atgolgin-84A $\Delta$ 1-557 were tested by trapping 100 Golgi bodies. When the optical trap is switched on it is possible to assess Golgi body behaviour to the trap because Golgi bodies are moving and if they get trapped they stop moving. Each Golgi body was categorised into “trapped”, if it was trapped, stopped movement and stayed in the trap position, “partially trapped” if it stopped movement at the trap but fell out of the trap when the microscope stage was moved (did not stay in the trap and moved away from the trap) or “not trapped” meaning it was not trapped and did not stop at the trap position. After trapping, the trapped Golgi body can be moved from the original position by moving the stage of the microscope to understand if the Golgi body remains trapped or if it leaves the trap.

Figure 6.1 (Appendix I, Movie 23) shows an example of a trapping event during ST-GFP overexpression. A Golgi body is trapped (black arrow in the schematic representation A corresponding to the white arrow in the micrograph B) and the stage is moved 2  $\mu$ m to the right in x. The Golgi body stays trapped for the 2  $\mu$ m translation (C and D). At the start of the translation there are three Golgi bodies in close proximity with the trap but these three (red arrow) do not get trapped.

A similar procedure is applied to Golgi bodies labelled by GFP-Atgolgin-84A $\Delta$ 1-557 as observed in Figure 6.2 (Appendix I, Movie 24). Interestingly, several Golgi bodies labelled by the mutant are trapped at the same time in one trapping event which was not observed for ST-GFP overexpression (black arrow in A corresponding to white arrow in B). The trapped Golgi bodies are moved and all remain trapped for the duration of the translation. Afterwards, the Golgi bodies are moved in the opposite direction, returning to the original position and during this procedure several different Golgi bodies far from the trap position get trapped and it is possible to observe that these other Golgi bodies appear from a different focal plane

which shows the distance from where they were pulled into the trap (Figure 6.2E and F, red arrow). At the end of the trapping event, with the trap still on, it is possible to count approximately twelve Golgi bodies trapped at the same time (Figure 6.2G and H). Several clusters of Golgi bodies are observed during expression of GFP-Atgolgin-84A $\Delta$ 1-557 (Figure 6.3, Appendix I, Movie 25).

Each trapping event similar to what was described for above ST-GFP, was scored into one of the three categories: “trapped”, “partially trapped” or “not trapped” in three independent experiments, and 100 Golgi bodies were counted per experiment and per condition. Figure 6.4 represents the 100-Golgi bodies test in cells expressing ST-GFP (the wild-type control with fluorescently labelled Golgi body), compared to the overexpression of the GFP-Atgolgin-84A $\Delta$ 1-557 or the co-expression of GFP-Atgolgin-84A $\Delta$ 1-557 with mRFP-AtCASP $\Delta$ 1-664. In the co-expression, expression of the constructs can be detected in two independent channels for the different fluorophores (Figure 6.5, Appendix I, Movie 26) Less Golgi bodies are trapped when GFP-Atgolgin-84A $\Delta$ 1-557 is expressed compared to the ST-GFP control. More Golgi bodies exit the trap in the GFP-Atgolgin-84A $\Delta$ 1-557+mRFP-AtCASP $\Delta$ 1-664 compared to GFP-Atgolgin-84A $\Delta$ 1-557 alone. The histogram gives a good indication of differences between the three conditions (Figure 6.4). Tables 6-1 and 6-2 give information about significance and what it represents spatially i.e. what happened to the trapped Golgi body during the trapping event. Therefore the data was separated and analysed for two different events (Tables 6-1 and 6-2). The first characterisation aims to answer the question “how many Golgi bodies are trapped?” in each condition. The second analysis asked the question “how many Golgi bodies remain trapped during the 2  $\mu$ m translation?”. This comparison will allow to determine the significance of the data and understand better how the Golgi body behaved during the trapping event.

During overexpression of GFP-Atgolgin-84A $\Delta$ 1-557 less Golgi bodies were trapped than in the ST-GFP (Table 6-1A) because even though

apparently more Golgi fall into the trap in the mutant, it is only counted yes or no for trapping and not how many Golgi for trapping event. This difference is not due to randomness given the p-value of  $3.11 \times 10^{-7}$  in the Chi-squared test. The Golgi bodies in these clusters were tested for trapping but it is not possible to move them away from the cluster and it is difficult to trap them. Therefore the clusters were avoided and only single Golgi were tested for trapping.

Only 60% of the mutant labelled Golgi bodies stay in the trap for the translation compared to 83% for the wild-type (Table 6-1B). This difference is also very significant with a p-value of  $2.27 \times 10^{-10}$ . When GFP-Atgolgin-84A $\Delta$ 1-557 and mRFP-AtCASP $\Delta$ 1-664 are co-expressed, there is no significant difference in the amount of Golgi bodies trapped compared to the ST-GFP control (Table 6-2A) with a p-value of 0.314 ( $>0.05$ ) in the Chi-squared test. The number of Golgi bodies that could be moved in GFP-Atgolgin-84A $\Delta$ 1-557+mRFP-AtCASP $\Delta$ 1-664 was 61%, compared to 74% in the ST-GFP which is significant in the Chi-squared test with a p-value of 0.0009 (Table 6-2B).

Two colours can be detected with dual colour TIRF as shown in Figure 6.5. Figure 6.6 (Appendix I, Movie 27) shows an example of how some Golgi bodies trapped during the expression of both GFP-Atgolgin-84A $\Delta$ 1-557 and mRFP-AtCASP $\Delta$ 1-664 can produce long tubules. The Golgi bodies show protruding structures that extend a long distance from the Golgi bodies. In Figure 6.6A a structure labelled by both GFP-Atgolgin-84A $\Delta$ 1-557 and mRFP-AtCASP $\Delta$ 1-664 reaches close proximity with a structure with several tubules (red arrow). Both connect and move together (Figure 6.6B). These tubules can extend for a long distance (Figure 6.6C and D) and seem to become in contact with other tubules. Some of these tubules disconnect from the ring-shaped structures and move alone (Figure 6.6E and F). Many of the Golgi bodies expressing double mutant have long tubules.



## 6.3 Discussion

The use of optical tweezers allows the assessment of how easily Golgi bodies labelled by the golgin mutant form Atgolgin-84A $\Delta$ 1-557 will fall into the optical trap and can be moved upon trapping in comparison to wild-type Golgi bodies. To label the wild-type Golgi bodies ST-GFP was used which does not affect the wild-type phenotype of the Golgi bodies or causes any change in dynamics. To assess this one hundred Golgi bodies were tested for the expression of GFP-Atgolgin-84A $\Delta$ 1-557 or GFP-Atgolgin-84A $\Delta$ 1-557+mRFP-AtCASP $\Delta$ 1-664 and compared to expression of ST-GFP. If a Golgi body stops moving at the trap position it means it was trapped. If the Golgi body does not stop movement at trap position it means it was not trapped. By comparison if more or less Golgi bodies were trapped it can be hypothesised that Golgi bodies are more or less tethered to other organelles such as ER or other structures such as Golgi matrix components or tubules. Tethering to other structures can prevent movement and therefore Golgi bodies could be difficult to trap or easily trapped depending on a strong or weak connection to those structures. Trapping behaviour of Golgi bodies labelled by mRFP-AtCASP $\Delta$ 1-664 was already described in the literature where it was suggested that AtCASP acts as a partial tether (Osterrieder *et al.*, 2017). ST-GFP trapping is also well-described in the literature (Sparkes *et al.*, 2006; Osterrieder *et al.*, 2017) and these trapping events were repeated during this work. As expected we can trap a Golgi body labelled by ST-GFP and it is possible to trap more than 90% of the Golgi bodies tested.

There is a significant reduction in the number of Golgi bodies trapped when compared to ST-GFP (Table 6-1A). It could be hypothesised that without long coiled-coil domains it would be easier to trap the Golgi bodies, if these are the motif for the tethering. In fact, the expression of the deletion mutant causes three different sub-populations of Golgi bodies with different phenotypes and different response to the optical trap, i.e. in each sample Golgi bodies with no tubules (an example of this is Figure 6.2), Golgi bodies

with a long tubule (data not shown but similar to Figure 6.6) and Golgi bodies in clusters (Figure 6.3) were observed. This might be due to transient expression where expression levels can differ between cells. The event illustrated in Figure 6.2 is only observed when there are no tubules detected protruding from the GFP-Atgolgin-84A $\Delta$ 1-557-labelled compartments. In this case, i.e. without tubules, several Golgi bodies are captured at the same time once the trap is on. Several Golgi bodies observed show tubules, and the preliminary observations indicate that this seems to prevent movement in general but this would have to be assessed by repeating the experiment only trapping Golgi bodies with tubules or using other analyses methods. Several clusters were observed (Figure 6.3), in which tubules wrap these compartments together, and these were excluded from trapping scoring as it was not possible to trap any of them as if they were “glued together”. Therefore it is not surprising that trapping is in general more difficult than in the wild-type. Considering this, moving the Golgi bodies with tubules means having a force opposing to the force created by the movement of the stage and as expected the Golgi bodies do not stay in the trap (Table 6-1B). Another feature that would interfere with trapping behaviour is the remaining short putative coiled-coil region, which may confer some tethering ability and there might be other tethers involved.

Co-expression of GFP-Atgolgin-84A $\Delta$ 1-557 with mRFP-AtCASP $\Delta$ 1-664 was also tested, and the number of trapped Golgi bodies was not significantly different from the wild-type (Table 6-2A). It is described in Osterrieder *et al.* (2017) that the mRFP-AtCASP $\Delta$ 1-664 affects the trapping behaviour and more Golgi bodies are trapped in comparison to wild-type. Therefore as the mRFP-AtCASP $\Delta$ 1-664 makes trapping easier this compensates for the tubule effect which could explain the lack of difference compared to the wild-type. If mRFP-AtCASP $\Delta$ 1-664 makes the Golgi bodies less tethered to other structures, the tubules created by GFP-Atgolgin-84A $\Delta$ 1-557 overexpression would not have a strong effect in preventing movement. In the GFP-Atgolgin-84A $\Delta$ 1-557+mRFP-AtCASP $\Delta$ 1-664

samples (Figure 6.6) Golgi bodies without tubules were rarely observed and it would be expected that Golgi bodies in this case would be more difficult to move. Only during the attempt to move the Golgi bodies is it possible to understand the effect of tubules. It is significantly more difficult to move the co-expression GFP-Atgolgin-84A $\Delta$ 1-557+mRFP-AtCASP $\Delta$ 1-664 than the ST-GFP Golgi bodies (Table 6-2B) which suggests that the mutants are involved in different tethering events. Potentially mRFP-AtCASP $\Delta$ 1-664 affects tethering to other organelles such as the ER and it is not involved in the long tubules effect. The tubules extend out of the Golgi bodies preventing movement even when mRFP-AtCASP $\Delta$ 1-664 lacking the coiled-coil domains is not connecting to other organelles or structures.

The mechanism for tubule formation and extension is unclear. The tubules seem to move as independent structures able to capture a Golgi that comes in close proximity (Figure 6.6A and B). Some of the tubules break free from the GFP-Atgolgin-84A $\Delta$ 1-557+mRFP-AtCASP $\Delta$ 1-664-labelled compartments and move alone (Figure 6.6E and F). This indicates that the tubules might be an independent structure. The fast extension of the tubules does not suggest newly synthesised membrane components and instead suggests that possibly they are coiled around the organelle and only extend when an extra connection or contact area is needed. The tubules could have a role in communication between Golgi and other organelles. They could be a response to maintain connections with the aim of reducing spatial separation between structures when the golgins are partially or fully non-functional.

**The results described in this chapter provide a good starting method to study the biophysical forces involved in Golgi tethering and demonstrate that the effect of golgins lacking coiled-coil domains are not random and can be quantified using optical tweezers. Mutation of one or more golgins resulted in the alterations of the trapping properties of the Golgi bodies. It also confirms previous data**

**(Osterrieder *et al.*, 2017) suggesting a key role of golgins in maintaining physical connectivity between Golgi and other structures or organelles. Future studies could involve force measurements to compare golgin mutant expression with wild-type plants and the use of stably transformed plants constitutively expressing golgin deletion mutants or plant mutant lines lacking golgins. It would be interesting to look at the connection between ER and Atgolgin-84A $\Delta$ 1-557-labelled compartments using optical tweezers and assess how amenable to be disrupted this connection is compared to wild-type. This would require higher magnification in the TIRF microscope coupled to the optical tweezers. The methodology developed here will enable future studies concerning the molecular and physiological role of golgins in tethering to other organelles or movement components and can also be used to develop a method to study Golgi membrane extensions.**

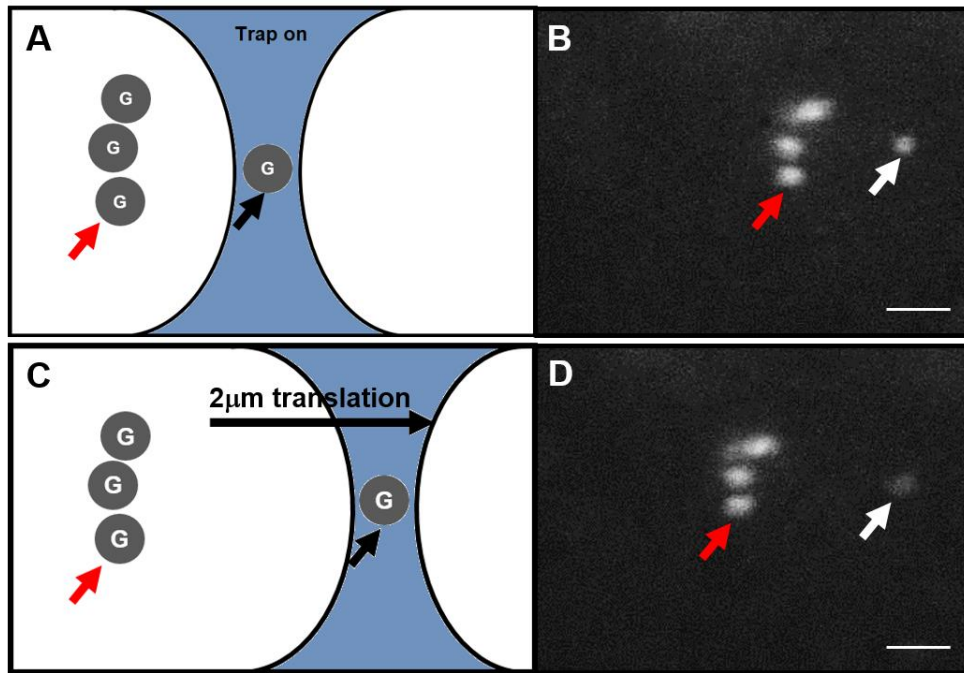


Figure 6.1: Trapping event during overexpression of ST-GFP (Appendix I, Movie 23). The left is the schematic representation of the trapping event. On the right are the micrographs from the trapping event. The blue area indicates the trap position in relation to the stage movement. The exact trap position is where the trapped Golgi body is and indicated by the black/white arrows. (A) One Golgi body is trapped and moved (B) and the other Golgi bodies surrounding it do not move easily into the trap. At the end of the trapping event, only one Golgi body remains captured (C). The translation event represents the movement of the stage. Scale bars, 2  $\mu\text{m}$ .

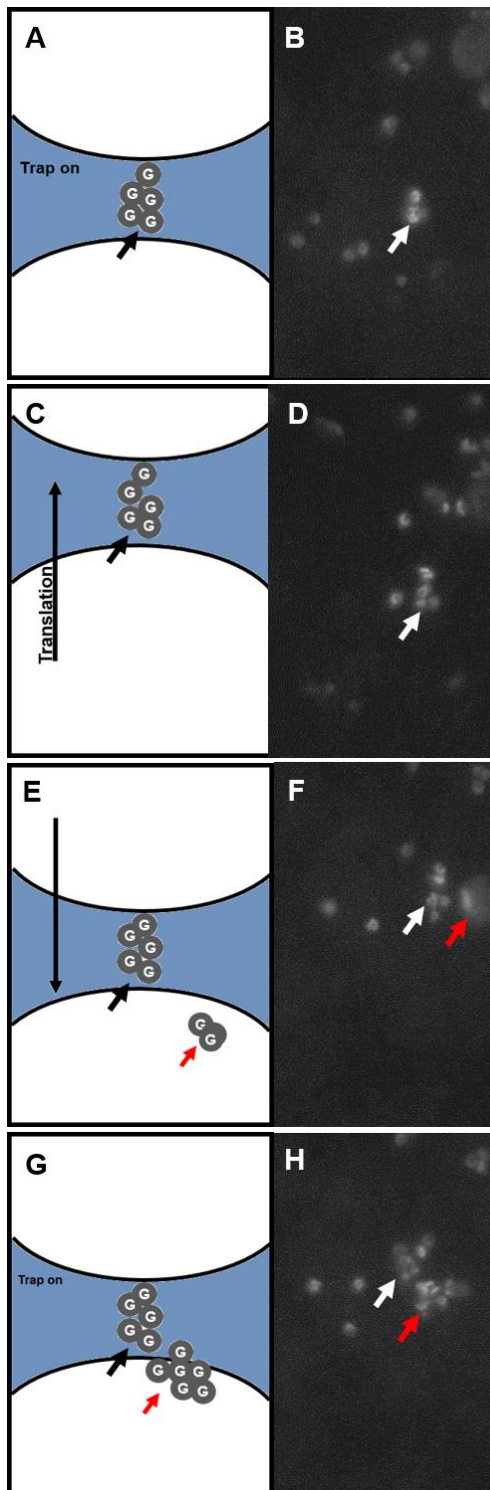


Figure 6.2: Trapping event during overexpression of GFP-Atgolgin-84A $\Delta$ 1-557 (Appendix I, Movie 24). The left panel shows the schematic representation of the trapping event. The right hand side shows the micrograph from the trapping event. The blue area indicates the trap position in relation to the stage movement. The exact trap position is where the trapped Golgi body is and indicated by the black/white arrows.

(A and B) Several Golgi bodies are trapped at once (black arrow). (C and D) The stage is moved and the Golgi bodies remain trapped. (E and F) The stage is moved down and several Golgi bodies in a cluster from another focal plane are pulled to the trap (red arrow). (G and H) At the end of the trapping event, many Golgi bodies remain in the trap >12. The translation event represents the movement of the stage.

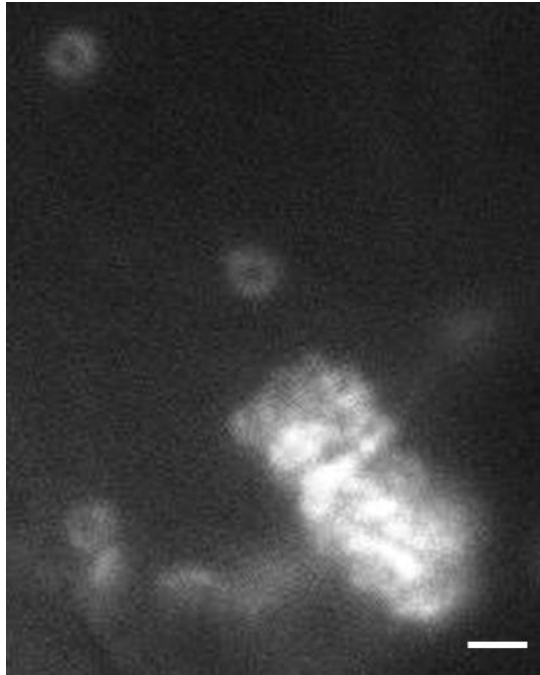


Figure 6.3: Aggregates of Golgi bodies during over expression of GFP-Atgolgin-84A $\Delta$ 1-557 (Appendix I, Movie 25). Scale bar, 1  $\mu$ m.

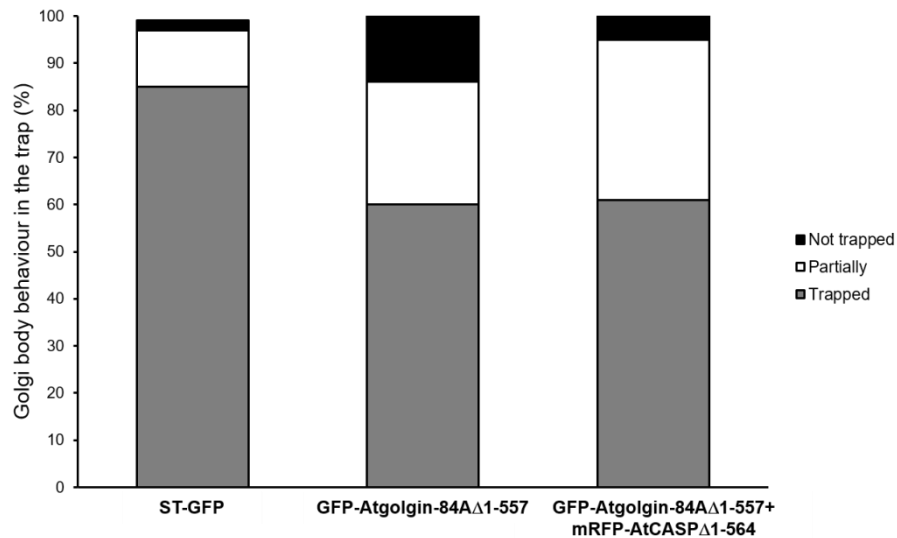


Figure 6.4: Golgi bodies labelled by ST-GFP, Atgolgin-84A1-557 and the co-expression of GFP-Atgolgin-84A $\Delta$ 1-557 with mRFP-AtCASP $\Delta$ 1-664 were tested for trapping and their trapping characteristics were scored. Ring-shaped compartments that remained in the trap over the 2  $\mu$ m translation i.e. stopped movement at the trap and did not move away from trap position during movement of the stage (grey bars), escaped the trap during the translation i.e., start moving away from the trap (white bars) or were unable to be trapped i.e. did not stop movement at the trap position (black bars). Percentages displayed are based on weighted means from a set of 3 independent experiments.



Table 6-1: Mean of counted trapped Golgi bodies during the overexpression of GFP-Atgolgin-84A $\Delta$ 1-557 compared to the mean of trapped Golgi bodies expressing ST-GFP. (A) Mean of Golgi bodies scored as trapped plus partially trapped. (B) Golgi bodies that are trapped and stay trapped for the 2  $\mu$ m translation. Golgi bodies as shown in Figure 6.1 and 6.2 were scored in 3 independent experiments; 100 Golgi bodies were tested per experiment. Data represent mean $\pm$ SEM\*\*\*\*p<0.0001 (Chi-squared test).

### A

Construct	Mean $\pm$ SEM	P
ST-GFP	98 $\pm$ 0.379	**** 3.11X10 <sup>-7</sup>
GFP-Atgolgin-84A $\Delta$ 1-557	86 $\pm$ 0.841	

### B

Construct	Mean $\pm$ SEM	P
ST-GFP	83 $\pm$ 0.44	**** 2.27X10 <sup>-10</sup>
GFP-Atgolgin-84A $\Delta$ 1-557	60 $\pm$ 1.55	

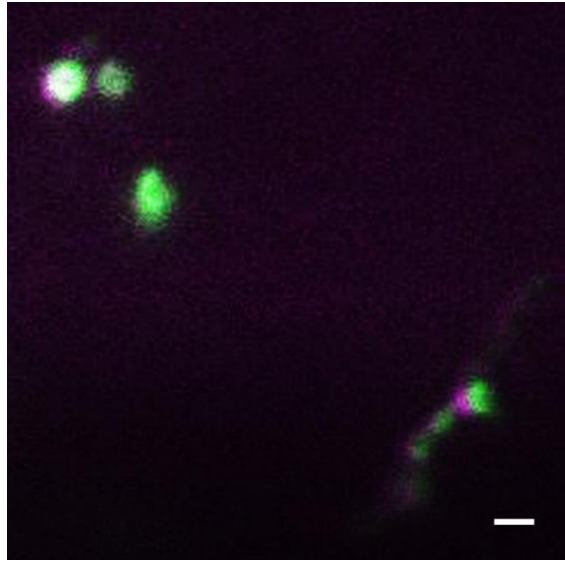


Figure 6.5: Co-expression of GFP-Atgolgin-84A $\Delta$ 1-557 and mRFP-AtCASP $\Delta$ 1-564 imaged with a TIRF microscope with two-colours imaging. GFP-Atgolgin-84A $\Delta$ 1-557 is imaged in the green channel with one of the cameras and mRFP-AtCASP $\Delta$ 1-564 is imaged in the red channel with the other camera (Appendix 1, Movie 26). Scale bar, 1  $\mu$ m.

Table 6-2: Mean of counted trapped Golgi bodies during the co-expression of GFP-Atgolgin-84A $\Delta$ 1-557 with mRFP-AtCASP $\Delta$ 1-664 compared to the mean of trapped Golgi bodies expressing ST-GFP. (A) Mean of Golgi bodies scored as trapped plus partially trapped. (B) Golgi bodies that are trapped and stay trapped for the 2  $\mu$ m translation. Golgi bodies as shown in Figure 6.1 and 6.6 were scored in 3 independent experiments; 100 Golgi bodies were tested per experiment. Data represent mean  $\pm$ SEM\*\*\* $p$ <0.001 (Chi-squared test).

### A

Construct	Mean $\pm$ SEM	<i>P</i>
ST-GFP	93 $\pm$ 0.467	0.314
GFP-Atgolgin-84A $\Delta$ 1-557 +mRFP-AtCASP $\Delta$ 1-664	95 $\pm$ 0.067	

### B

Construct	Mean $\pm$ SEM	<i>P</i>
ST-GFP	74 $\pm$ 0.817	*** 0.0009
GFP-Atgolgin-84A $\Delta$ 1-557 +mRFP-AtCASP $\Delta$ 1-664	61 $\pm$ 0.757	

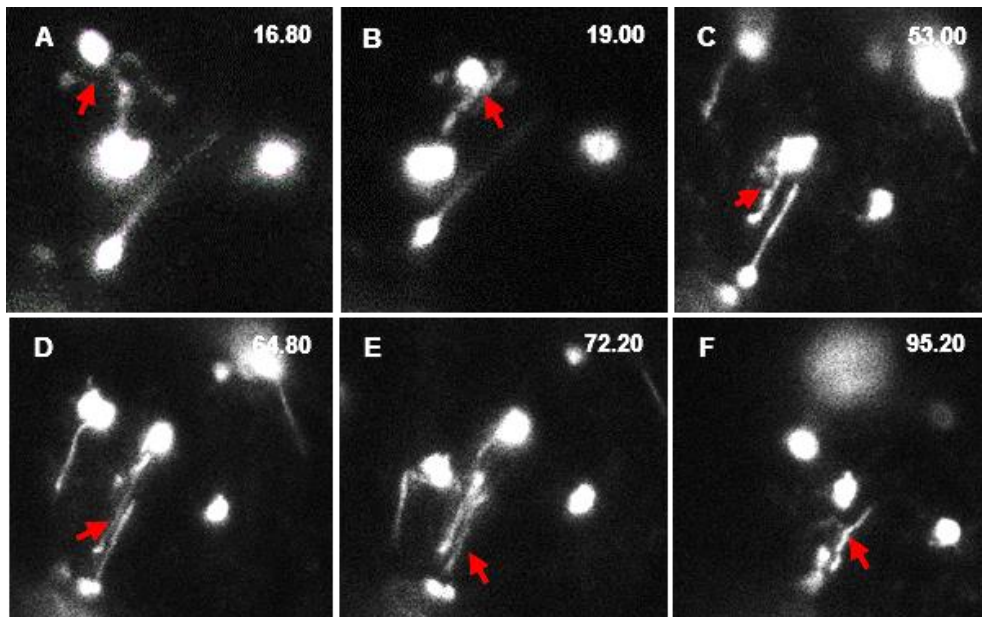


Figure 6.6: Co-expression of GFP-Atgolgin-84A $\Delta$ 1-557 and mRFP-AtCASP $\Delta$ 1-564 imaged with a TIRF microscope. The ring-shaped compartments show protruding long structures (Appendix I, Movie 27). (A) A Golgi body comes into contact with tubules (B) Golgi body seems to connect with this tubular structure and moves with it. (C and D, red arrow) The protruding tubules extend (E and F) a tubule detaches from the ring-shaped structure and moves free from Golgi bodies (red arrow). Time in seconds.

## 7. The effect of overexpression of Atgolgin-84A in protein trafficking

### 7.1 Introduction

The hypothesis of this work is that Atgolgin-84A is a tethering factor at the ER-Golgi interface, and. chapter 4 the localisation of the protein was investigated. Moreover, aggregates of Golgi bodies were observed during the overexpression of fluorescent forms of Atgolgin-84A. The overexpression of the full-length protein is very toxic for the plant cells. In chapter 5 the effect of the overexpression of a truncated version of the golgins without most of the coiled-coil domain region was assessed in tobacco leaf cells. Indeed, when the putative motif for the tethering, the coiled-coil region was deleted another strong phenotype was observed. The compartments labelled by the Atgolgin-84A $\Delta$ 1-557 exhibit long tubular structures. All together the results point towards a localisation of the golgin at the *cis*-Golgi and possibly at a pre-*cis*-Golgi subcompartment. The effects in disrupting the Golgi stack either by generating pairs of Golgi bodies or by the induction of long tubules could influence the entry of cargo into the Golgi. A similar role in tethering vesicles to Golgi membranes and in maintaining Golgi stacking has been suggested for the mammalian Golgi (Seemann *et al.*, 2000b; Short *et al.*, 2005). In this chapter it is hypothesised that if the plant golgins have a role in tethering the ER to the Golgi, as it has been shown for AtCASP in Osterrieder *et al.* (2017), also overexpression of a truncated golgin, in this study specifically Atgolgin-84A $\Delta$ 1-557 could be predicted to disrupt transport of proteins between ER and Golgi. Mammalian golgins have been implicated in tethering transport vesicles and it has been shown that golgins confer specificity to these tethering events at the Golgi (Malsam *et al.*, 2005; Wong and Munro, 2014).

This chapter will investigate a potential role for Atgolgin-84A and later for AtCASP as a biochemical control in protein trafficking. An effect on protein secretion is evaluated during the overexpression of full-length golgins and truncated versions, by two different methods: a secretion assay using confocal microscopy to image cargo protein destination upon overexpression of Atgolgin-84A and Atgolgin-84A $\Delta$ 1-557 and trial runs of an enzymatic assay that measures the activity of the secretory marker  $\alpha$ -amylase from barley during expression of Atgolgin-84A, Atgolgin-84A $\Delta$ 1-557 and AtCASP and AtCASP $\Delta$ 1-564.

## **7.2 Results**

### **7.2.1 A secretory assay using confocal microscopy**

To test the hypothesis that golgins have an effect on protein trafficking a signal peptide (SP) from the *A. thaliana* chitinase fused to mCherry (SP-mCh) was used as cargo. SP-mCh has been used before as a marker for the default secretion pathway (Soares Da Costa *et al.*, 2010). SP-mCh enters the secretory pathway via the signal peptide and after cleavage of the signal peptide mCherry is transported to the Golgi and as it is lacking any other sorting signals by default arrives at the extracellular matrix as seen in Figure 7.1A. If overexpression GFP-Atgolgin-84A or GFP-Atgolgin-84A $\Delta$ 1-557) have an effect on protein transport it would be expected that SP-mCh would be retained in the ER without accumulation of mCherry in the extracellular matrix for example as illustrated in Figure 7.1B. In this experiment SP-mCh was infiltrated alone or in combination with effectors (Atgolgin-84A full-length and the truncated protein GFP-Atgolgin-84A $\Delta$ 1-557).

SP-mCh alone labels the apoplast as expected from the literature (Soares Da Costa *et al.*, 2010) (Figure 7.3a, A). During co-expression of SP-mCh with Atgolgin-84A or Atgolgin-84A $\Delta$ 1-557 mCherry was detected

predominantly in the vacuole and most cells were not showing apoplast labelling (Figure 7.3F and I) which is very different from the control where SP-mCh was infiltrated alone (Figure 7.3a, A). When SP-mCh and Atgolgin-84A or Atgolgin-84A $\Delta$ 1-557 were infiltrated together and imaged 3 days after infiltration. The effect described above was not observed in all the cells and the results were not consistent i.e., some cells would have apoplast labelling and other cells would have vacuole labelling. It was unclear if the labelling of the vacuole could be due to overexpression and if Atgolgin-84A/ Atgolgin-84A $\Delta$ 1-557 were expressed fast enough to produce a dominant negative effect over the native golgins before mCherry reaches the Golgi body. Therefore Atgolgin-84A or Atgolgin-84A $\Delta$ 1-557 were infiltrated 24h before SP-mCh infiltration. The cells were imaged 3 days after the SP-mCh infiltration and consequently 4 days after infiltration of the golgins (see timeline Figure 7.2). The majority of cells observed had the effect shown in Figure 7.3F and I and these was observed in at least three independent repeats. Atgolgin-84A and Atgolgin-84A $\Delta$ 1-557 were also infiltrated alone and detected in punctate compartments (Figure 7.3a, B and C). It appears that mCherry was re-directed to the vacuole after overexpression of GFP-Atgolgin-84A and Atgolgin-84A $\Delta$ 1-557.

The cells with different labelling were categorised as shown in Figure 7.4 and counted. Figure 7.5 shows the number of cells with different mCherry localisation during overexpression of GFP-Atgolgin-84A or GFP-Atgolgin-84A $\Delta$ 1-557. Figure 7.5A shows the secretion assay if the cargo and effectors are infiltrated together. Figure 7.5B shows the secretion assay if effectors are infiltrated 24h before the cargo infiltration. The effect of Atgolgin-84A and Atgolgin-84A $\Delta$ 1-557 is more drastic if they are infiltrated before the SP-mCherry. As shown in Figure 7.5B more cells have vacuoles and less apoplast labelling. In the single infiltration of SP-mCh the fluorescence is detected in the apoplast and some vacuole labelling is detected most probably due to overexpression. When in co-expression with the golgins the

localisation of mCherry changes drastically and most of the protein is found in the vacuole and a few cells also have ER labelling (Figure 7.4).

Given the surprising accumulation of SP-mCh in the vacuole it was of interest to test Atgolgin-84A and Atgolgin-84A $\Delta$ 1-557 using a biochemical secretion assay that is well described in the literature (Phillipson *et al.*, 2001; Silva-Alvim *et al.*, 2018) for comparison. This method also allowed for testing of another golgin AtCASP and the respective truncation AtCASP $\Delta$ 1-564 as a comparative control described in chapter 5. Furthermore it allowed the comparison between fluorescent fusions and non-tagged effector proteins. Due to the time limitations of this project AtCASP was not tested using SP-mCh as secretion marker as described for Atgolgin-84A since GFP-AtCASP and GFP-AtCASP $\Delta$ 1-564 versions were not available in the laboratory.

### 7.2.2 A secretory assay using $\alpha$ -amylase

Barley  $\alpha$ -amylase (amy) has been used as a marker to quantify exocytosis versus cell retention in plant cells (Phillipson *et al.*, 2001). This enzyme from the aleurone layer has an important role in seed germination as it mobilises the starch reserves of the endosperm during seed germination. It is also used in breweries in the malting process due to being highly stable and can be incubated at 60°C. For this reason it has been developed as a tool to measure protein trafficking through the plant endomembrane system. *N. tabacum* and *N. benthamiana* mesophyll protoplasts do not show detectable  $\alpha$ -amylase activity, and therefore are the ideal model plant systems for expression of  $\alpha$ -amylase. The results obtained from fluorescence microscopy in section 7.2.1 gave a good indication of the effect of Atgolgin-84A and Atgolgin-84A $\Delta$ 1-557 in the secretory pathway and therefore it was decided to undertake a trial to using a secreted enzyme like  $\alpha$ -amylase as a secretion marker (Phillipson *et al.*, 2001). This technique also allows for comparison between tagged and untagged golgins. Atgolgin-84A



and AtCASP and Atgolgin-84A $\Delta$ 1-557 or AtCASP $\Delta$ 1-564 were cloned into double expression vectors optimised for transformation of protoplasts with a GUS reporter gene (Gershlick *et al.*, 2014; Silva-Alvim *et al.*, 2018) and versions with YFP fluorescent protein as illustrated in Figure 7.6A. AtCASP constructs were included in the  $\alpha$ -amylase experiment as a control golgin only. It was outside the remit of this project to investigate the role of AtCASP in secretion.

Plasmid DNA for the different constructs was tested in a GUS assay beforehand in order to quantify plasmid transfection rates. In order to compare different effectors (the molecules affecting the secretory pathway) it is important to normalise expression levels between different constructs. The cytosolic reporter GUS has been successfully used as an internal marker to distinguish ER stress from general cell mortality (Leborgne-Castel *et al.*, 1999) and is used in effector dose-response assays in vacuolar protein sorting research (Gershlick *et al.*, 2014). The GUS expression as internal standard can be measured enzymatically upon transfection and the result is applied for equalisation of different DNA preparations. Figure 7.6B shows a pilot assay to compare GUS activity and consequently protoplast transfection efficiency of the new constructs. To be able to compare the effect of golgins and mutants plasmid concentrations were chosen in order to yield comparable GUS expression levels.

The GUS activity levels in Figure 7.6B allow for normalisation of the transfection efficiency. Therefore according to this pilot assay the amount of plasmid for all constructs was calculated for protoplast electroporation and this was used for the  $\alpha$ -amylase assay and GUS assay as described in chapter 2.  $\alpha$ -amylase was used as control cargo (Figure 7.7A). Figure 7.7A shows the secretion index for two technical replicates of each construct. YFP-Atgolgin-84 shows approximately half the secretion index of the control which means that the cargo is being retained in the cells. Surprisingly, Atgolgin-84A $\Delta$ 1-557 shows approximately the same levels of exocytosis compared to the control. YFP-AtCASP does not seem to produce an effect.

AtCASP $\Delta$ 1-564 protein has a decrease in secretion index when compared to the control. The untagged versions decrease the secretion index except for AtCASP that shows similar levels as the  $\alpha$ -amylase control. Total activity of the  $\alpha$ -amylase shows that the electroporation was successful, the transfection was efficient and the co-expression with golgins did not affect the activity of the enzyme (Figure 7.7B).

These results were obtained in *N. benthamiana* since this system is optimized in this species (Silva-Alvim *et al.*, 2018). The same approach used for *N. tabacum* on the confocal secretion assay was tested in *N. benthamiana*. Interestingly SP-mCherry was not detected in the vacuole in the presence of GFP-Atgolgin-84A or GFP-Atgolgin $\Delta$ 1-557 as observed in *N. tabacum* and instead is detected in the apoplast (Figure 7.8C and D). Surprisingly, SP-mcherry has cytoplasmic localisation before being detected in the vacuole (Figure 7.8A and B).

Due to time constraints it was not possible to undertake further experiments to perfect of this assay.

## 7.3 Discussion

In the endomembrane system there is a constant and selective transport of cargo between compartments. The cargo is collected by transporters that can be vesicles, for example in mammalian cells, and has to be transported and finally be delivered to the correct destination. Many proteins are involved in these events such as SNAREs as described in detail in chapter 1, section 1.1.1. Recent publications demonstrated in a very elegant way, using a relocation strategy, that several mammalian golgins can tether vesicles (Wong and Munro, 2014). These golgins are also selective. For example, *cis*-golgins would tether cargo that has to transit from ER to the Golgi and golgins at the *trans*-Golgi would capture vesicles carrying cargo passing from the endosome to the Golgi. Golgins have been suggested to play a role in vesicle fusion by attaching the vesicle to the destination organelle and then bringing it close to allow for example, SNARE proteins on opposite membranes to interact (Malsam *et al.*, 2005; Drin *et al.*, 2008). Considering the localisation of Atgolgin-84A and Atgolgin-84A $\Delta$ 1-557 as described in chapters 4 and 5 and the dramatic phenotypes observed and the findings mentioned above in mammalian cells Atgolgin-84A and Atgolgin-84A $\Delta$ 1-557 were co-expressed with a secreted molecule in order to test if there would be changes in the trafficking of model secretory proteins. Non-tagged and fluorescently-tagged versions of Atgolgin-84A, Atgolgin-84A $\Delta$ 1-557, AtCASP and the mutant AtCASP $\Delta$ 1-564 were also tested using an enzymatic assay. Interesting to note that, CASP did not show tethering activity in the gain-of-function assays in mammalian cells (Wong and Munro *et al.*, 2014) but it is also suggested that CASP has this tethering function only by interaction with other golgins or other proteins.

## Using a secreted mCherry construct version as a marker for secretion/retention

The first assay took advantage of live cell imaging and a secreted version of the mCherry fluorescent protein. Lacking any other sorting signal, the final destination of SP-mCh is the apoplast after passing through the Golgi stacks. The golgins were infiltrated before SP-mCh and in this set-up mCherry was re-directed to the vacuole (Figure 7.3). It appears that it takes longer for the fluorescent tagged golgin to have a dominant negative effect than it takes SP-mCherry to complete the route. The infiltrated golgins have to be already in the Golgi before SP-mCh expression for cargo to be diverted to the vacuole efficiently (Figure 7.5). The secretion of mCherry should be a fast process considering the relatively small size of the molecule and therefore it could possibly pass through the Golgi before the Atgolgin-84A or truncation has an effect. This can be due to the size of a molecule like GFP-Atgolgin-84A or the time to correctly fold the protein or the time necessary to titrate out putative native golgins in the *N. tabacum* cells. Considering this, only results on Figure 7.5B will be discussed in detail.

Around 10% of the cells expressing Atgolgin-84A show mCherry in the other location apart from vacuoles and apoplast (vacuoles, ER and punctae). This can be due to overexpression and the cargo still in transit or the golgin could cause a delay in ER export and the punctae observed could be pre-vacuolar compartment labelling. 90% of the cells show vacuolar labelling and only 5% of these show mCherry in the apoplast, and the latter is probably due to overexpression of SP-mCh or lower levels of Atgolgin-84A expression that are not sufficient to produce an effect in these cells. The mutant golgin shows very similar effects and distribution pattern to the full-length protein. It can be hypothesised that both fusions can be causing the same effect as they disrupt the tether between the two organelles which is important for transport between ER and Golgi. It could be that in the full-length protein the fluorophore tag is blocking the coiled-coil domain region and this fusion

would result in a non-fully functional golgin. This could explain why the effect of the untagged full-length protein in the amylase assay is different (Figure 7.7A) and that secretion decreases in the untagged versions. There is also a possibility that having overexpression of golgin impairs trafficking between ER and Golgi. Atgolgin-84A native expression levels may be very low and an excess of golgin might collapse the pathway. It was shown in chapter 4 that Atgolgin-84A induces pairs of Golgi bodies and that could possibly affect the structure of the organelle impairing entry of cargo into the Golgi. It is also important that part of the coiled-coil region remains in deletion mutant and might still retain some tethering function. In the case of the mutant without coiled-coil domains the distance between ER and Golgi might be longer or the connection between compartments is not strong enough to give support to events of docking of transporters of cargo.

Expression of GFP-Atgolgin-84A and GFP-Atgolgin-84A $\Delta$ 1-557 re-direct most of the detected mCherry to the vacuole. If entry into the Golgi would be severely compromised it is possible that an alternative pathway is active and exporting cargo from ER or there is a route directly from *cis*-Golgi to vacuole. The cells might be responding to the overexpression by exporting unnecessary cargo from the ER and send it to the vacuole for degradation (Wang *et al.*, 2017). Soluble proteins do not require signals to mediate secretion but they require sorting signals to avoid secretion and reach vacuoles or other organelles instead. The accumulation of SP-mCherry in the vacuole upon overexpression of Atgolgin-84A or the deletion mutant might be due to the cells sending unnecessary cargo for degradation and because entry in the Golgi is impaired the cells may be using a different route to reach the vacuole. Thus it can be hypothesised that cargo can bypass the Golgi to reach the vacuole.

## Using $\alpha$ -amylase activity to measure secretion upon golgins overexpression

The secretion assay described in section 7.2.1 gave a good indication that golgins have a role in the protein trafficking from ER to Golgi. Quantification of fluorescence imaging can be biased by the volume of the cell compartment and overexpression of the secretion markers and by relying on visual assessment of protein localisation. Therefore a trial run of a biochemical secretion assay was undertaken.

The secretion index (SI) obtained from expression of the golgins and truncations show that golgins change the secretion/retention of  $\alpha$ -amylase. Using this assay allows testing of untagged versions of each golgin and truncation. All constructs show lower SI for tagged and untagged versions except for YFP-Atgolgin-84A $\Delta$ 1-557 that shows the same SI compared to the control (Figure 7.7A). This means that the overexpression of YFP-Atgolgin-84A, YFP-AtCASP, YFP-AtCASP $\Delta$ 1-564, Atgolgin-84A, Atgolgin-84A $\Delta$ 1-557, AtCASP, AtCASP $\Delta$ 1-564 caused a retention of amylase inside the cells and therefore a decrease of detected extracellular amylase activity in the medium. YFP-AtCASP and AtCASP showed less effect in blocking exocytosis than any of the other effectors but significance of this data would have to be confirmed by independent repeats.

These preliminary results gave a good confirmation of what was observed in the secretion assay by confocal microscopy (section 7.2.1). This experiment requires further repeats to confirm these results and controls, for example a positive control for retention, a molecule that is already described as blocking the trafficking between ER and Golgi such as Sar1-GTP locked dominant negative mutant that impairs COPII transport and was already used for this type of experiments (Phillipson *et al.*, 2001).

Expression of the golgin fusions can also be optimised since in the GUS activity assay the results for GUS activity are usually higher for other

constructs tested in this assay. This can be achieved using protocols for DNA extraction that result in higher yields and this is very important for the efficiency of the  $\alpha$ -amylase assay.

Another limitation is the timing of expression of the proteins. This assay is optimised for the expression of amylase but the golgins have different time requirements for optimal protein expression. In section 7.2.1 the time-course for the secretion was optimised for confocal imaging. The full-length fusions are only observed in the Golgi 3 days after infiltration therefore before dominant negative effect the levels of the fusions might not be high enough to disrupt the pathway. Indeed, the a more drastic effect was obtained when the golgins are already being expressed 24h before the cargo. In the protoplasts transformation the optimised set-up for expression of effectors (molecules that affect retention/secretion) means that golgin/deletion mutants have to be necessarily transfected together. Due to viability of protoplasts only the expression at 24h was tested. The expression of the fusions could have been monitored by fluorescence microscopy since half of the fusions are tagged with YFP but due to time limitations this was not tested. Furthermore, this experiment was performed in *N. benthamiana* as the  $\alpha$ -amylase assay was established and optimised in this species and the protoplasting results obtained are considerably better in *N. benthamiana* (Silva-Alvim *et al.*, 2018). To confirm the results obtained in section 7.2.1 in *N. benthamiana* the same approach was tested in this species but surprisingly, SP-mCh was not retained in the cells as in *N. tabacum* (Figure 7.8). These results suggest that possibly in *N. benthamiana* most of SP-mCh does not enter the ER and therefore does not enter the secretory pathway and might be secreted as a leaderless protein. For future optimisations SP-mCh is probably not the best choice as cargo for *N. benthamiana* system. The golgin fusions can be tested in *N. tabacum* protoplasts in the future to fit with the microscopy assay but another secretion marker should be tested.

In conclusion in this chapter it has been shown that expression of Atgolgin-84A and truncation Atgolgin-84A $\Delta$ 1-557 can have a major effect on the transport of a marker protein in the secretory assay.  $\alpha$ -amylase secretion assays are a powerful tool to study trafficking in plant cells but have to be further optimised for the expression of the golgins. Taken together the results indicate that golgins have a role in protein trafficking. It remains unclear if the effect is direct because plant golgins, similar to golgins in mammalian cells, are involved in tethering of specific transporters or because competition with the native golgins affects tethering of ER and Golgi which is important for protein transport from ER to Golgi.



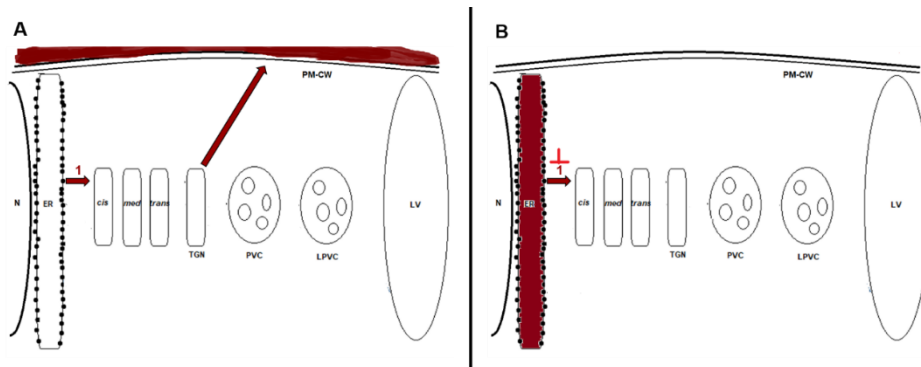


Figure 7.1: Schematic diagram of secretory pathway blockage by overexpression of Atgolgin-84A or Atgolgin-84A $\Delta$ 1-557. (A) SP-mCh alone: SP-mCh default pathway showing mCherry labelling the extracellular matrix. This is the conventional pathway described in Chapter 1, Figure 1.1. (B) Considering the hypothesis that overexpression of Atgolgin-84A would have an effect in the ER-to-Golgi trafficking, SP-mCh labelling the ER and not the extracellular matrix when co-infiltrated with Atgolgin-84A or Atgolgin-84A $\Delta$ 1-557 would be one possible outcome.

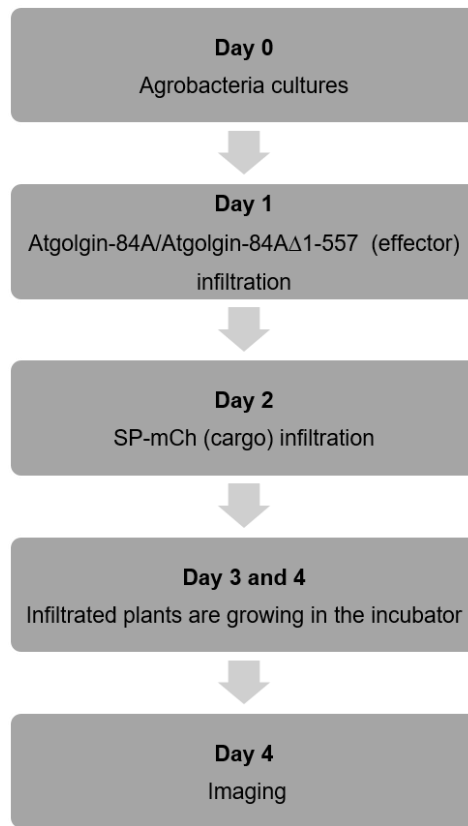


Figure 7.2: Timeline of infiltration for the secretion assay imaging. The protocol starts with set up of Agrobacteria cultures on day 0. The effector is infiltrated on day 1. On day 2 i.e. 24h after effector infiltration, the cargo was infiltrated. The plants were left to grow in the incubator and at day 4 (4 days after first infiltration of effector, 3 days after infiltration of cargo) plants are imaged.

### Controls

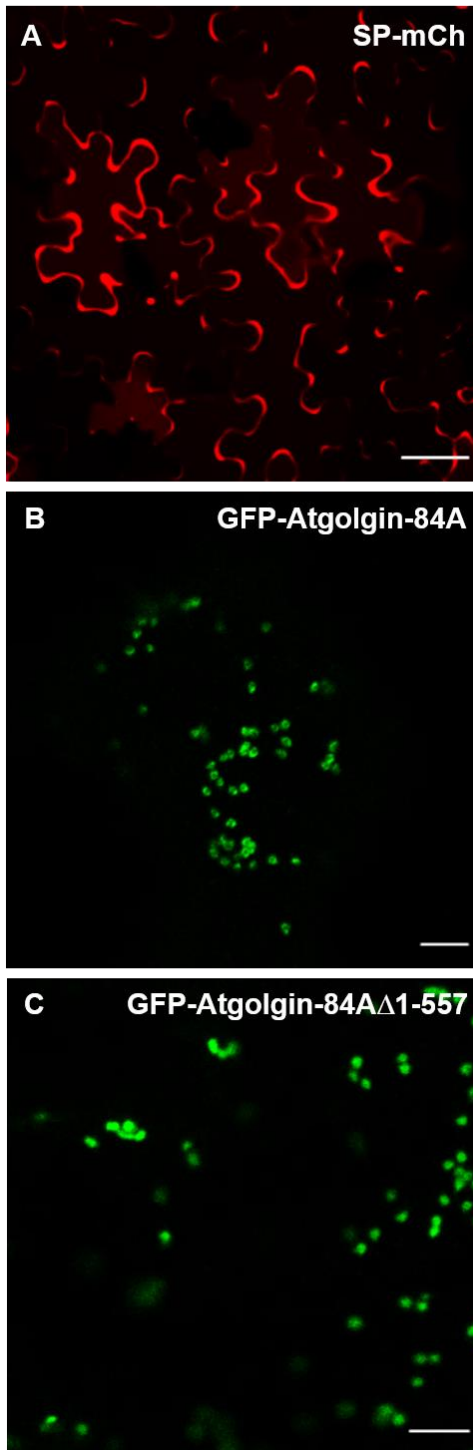


Figure 7.3a: Secretion assay using transient expression in *N. tabacum*. All fluorescent fusions were expressed alone (A-C) as controls. (A) SP-mCherry was detected in the apoplast. (B and C) Atgolgin-84A and Atgolgin-84A $\Delta$ 1-557 were detected in green dots (B and C). (D-I) Co-expression of Atgolgin-84A or Atgolgin-84A $\Delta$ 1-557 with SP-mCherry. (D and G) Red channel showing SP-mCherry fluorescence. (E and H) Green channel for co-expression showing only the golgins and truncated golgins version. (F and I) Expression of GFP-Atgolgin-84A or GFP-Atgolgin-8A $\Delta$ 1-557 changes SP-mCherry localisation and mCherry is detected predominantly in the vacuole. Scale bars, (A, D, E, F, G, H and I) 50  $\mu$ m; (B) 10  $\mu$ m and (C) 5  $\mu$ m.

### Atgolgin-84A+SP-mCh

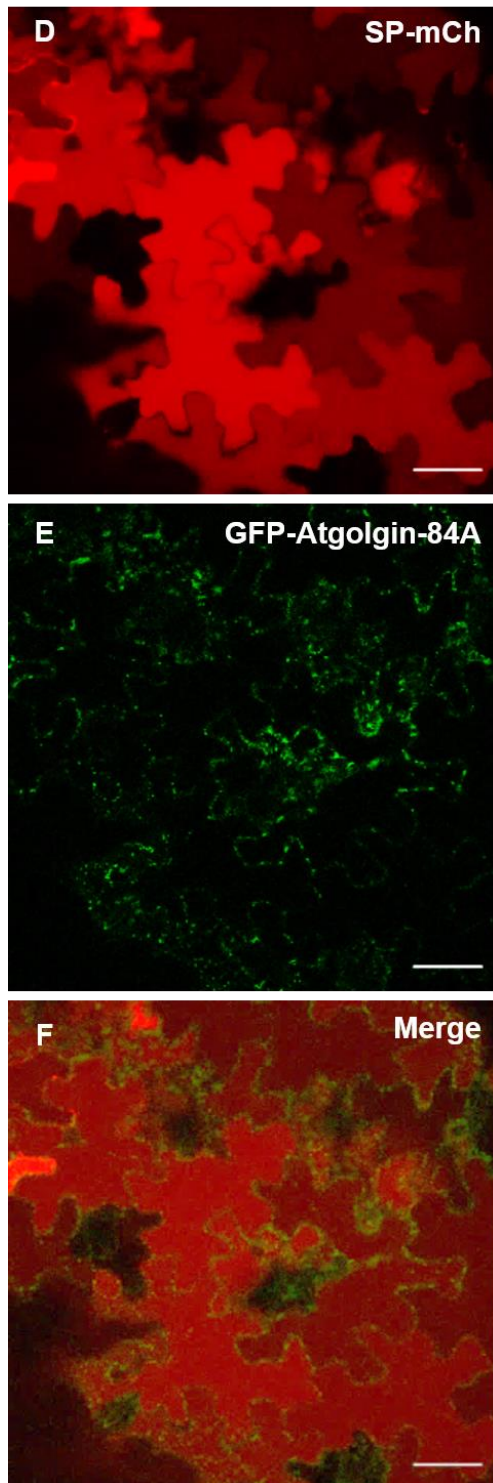


Figure 7.3b: Secretion assay using transient expression in *N. tabacum*. All fluorescent fusions were expressed alone (A-C) as controls. (A) SP-mCherry was detected in the apoplast. (B and C) Atgolgin-84A and Atgolgin-84A $\Delta$ 1-557 were detected in green dots (B and C). (D-I) Co-expression of Atgolgin-84A or Atgolgin-84A $\Delta$ 1-557 with SP-mCherry. (D and G) Red channel showing SP-mCh fluorescence. (E and H) Green channel for co-expression showing only the golgins and truncated golgins version. (F and I) Expression of GFP-Atgolgin-84A or GFP-Atgolgin-84A $\Delta$ 1-557 changes SP-mCherry localisation and mCherry is detected predominantly in the vacuole. Scale bars, (A, D, E, F, G, H and I) 50  $\mu$ m; (B) 10  $\mu$ m and (C) 5  $\mu$ m.

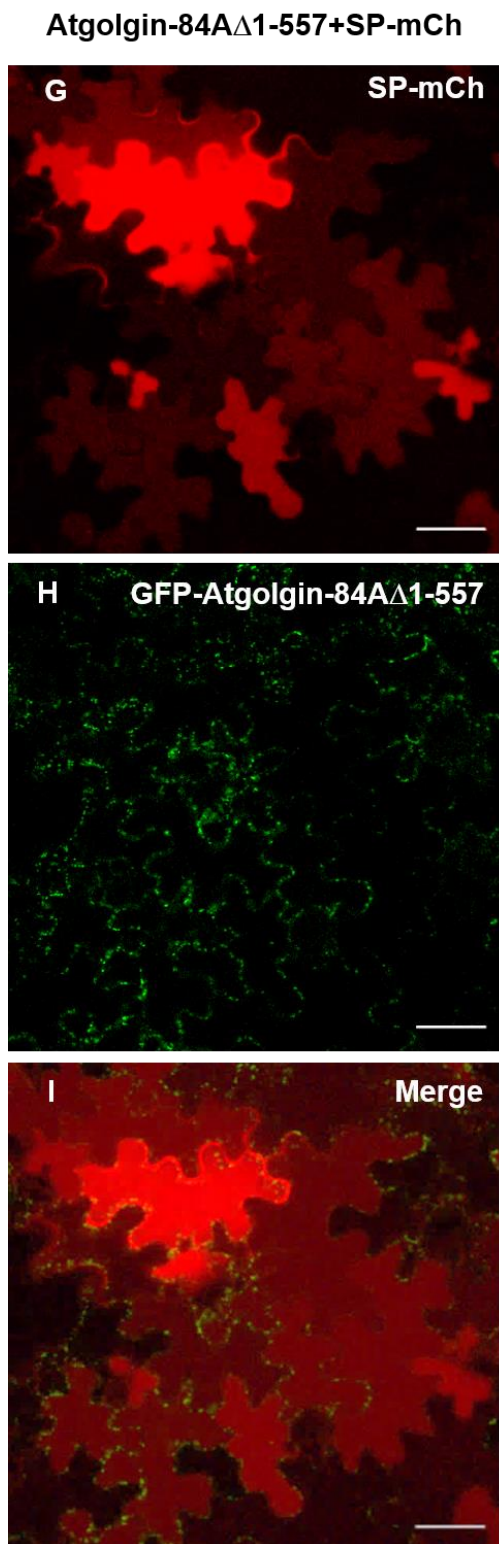


Figure 7.3c: Secretion assay using transient expression in *N. tabacum*. All fluorescent fusions were expressed alone (A-C) as controls. (A) SP-mCherry was detected in the apoplast. (B and C) Atgolgin-84A and Atgolgin-84A $\Delta$ 1-557 were detected in green dots (B and C). (D-I) Co-expression of Atgolgin-84A or Atgolgin-84A $\Delta$ 1-557 with SP-mCherry. (D and G) Red channel showing SP-mCh fluorescence. (E and H) Green channel for co-expression showing only the golgins and truncated golgins version. (F and I) Expression of GFP-Atgolgin-84A or GFP-Atgolgin-84A $\Delta$ 1-557 changes SP-mCherry localisation and mCherry is detected predominantly in the vacuole. Scale bars, (A, D, E, F, G, H and I) 50  $\mu$ m; (B) 10  $\mu$ m and (C) 5  $\mu$ m.

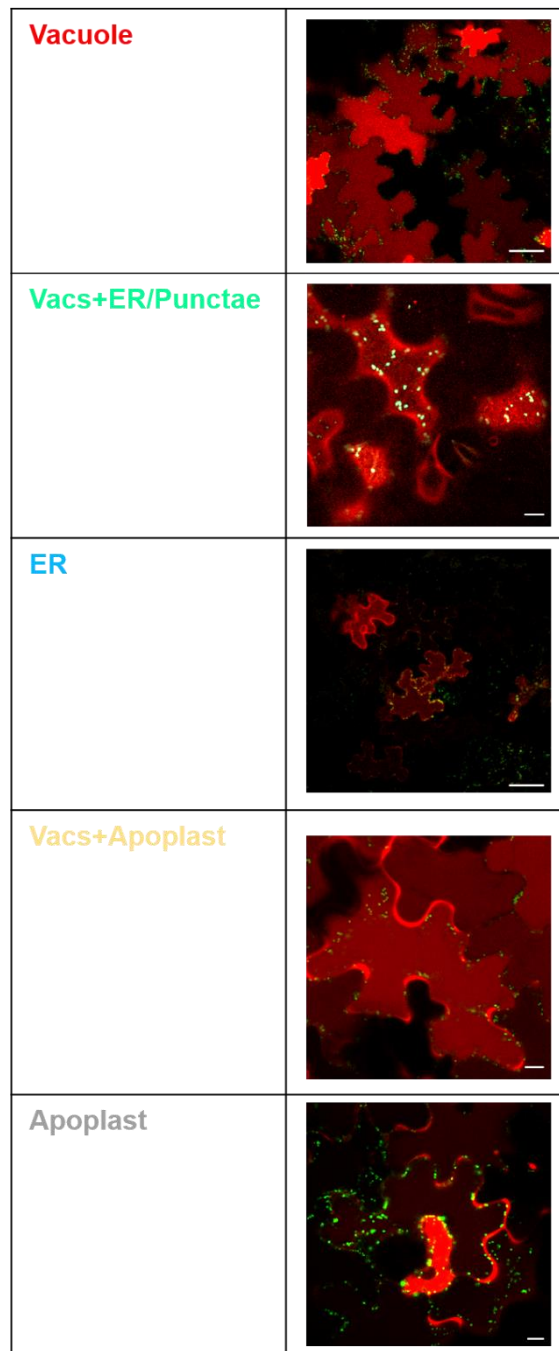


Figure 7.4: Example of each category used for the quantification from the co-expression of SP-mCh with GFP-Atgolgin-84A $\Delta$ 1-557. Each image contains at least one cell from the category. Scale bars, Vacuole 50 $\mu$ m; Vacs+Apoplast 10 $\mu$ m; ER 50 $\mu$ m; Vacs+Apoplast 10 $\mu$ m; Apoplast 10 $\mu$ m.

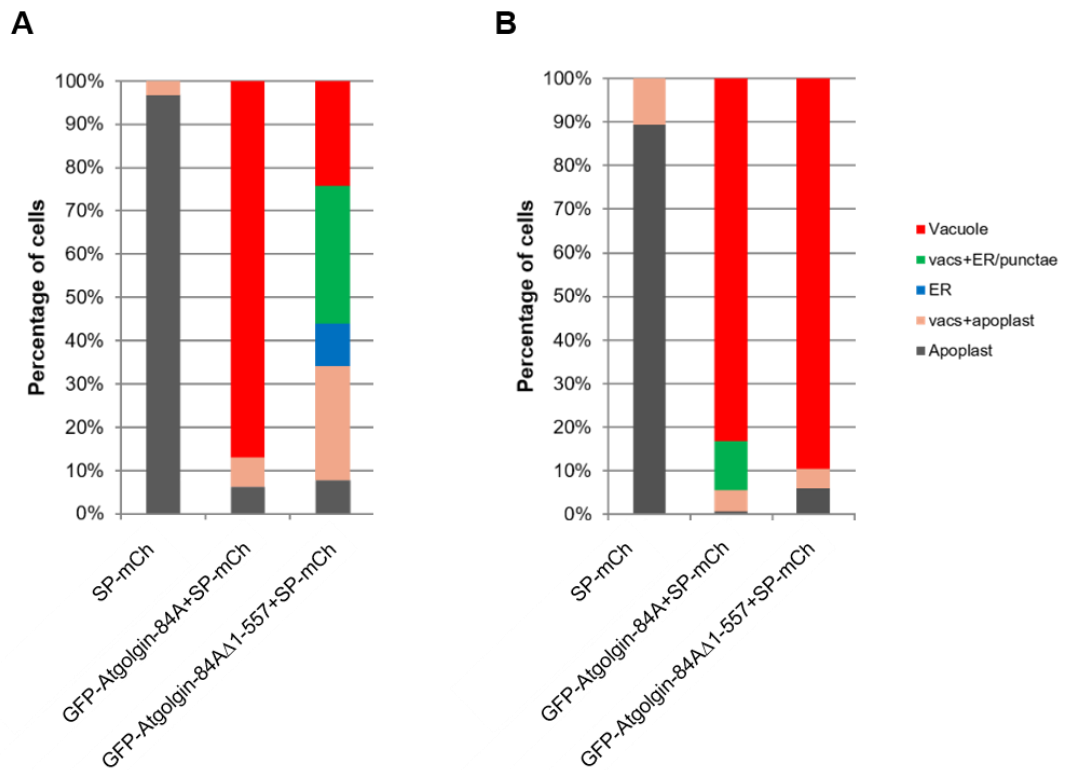


Figure 7.5: Quantification of the amount of cells showing different labelling by mCherry. (A) Shows localisation of mCherry when effectors and cargo are infiltrated together and imaged 4dpi. (B) Shows localisation of mCherry when effectors are infiltrated 24h before SP-mCherry and cells are imaged 3 days after SP-mCherry infiltration and consequently the effectors 4dpi.  $n \geq 47$  (minimum 47 cells were scored per condition).  $n$ , number of cells counted per each different protein expression combination in three independent experiments.

on the left.

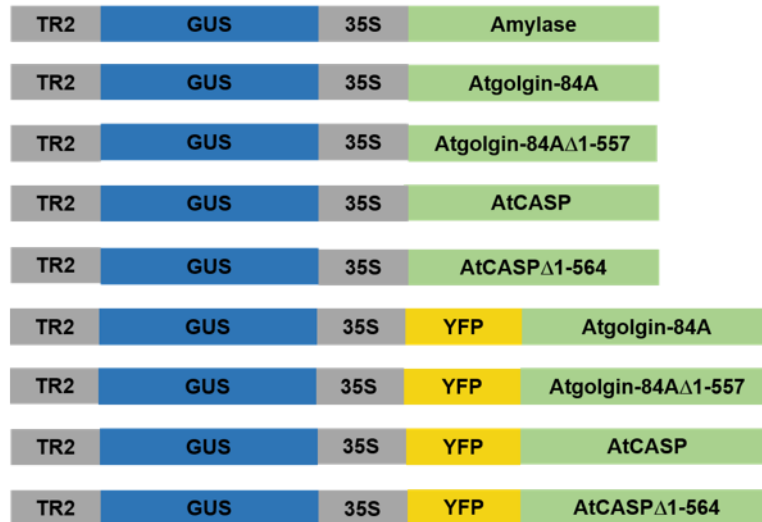
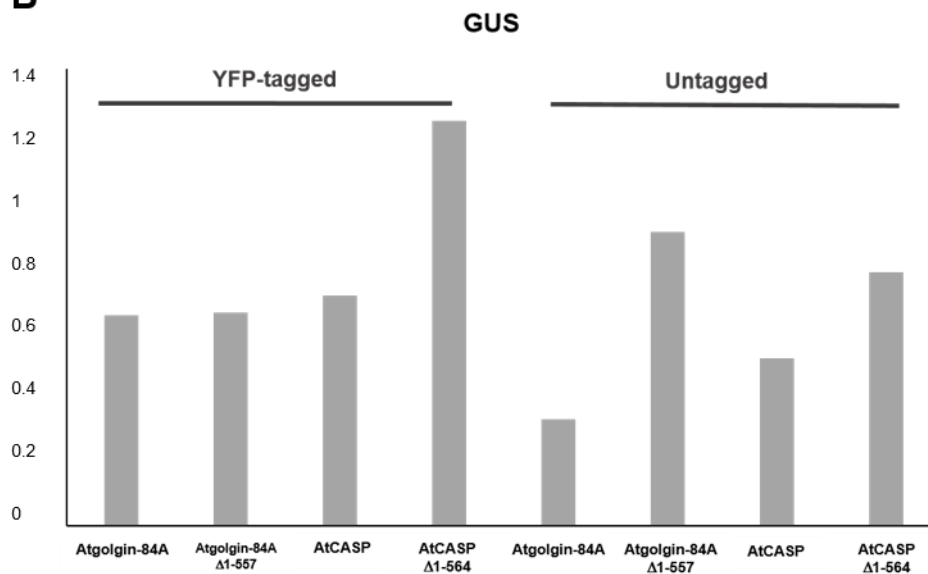
**A****B**

Figure 7.6: Pilot test for expression of golgins and truncations using GUS assay in transfected *N. benthamiana* protoplasts. (A) Atgolgin-84A and AtCASP and respective versions without coiled-coil domains were sub-cloned into GUS double vector. (B) The amount of DNA to use in the  $\alpha$ -amylase assay was adjusted according to the expression in the pilot GUS activity assay. GUS activity units are measured as absorbance at 405 nm and considered as arbitrary.



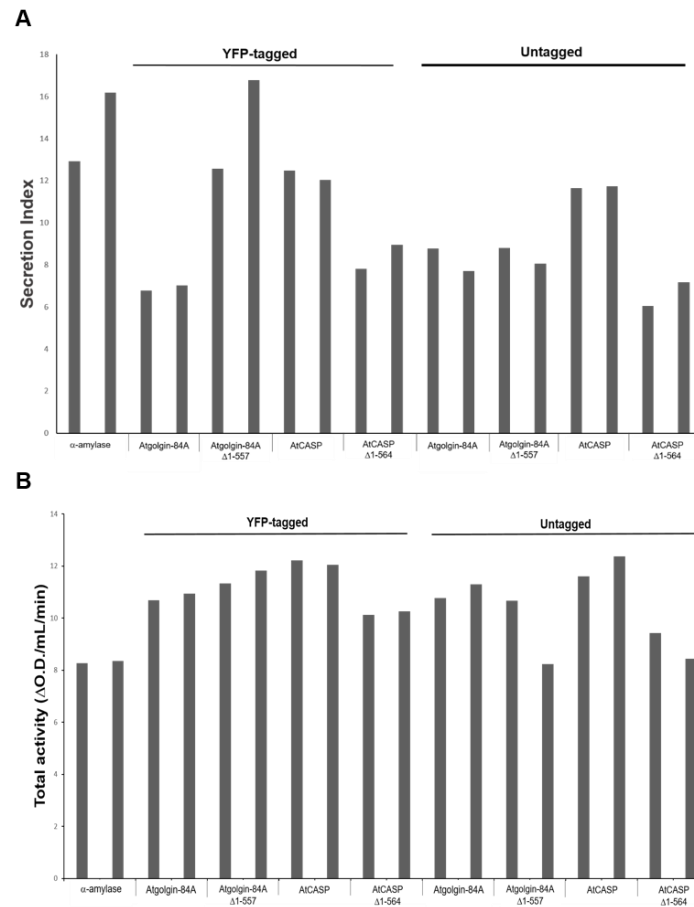


Figure 7.7: Co-expression of  $\alpha$ -amylase and golgins fusions in *N. Benthamiana* protoplasts as described in chapter 2, section 2.3. Protoplasts were transfected with  $\alpha$ -amylase plasmid alone or together with the plasmid encoding YFP-tagged and untagged versions of Atgolgin-84A full-length, the deletion mutant Atgolgin-84A $\Delta$ 1-557, AtCASP full-length and the deletion mutant AtCASP $\Delta$ 1-564. The two bars represent replicates for each construct. (A) Protoplast suspensions were harvested to obtain cells and medium separately. The  $\alpha$ -amylase activity was measured for both medium and cell fractions, and the secretion index was calculated. The negative controls contain only cargo DNA. (B) Shows the total activity of medium plus cell samples to confirm the relative transfection efficiency. Units of  $\alpha$ -amylase activity are  $\Delta$ O.D./mL/min and secretion index units are considered as arbitrary.

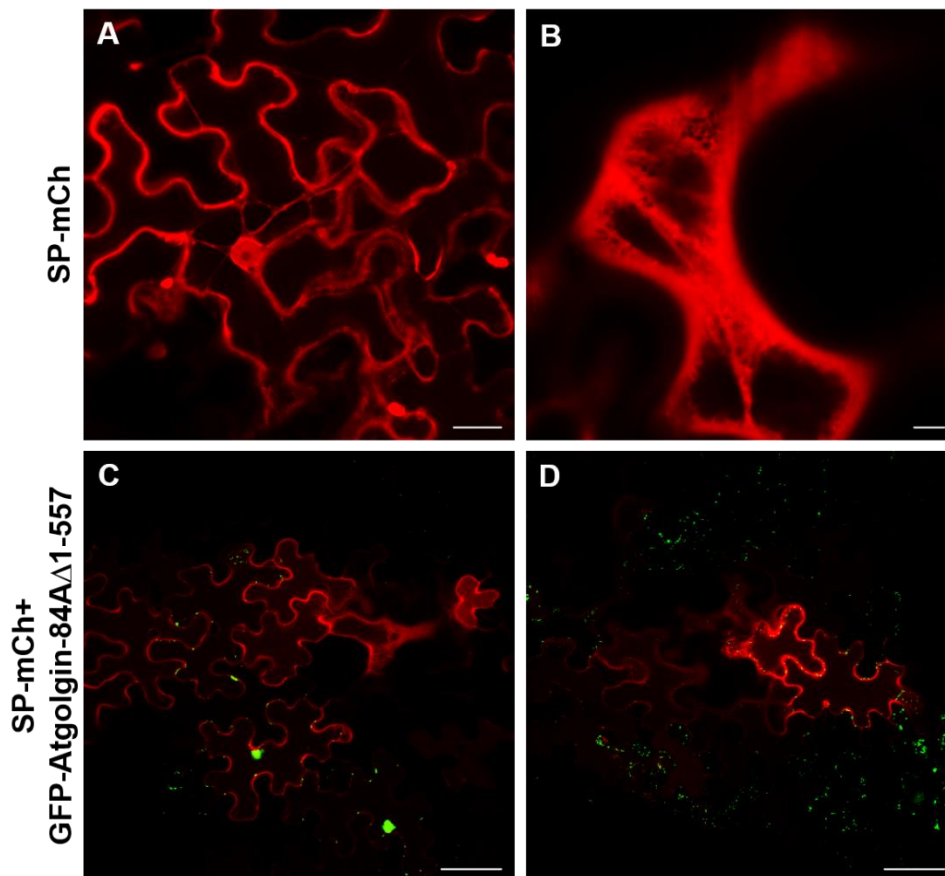


Figure 7.8: Co-expression of SP-mCherry with GFP-Atgolgin-84A $\Delta$ 1-557 in *N. benthamiana*. (A) Expression of SP-mCh alone in *N. benthamiana* 3 dpi. Apoplast is labelled but also the cytoplasmic strands and mCherry is detected inside the nucleus. (B) Cytoplasmic labelling of SP-mCh in *N. benthamiana*. (C and D) Overexpression of GFP-Atgolgin-84A $\Delta$ 1-557 does not re-direct SP-mCh to the vacuole and mCherry is detected in the apoplast and cytoplasm. Scale bars, (A) 20 $\mu$ m; (B) 5 $\mu$ m; (C and D) 50 $\mu$ m.

## 8.1 General Discussion and future work

The aims of this work were to study the Arabidopsis protein Atgolgin-84A in terms of subcellular localisation but also to characterise the putative functions of this golgin. Recent advances in confocal microscopy brought about dramatically increased image resolution and allowed for unprecedented imaging of Golgi cisternae and ER.

### **The features of predicted Atgolgin-84A structure show characteristics of a tether and similarity with human golgin-84**

The first task of the project was to get predictions about the Atgolgin-84A structure and features. Atgolgin-84A was identified by structural characteristics of human golgin-84 namely the transmembrane domain (Latijnhouwers *et al.*, 2007). It was important that before looking into localisation and putative functions of the protein in silico characterisation was updated using bioinformatics tools with publicly available data and also using the information about the human golgin-84 described recently (Wong *et al.* 2017). The data obtained was a good indication that Atgolgin-84A could have high flexibility due to its long-coiled coil domains that have been described to extend to reach into the cytoplasm in other golgins (Cheung *et al.*, 2015, for review Wong *et al.*, 2017). Another important feature found in human golgin-84 is that the N-terminal deletion abolishes the tethering ability of capturing cargo vesicles (Wong *et al.*, 2017). More specifically the Trp3 mutation seems to play a crucial role in this function. This amino acid is conserved in *A. thaliana* golgin-84A and other plant species. In the future would be interesting to investigate more about this amino acid and the first 40 amino acids of Atgolgin-84 to understand if the sequence that determines recognition and tethering of transporters would be conserved in plants. The molecule seems to have phosphorylation sites and although there is some

information that these were tested experimentally not much detail is given in databases therefore further experiments would be needed to confirm any of this data. If Atgolgin-84A can be phosphorylated in order to regulate its function and the deletion of the long coiled-coil domains exposed some phosphorylation sites than Atgolgin-84A $\Delta$ 1-557 could lose its tethering function by impaired interaction with other golgins, Rab proteins or tethering factors or by dissociation from the Golgi membrane (Witkos and Lowe, 2016). Also this *in silico* analysis helped to confirm that there is a short coiled-coil domain remaining in the Atgolgin-84A $\Delta$ 1-557 and this could have some residual function.

### **Atgolgin-84A could be part of a scaffold involved in shape, size and orientation of the Golgi stack and partially localised in a pre-*cis*-Golgi compartment**

Using the Airyscan detector it was possible to see that Atgolgin-84A does not completely co-localise with *cis*-Golgi markers and the data here obtained implies that there is a sub-compartment before the true Golgi, between ER and Golgi. In plant cells there is no evidence for an ER-Golgi intermediate compartment (ERGIC) but this could be an equivalent.

One of the limitations of this project was the lack of characterisation of ERES markers with high-resolution in the literature. Recent developments in confocal imaging allows for a re-definition of localisation of well described markers and as observed during this work a re-definition of Golgi subcompartments and the ER-Golgi interface.

Atgolgin-84A seems to lose its ring-shape when co-expressed with markers for COPII components which is the case of AtSar1a. The few ring-shape structures that could be observed looked like the COPII component co-localise on this same sub-compartment. These findings do not exclude that other markers could label the exit sites at the ER. In fact isoforms of AtSar1 have been described to have distinct localisations using

immunofluorescence and structured illumination microscopy (SIM) (Zeng *et al.*, 2015). AtSar1a was found in the peri-Golgi region and AtSar1c was largely separated from the Golgi in Arabidopsis and tobacco (Zeng *et al.*, 2015). It would be interesting to obtain imaging of these and other COPII components with the Airyscan detector as these processes are dynamic which requires fast live high-resolution imaging and may give different results from the ones using other microscopy techniques such as SIM.

Another question is: how does the Atgolgin-84A reaches the Golgi membrane and possibly Golgi matrix/scaffold? In fact 2 days post-infiltration GFP-Atgolgin-84A is detected in punctae, cytoplasm and pleomorphic structures. Interestingly, this was observed during the BFA treatment which is very different from what is observed for Golgi markers such as ST or MnSI. At 3 days post-infiltration the golgin is in the ring-shaped compartments and these are sometimes in pairs or aggregates of more than two Golgi bodies. This was the first indication that Atgolgin.84A can act as a tethering factor.

By imaging with Airyscan detection the Atgolgin-84A-labelled compartment looks larger in relation to the ER than previously with conventional confocal microscopy detection. It seems that the ER and Golgi fit around each other re-shaping to adjust the Golgi to the lacunae of the ER.

Interestingly, Atgolgin-84A shows tubules during BFA wash-out and these were also observed during expression of Atgolgin-84A $\Delta$ 1-557. This could indicate that Atgolgin-84A is involved the assembly of new Golgi stacks or for Golgi stacking maintenance. During reassembly of the Golgi stack, in the case of BFA washout Atgolgin-84A labels tubular structures until the Golgi stack is reassembled and Atgolgin-84A $\Delta$ 1-557 without coiled coil domains is not able to keep the Golgi stacking together and what it is observed in the disassembly of the stack by the appearing of long tubules. Also Atgolgin-84A does not go back to the ER during BFA washout contrary to what happens for *cis*- and *trans*-Golgi markers. This might be a strong indication for the existence of a Golgi matrix in which Atgolgin-84A stays during the BFA treatment. Possibly the Atgolgin-84A interacts with other components of the matrix and this bounds are strong enough for the Atgolgin-

84A to stay in the matrix and possibly serving as a scaffold for reassembly of the Golgi or for Golgi biogenesis events.

More interestingly the deletion of the coiled coil domains does not seem to affect the localisation of the Atgolgin-84A upon BFA treatment. Possibly the remaining coiled-coil region in the structure is enough to keep to Atgolgin-84A in the matrix. Furthermore interactors of full-length and Atgolgin-84A $\Delta$ 1-557 could be compared by using a technique of co-immunoprecipitation. If Atgolgin-84A $\Delta$ 1-557 is mainly localised at the lumen of the Golgi and the full-length is reaching out to the cytoplasm it can be hypothesised that the interactors could be at least in part different.

The tubules are similar to what was observed for a non-functional version of ERD2, a receptor that mediates accumulation of soluble protein in the ER, where long tubules were also observed (Silva-Alvim *et al.*, 2018). It would be of interest to co-express Atgolgin-84A $\Delta$ 1-557 and non-functional ERD2 to investigate if these tubules co-localise. This could be a good indication that these proteins are involved in related mechanisms and therefore causing similar perturbations to Golgi structure.

Indeed, there are effects in tethering when the long coiled coil domains are deleted. The ring-shaped compartments flip more to a sideways view instead of the usual face view. The ring-shaped structures labelled by Atgolgin-84A $\Delta$ 1-557 can rotate. Considering the Golgi bodies are mainly observed in face view this suggests that the Golgi body is more efficient in this orientation. Therefore it is not surprising that for instance we observe effects in protein trafficking. Moreover it was observed that is possible to capture more than one Golgi body at the same time using an optical trap. Sometimes around 20 Golgi bodies can be trapped in the same trapping event. Repetitions with quantifications would be needed to understand this result but it is another good indication that the deletion of long coiled domains causes the Golgi bodies Surprisingly less Golgi bodies are amenable to trapping when compared to wild-type. This is due to the fact that the method is to count only yes or no for trapping and not how many Golgi bodies fall into

the trap in each trapping event. The fact that several Golgi bodies fall into the trap at the same time suggests that the Golgi bodies are looser which points to a role of Atgolgin-84A in tethering of Golgi bodies to other structures. The GFP-Atgolgin-84A $\Delta$ 1-557 possibly has to be in high concentration to titrate out the native golgin and maybe this is a slow process. Atgolgin-84A may be the other tether that it still keeping the ER and Golgi connected when a truncation of AtCASP is expressed and as described in Osterrieder *et al.* (2017), the ER still follows the Golgi bodies but a gap is induced between both compartments. The trapping data here present confirms that AtCASP has an effect in tethering since AtCASP $\Delta$ 1-564 abolishes the effect of Atgolgin-84A $\Delta$ 1-557. This indicates that these two golgins have different functions but work at the same tethering events at the pre-*cis*-Golgi compartment level. In future, to test this optical tweezers could be used in a method similar to what is described in Gao *et al.* (2016). The Golgi bodies with tubules would be trapped, moved and released from the trap to see if they would go back to initial position. Also comparing how much laser power and, in a more quantifiable manner, measuring how much force is required to move a Golgi body would be of interest. Tracking analysis should be done with GFP-Atgolgin-84A $\Delta$ 1-557 and to test if movement can be impaired in the same way it can be impaired in a Golgi labelled by ST-GFP using drugs such Latrunculin B or expression of motor proteins mutants that are used to impair movement (Gao *et al.*, 2016; Osterrieder *et al.*, 2017). Optical tweezers coupled to a confocal microscope could be used to track the tips of ER tubules while trapping a Golgi body expression Atgolgin-84A or the truncation Atgolgin-84A $\Delta$ 1-557 as it was obtained for AtCASP expression (Osterrieder *et al.*, 2017).

It would be interesting to also quantify how often it is possible to trap a high number of Golgi bodies and this could be compared to stable expression in *A. thaliana* considering these different phenotypes might be due to different levels of expression in transient transformation.

AtCASP $\Delta$ 1-564 has been shown to have an effect in tethering to the ER. When co-expressed with Atgolgin-84A $\Delta$ 1-557 there was no effect in the number of Golgi bodies trapped. If AtCASP $\Delta$ 1-564 weaken the tether to the ER this would compensate the effect of Atgolgin-84A $\Delta$ 1-557 that alone makes the Golgi bodies more difficult to trap. This suggests that AtCASP and Atgolgin-84A may be involved in different tethering events.

### **Atgolgin-84A $\Delta$ 1-557 can impair exocytosis of a secretory marker**

Considering the recent works the ability of human golgin-84 to tether specific cargo vesicles and Atgolgin-84A as a potential pre-*cis*-Golgi-ER-tether was tested for effects in the protein trafficking. Interestingly both expression of full-length protein and Atgolgin-84A $\Delta$ 1-557 impaired exocytosis and the cargo marker was re-directed to the vacuole potentially interfering with ER-to-Golgi transport. It can be hypothesised that the N-terminal region of the protein could be essential for trafficking to the Golgi or within the Golgi. In the case of full-length the recognition of the cargo transporter might be impaired due to GFP masking the first N-terminal amino acids. In the case of Atgolgin-84A $\Delta$ 1-557 that region was deleted. Therefore, both have a similar effect. This indicates an alternative export from the ER or Golgi. If ER-Golgi transport is impaired then a route could be active to export the cargo from the ER bypassing the Golgi and reaching the vacuole if this cargo was sent for degradation. The Golgi-independent route has been reported previously, for example in Hara-Nishimura *et al.* (1998) and when trafficking is impaired in tobacco epidermal cells (Pereira *et al.*, 2013).

One hypothesis is that Atgolgin-84A is not able to recognise the cargo and docking of the transporter to the Golgi does not occur. If the cargo reaches the Atgolgin-84A labelled compartment then perhaps it cannot travel within the Golgi stack and exits the Golgi at the pre-*cis*-Golgi or before the *trans*-Golgi. Another hypothesis is that Golgi stack morphology is so



compromised due to a partially non-functional Atgolgin-84A expression that proteins are not going through post-translational modifications efficiently and there might be a quality control within the Golgi and this cargo protein is sent to degradation in the vacuole. Also using another cargo such as a fluorescent-tagged vacuolar sorting determinant that follows the conventional COPII-dependent pathway to reach the vacuole or a medial/trans Golgi marker would be useful to confirm the results with SP-mCherry. The cargo could enter the Golgi but cannot progress within the Golgi stack and it exits the Golgi directly to the vacuole possibly for degradation. If the cargo was not being transported from ER to the Golgi it is typical to observe accumulation in the ER and this was never observed in the case of the golgin and Atgolgin-84A $\Delta$ 1-557. In contrast the trafficking through the Golgi is a fast process and the accumulation in the Golgi might not be detectable.

The  $\alpha$ -amylase assay is a robust method to study the effect of the golgin in the protein transport but these experiments have to be further optimised for the expression of the golgins and tested for other expression time-points to mimic the time-points for the imaging secretion assay. This can be optimised by monitoring expression in protoplasts using the fluorescent tagged versions of the constructs. From the confocal assay it is known that the Atgolgin-84A only has an effect in cargo transport after 24h of expression therefore the amylase assay could only start 24h after the expression of golgins which could be achieved by infiltration of the golgin, protoplast preparation and electroporation with a secretory marker 24h after. This experiment should be repeated also with other controls such as effector proteins that have been described to impair the secretory pathway such as the dominant negative mutant of Sar1-GTP locked version.

In summary:

- Atgolgin-84A acts as a tether at the newly described pre-*cis*-Golgi compartment
- It has a potential role in regulating ER-Golgi transport
- May be involved in maintaining Golgi stacking, orientation and size.

## REFERENCES

Altschul S. F., Madden T. L., Schäffer A. A., Zhang J., Zhang Z., Miller W. and Lipman D. J. (1997). *Gapped BLAST and PSI-BLAST: a new generation of protein database search programs. Nucleic Acids Res.* 25, 3389–3402.

Alvarez C., Garcia-Mata R., Hauri H. P., and Sztul E. (2001). The p115-interactive Proteins GM130 and Giantin participate in Endoplasmic Reticulum-Golgi traffic. *J. Biol. Chem.* 276, 2693–2700.

Andreeva A.V., Zheng H., Kutuzov M. A., Evans D. E. and Hawes C. R. (2000). Organization of transport from endoplasmic reticulum to Golgi in higher plants Plant ER and GA visualization with green fluorescent protein (GFP) Plant homologues of the proteins involved in ER-to-GA transport. *Biochemical Society Transactions*, 505-512.

Appenzeller-Herzog C. and Hauri H. P. (2006). The ER-Golgi intermediate compartment (ERGIC): in search of its identity and function. *J Cell Sci* 119, 2173-83.

Barlow L. D., Nývltová E., Aguilar M., Tachezy J. and Dacks J. B. (2018). A sophisticated, differentiated Golgi in the ancestor of eukaryotes. *BMC Biology*, 16-27.

Bar-Peled M. and Raikhel N. V. (1997). Characterization of AtSEC12 and AtSAR1. Proteins likely involved in endoplasmic reticulum and Golgi transport. *Plant Physiol* 114, 315–324.

Bascom R. A., Srinivasan S. and Nussbaum R. L. (1999). Identification and characterization of golgin-84, a novel Golgi integral membrane protein with a cytoplasmic coiled-coil domain. *J. Biol.Chem.* 274, 2953–2962.

Batoko H., Zheng H.Q., Hawes C. and Moore I. (2000). A Rab1 GTPase is required for transport between the endoplasmic reticulum and Golgi apparatus and for normal Golgi movement in plants. *The Plant cell*. 12, 2201–2218.

Bevis B. J., Hammond A. T., Reinke C. A. and Glick B. S. (2002). *De novo* formation of transitional ER sites and Golgi structures in *Pichia pastoris*. *Nat Cell Biol* 4, 750-6.

Boevink P., Oparka K., Santa Cruz S., Martin B., Betteridge A. and Hawes C. (1998). Stacks on tracks: the plant Golgi apparatus traffics on an actin/ER network. *Plant J* 15, 441-447.

Brandizzi F., Snapp E. L., Roberts A. G., Lippincott-Schwartz J. and Hawes C. (2002). Membrane protein transport between the endoplasmic reticulum and the Golgi in tobacco leaves is energy dependent but cytoskeleton independent: evidence from selective photobleaching. *Plant Cell* 14, 1293-1309.

Burguete A. S., Fenn T. D., Brunger A. T. and Pfeffer S. R. (2008). Rab and Arl GTPase family members cooperate in the localization of the golgins GCC185. *Cell* 132, 286–298.

Burkhard P., Stetefeld J. and Strelkov S. V. (2001). Coiled coils: a highly versatile protein folding motif. *Trends Cell Biol* 11, 82-8.

Cao P., Renna L., Stefano G. and Brandizzi F. (2016). SYP73 Anchors the ER to the actin cytoskeleton for maintenance of ER integrity and streaming in Arabidopsis. *Current Biology* 26, 3245–3254.

Chatre L., Brandizzi F., Hocquellet A., Hawes C. and Moreau P. (2005). Sec22 and Memb11 are v-SNAREs of the anterograde endoplasmic reticulum-Golgi pathway in tobacco leaf epidermal cells. *Plant Physiol* 139, 1244-54.

Chen J., Stefano G., Brandizzi F. and Zheng H. (2011). Arabidopsis RHD3 mediates the generation of the tubular ER network and is required for Golgi distribution and motility in plant cells. *J Cell Sci* 124, 2241-52.

Cheung P. P., Limouse C., Mabuchi H. and Pfeffer S. R. (2015). Protein flexibility is required for vesicle tethering at the Golgi. *eLife* 4, e12790. doi:10.7554/eLife.12790.

Chrispeels M. J. and Herman E. M. (2000). Endoplasmic reticulum-derived compartments function in storage and as mediators of vacuolar remodeling via a new type of organelle, precursor protease vesicles. *Plant physiology* 123, 1227–1234.

Clough S.J. and Bent A.F. (1998). Floral Dip: A Simplified Method for Agrobacterium-Mediated Transformation of Arabidopsis thaliana. *The Plant Journal* 16, 735-743.

Crofts A. J. A., Leborgne-castel N., Hillmer S., Robinson D. G. D., Phillipson B., Carlsson L. E., Ashford D. A. and Denecke J. (1999). Saturation of the endoplasmic reticulum retention machinery reveals anterograde bulk flow. *The Plant cell* 11, 2233–48.

Curtis, M. and Grossniklaus U. (2003). A Gateway Cloning Vector Set for High-Throughput Functional Analysis of Genes in Planta. *Plant Physiology* 133, 462–469.

Da Silva L. L., Snapp E. L., Denecke J., Lippincott-Schwartz J., Hawes C. and Brandizzi F. (2004). Endoplasmic reticulum export sites and Golgi bodies behave as single mobile secretory units in plant cells. *Plant Cell* 16, 1753-1771.

Delorenzi M. and Speed T. (2002). An HMM model for coiled-coil domains and a comparison with PSSM-based predictions. *Bioinformatics* 18, 617-25.

De Marcos Lousa C., Gershlick D.C. and Denecke J. (2012). Mechanisms and concepts paving the way towards a complete transport cycle of plant vacuolar sorting receptors. *The Plant Cell*. 24, 1714–32.

d'Enfert C., Gensse M. and Gaillardin C. (1992). Fission yeast and a plant have functional homologues of the Sar1 and Sec12 proteins involved in ER to Golgi traffic in budding yeast. *EMBO J* 11, 4205–4211.

Diao A., Rahman D., Pappin D. J., Lucocq J. and Lowe M. (2003). The coiled-coil membrane protein golgin-84 is a novel Rab effector required for Golgi ribbon formation. *J Cell Biol* 160, 201-12.

Donaldson J. G. and Jackson C. L. (2011). ARF family G proteins and their regulators: roles in membrane transport, development and disease. *Nat Rev Mol Cell Biol* 12, 362-75.

Donohoe B. S., Kang B. H. and Staehelin L. A. (2007). Identification and characterization of COPIa- and COPIb-type vesicle classes associated with plant and algal Golgi. *Proc Natl Acad Sci USA* 104, 163-8.

Drin G., Morello V., Casella J. F., Gounon P. and Antony B. (2008). Asymmetric tethering of flat and curved lipid membranes by a golgin. *Science* 320, 670–673.

Du W., Tamura K., Stefano G., Brandizzi F. (2013). The integrity of the plant Golgi apparatus depends on cell growth-controlled activity of GNL1. *Mol Plant* 6, 905-15.

Durek P., Schmidt R., Heazlewood J. L., Jones A., Maclean D., Nagel A., Kersten B., Schulze W. X. (2010). PhosPhAt: the *Arabidopsis thaliana* phosphorylation site database. An update. *Nucleic Acids Research* 38, 828-834.

Efimov A., Kharitonov A., Efimova N., Loncarek J., Miller P. M., Andreyeva N., Gleeson P., Galjart N., Maia A. R. R., McLeod I. X., Yates

J.R., Maiato H., Khodjakov A., Akhmanova A. and Kaverina I. (2007). Asymmetric CLASP-dependent nucleation of non centrosomal microtubules at the *trans*-Golgi network. *Developmental Cell* 12, 917–930.

Faso C., Chen Y.N, Tamura K., Held M., Zemelis S., Marti L., Saravana R., Hummel E., Kung L., Miller E. (2009). A missense mutation in the *Arabidopsis* COPII coat protein Sec24A induces the formation of clusters of the endoplasmic reticulum and Golgi apparatus. *Plant Cell* 21, 3655–3671.

Fazal F. M. and Block S. M. (2011). Optical tweezers study life under tension. *Nat Photonics* 5, 318-321.

Foresti, O. and Denecke, J. (2008). Intermediate organelles of the plant secretory pathway: identity and function. *Traffic* 9, 1599-612.

Foresti O., Gershlick D. C., Bottanelli F., Hummel E., Hawes C. and Denecke, J. (2010). A recycling-defective vacuolar sorting receptor reveals an intermediate compartment situated between prevacuoles and vacuoles in tobacco. *The Plant Cell* 22, 3992–4008.

Fridmann-Sirkis Y., Siniosoglou S. and Pelham H. R. (2004). TMF is a golgin that binds Rab6 and influences Golgi morphology. *BMC Cell Biol* 5, 18.

Ganley I. G., Espinosa E. and Pfeffer S. R. (2008). A syntaxin 10 SNARE complex distinguishes two distinct transport routes from endosomes to the *trans*-golgi in human cells. *The Journal of Cell Biology* 180, 159–172.

Gao H., Metz J., Teanby N. A., Ward A. D., Botchway S. W., Coles B., Pollard M. and Sparkes I. (2016). *In vivo* quantification of peroxisome tethering to chloroplasts in tobacco epidermal cells using optical tweezers. *Plant Physiology* 170, 263–272.

Geldner N., Anders N., Wolters H., Keicher J., Kornberger W., Muller P., Delbarre A., Ueda T., Nakano A. and Jurgens G. (2003). The Arabidopsis GNOM ARF-GEF mediates endosomal recycling, auxin transport, and auxin-dependent plant growth. *Cell* 112, 219-30.

Gershlick D. C., Lousa C. D. M., Foresti O., Lee A. J., Pereira E. A., Luis L. P., Bottanelli F., Denecke J. and daSilva, L. L. P. (2014). Golgi-dependent transport of vacuolar sorting receptors is regulated by COPII, AP1, and AP4 protein complexes in tobacco. *The Plant cell* 26, 1308–29.

Gillingham A. K., Pfeifer A. C. and Munro S. (2002). CASP, the alternatively spliced product of the gene encoding the CCAAT-displacement protein transcription factor, is a Golgi membrane protein related to giantin. *Mol Biol Cell* 13, 3761-74.

Gillingham A. K., Tong A. H., Boone C. and Munro S. (2004). The GTPase Arf1p and the ER to Golgi cargo receptor Erv14p cooperate to recruit the golgin Rud3p to the *cis*-Golgi. *J Cell Biol* 167, 281-92.

Gilson P. R., Vergara C. E., Kjer-Nielsen L., Teasdale R. D., Bacic A. and Gleeson, P. A. (2004). Identification of a Golgi-localised GRIP domain protein from *Arabidopsis thaliana*. *Planta* 219, 1050–1056.

Glick B. S. (2002). Can the Golgi form *de novo*? *Nat Rev Mol Cell Biol* 3, 615-9.

Hanson M. R. and Sattarzadeh A. (2013). Trafficking of proteins through plastid stromules. *Plant Cell* 25, 2774–2782.

Hanton S.L., Bortolotti L. E., Renna L., Stefano G. and Brandizzi F. (2005). Crossing the divide - transport between the endoplasmic reticulum and Golgi apparatus in plants. *Traffic* 6, 267-277.

Hara-Nishimura I. I., Shimada T., Hatano K., Takeuchi Y. and Nishimura M. (1998). Transport of storage proteins to protein storage vacuoles is

mediated by large precursor-accumulating vesicles. *Plant Cell* 10, 825-36.

**Hauri H. P. and Schweizer A.** (1992). The endoplasmic reticulum-Golgi intermediate compartment. *Curr. Opin. Cell Biol.* 4, 600-608.

Hawes C. (2005). Cell biology of the plant Golgi apparatus. *New Phytol* 165, 29-44.

Hawes, C. and Satiat-Jeunemaitre, B. (2005). The plant Golgi apparatus-going with the flow. *Biochim Biophys Acta* 1744, 466-80.

Hawes C., Schoberer J., Hummel E. and Osterrieder A. (2010). Biogenesis of the plant Golgi apparatus. *Biochem. Soc. Trans.* 38, 761–767.

Hayes G. L., Brown F. C., Haas A. K., Nottingham R. M., Barr F. A. and Pfeffer S. R. (2009). Multiple rab GTPase binding sites in GCC185 suggest a model for vesicle tethering at the *trans*-Golgi. *Molecular Biology of the Cell* 20, 209–217.

He C. Y., Ho H. H., Malsam J., Chalouni C., West C. M., Ullu E., Toomre D. and Warren G. (2004). Golgi duplication in *Trypanosoma brucei*. *J Cell Biol* 165, 313-21.

Helms J. B. and Rothman J. E. (1992). Inhibition by Brefeldin A of a Golgi membrane enzyme that catalyses exchange of guanine nucleotide bound to ARF. *Nature* 360, 352-4.

Hong, W. and Lev, S. (2014). Tethering the assembly of SNARE complexes. *Trends Cell Biol.* 24, 35–43.

Huff J., Bathe W., Netz R., Anhut T. and Weisshart K. (2015). The Airyscan Detector from ZEISS Confocal Imaging with Improved Signal-to-Noise Ratio and Superresolution. Technology note, *Carl Zeiss Microscopy GmbH*, Germany.



Hummel E., Schmickl R., Hinz G., Hillmer S. and Robinson D. G. (2007). Brefeldin A action and recovery in *Chlamydomonas* are rapid and involve fusion and fission of Golgi cisternae. *Plant Biol* 9, 489-501.

Johansen J. N., Chow C. M., Moore I. and Hawes, C. (2009). AtRABH1b and AtRAB-H1c GTPases, homologues of the yeast Ypt6, target reporter proteins to the Golgi when expressed in *Nicotiana tabacum* and *Arabidopsis thaliana*. *J. Exp. Bot.* 60, 3179–3193.

Jones D.T. (1999). *Protein secondary structure prediction based on position-specific scoring matrices*. *J Mol Biol.* 292, 195–202.

Jones D. T. and Cozzetto D. (2014). DISOPRED3: Precise disordered region predictions with annotated protein binding activity. *Structural Bioinformatics*.

Kang B. H. and Staehelin L. A. (2008) ER-to-Golgi transport by COPII vesicles in Arabidopsis involves a ribosome-excluding scaffold that is transferred with the vesicles to the Golgi matrix. *Protoplasma*, 51-64.

Karimi M., De Meyer B. and Hilson P. (2005). Modular cloning and expression of tagged fluorescent protein in plant cells. *Trends Plant Sci* 10, 103-105.

Kelley L. A., Mezulis S., Yates C. M., Wass N. M. and Sternberg M. J.E. (2015). The Phyre2 web portal for protein modeling, prediction and analysis. *Nature Protocols* 10, 845–858.

Langhans M., Hawes C., Hillmer S., Hummel E. and Robinson D. G. (2007). Golgi regeneration after Brefeldin A treatment in BY-2 cells entails stack enlargement and cisternal growth followed by division. *Plant Physiol* 145, 527-38.

Latijnhouwers M., Hawes C. and Carvalho C. (2005a) Holding it all together? Candidate proteins for the plant Golgi matrix. *Curr. Opin.Plant Biol.* 8, 632–639.

Latijnhouwers M., Hawes C., Carvalho C., Oparka K., Gillingham A. K. and Boevink P. (2005b). An *Arabidopsis* GRIP domain protein locates to the *trans*-Golgi and binds the small GTPase ARL1. *Plant J.* 44, 459–470.

Latijnhouwers M., Gillespie T., Boevink P., Kriechbaumer V., Hawes C. and Carvalho C. M. (2007). Localization and domain characterization of *Arabidopsis* golgin candidates. *J. Exp. Bot.* 58, 4373–4386.

Leborgne-Castel N., Jelitto-Van Dooren E. P., Crofts J. and Denecke J. (1999). Overexpression of BiP in tobacco alleviates endoplasmic reticulum stress. *The Plant cell* 11, 459–470.

Lin Y. C., Chiang T. C., Liu Y. T., Tsai Y. T., Jang L. T. and Lee F. J. S. (2011). ARL4A acts with GCC185 to modulate Golgi complex organization. *Journal of Cell Science* 124, 4014–4026.

Linstedt A. D. and Hauri H. P. (1993). Giantin, a novel conserved Golgi membrane protein containing a cytoplasmic domain of at least 350 kDa. *Mol Biol Cell* 4, 679-93.

Lowe M. (2011). Structural organization of the Golgi apparatus. *Curr Opin Cell Biol.* 23, 85–93.

Lu L. and Hong W. (2003). Interaction of Arl1–GTP with GRIP domains recruits autoantigens Golgin-97 and Golgin-245/p230 onto the Golgi. *Mol. Biol. Cell* 14, 3767–3781.

Malsam J., Satoh A., Pelletier L. and Warren G. (2005). Golgin tethers define subpopulations of COPI vesicles. *Science* 307, 1095-8.

Marion J., Bach L., Bellec Y., Meyer C., Gissot L. and Faure J-D (2008). Systematic analysis of protein subcellular localization and interaction

using high-throughput transient transformation of Arabidopsis seedlings. *The Plant Journal* 56, 169–179.

Matheson L. A., Hanton S. L., Rossi M., Latijnhouwers M., Stefano G., Renna L. and Brandizzi F. (2007). Multiple roles of ADP-ribosylation factor 1 in plant cells include spatially regulated recruitment of coatomer and elements of the Golgi matrix. *Plant Physiol* 143, 1615-27.

Mathur J., Mammone A. and Barton K. A. (2012). Organelle Extensions in Plant Cells. *Journal of Integrative Plant Biology* 54, 851–867.

Misteli T. and Warren G. (1995). Mitotic disassembly of the Golgi apparatus *in vivo*. *J Cell Sci* 108, 2715-27.

Movafeghi A., Happel N., Pimpl P., Tai G. H., Robinson D. G. (1999). Arabidopsis Sec21p and Sec23p homologs. Probable coat proteins of plant COP coated vesicles. *Plant Physiol* 119, 1437–1446.

Munro S. (2011). The golgin coiled-coil proteins of the Golgi apparatus. *Cold Spring Harb Perspect Biol*, 1-3(6).

Murashige T. and Skoog F. (1962). A Revised Medium for Rapid Growth and Bio Assays with Tobacco Tissue Cultures. *Physiologia Plantarum*, 473-497.

Nebenfuhr A., Gallagher L. A., Dunahay T. G., Frohlick J. A., Mazurkiewicz A. M., Meehl J. B. and Staehelin L. A. (1999). Stop-and-go movements of plant Golgi stacks are mediated by the acto-myosin system. *Plant Physiol* 121, 1127-1142.

Osterrieder A., Hummel E., Carvalho C. M. and Hawes C. (2009a). Golgi membrane dynamics after induction of a dominant negative mutant Sar1 GTPase in tobacco. *Journal of Experimental Botany*, 1-18.

Osterrieder A., Carvalho C. M., Latijnhouwers M., Johansen J. N., Stubbs C., Botchway S. and Hawes C. (2009b). Fluorescence lifetime imaging

of interactions between Golgi tethering factors and small GTPases in plants. *Traffic* 10, 1034–1046.

Osterrieder A., Hummel E., Carvalho C. M. and Hawes, C. (2010). Golgi membrane dynamics after induction of a dominant-negative mutant Sar1 GTPase in tobacco. *J. Exp. Bot.* 61, 405–422.

Osterrieder A. (2012). Tales of tethers and tentacles: golgins in plants. *Journal of Microscopy* 247, 68–77.

Osterrieder A., Sparkes I. A, Botchway S.W., Ward A., Ketelaar T., De Ruijter N. C. A and Hawes C. (2017). Stacks off tracks: a role for the golgin AtCASP in plant endoplasmic reticulum-Golgi apparatus tethering. *Journal of Experimental Biology* 68, 3339–3350.

Pelletier L., Stern C. A., Pypaert M., Sheff D., Ngo H. M., Roper N., He C. Y., Hu K., Toomre D., Coppens I., Roos D. S., Joiner K. A. and Warren G. (2002). Golgi biogenesis in *Toxoplasma gondii*. *Nature* 418, 548-52.

Pereira C., Pereira S., Satiat-Jeunemaitre B. and Pissarra J. (2013). Cardosin A contains two vacuolar sorting signals using different vacuolar routes in tobacco epidermal cells. *The Plant Journal* 76, 87–100.

Perico C. and Sparkes I. (2018). Plant organelle dynamics: cytoskeletal control and membrane contact sites. *New Phytologist* 381–394.

Pernet-Gallay K., Antony C., Johannes L., Bornens M., Goud B. and Rios R. M. (2002). The overexpression of GMAP-210 blocks anterograde and retrograde transport between the ER and the Golgi apparatus. *Traffic* 3, 822-32.

Phillipson B. A., Pimpl P., da Silva L. L., Crofts A. J., Taylor J. P., Movafeghi A., Robinson D. G. and Denecke J. (2001). Secretory bulk flow of soluble proteins is efficient and COPII dependent. *Plant Cell* 13, 2005–2020.

Pimpl P., Taylor J. P., Snowden C., Hillmer S., Robinson D. G. and Denecke J. (2006). Golgi-mediated vacuolar sorting of the endoplasmic reticulum chaperone BiP may play an active role in quality control within the secretory pathway. *The Plant cell* 18, 198-211.

Kriechbaumer V., Botchway S. W., Slade S. E., Knox K., Frigerio L., Oparka K. and Hawes C. (2015). Reticulomics: Protein-Protein Interaction Studies with Two Plasmodesmata-Localized Reticulon Family Proteins Identify Binding Partners Enriched at Plasmodesmata, Endoplasmic Reticulum, and the Plasma Membrane. *Plant Physiol.* 169, 1933-45.

Ramirez I. B. and Lowe M. (2009). Golgins and GRASPs: holding the Golgi together. *Seminars in Cell & Developmental Biology* 20, 770–779.

Renna, L., Hanton, S. L., Stefano, G., Bortolotti, L., Misra, V. and Brandizzi, F. (2005). Identification and characterization of AtCASP, a plant transmembrane Golgi matrix protein. *Plant Mol. Biol.* 58, 109–122.

Robinson D.G., Langhans M., Saint-Jore-Dupas C. and Hawes C. (2008). BFA effects are tissue and not just plant specific. *Trends Plant Sci* 13, 405-8.

Rosing M., Ossendorf E., Rak A., and Barnekow A. (2007). Giantin interacts with both the small GTPase Rab6 and Rab1. *Exp. Cell Res.* 313, 2318–2325.

Runions J., Brach T., Kühner S. and Hawes C. (2005). Photoactivation of GFP reveals protein dynamics within the endoplasmic reticulum membrane. *J Exp Bot* 57, 43–50.

Saint-Jore C.M., Evins J., Batoko H., Brandizzi F., Moore I. and C. Hawes (2002). Redistribution of membrane proteins between the Golgi apparatus and endoplasmic reticulum in plants is reversible and not dependent on cytoskeletal networks, *Plant J* 29, 661-78.

Satiat-Jeunemaitre B., Cole L., Bourett T., Howard R. and Hawes C. (1996). Brefeldin A effects in plant and fungal cells: something new about vesicle trafficking? *J Microsc* 181, 162-77.

Satoh A., Wang Y., Malsam J., Beard M. B. and Warren G. (2003). Golgin-84 is a Rab1 binding partner involved in Golgi structure. *Traffic* 4, 153–161.

Seemann J., Jokitalo E., Pypaert M. and Warren G. (2000a). Matrix proteins can generate the higher order architecture of the Golgi apparatus. *Nature* 407, 1022-6.

Seemann J., Jokitalo E. J. and Warren G. (2000b). The role of the tethering proteins p115 and GM130 in transport through the Golgi apparatus *in vivo*. *Mol Biol Cell* 11, 635-45.

Schoberer J. and Strasser R. (2011). Sub-Compartmental Organization of Golgi-Resident N-Glycan Processing Enzymes in Plants. *Molecular Plant* 4, 220–228.

Schoberer J., Runions J., Steinkellner H., Strasser R., Hawes C. and Osterrieder A. (2010). Sequential depletion and acquisition of proteins during Golgi stack disassembly and reformation. *Traffic* 11, 1429–1444.

**Schweizer A., Fransen J. A., Matter K., Kreis T. E., Ginsel L. and Hauri H. P.** (1990). Identification of an intermediate compartment involved in protein transport from endoplasmic reticulum to Golgi apparatus. *Eur. J. Cell Biol.* 53,185-196.

Short, B., Haas, A. and Barr, F. A. (2005). Golgins and GTPases, giving identity and structure to the Golgi apparatus. *Biochim Biophys Acta* 1744, 383-95.

Silva-Alvim F. A. L., An J., Alvim J. C., Foresti O., Grippa A., Pelgrom A., Adams T. L., Hawes C., and Denecke J. (2018). Predominant Golgi

Residency of the Plant K/HDEL Receptor Is Essential for its Function in Mediating ER Retention *Plant Cell* doi:10.1105/tpc.18.00426.

Soares Da Costa D. S., Pereira S., Moore I. and Pissarra J. (2010). Dissecting cardosin B trafficking pathways in heterologous systems. *Planta* 232, 1517-30.

Sohda M., Misumi Y., Yamamoto A., Nakamura N., Ogata S., Sakisaka S., Hirose S., Ikehara Y. and Oda K. (2010). Interaction of golgin-84 with the COG complex mediates the intra-Golgi retrograde transport. *Traffic* 11, 1552–1566.

Spang A., Shiba Y. and Randazzo P. A. (2010). Arf GAPs: gatekeepers of vesicle generation. *FEBS Lett.* 18; 584 (12): 2646-51.

Sparkes I. A., Ketelaar T., de Ruijter N. C. A. and Hawes C. (2009). Grab a Golgi: laser trapping of Golgi bodies reveals *in vivo* interaction with the endoplasmic reticulum. *Traffic* 10, 567–571.

Sparkes I., Frigerio, L., Tolley N. and Hawes C. (2009). The plant endoplasmic reticulum: a cell-wide web. *Biochemical Journal*, 423 (2) 145-155.

Sparkes I., Runions J., Kearns A. and Hawes C. (2006). Rapid, transient expression of fluorescent fusion proteins in tobacco plants and generation of stably transformed plants. *Nature protocols* 1, 2019-25.

Sparkes I., Tolley N., Aller I., Svozil J., Osterrieder A., Botchway S., Mueller C., Frigerio L., and Hawes C. (2010) Five *Arabidopsis* Reticulon Isoforms Share Endoplasmic Reticulum Location, Topology, and Membrane-Shaping Properties. *Plant Cell*. 22(4): 1333–1343.

Sparkes I., White R. R., Coles B., Botchway S. W. and Ward A. (2018). Using optical tweezers combined with total internal reflection microscopy

to study interactions between the ER and Golgi in plant cells. *Methods in Molecular Biology* 1691, 167–178.

Staehelein L. A. and Chapman R.L. (1987). Secretion and membrane recycling in plant cells: novel intermediary structures, visualized in ultrarapidly frozen sycamore and carrot suspension-culture cells L.A. *Planta* 171: 43-57.

Staehelein A. L. (1997). The plant ER: a dynamic organelle composed of a large number of discrete functional domains. *The Plant Journal* 11, 1151-1165.

Staehelein L. A., Giddings T. H. Jr, Kiss J. Z. and Sack F. D. (1990). Macromolecular differentiation of Golgi stacks in root tips of *Arabidopsis* and *Nicotiana* seedlings as visualized in high pressure frozen and freeze-substituted samples. *Protoplasma* 157, 75-91.

Staehelein L. A. and Moore I. (1995). The plant Golgi apparatus: structure, functional organisation and trafficking mechanisms. *Annu Rev Plant Physiol and Plant Mol Biol* 46, 261-288.

Stefano G., Renna L., Chatre L., Hanton S. L., Moreau P., Hawes C. and Brandizzi F. (2006). In tobacco leaf epidermal cells, the integrity of protein export from the endoplasmic reticulum and of ER export sites depends on active COPI machinery. *Plant J* 46, 95–110.

Stefano G., Renna L., Moss T., McNew J.A. and Brandizzi F. (2012). In *Arabidopsis*, the spatial and dynamic organization of the endoplasmic reticulum and Golgi apparatus is influenced by the integrity of the C-terminal domain of RHD3, a non-essential GTPase, *Plant J* 69, 957-66.

Stefano G., Hawes C. and Brandizzi F. (2014). ER - the key to the highway. *Curr Opin Plant Biol* 2230-8.



Stevenson N. L., Bergen D. J. M., Skinner R. E. H., Kague E., Martin-Silverstone E., Brown K. A. R., Hammond C. L., and Stephens D. J. (2017). Giantin-knockout models reveal a feedback loop between Golgi function and glycosyltransferase expression. *J Cell Sci.* 130 (24), 4132–4143.

Strasser R., Stadlmann J., Svoboda B., Altmann F., Ossl J. G. I. and Mach L. (2005). Molecular basis of N-acetylglucosaminyltransferase I deficiency in *Arabidopsis thaliana* plants lacking complex N-glycans. *Biochem. J.* 387, 385–391.

Strasser R. (2016). Plant protein glycosylation. *Glycobiology* 1–14.

Sztul E. and Lupashin V. (2006). Role of tethering factors in secretory membrane traffic. *American Journal of Physiology-Cell Physiology* 290, C11–C26.

Takeuchi M., Tada M., Saito C., Yashiroda H. and Nakano A. (1998). Isolation of a tobacco cDNA encoding Sar1 GTPase and analysis of its dominant mutations in vesicular traffic using a yeast complementation system. *Plant Cell Physiol* 39, 590–599.

Takeuchi M., Ueda T., Sato K., Abe H., Nagata T., Nakano A. (2000). A dominant negative mutant of Sar1 GTPase inhibits protein transport from the endoplasmic reticulum to the Golgi apparatus in tobacco and *Arabidopsis* cultured cells. *Plant J* 23, 517–525.

Thompson J. D., Higgins D. G., and Gibson T. J. (1994) Clustal-W – Improving the Sensitivity of Progressive Multiple Sequence Alignment through Sequence Weighting, Position-Specific Gap Penalties and Weight Matrix Choice. *Nucleic Acids Res* 22, 4673-4680.

Ueda K. (1997). The synchronous division of dictyosomes at the premitotic stage. *Ann Bot* 80, 29-33.

- Uemura T., Ueda T., Ohniwa R. L., Nakano A., Takeyasu K. and Sato M. H. (2004). Systematic analysis of SNARE molecules in Arabidopsis: dissection of the post-Golgi network in plant cells. *Cell Struct Funct* 29, 49-65.
- Vitale A. and Denecke J. (1999). The endoplasmic reticulum-gateway of the secretory pathway. *The Plant cell* 11, 615-28.
- Vitale A. and Raikhel, N. (1999). What do proteins need to reach different vacuoles? *Trends in plant science* 4, 149–155.
- Vitale A. and Boston R. S. (2008). Endoplasmic reticulum quality control and the unfolded protein response: insights from plants. *Traffic* 9, 1581-8.
- Wang X., Cai Y., Wang H., Zeng Y., Zhuang X., Li B. and Jiang L. (2014). *Trans*-Golgi network-located AP1 gamma adaptins mediate dileucine motif-directed vacuolar targeting in Arabidopsis. *The Plant cell* 26, 4102-4118.
- Wang P., Hawes C. and Hussey P. J. (2017). Plant endoplasmic reticulum-plasma membrane contact sites. *Trends in Plant Science* 22, 289–297.
- Wang P., Mugume Y. and Bassham D. C. (2017). New advances in autophagy in plants: regulation, selectivity and function. *Seminars in Cell & Developmental Biology* (17) 30129-5.
- Ward J. J., Sodhi J. S., McGuffin L. J., Buxton B. F. and Jones D. T. (2004). *Prediction and functional analysis of native disorder in proteins from the three kingdoms of life. J. Mol. Biol.* 337, 635–645.
- Williams D., Hicks S. W., Machamer C. E. and Pessin J. E. (2006). Golgin-160 is required for the Golgi membrane sorting of the insulin-responsive glucose transporter GLUT4 in adipocytes. *Mol Biol Cell.* 17, 5346-55.

- Witkos T. M. and Lowe M. (2016). The Golgin Family of Coiled-Coil Tethering Proteins. *Frontiers in Cell and Developmental Biology* 3, 86.
- Wong M. and Munro S. (2014). The specificity of vesicle traffic to the Golgi is encoded in the golgins coiled- coil proteins. *Science* 346, 6209.
- Wong M., Gillingham A. K. and Munro S. (2017). The golgin coiled-coil proteins capture different types of transport carriers via distinct N-terminal motifs. *BMC Biology* 15.
- Xiang Y. and Wang Y. (2010). GRASP55 and GRASP65 play complementary and essential roles in Golgi cisternal stacking. *J Cell Biol* 188, 237–251.
- Xiang Y. and Wang Y. (2011). New components of the Golgi matrix. *Cell Tissue Res.* 344, 365–379.
- Yadav S., Puthenveedu M. A. and Linstedt A. D. (2012). Golgin-160 recruits the dynein motor to position the Golgi apparatus. *Dev. Cell* 23,153–165.
- Yang Y. D., Elamawi R., Bubeck J., Pepperkok R., Ritzenthaler C., Robinson D. G. (2005). Dynamics of COPII vesicles and the Golgi apparatus in cultured *Nicotiana tabacum* BY-2 cells provides evidence for transient association of Golgi stacks with endoplasmic reticulum exit sites. *Plant Cell* 17, 1513–1531.
- Yu I-M. and Hughson F. M. (2010). Tethering factors as organizers of intracellular vesicular traffic. *Annu. Rev. Cell Dev. Biol.* 26, 137–156.
- Zeng Y., Chung K.P., Li B., Lai C. M., Lam S. K., Wang X., Cui Y., Gao C., Luo M., Wong K.B., Schekman R. and Jiang L. (2015). Unique COPII component AtSar1a/AtSec23a pair is required for the distinct function of protein ER export in *Arabidopsis thaliana*, *Proc Natl Acad Sci USA* 112, 14360-5.

Zhang M., Wu F., Shi J., Zhu Y., Zhu Z., Gong Q. and Hu J. (2013). ROOT HAIR DEFECTIVE 3 family of dynamin-like GTPases mediates homotypic endoplasmic reticulum fusion and is essential for Arabidopsis development. *Plant Physiol* 163, 713-20.

Zinchuk V. and Zinchuk O. (2008). Quantitative colocalization analysis of confocal fluorescence microscopy images. *Current Protocols in Cell Biology* 4: 19.

Zulawski M., Braginets R. and Schulze W. X. (2013). PhosPhAt goes kinases-searchable protein kinase target information in the plant phosphorylation site database PhosPhAt. *Nucleic Acids Research* 41.